The biofilm formation of *Mycobacterium abscessus* and *Mycobacterium chimaera* and its impact on antimicrobial susceptibility.

Inaugural - Dissertation
to obtain the academic degree

Doctor rerum naturalium (Dr. rer. nat.)

Submitted to the Department of Biology, Chemistry and Pharmacy
of the Freie Universität Berlin

by

Anna Maria Oschmann-Kadenbach
née Oschmann, from Munich, Germany

Berlin, 2023

This work was accomplished between March 2018 and June 2021 at the Robert Koch Institute under the supervision of Dr. Astrid Lewin.

1st Reviewer: Dr. Astrid Lewin

2nd Reviewer: Prof. Dr. Peter Robin Hiesinger

Date of Defense: **24.04.2023**

Table of Contents

Statutory Declaration

I herewith declare that I have composed the present thesis myself and without use of any other than the cited sources and aids. Sentences or parts of sentences quoted literally are marked as such; other references with regard to the statement and scope are indicated by full details of the publications concerned.

The thesis in the same or similar form has not been submitted to any examination body and has not been published. This thesis was not yet, even in part, used in another examination or as a course performance.

Anna Maria Oschmann-Kadenbach

Berlin, December 23, 2022

Acknowledgement

At first I want to thank my supervisor at the Freie Universität Berlin Prof. Dr. Peter Robin Hiesinger for his support and the correction of this thesis.

Special thanks go to Dr. Astrid Lewin who has been such an inspiration and guidance through all of my years in the mycobacterial research field. I'm more than grateful that you have taken your time to support and supervise me and to push me forward. Thank you very much!

Further gratitude goes to all of the great people of FG14 and FG16 at the RKI that have welcomed and put up with me. Well knowing that I cannot mention all and that I will probably do some of them wrong, I want to highlight Katharina Konrat, Elisabeth Kamal, Genna Sohl, Hubert Schäfer, Linus und Leonard for their noteworthy support.
Of course I also want to thank the bioinformatic guys from Torsten Semmler (NG1), the proteome people from Jörg Döllinger (ZBS6), the sequencers from Andrea Thürmer (MF2) and (last but surely never least!) Christoph Schaudinn (ZBS4) for every amazing minute I was able to spent with you in the microscopy catacombs and the astonishing insights you gave me in the hidden worlds of light and electron microscopy. Without you this work would be far less beautiful.

At last, my thanks go to my extraordinary parents, my family and friends, including those who are not with us anymore, and the most fabulous husband you can wish for when you have to finish a doctoral thesis.

Abstract

Background

The biofilm formation of nontuberculous mycobacteria (NTM) gained more and more attention in the past years. NTM biofilms were found in contaminated medical devices causing globel outbreaks and in the lung cavities of patients where they complicate treatment. These findings raised the attention on NTM biofilms.

Methods

In the present study, a porous glass bead (PGB) biofilm cultivation model was adjusted to *Mycobacterium abescessus* and *Mycobacterium chimaera*. The biofilms were cultivated in different media and the bacteria quantified using multiple experimental approaches (CFU, ATP and qPCR quantification). The biofilms were further analysed in structure and composition and their susceptibility towards disinfectants and antibiotics was tested. Further, the proteome and transcriptome expression profiles of two *M. chimaera* isolates were analysed to identify biofilm specific genes.

Results

All tested isolates formed surface attached biofilms, including rough *M. abscessus* isolates. Strong differences in the structures were found between the isolates also within one species and, in *M. abscessus*, even between different colony morphotypes of the same isolate. Moreover, it was found that the used medium had a fundamental influence on growth and structure of the cultivated biofilms, affecting for example the expression of a cording phenotype in smooth *M. abscessus* isolates.

In all cases the biofilms showed an enhanced biomass of extracellular matrix (ECM) components when compared to the corresponding suspension. Most impressively it was found that the biofilm of the outbreak strain ZUERICH-1 consists of an extremely enhanced amount of protein compared to the other *M. chimaera* isolates. The differences in the composition of the biofilms were less isolate specific in *M. abscessus* than in *M. chimaera*.

The proteome and the transcriptome analysis revealed the expression of biofilm specific genes (e.g. *glmM, glgX, pepN*) including genes of the type VII secretion systems.

Finally, it was found that that the biofilms provide enhanced tolerance to antibiotics and disinfectants with the exception of sodium hypochlorite. In this case, the suspension of all *M. chimaera* isolates were more tolerant than the corresponding biofilm. An interesting finding was, that the outbreak strain *M. chimaera* ZUERICH-1 presents an enhanced tolerance to peracetic acid (PAA) in comparison to the other isolates. It is important to mention, that commonly recommended concentrations of disinfectants were not able eradicate the biofilms of several isolates tested.

Conclusion

The PGB model is well suited for cultivation of different NTM biofilms and is highly applicable to various analysis methods. The biofilms of the tested species provide very different characteristics highly depending on the cultivation condititons. It was possible to identify biofilm specific genes, which could be a first step to define a basic NTM biofilm genotype.

Finally it was found that antimicrobials commonly used to inactivate NTM fail to eradicate or reduce the biofilms. It will be necessary to adjust the common laboratory methods to include NTM biofilms.

Zusammenfassung

Hintergrund

In den letzten Jahres rückte die Biofilmbildung von nichttuberkulösen Mykobakterien (NTM) immer mehr in den Fokus der Forschung. Biofilme wurden in kontaminierten medizinischen Geräten gefunden, durch die ein globaler nosokomialer Ausbruch ausgelöst wurde, sowie in den Lungencaveolen von Patienten, wodurch die Behandlung der Infektion deutlich erschwert wurde. Diese Fälle führten letztlich zu einem erhöhten Interesse an der Biofilmbildung von NTM.

Methoden

In der vorliegenden Studie wurde eine Kultivierungsmethode basierend auf der Nutzung von Porous Glass Beads (PGBs) verwendet, die auf *Mycobacterium abscessus* und *Mycobacterium chimaera* angepasst wurde. Die Biofilme wurden in verschiedenen Medien kultiviert und die Bakterien mit unterschiedlichen experimentellen Methoden quantifiziert (CFU, ATP und qPCR-Quantifizierung). Die Biofilme wurden anschließend in Hinsicht auf ihre Struktur, ihre Zusammensetzung und ihre Empfindlichkeit gegenüber Desinfektionsmitteln und Antibiotika untersucht. Weiterhin wurden die Expressionsprofile aus Proteome und Transcriptome zweier *M. chimaera* Isolate analysiert, um biofilmspezifische Gene zu identifizieren.

Ergebnisse

Alle getesteten Isolate bildeten adhärente Biofilme, inklusive der rauhen *M. abscessus* Isolate. Zwischen den Isolaten derselben Spezies wurden deutliche Unterschiede in der Biofilmstruktur festgestellt und in *M. abscessus* auch zwischen den unterschiedlichen Morphotypen des selben Isolates. Weiterhin konnte gezeigt werden, dass das Medium einen fundamentalen Einfluss auf das Wachstum und die Struktur der kultivierten Biofilme hat. Beispielsweise beeinflusste das Medium die Ausbildung eines 'Cording'-Phenotyps bei glatten *M. abscessus* Isolaten.

In allen Fällen zeigte sich, dass die Biofilme eine erhöhte Biomasse an extrazellulärer Matrix produzierten, wenn diese mit der zugehörigen Suspension verglichen wurden. Herausstechend war dabei die extrem erhöhte Proteinproduktion im Biofilm des Ausbruchsstammes ZUERICH-1 im Vergleich zu den anderen *M. chimaera*. Die Unterschiede der Zusammensetzung waren in den Biofilmen von *M. abscessus* weniger Isolat-spezifisch als in denen von *M. chimaera*.

Durch die Proteome- und Transcriptomeanalyse konnten mehrere biofilmspezifische Gene identifiziert werden (z.B. *glmM, glgX, pepN*), eingeschlossen gene des Typ 7 Sekretionssystems.

Abschließend konnte gezeigt werden, dass die Biofilmbildung zu einer erhöhten Toleranz gegenüber Antibiotika und Desinfektionsmitteln führt, allerdings mit Ausnahme von Natriumhypochlorit. Bei diesem zeigte sich, dass die Suspensionen aller *M. chimaera* Isolate deutlich toleranter waren, als die zugehörigen Biofilme. Interessant war, dass der Ausbruchsstamm *M. chimaera* ZUERICH-1 im Vergleich zu den anderen Isolaten, eine erhöhte Toleranz gegenüber Peressigsäure (PAA) zeigte. Wichtig ist, dass keine der empfohlenen Desinfektionsmittelkonzentrationen ausreichend war um die Biofilme verschiedener Isolate vollständig abzutöten.

Fazit

Das PGB Modell eignet sich sehr gut für die Kultivierung von NTM-Biofilmen und ist darüber hinaus gut an verschiedene weitere Analysemethoden anpassbar. Die Biofilme der getesteten Spezies zeigten sehr unterschiedliche Eigenschaften basierend auf den Kultivierungsumständen. Es war möglich

mehrere biofilmspezifische Gene zu identifizieren, die dabei helfen können einen grundlegenden NTM-Biofilm Genotyp zu definieren.
Final wurde festgestellt, dass üblicherweise für NTM verwendete antimikrobielle Substanzen nicht in der Lage sind die Biofilme abzutöten oder zu reduzieren. Langfristig wird es daher notwendig sein die gängigen Labormethoden auf die Nutzung von NTM-Biofilmen anzupassen.

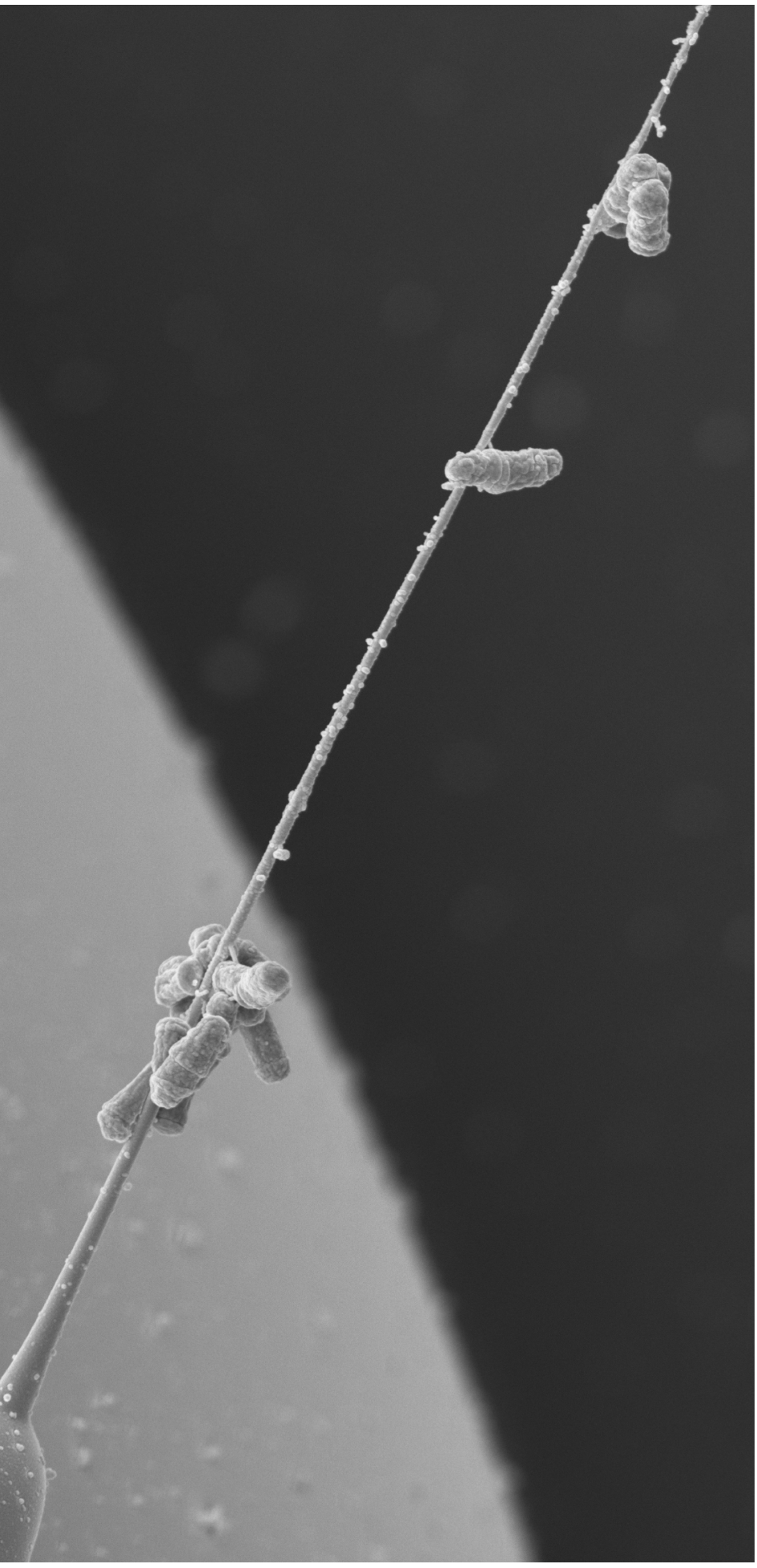

Chapter 1

Introduction

1.1 Nontuberculous Mycobacteria (NTM)

Today, the genus *Mycobacterium* comprises over 200 species[1]. In the past decades, a broad range of new mycobacterial species was described, mainly promoted by the improvement of sequencing techniques and corresponding evaluation methods [1].
Mycobacteria are often sorted into groups, while the commonest way is to differentiate between species that belong to the *Mycobacterium tuberculosis*-complex (MTC) and the so-called nontuberculous mycobacteria (NTM) or mycobacteria other than tuberculosis (MOTT). Due to their special characteristics, *Mycobacterium leprae* and *Mycobacterium lepromatosis* are grouped separately.
As implied by the name, the MTC contains *Mycobacterium tuberculosis* (MTB) and closely related pathogenic mycobacteria, like *Mycobacterium bovis* or *Mycobacterium africanum*. Its undeniable importance as 'the world's top infectious killer' [2] makes MTB the most well known and most intensively studied representative of the genus *Mycobacterium*.
The major part of mycobacteria, though, belongs to the NTM, including almost 200 species. These are further categorized in slow and rapid growing species, depending on their individual time to grow as visible colony on agar or in liquid media. Slow growing mycobacteria (SGM) representatives usually take at least seven days, while rapid growing mycobacteria (RGM) form colonies within two to seven days; species of the *Mycobacterium terrae*-complex have been categorized as intermediate [2]. The slow growth rate of mycobacteria enables adaptation to stress, such as anitmicrobial agents, before cells are killed [3]. It is supposed that rapid growers are the more ancestral group, from which the slow growing species have evolved [4].
The research on the mycobacterial taxonomy led to the proposal to split up the mycobacteria to multiple genera [5, 6]. Especially species of the NTM were classified in four new genera, namely *Mycobacteroides*, *Mycolicibacter*, *Mycolicibacterium* and *Mycolicibacillus*. This was highly criticised as it causes a bunch of complications and confusions in particular in the clinical field [7]. Congruent with the proposal of well-known representatives of the mycobacterial research field to ignore the renaming of the genera [7], this work will also refer to all species as *Mycobacterium*.

1.1.1 Clinical Relevance

About 140 NTM species are opportunistic pathogens that are of special clinical interest [8]. While representatives of the MTC cause tuberculosis and are classified as pathogenic to humans, the diversity of NTM species results in variable clinical presentations. Still, the commonest is NTM pulmonary disease (NTM-PD), which is similar to tuberculosis. Besides this, NTM can cause severe skin or cuticular lesions, lymphatic infections and other disseminated infections [9]. The most important risk factor for NTM-PD is the susceptibility of the host. Often, immunocompromised individuals suffering from pulmonary disease such as cystic fibrosis (CF), display an increased prevalence of NTM infection [10]. NTM-PD shows a high mortatily rate of over 25% [11]. Patients infected with the rapid growing species *Mycobacterium abscessus* present a cure rate ranging between 25 - 58 % [12, 13, 14] and patients with a *Mycobacterium avium*-complex (MAC) pulmonary disease (MAC-PD) display a relapse rate of reinfection around 4 - 12 % [15, 16, 17] showing the need for better and more sufficient treatment and susceptibility evaluation.

[1] List of Prokaryotic names with Standing in Nomenclature - Genus *Mycobacterium*
`www.dsmz.de` - last checked January 11, 2023
[2] World Health Organisation - Tuberculosis
`www.who.int` - last checked January 11, 2023

The identification of NTM infections is often done by repeated isolation, cultivation and acid-fast bacteria (AFB) staining (e.g. Ziehl-Neelson) as well as the idenfication via automated commercial tests. Thereby the first approach is to distingiush between NTM or MTB infection [18]. Further the species can be identifed by polymerase chain reaction (PCR), sequencing or MALDI-TOF [8]. Meanwhile, these techniques allow a very specific identification of the species or subspecies which is a prerequisite to adjust and optimise medical treatment. The detailed genetic identification of the infecting NTM strain has moreover gained importance in non-treatable patients. In a few cases of non-treatable patients suffering from severe NTM-PD, treatment of these patients using phages was successfully completed [19]. In such cases the concrete genetic identification of the infection strain is fundamental to enable accurate treatment using phages.

1.1.1.1 Epidemiology and Distribution

NTM are ubiquitous bacteria and are regularly isolated from environmental specimens, such as soil or water. This indicates that the common infection route disperses from environmental sources [21, 22]. Especially MAC and other NTM species like *Mycobacterium gordonae* are regularly isolated from water pipes or taps [23].

Within the NTM, the global predominant species belong to the MAC, representing approximately 50 % of all species isolated from pulmonary specimens (see figure 1.1.1) [20, 24]. Only few laboratories distinguish the infection by MAC to individual species like e.g. *Mycobacterium chimaera*.

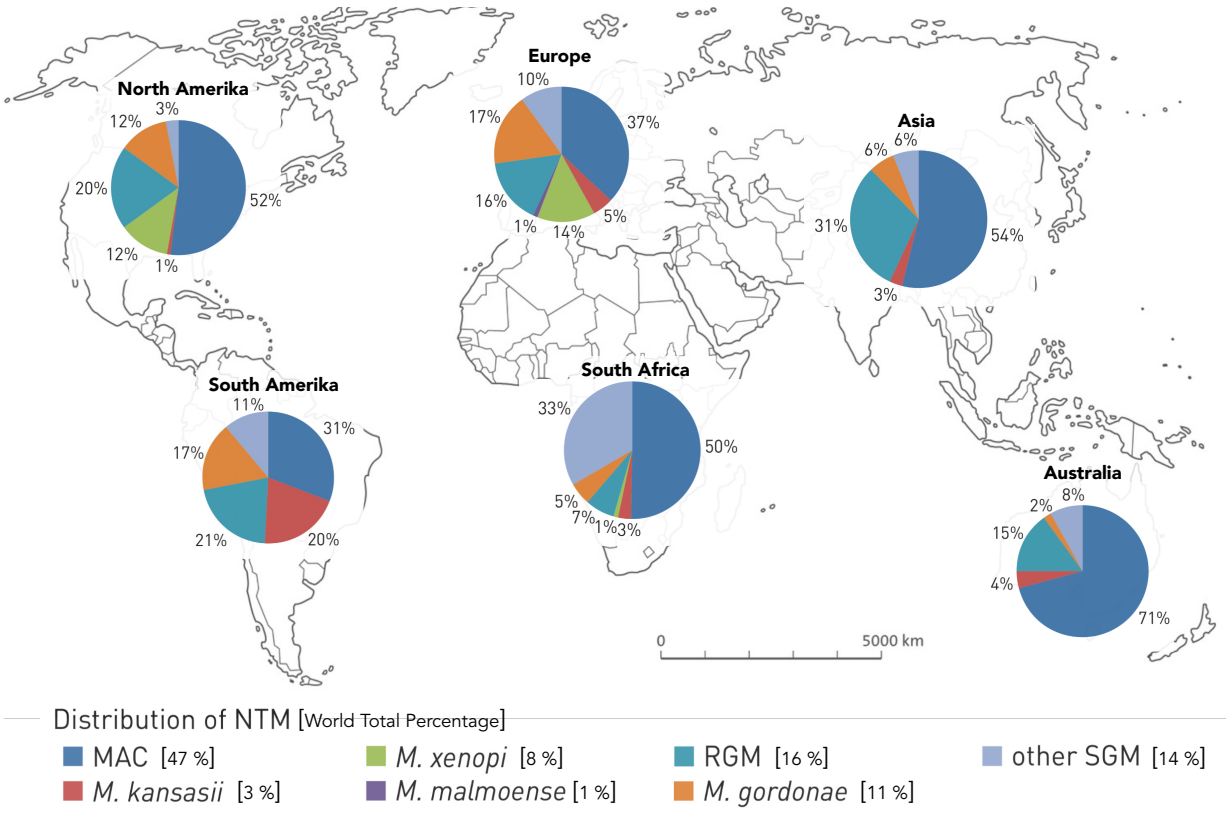

Figure 1.1.1: Geographic diversity of NTM [2013]

Diagramms and data adopted and adjusted from [20]. Presented is the world wide percentual distribution of relevant NTM species isolated from specimens. Pie charts display the distribution within the specific continental region.
MAC - *Mycobacterium avium* Complex; RGM - rapid growing mycobacteria; SGM - slow growing mycobacteria

Among rapid growing mycobacteria *M. abscessus* is the most frequently isolated species [20, 25]. RGM are especially predominant in East Asia were they can display over 50 % of all isolated NTM species [26, 27]. In a recent publication from He et al. (2022) focussing on southern coastal areas of China, *M. abscessus* was found to be the major identified NTM species (approx. 41 %) followed by MAC species (approx. 29 %) (Preprint [28]) displaying how distribution patterns can vary on regional levels.

The incidence of mycobacterial infection, especially NTM-PD, raised in past decades [29, 30, 31, 32]. Depending on the global location, the incidence of NTM-PD is ranging between 0.2 - 9.8/100,000 people [33, 34]. Thereby the infection with NTM displays an alarming growth rate [35, 36]. The incidence of pulmonary NTM infections in England and Ireland for example raised from about 5.6/100,00 cases in 2007 to a total of 7.6/100,000 in 2012 [37].
While the annual prevalence of MTB infection in Canada decreased, the incidence of NTM disease displays the contrary trend [33]. A similar increase of NTM infection was reported in multiple countries and regions world wide. Especially in third world countries, NTM infections are, due to insufficient diagnostic methods and the similar clinical presentation, misidentified as multi-drug resistant MTB [38, 39, 40]. As a result, NTM infected patients are treated with inappropriate antibiotics as NTM are often resistant to common MTB drugs [36]. Another factor supporting the presumable high underestimation of infection counts is the fact that NTM-PD is not a notifiable disease [25, 41]. Therefore, sufficient and accurate global data collection is not possible. It can be assumed that the true numbers of NTM-PD are much higher, presenting how important it is, to increase research on these organisms.

1.1.2 Treatment

At the moment only few drugs show bactericidal activity against MAC or *M. abscessus* [36]. Treatment often fails due to different outcomes of clinical susceptibility testing results and the 'real' outcome in patient treatment [42, 43]. Susceptibility testing of mycobacteria is usually done in micro-dilution procedures. However, the outcome of these susceptibility testings is not reflected in the treatment outcome [43]. Since several mycobacteria including *M. abscessus* have been found to also form biofilms in the cavities of the patients lung, the need for adjusted susceptibility testing methods gets obvious [44].

MAC is commonly treated with a general macrolide-based multidrug regimen, while *M. abscessus* treatment includes a combination of macrolides combined with parental antibiotics (e.g. aminoglycoside + cefoxitin, imipenem or tigecycline) given over a time period usually ranging between 18 - 24 month [12, 15, 36]. Tigecycline is the only newly discovered antibiotic specifically focussing on the treatment of NTM infection [36, 45]. Due to the limitation of NTM specific drugs, newly established MTB antibiotics are also tested for NTM. One of the most hopeful substances is bedaquiline (also referred to as TMC207), which was established to enable treatment of patients infected with extensively drug resistant tuberculosis (XDR TB). In case of NTM, bedaquiline does not display bactericidal activity but triggers bacteriostatic behaviour of *M. avium* in mouse model [46, 47]. As bacteriostatic conditions are often shifting bacteria to a dormancy state, which reduces the efficiency of common antibiotics that specifically attack metabolic processes during growth, the use of bedaquiline against NTM could exacerbate the infection. Moreover, it was shown that *Mycobacterium intracellulare* is aquiring resistance shortly after bedaquiline treatment [48]. This underlies the need for appropriate susceptibility testing of NTM to improve treatment and improve antibiotic stewardship [36].

1.1.3 Disinfection procedures

As NTM are widely distributed in the human environment they also appear in unwanted surroundings such as footbaths, tattoo ink or medical devices [49, 50]. The association of NTM infection in the healthcare environment is to be rated as a major problem [51]. Since waterborne healthcare-associated infections with NTM are a rising and underestimated problematic [52, 53, 54], the screening of qualified eradication mechanisms is necessary.

Disinfection procedures for water-based environments often include chlorine or chloramine based disinfection which usually enable efficient eradication of the microflora. In the US, drinking water systems are commonly treated with low levels of chlorine[3]. Disinfection at such low levels is currently harmless for humans but is also ineffective against NTM colonisation of water pipes and moreover leads to positive selection of these bacteria in such environments why NTM are usually declared as to be resistant towards chlorine [23, 55, 56, 57].
Depending on the disinfection procedure (e.g. instrument or surface disinfection) different agents are of common use. For disinfection of medical instruments a disinfection using 2 % of glutaraldehyde (GA) for a time period ranging between 60 minutes and several hours, is commonly recommended[4].
In case of the disinfection protocols of the water reserviors of medical devices such as heater-cooler units (HCUs) or extracorporal membrane oxigenation (ECMO), disinfectants containing peracetic acid (PAA) or sodium hypochlorite [free active chlorine (FAC)] are recommended. Due to the corrosive properties of PAA, disinfectants containing this agent can only be used in low concentrations for short time periods in devices made of metal. For example for HCUs, the recommended disinfection protocol using PAA as working agent currently prescribes a concentration of about 0.1 % for an exposure time of 10 minutes[5]. Since NTM biofilms have been found in such machines, although regular disinfection was performed, it can be assumed that these recommendations are not suitable to prevent outbreaks by NTM in the clinical environment.

[3] US Department of Health - Drinking Water Protection
`www.health.state.mn.us` - last checked January 11, 2023

[4] Robert Koch - Institute, Liste der geprüften Desinfektionsmittel und -verfahren
`www.rki.de` - last checked January 11, 2023

[5] LivaNova Operating instructions Heater Cooler T3; Version 02/2020
`www.livanovamediaprod.` - last checked January 11, 2023

1.1.4 General Characteristics of NTM

The genetic inter- and intraspecies diversity among NTM is comparatively huge and complicates to generalize phenotypic characteristics [58]. Though, certain characteristics are present in all mycobacteria, including the rod-like shape, a very thick hydrophobic cell wall and a high genomic GC-content ranging around 65 %. NTM are environmental opportunistic pathogens that have settled in a wide range of different environmental niches, such as water, soil, wood or even amoeba [23, 59]. In the immediate surrounding of human beings, NTM most often appear in the pipes and water supplies of bathrooms, such as in shower heads or taps but also in the medical environment where they can cause severe global outbreaks [56, 60]. For most people, these neighbours are of no danger, while especially for immunocompromised this cohabitation can have problematic consequences, such as for example severe lung infection similar to tuberculosis [21].

1.1.5 The Cell Envelope

Mycobacteria belong to the phylum of *Actinobacteria* in the order of *Corynebacteriales*. Thereby they share their special construction of the cell envelope with other genera in this order. As the cell envelope displays in the figurative sense the face of the bacteria, its structure and composition are of great importance for the primary interaction with the host and the environment [61]. In general, the cell envelope is built in multiple layers (figure 1.1.3) starting from the inside with the cytoplasmic membrane, followed by the cell wall and surface lipids (approx. 40 nm) which majorly contribute to virulence and host interaction [61].

The mycobacterial cell wall is an important factor that contributes fundamentaly to the success of these bacteria during the infection process. The waxy character of the cell envelope is due to its composition of multiple long chain fatty acids, the mycolic acids (MA), resulting in an extreme hydrophobic barrier [63, 64]. This allows mycobacteria naturally to withstand a wide range of antimicrobial agents such as antibiotics or disinfectants especially those that are of hydrophilic structure [65].

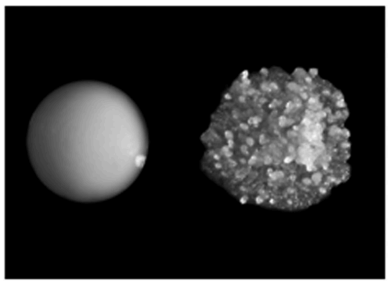

Figure 1.1.2: Smooth and Rough colony morphology of *M. abscessus*

Figure adopted from [62]. Presented is a macrophotography of both distinct colony morphotypes of *M. abscessus* - smooth (left) and rough (right).

The cell wall of mycobacteria is constructed of two inner layers, a peptidoglycan and an arabinogalactan layer. The peptidoglycan layer contributes to the stability of the cell and maintains the osmotic balance [66]. It is constructed of short peptides and glycan strands linked to variable amino acids. The arabinogalactan layer is composed of highly branched arabinose and galactose [67]. The arabinogalactan is further covalently linked to a layer of MA which compose the so-called inner leaflet. MAs are long-chain fatty acids which exclusively appear in representatives of the *Corynebacteriales*. In the mycobacterial cell envelope, they majorly contribute to its waxy and hydrophobic characteristics [61, 64, 68, 69].

The inner leaflet is surrounded by the highly heterogeneous outer leaflet, a layer composed of surface lipids, lipoglycan and proteins. The composition of this layer is species-specific as it contains a broad range of different adaptable molecules [e.g. glycopeptidolipids (GPL) or phenolic glycolipids (PGL; only present in SGM)] [64]. It also contains trehalose monomycolate (TMM) and trehalose dimycolate (TDM), latter also known as 'cord-factor', which are molecules produced by esterification of trehalose with mycolic acids [69].

The presence or absence of certain lipids in the mycobacterial cell envelope relates in different species to the development of multiple morphological presentations such as the colony structure or color [70]. The lipid diversity can also result in smooth and rough colony morphotypes (figure 1.1.2) that besides their appearance, often also gain other properties, such as an enhanced antimicrobial resistance [62, 64, 71]. This morphological change does not appaer in all mycobacteria, but e.g. *Mycobacterium kansasii*, *M. abscessus*, *M. gordonae* and *M. avium* have been reported to display these different morphotypes [72].

1.1.5.1 Glycopeptidolipids (GPL)

The outer surface of many NTM contains glycopeptidolipids (GPL), which can either occur as di- (apolar) or triglycosylated (polar) GPL. They are very heterogeneous in structure and properties, as they can vary in length of the lipid chain and/or in the hydroxylation/*0*-methylation status of the monosaccharides [73]. These different types of GPL are displayed in different species of NTM. The species of the MAC produce highly antigenic serovar-specific GPL (ssGPL) while each individual strain of *M. avium* for example is only expressing one type of ssGPL [72].
In *M. abscessus*, so-called nonserovar-specific GPL are produced besides polar GPLs. The latter contributes to the varying properties of the cell envelopes of the different NTM species.
GPL are a major surface component of MAC species where they influence the production of pro- and anti-inflammatory cytokines and control the process of phagosome-lysosome fusion [72] playing a large role in the pathogenesis and virulence during infection and host interaction. They induce the production of interferon γ and TNFα, thereby triggering the immune response of the host [74].
It was further shown that the absence of GPL on the MAC cell surface results in the loss of the ability to form biofilm [75, 76, 77], which is directly linked to virulence of MAC [78].
The absence or presence of GPL in the cell envelope of NTM also contributes to the colony morphotype of the isolate. In multiple species the lack of GPL on the cell surface resulted in the phenotypic presentation of rough colony morphotypes (figure 1.1.2). Especially in *M. abscessus* this phenotypical shape shifting is of great importance and is therefore intensively studied [73, 76, 77, 79]. The phe-

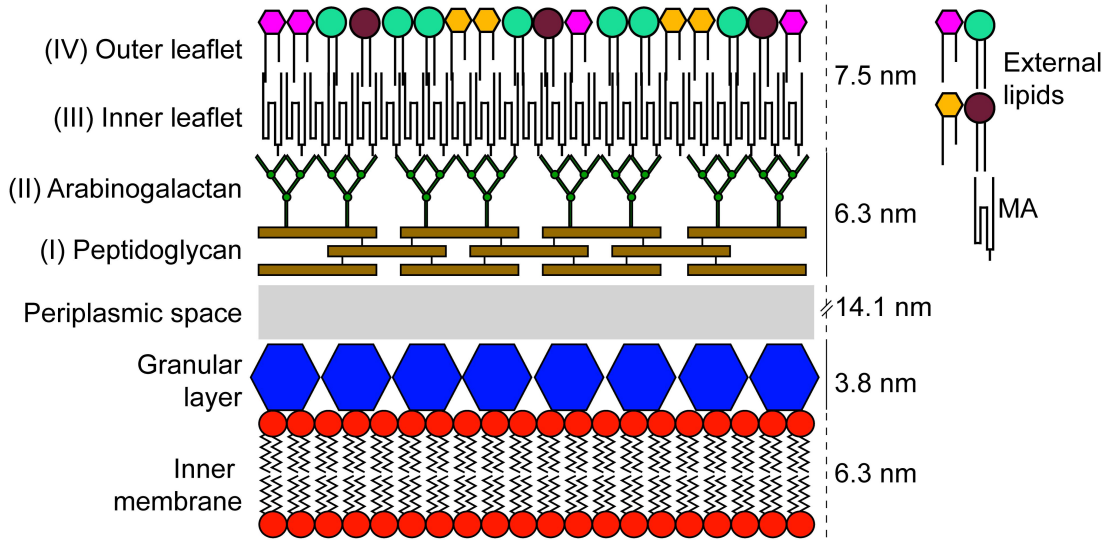

Figure 1.1.3: Mycobacterial Cell envelope structure

Figure adopted from [64]. The mycobacterial cell envelope is composed of multiple layers, while especially the outer layers largely contain lipids and hydrophobic molecules supporting the waxy nature of mycobacterial cells. Especially the external lipids contribute to the bacterial shape, surface and color. MA - mycolic acids

notypical change from smooth to rough is in most cases non-reversible as it is caused by mutation [e.g. single nucleotide polymorphism (SNP)] in genes of the so-called GPL-cluster or GPL-locus [79]. Depending on the species, the according genes in the GPL-locus vary, though the overall GPL-locus remains similar and the structure itself is highly conserved in mycobacteria [73, 80, 81]. The included genes are not exclusively responsible for GPL synthesis but majorly contribute to it.

1.1.5.2 Cord Factor

One of the most interesting characteristic of mycobacteria is the so-called cording phenotype of MTB which was described in 1884 by Robert Koch himself while analysing the special characteristics of the tuberculosis disease [83].
Actually 'cord factor' is another name for the glycolipid molecule trehalose dimycolate (TDM) which is a lipid found on the cell envelope of MTB [84]. It is synthesized by the esterification of trehalose with mycolic acids and is therefore limited to bacterial species that harbour these lipids. When expressed, TDM enables the formation of a specific phenotype in which the bacteria start to align in cords (figure 1.1.4).

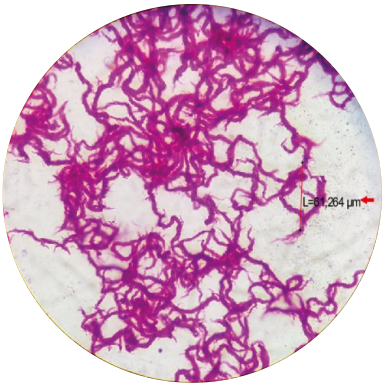

Figure 1.1.4: Cord factor formation of *M. tuberculosis*
Figure adopted and adjusted from [82]. MTB was stained with Ziehl-Neelsen.

This special formation of bacteria was used in specimen samples to identify and diagnose MTC infection [85, 86]. However, the cord factor formation was meanwhile also described in multiple NTM species including opportunistic pathogenic species e.g. *Mycobacterium marinum*, *M. abscessus* or *M. avium* [87, 88, 89, 90].
The cording of MTB is related to virulence behaviour, commonly recognised as a phenotype developed during infection. TDM is reported to inhibit phagosome-lysosome fusion, induce cytokine secretion and was identified as a key driver of secondary and cavitary disease type of tuberculosis [91].

1.1.6 *Mycobacterium abscessus*

M. abscessus is one of the widest distributed multi-drug resistant mycobacterial species [33]. It is usually differentiated in three subspecies *M. abscessus* sups. *abscessus*, *M. abscessus* sups. *bolletii* and *M. abscessus* sups. *massiliense*. The species is one of the most dangerous NTM, causing severe, often untreatable infections. *M. abscessus* is not only causing pulmonary infection but is also a prominent NTM species causing skin infections. They have caused several outbreaks in the medical and cosmetic environment [50, 92, 93]. Though *M. abscessus* is also an environmental species, direct transmission between patients was meanwhile documented [94]. The severity of an infection with *M. abscessus* is presumably supported by the biofilm formation within the cavities of the patients lung [95]. Thereby the biofilm formation of *M. abscessus* and other species in CF-patients impede the effects of the antibiotic treatment and are the most likely reason why the results of laboratory susceptibility testing and treatment success are often not consistent [43].

One of the most prominent characteristics of *M. abscessus* is the shape shifting of the two morphotypes smooth and rough which causes a variety of changes in the virulence and susceptibility of each phenotypic variant. Smooth strains appear in a round, even colony shape while rough on the opposite display a ragged, hilly form (figure 1.1.2). The rough morphotypes present other physical properties,

resulting in an enhanced hydrophobicity and repellent interface [73]. The loss of GPL, which causes the rough colony morphology, results in an extreme aggregation or clumping of rough *M. abscessus* isolates [77].
The morphotypes of *M. abscessus* show certain virulence strategies. While rough isolates have been shown to replicate intracellularly in macrophages resulting in cell lysis, smooth strains persist and/or decline during intracellular growth [77]. Moreover, the polar GPL of smooth *M. abscessus* isolates were shown to interact with mitochondrial cyclophilin D, resulting in an inhibition of apoptosis. In contrast, rough variants induce apoptosis in phagelysosomes [96]. It was shown that the shift from smooth to rough morphotype is occurring or induced during long term infection. Studies have displayed that from the start of the infection with a smooth *M. abscessus* variant, the infectious isolates from patient sputum change over time to rough morphotypes [97, 98, 99]. This underlies the assumption that the phenotypical shift is related to the adaptation to the infection status. Wiersma et al (2020) showed that the cell surface of *M. abscessus* is actively remodeled when the environmental conditions are adjusted to conditions similar to what is present during infection [100] .
The morphological shift of *M. abscessus* is assumed to result in an enhanced tolerance towards certain antimicrobials. Still, in most cases it is unclear whether this effect is directly linked to the absence of GPL and thereby the chemical change of the cell surface or the enhanced aggregation of the rough *M. abscessus* isolates. The clumping of the bacteria simply physically hinders antimicrobials to reach bacteria inside the aggregates while the enhanced hydrophobicity of the cell surface displays a chemical barrier against certain antibiotics. The differentiation is tricky but finally does not override the fact that rough variants present a reduced susceptibility towards antimicrobial agents when compared to smooth counterparts [97, 101].
The severity of the *M. abscessus* infection and the ability to shift from a certain phenotype to another display highly problematic topics for the clinical environment [33]. Not just that rough *M. abscessus* isolates seem to be more virulent, they are moreover not easy to cultivate and to work with. Since *M. abscessus* is generally hard to treat with high failure rates, the intensive testing of the susceptibility of this species is of high clinical interest. Because *M. abscessus* was found to form biofilms in the lung cavities of patients [95], it is of high research interest to establish a reliable biofilm model for susceptibility testing for routine use.

1.1.7 *Mycobacterium chimaera*

The species of *Mycobacterium chimaera* was first described in 2004 as a close relative of *Mycobacterium intracellulare* [102]. In previous publications, *M. chimaera* was often identified as *M. intracellulare* and the DSMZ German Collection of Microorganisms actually refers to it as *Mycobacterium intracellulare* subspecies *chimaera*[6]. Both are closely related to *M. avium*, belonging to the so called *Mycobacterium avium*-complex (MAC) [102]. The MAC species are slow growing, environmental mycobacteria that are distributed world wide and are often isolated from plumbing facilities such as shower heads and tap water [103]. This preference for water based environments presumably also promoted an ongoing global outbreak of *M. chimaera* that started in 2013 which was lately categorised as the most influential NTM outbreak in the past years [104].

[6] DSMZ German Collection of Microorganisms - *Mycobacterium chimaera* ZUERICH-1
`www.dsmz.de` - last checked January 11, 2023

At the production site, medical devices - so-called heater-cooler units (HCUs) were contaminated with *M. chimaera*. During open-chest or cardiopulmonary bypass surgery, HCUs are used to keep the patients' blood at a specific temperature level. Thereby the open ventilation led to the spread of *M. chimaera* from the contaminated water cooling circuit via bio-aerosols into the operating room. That led to the contamination of surfaces, surgical sites and/or prosthetic materials [105, 106, 107]. This finally resulted in disseminated infections which are characterised by a long latency of several months to years and unspecific symptoms. As a consequence, the number of cases was underestimated [107]. As of 2018, a global total of meanwhile > 150 patients has been linked to the outbreak with a fatality rate of approximately 50 % [104].

Figure 1.1.5: Biofilm in HCUs
Figure adopted from [108]. Displayed is the biofilm formation within the water tanks and circuits of HCUs.

The correlation of the globally distributed *M. chimaera* infections was identified by an international team of researchers and institutes that were able to follow-up the route of infection to the production site of the HCUs by whole genome sequencing and phylogenetic analysis [109]. The globally accumulated bacterial isolates from contaminated HCUs were sequenced and compared on a genome level to samples taken from the production site of a specific HCU manufacturer. As a result, the isolate ZUERICH-1 was identified to be globally present in samples of patients as well as to be closely related to the isolate collected at the production site.

Usually, medical devices like HCUs and similar machines like ECMOs (extracorporal membrane oxigenation) underlie strict disinfection and cleaning procedures. At the beginning of the *M. chimaera* outbreak, the recommendation for the responsible heater-cooler units T3 from Sorin inlcuded a 14 day cycle disinfection of the internal tanks and tubes for 10 min with either $\sim$ 0.1 % sodium hypochlorite or $\sim$ 0.045 % peracetic acid[7]. Since the outbreak carried on, the recommendation of the manufacturers were modified several times. Meanwhile, a disinfection routine of a 14 day cycle using either $\sim$ 0.1 % sodium hypochlorite or $\sim$ 0.1 % peracetic acid based disinfectants for an incubation time of 10 minutes is recommended[8]. These adaptations focussed on peracetic acids but did not improve the recommendations for sodium hypochlorite. A potential reason could be, that higher concentrations of sodium hypochlorite interfere with the machines internal materials and can therefore not be recommended.
In the meantime other methods were developed that resulted in the sealing of the ventilation system or the rerouting of the HCU in a separate room beside the operating hall. Updated disinfection procedures as well as intensive cleaning and the replacement of contaminated tubes still could not prevent reemergence of the bacteria [110].

[7] Heater-cooler system 3T operating instructions. Version 09/2015. Sorin Group/LivaNova `livanova.com/Sorin_T3_HCU` - last checked January 11, 2023
[8] Heater-cooler system 3T operating instructions. Version 02/2020. LivaNova `livanova.com/T3/productsite` - last checked January 11, 2023

1.2 Mycobacterial Biofilms

Biofilms have been defined as communities of microorganisms, that attach to a surface and/or each other and embed themselves in an extracellular matrix [111, 112, 113]. Further, the biofilm phenotype is linked to specific genetic expression profiles that distinguish this lifestyle from the planktonic lifestyle [111, 112]. In some species the biofilm specific expression profiles are already described and certain biofilm relevant genes have been identified [111, 113]. In mycobacteria, though, is the knowledge rather small.
Biofilms are usually formed in so-called interphases between two different physical states: air-solid, solid-liquid and air-liquid [113, 114]. Especially air-liquid interphase biofilms are well-known since they often appear as a sort of side-effect during the planktonic cultivation of bacteria in broth. In the laboratory environment mycobacterial biofilms are often cultivated as floating air-liquid interface pellicle biofilms, still this form of biofilm cultivation has major limitations for further experimental protocols [115, 116].
The genetic profile of NTM biofilms is not yet extensively described. Due to the strong genetic diversity in mycobacteria it is quite unlikely to find or describe a general 'biofilm'-expression pattern. In a few mycobacterial species, including *M. smegmatis* and *M. tuberculosis*, genes relevant for biofilm formation were described but were not further analysed in NTM biofilms yet [113, 115].
Among these, genes encoding for membrane transporter proteins which are involved in the synthesis of the mycobacterial cell envelope have been found to influence the ability of mycobacteria to form biofilms. The mycolic-acid transporter MmpL11 for example, contributes majorly to biofilm formation in *M. smegmatis* and *M. tuberculosis* [117, 118]. Mutants lacking MmpL11 function displayed lower levels of mycolic acids on the cell surface and altered biofilm formation. Another prominent gene that found to be involved in mycobacterial biofilm formation was the gene *groEL1*. Mutants of *M. smegmatis* lacking a functioning *groEL1* gene display reduced biofilm formation and maturation [119]. Another factor that was linked to mycobacterial biofilm formation was the type VII secretion system (T7SS). Secretion systems are present in a broad range of organisms. In mycobacteria, 5 T7SSs were identified meanwhile (ESX 1 - 5). Though the ESX-systems have different functions, they often interact. They have been linked to communication processes and horizontal gene transfer in mycobacteria. These functions are commonly displayed in biofilms [120].

1.2.1 Biofilm Properties and Functions

As biofilms often contain several microbial species, the description of 'general' characteristics is rather difficult. Though, all biofilms display certain properties and functions.
At first, the formation of biofilms is following a distinct lifecycle (figure 1.2.1) [112, 114]. Thereby the attachment or adhesion to a biotic or abiotic surface is the initial step for biofilm accumulation. Afterwards the according microorganism starts to replicate within a colony attached to the surface. In this step, an extracellular matrix (ECM) is produced which covers and protects the bacteria. During the following growth the biofilm is maturating, thereby more and more microorganisms are accumulating within the structure and often the composition of the ECM changes as a reaction to the changing conditions in the biofilm [112, 114]. While maturation and stagnation precede, the microorganisms also leave and disperse from the biofilm (either actively or by external pressure).

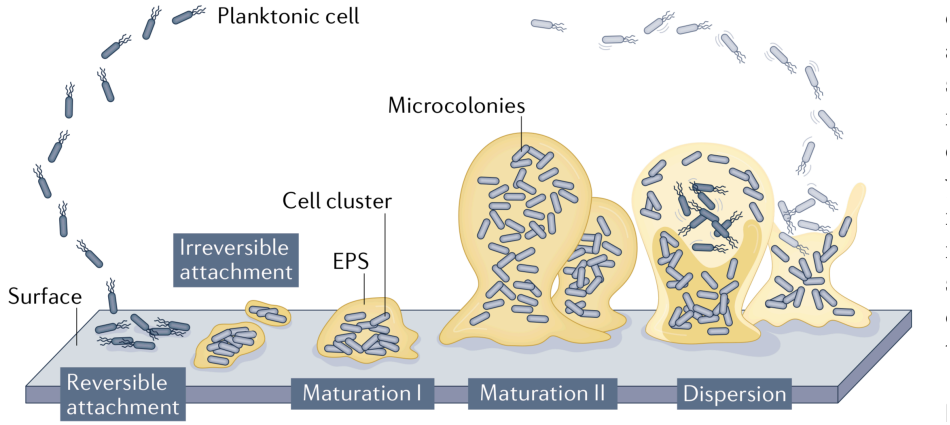

Figure 1.2.1: Biofilm lifecycle
Figure was adopted from [114].
The biofilm formation follows a distinct lifecycle starting by the irreversible attachment to a surface followed by growth and maturation of the biofilm resulting in final dispersion of single cells from the community. During maturation an extracellular polymeric substance (EPS) or extracellular matrix (ECM) is produced which mainly is meant to provide protection for the bacteria in the biofilm. The composition of the ECM changes over time. When nutrient levels are to low and/or the biofilm community faces external pressures (e.g. antimicrobials) the bacteria disperse from the colony.

1.2.2 Adhesion

The adhesion to a surface belongs to the main characteristics of biofilms [111]. Still, biofilms can also form without distinct attachment to a unnatural surface. A prominent and common example is the formation of biofilms at air-liquid interphases. These floating biofilms are not necessarily attached to a surface but the microorganisms in the structure attach to each other [113].
The surface adhesion of bacteria is a critical point for biofilm formation. Therefore some species have evolved different strategies to enable the attachment. While in general extracellular DNA (eDNA) and certain protein structures are linked to the surface attachment processes in biofilm formation, some bacteria show the expression of specific genes that are directly linked to surface attachment [112, 113, 121]. In *Escherichia coli* for example the production of the curli protein structure is majorly involved in surface attachment [121]. Also other amyloid fibril structures are found to be important for the adhesion to abiotic and biotic substrates [122].

1.2.3 Structure

The variability in biofilms structures is majorly depending on the composition of the microorganisms within and the surrounding extracellular matrix ECM [114].
Commonly, biofilms are formed in multilayered structures, though, especially in the beginning of biofilm formation, a mono-layered distribution of bacteria can appear. One of the most prominent biofilm structures documented is the mushroom-like biofilm of *Pseudomonas aeruginosa*, which is resulting from the active migration of bacteria in order to form a biofilm structure that provides optimal conditions for nutritent and oxygen supply [123]. The biofilms are linked to the surface with a smaller part of bacteria and form on top a mushroom-like cap.
The structure of biofilms is mainly depending on the environmental circumstances. Environments in which high external pressures and shear forces are common, the abrasion of bacteria from the biofilm leads to smooth biofilm surfaces with high bacterial density [124]. Still, in most natural environments, multi-layered biofilms are the predominant structure. Especially bacteria in the inner parts of the biofilm are often thickly packed in ECM and other bacteria. This leads to reduced nutrient and oxygen availability. In order to prevent such stresses, biofilms are found to form cavities and

tunnels that enable the passage of medium and nutrients also to inner biofilm areas [112]. Moreover, the microorganisms have established nano-tubular structures, so-called nanowires, that are involved in oxygen transport, metabolic cross-feeding and communication between bacteria [113, 125, 126].

1.2.4 Extracellular Matrix (ECM)

Such as the biofilm structure, the composition of the extracellular matrix (ECM) shows an enormous amount of variation which is depending on the combination of microorganisms in the biofilm and the environmental circumstances [127].
During the first steps of biofilm formation, the ECM is majorly composed of substances that usually contribute to the adhesion of the bacteria. With time, the composition in the ECM changes, including also components of dead bacteria. In general, the ECM is composed of different molecules, namely exopolysaccharides, proteins, eDNA and lipids but the most abundant substance is water [128].
In the pellicle-biofilms of NTM, eDNA and mycolic acids were found to display major components of the ECM [129]. In more recent studies, cellulose was identified as a component of the mycobacterial ECM in surface attached biofilms [130, 131]. It was also found, that a range of various lipids in mycobacteria play an important role in subtrate attachment [116].
The ECM fulfils a range of different functions. It contributes majorly to the adhesion, the structure and is giving stability. It acts as a nutrient supply on the one hand and as a protection on the other [127, 128]. During the maturation of the biofilm, the ECM grows thicker and less permeable for nutrients or antimicrobial substances. As a result, a gradient of nutrient and oxygen levels occurs. The bacteria in the biofilm adapt to these gradients. The inner parts of the biofilm provide anaerobic and starvation stresses forcing the bacteria to either die or change to dormant or persisting metabolic growth stages [128]. Genes related to these stresses are often found in proteome or transcriptome analysis.

1.2.5 Communication and Nanowires

Microorganisms display inter- and intra-species communication among the members of the biofilm community [112, 113]. These communication processes are fundamental for the development and survival of the biofilm. The biofilm communication relies on different mechanisms which can either be based on chemical distribution or electrical signalling [113, 132]. The quorum sensing of biofilms is based on incorporation and distribution of chemicals. Using specific molecules for signal transduction, microorganisms in a biofilm react to environmental stresses such as antimicrobial substances. In *P. aeruginosa* for example, quorum sensing mediates the expression of catalase and superoxide dismutase genes in order to control the susceptibility to hydrogen peroxide [133].
Nanotubular structures called nanowires are build between bacteria and used for the sharing of nutrients, oxygen and also genetic information (e.g. plasmids) [113, 126]. It was shown that conjugation is enhanced in biofilms when compared to planktonic cells [134] which is presumably favoured by the formation of nanowires. Nanowires are also important for signalling processes in the biofilm that is based on the electron transport among these nanotubes between the bacteria, enabling them to react and interact with aimed purposes to, for example, external stresses [125].

1.3 Aim of the study

The present study analysed two important species of nontuberculous mycobacteria that have majorly contributed to the spread of NTM in nosocomial infection and are problematic to either treat or eradicate. Both species, *M. abscessus* and *M. chimaera* are capable of biofilm formation which in both cases is considered to be a fundamental reason for the success of each species.
Biofilm formation of mycobacteria is not yet investigated well enough to evaluate its impact on the susceptibility behaviour towards antimicrobials although mycobacterial biofilms gain more and more attention as described in the previous sections [3, 44].

The aim of this study was to (1) adjust an approved biofilm cultivation method to the use with *M. abscessus* and *M. chimaera*, (2) to investigate the general structure and composition of the biofilms, (3) to identify biofilm specific genes and finally, (4) to evaluate the impact of the biofilm formation of these NTM species on their susceptibility towards common antimicrobials.

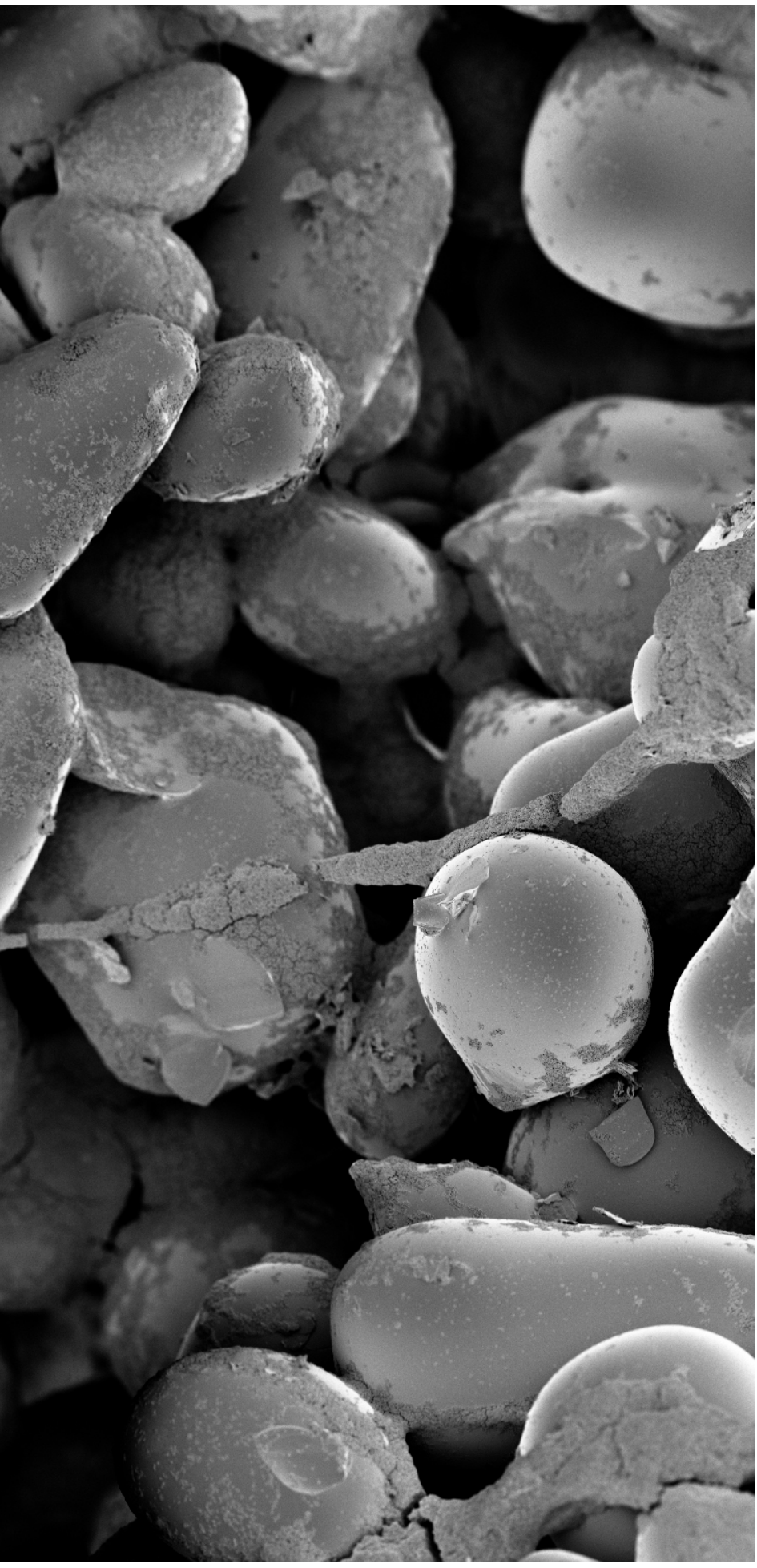

Chapter 2

Material and Methods

2.1 Isolate collection

2.1.1 Rapid growing mycobacteria (RGM)

Two pairs of genetic isoform isolates were chosen from the *M. abscessus* strain collection of Dr. Astrid Lewin (Unit 16; Robert Koch - Institute). The four isolates were isolated from respiratory samples taken at different time points of the *M. abscessus* infection of the two patients.
One isolate of each sample pair showed genetic variation in the *mps2* gene of the GPL-locus and thus a morphological shift from a smooth to a rough phenotype (table 2.1.1).
The isolates $09/13^{sm}$ and $58/15^{rg}$ were isolated from a patient suffering from a persistent *M. abscessus* infection. Both isolates were further analysed by Lewin et al. [97].

Table 2.1.1: *Mycobacterium abscessus* isolates

Isolate	Morphology	*mps2* frameshift	Patient ID	ENA Accession Nr.
$25/14^{sm}$	smooth	Deletion 5191-5192 (-AT)	Patient D	ERS4791659
$35/14^{rg}$	rough			ERS4791674
$09/13^{sm}$	smooth	Insertion 5289 (+C)	Patient C [97]	ERS4791737
$58/15^{rg}$	rough			ERS4791694

Photographies are provided in supplementary figure S.1

2.1.2 Slow growing mycobacteria (SGM)

Four *M. chimaera* isolates have been chosen with respect to the global outbreak caused by contaminated HCUs. Besides the outbreak strain ZUERICH-1, three other *M. chimaera* isolates from different origin and with different phylogenetic distance have been chosen (table 2.1.2). Two water isolates, FR-35 and FR-41, and a sporadic patient isolate, UP-11, were selected. All isolates were analysed before by van Ingen et al (2017) using whole genome sequencing in order to identify isolates responsible

Table 2.1.2: *Mycobacterium chimaera* and *Mycobacterium avium* isolates

Isolate	Origin	Phyl. Dist. *	ENA Accession Nr.
ZUERICH-1	Patient, Outbreak strain	0	CP015272 - CP015277
FR-35	Water from HCU, not outbreak related	1.8	ERR1464001
FR-41	Water from hospital sink, not outbreak related	2.1	ERR1464006
UP-11	Respiratory patient sample, not outbreak related	1.9	ERR1463918
M. avium ATCC 15769	Spleen of a tuberculous hen, internal control	-	-

* - Phylogenetic distance evaluated by van Ingen et al [109]; Photographies of *M. chimaera* isolates are provided in suppl. figure S.3

for the global outbreak [109]. Additional, a *M. avium* isolate was chosen which is recommended by the DIN 14348 as a reference strain for disinfectant testing.

2.2 Cultivation

In general, all isolates were processed in the same way throughout all experiments with the exception of, if not otherwise mentioned, a cultivation duration of 7 days for *M. abscessus* and 21 days for *M. chimaera* and *M. avium* ATCC 15769.
All experiments were performed in at least three individual biological replicates and moreover, each individual sample was processed in three technical replicates. The used media and materials were sterilized prior to use.

2.2.1 Used Media

Three different media were used in the present study with respect to the recommendations given for susceptibility testing. The medium with the most appropriate nutrients for the cultivation of NTM is the Middlebrook 7H9 broth (Beckton Dickinson, NJ, US) which is commonly supplemented with 10 % OADC (Beckton Dickinson, NJ, US). The OADC supplement is composed of oleic acid, albumin, dextrose and catalase which support the metabolism of mycobacteria and thereby promote optimal growth. For plating Middlebrook 7H11 + 10 % OADC (Beckton Dickinson, NJ, US) was used. Middlebrook 7H9 or 7H11 + 10 % OADC (MB-OADC) is the recommended medium used for stock cultivation and disinfectant testing.
The second medium is Mueller-Hinton II cation-adjusted broth (Beckton Dickinson, NJ, US). It is recommended for antibiotic testing of NTM while for slow growing mycobacteria (e.g. *M. chimaera*) Mueller-Hinton II cation adjusted + 5 % OADC (MH-OADC) is recommended. For rapid growing mycobacteria (e.g. *M. abscessus*) Mueller-Hinton II cation adjusted (MH) is used without being additionally supplemented.

2.2.2 Bacterial stock solutions

First, for all isolates stock solutions were produced as follows. From each isolate 5 x 100 µL of the originally provided sample were plated on MB-OADC and incubated at 37 °C for the above mentioned duration. Then, the bacteria from each plate were washed off with each 10 mL of MB-OADC + 10 % glycerin using sterile spatula and the resuspended bacteria collected in a 50 mL falcon tube. The solution was homogenized by ultrasonication for 20 min at 40 Hz (Bactosonic, BANDELIN, Germany) and stored at -80 °C in 1 mL aliquots.

2.2.3 Biofilm

The bacterial stock solution was thawed and diluted in MB-OADC to a concentration of 10^5 CFU/mL. A 24-well plate was prepared by adding one sterilized bead per well using sterile tweezers. Then, 1 mL of the diluted bacterial solution was added to each well and the plate sealed with Parafilm®M. The plates were incubated on an orbital shaker at 150 rpm with 37 °C as long as further analysis required.

2.2.4 Suspension

Suspension samples were cultivated and produced as specified by DIN EN 12353. Briefly, 5 x 200 µL of the undiluted bacterial stock were plated on MB-OADC and incubated at 37 °C for the above mentioned time (section 2.2).

2.2.5 Planktonic

Planktonic samples were produced for proteome and transcripome analysis. The bacterial stock solution was diluted to 10^5 CFU/mL in a total volume of 20 mL MB-OADC. The culture was transferred to a cell culture flask and incubated at 37 °C on an orbital shaker at 150 rpm for as long as further analysis required.

2.3 Sample Preparation

2.3.1 Biofilm

For quantifying the biofilm-associated bacteria, the cultivated beads (section 2.2.3) were taken from the 24-well plate with sterile tweezers and washed carefully by dipping twice in 2 mL of sterile water. Afterwards, each bead was transferred to a tube containing 1 mL of sterile water and placed into a sonicator (Bactosonic, BANDELIN, Germany). The bacteria were detached and homogenized for 20 min at 100 % 40 Hz.

2.3.2 Suspension

The suspension samples were cultivated as described above (section 2.2.4). The bacteria were washed off from the plate by adding 5 mL H_2O or H_2O + 0.1 % Tween 80 (depending on further experiments) and resuspending the colonies with a spatula. The suspension was collected in a 50 mL falcon tube and centrifuged for 15 min at 3,500 rpm. The supernatant was discarded and the pellet resuspended in fresh H_2O or H_2O + 0.1 % Tween 80. The centrifugation and resuspension was repeated three times and the pellet finally resuspended in the ten-fold volume (with respect to the pellet's volume) using H_2O or H_2O + 0.1 % Tween 80. Afterwards 1 mL of the sample were transferred to a fresh 2 mL tube and homogenized in a sonicator as described under section 2.3.1.

2.3.3 Planktonic

The samples of planktonic bacteria (section 2.2.5) were carefully resuspended to avoid settlement of bacteria. One mL of the sample were transferred to a fresh 2 mL tube and centrifuged at 5,000 rpm for 10 min at room temperature. The supernatant was discarded and the pellet resuspended in 1 mL of sterile water. The sample was then sonicated as described above (section 2.3.1).

2.4 Quantification methods

For all quantification methods (CFU counting, qPCR or ATP measurement) the used samples originated from the same biofilm, suspension or planktonic sample.

2.4.1 Colony forming unit (CFU)

To determine the number of colony forming units (CFUs), the samples were cultivated and prepared as described above (section 2.2, section 2.3). After sonication the samples were diluted in sterile water in steps of ten and each dilution plated by drop-plating (5 µL per sample) on plates of MB-OADC. The plates were incubated at 37 °C as long as required for the specific species and afterwards the number of colonies was counted and projected to a volume of 1 mL.

2.4.2 qPCR

As quantification of rough *M. abscessus* morphotypes by CFU counting is often problematic due to the strong clumping of the bacteria, another method for quantifying the bacteria associated in biofilm was established.
For both species, *M. abscessus* and *M. chimaera*, primers and probe (FAM-TAMRA) for qPCR were designed on the *rpoB* gene, respectively (table 2.4.1). The efficiency of the *M. chimaera rpoB* primers was tested at different temperatures to confirm the optimal conditions (supplementary figure S.4). The primers and probe for *M. abscessus* were well established and used as recommended [135].
For quantifying the number of bacteria, a standard of genomic DNA of either *M. abscessus* or *M. chimaera* was produced, based on the protocol described at section 2.6.1. The DNA was quantified using NanoDrop™ 2000 (Thermo Fisher Scientific, Germany) following the manufacturers instructions and the corresponding number of bacteria calculated by using the weight of genomic DNA per bacterium. The weight of each genome was calculated using the Molbio DNACalculator [1].

Table 2.4.1: Primers and Probes used for qPCR

Target Gene	Primer/Probe	Sequence (5' - 3')
M. abscessus rpoB	Mabs rpoB-FW	CGATAGAGGACTTCGCCTAACC
	Mabs rpoB-BW	TCGAGCACGTAAACTCCCTTTC
	Mabs rpoB-Probe	[FAM]-CCACTGACCGAACATCTATCCCGC-[TAMRA]
M. chimaera rpoB	Mch rpoB-FW	TGGACCAACGAGCAGATCAC
	Mch rpoB-BW	TGTTGTCCTTCTCCAGCGTC
	Mch rpoB-Probe	[FAM]-GGCTTCTCCGAGATCATGATGT-[TAMRA]

[1] Molbio DNACalculator
www.molbiotools.com/dnacalculator - last checked January 11, 2023

Table 2.4.2: Mastermix protocol for one single PCR reaction with purified DNA
DreamTaq buffer and polymerase from Thermo Fisher Scientific CA, USA

Ingredients	**Concentration**	**Volume** [µL]
DNA Template	-	10
10x DreamTaq buffer	-	2.5
dNTP Mix	10 mM	0.5
$MgCl_2$	25 mM	0.8
Primer_F	25 µM	0.5
Primer_R	25 µM	0.5
Probe	10 µM	0.5
ROX	10 µM	0.25
DreamTaq Polymerase	5 U / µM	0.125
H_2O	-	ad 25

Table 2.4.3: Cycler conditions for PCR and qPCR

Step	**Temperature** [°C]	**Time** [sec]*	**Cycle**
Initial denaturation	95	180 (120)	x1
Denaturation	95	30 (45)	
Annealing (T_a)	60	30 (45)	x40
Extension	72	60 (45)	
Final Extension	72	300 (300)	x1

* in brackets - time settings adjusted for qPCR

In order to make the bacterial DNA available for PCR, the samples were heated for 30 min to 96 °C afterwards cooled to room temperature. A DreamTaq - mastermix (Thermo Fisher Scientific, CA, USA) was prepared as described in table 2.4.2. The qPCR was performed as described in table 2.4.3 using an ARIAMx Real-time PCR System (Agilent, CA, USA). From the resulting C_t-values the number of bacteria was then calculated relative to the DNA standard.

2.4.2.1 PMA-qPCR

Because biofilms are known to contain a certain amount of eDNA, the samples for qPCR were labelled with PMA dye (propidium monoazide dye; 20 mM in H_2O Biotium, CA) prior to DNA extraction. The dye binds free DNA in the extracellular space of bacteria and also the DNA of dead bacteria (with disrupted cell wall). Preceding experiments showed the effectiveness of the PMA dye (supplementary figure S.7).
The bacterial samples were cultivated as described under section 2.2 and prepared till sonication as described under section 2.2.3. Thereafter, 100 µL of the sonicated sample were mixed with PMA following the manufacturers protocol. The samples then rested for 10 min in the dark and were thereafter illuminated for 5 min using a blue light table (wavelength 470 nm, Jena Analytik GmbH, Germany) in order to activate the PMA. Afterwards, the samples were centrifuged at 12,000 g for 10 min at 4 °C and the supernatant discarded to aviod further binding of DNA. The pellet was resuspended in 100 µL sterile water and the mixture heated for 30 min at 96 °C in order to make the DNA available for qPCR. The PMA-qPCR was performed as described under section 2.4.2.

2.4.3 ATP quantification

The metabolic activity of the bacteria during biofilm growth was analysed by measuring the amount of ATP. This was done by using the Bactiter-Glo™ Microbial Cell Viability Assay (Promega GmbH, Germany). Therefore, 50 µL of the sonicated bacteria were transferred to a white 96-well plate. Afterwards, 50 µL of the reactive solution were added and mixed by pipetting. Then, the plate was sealed and incubated in the dark for 30 min. The luminescence was measured by using a TECAN Infinite ® 2000 PRO reader (Tecan Trading AG, Switzerland) following the manufacturers instructions.

2.5 Characterisation of the Biofilm

2.5.1 Optimizing the Substrate

In order to optimize the subtratum for biofilm formation, four different bead types were tested. The isolates $25/14^{sm}$ and $35/14^{rg}$ were cultivated as described above (section 2.2.3) using either glass beads (GB)[2], collagen-coated glass beads (CB)[3], plastic beads (PB)[4] or porous glass beads (PGB)[5]. Afterwards the number of bacteria was determined by CFU counting (section 2.4.1).

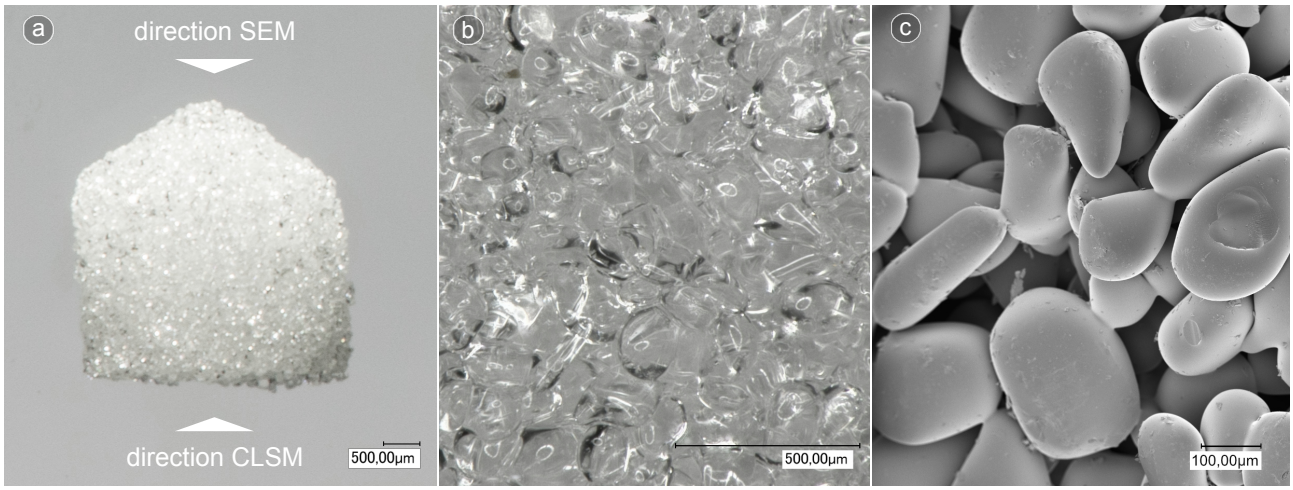

Figure 2.5.1: Porous Glass Beads
Upscaled images of porous glass beads (PGB; ROBU® Glasfilter-Gaerete GmbH, Germany) which were used as substrate for biofilm cultivation. The beads consist of glass particles, which are sintered together.
a) Sideward photography of a PGB. Labelled are the directions used for either SEM or CLSM imaging. Due to the cylindrical shape of the PGB different scanning direction had to be used for each microscopy procedure. **b)** Macrophotography of the glass particle structure of the PGB. **c)** SEM image of the glass particle structure of the PGB.

2.5.2 Growth curves

To analyse the growth in biofilm, each isolate was incubated as described above (section 2.2.3) for different periods of time. *M. abscessus* isolates were incubated for 1, 2, 3, 7 and 10 days in MB-OADC and MH; *M. chimaera* isolates were incubated for 3, 7, 10, 14, 21 and 28 days in MB-OADC and MH-OADC. Afterwards the CFU was analysed as described in section 2.4.1. Additionally, the metabolic activity was analysed as described in section 2.4.3. For *M. abscessus* isolates the number of bacteria was further determined by PMA-qPCR in order to assess the effect of the clumping of rough isolates on the CFU/mL.

2.5.3 Quantifying ECM components

As the amount of ECM was too low for analysis when using single biofilm beads, the experiments were performed with batch samples. Therefore, biofilm and suspension samples were cultivated as described above (section 2.2).
For biofilm batch samples, 24 beads were collected in a 50 mL flacon tube containing 10 mL sterile

[2] Ø 5 mm, Merck KGaA, Germany

[3] Ø 5 mm, glass beads coated with rat-collagen (Cat.No. 11179179001; Roche GmbH, Germany);
a collagen-solution was prepared as recommended by the manufacturer, sterile glass beads were coated with 10 µL collagen, respectively, dried for 60 min under fume hood and stored at 4 °C and used within a few days

[4] Ø 5 mm, Hoch Kugelfertigung, Germany

[5] Ø approx. 4 mm ROBU® Glasfilter-Gaerete GmbH, Germany

water. To produce suspension batch samples, one agar plate of cultivated bacteria was washed off with 10 mL of sterile water and the resuspended bacteria collected in a 50 mL falcon tube.
All samples were centrifuged at 8,000 rpm for 10 min at room temperature. The supernatant was discarded and the pellets resuspended in 10 mL of sterile water. Afterwards, the tubes were sonicated as described under section 2.3.1.
From each batch samples, the total number of bacteria was determined by PMA-qPCR (section 2.4.2). The resulting number of bacteria was used to finally set the total amount of ECM components in relation to the number of bacteria.
The quantification was performed from three biological replicates, each in three technical replicates.

2.5.3.1 DNA

In order to quantify the total amount of DNA per sample, 100 µL of the produced batch sample were used to analyse the amount of genome equivalents by qPCR (section 2.4.2). The amount of DNA was set in relation to the previously determined number of bacteria.

2.5.3.2 Proteins

Before protein quantification, a quantified standard of mycobacterial proteins was produced as described by Lewin et al. [136]. The amount of protein was determined using the Pierce™ BCA Protein Assay Kit (Thermo Fisher Scientific, MA USA) according to the manufacturers instructions.

50 µL of each biofilm or suspension batch sample, respectively, were transferred to a separate well of a clear bottom 96-black well plate (Greiner Bio-One International GmbH, Germany). An additional 50 µL of the serial dilutions of the mycobacterial protein standard were also transferred to the 96-well plate. Each sample and standard were processed in three technical replicates.
50 µL of staining solution [DMSO with 0.2 % SYPRO™ Orange protein gel stain (Thermo Fisher Scientific, MA USA)] was added to each well and mixed carefully. The plate was incubated in the dark at room temperature for 30 min and the fluorescence ($470_{\,Ex}$ /$570_{\,Em}$) was subsequently measured in a TECAN microplate reader (TECAN Trading AG, Switzerland). The mass of protein per well was calculated using a standard curve generated from the mycobacterial protein standard and related to the additional number of bacteria in order to determine the amount of protein per bacterium.

2.5.3.3 Lipids

To determine the amount of lipids per bacterium, 5 mL of the prepared batch samples were transferred to a fresh 50 mL falcon tube and centrifuged at 8,000 g for 15 min at 4 °C. The supernatant was discarded. Afterwards, each pellet was resuspended in the 20-fold volume (with respect to the pellet's volume) of 2:1 chloroform/methanol. The tubes were sonicated for 20 min at 40 Hz and then incubated overnight at room temperature.
The next day, the samples were centrifuged at 8,000 g for 15 min at 4 °C. The supernatant containing the solved lipids was carefully transferred to a fresh, pre-weighted 50 mL falcon tube without disturbing the pellet. Subsequently, the supernatant was left to evaporate under the fume hood completely for 2-3 days.
Then, the falcon tube was weighed again and from the difference in weight, the amount of lipids was calculated. Finally, the amount of lipids was set in relation to the number of bacteria.

2.5.4 Microscopic Evaluation

The pictorial representation of the biofilms on PGBs was done in order to display on the one hand the structure of the biofilm and on the other hand the distribution of ECM components in the biofilm. Therefore, the biofilms were cultivated as described above (section 2.2.3) for either 7 (*M. abscessus*) or 21 (*M. chimaera*) days. Afterwards, the biofilm beads were transferred to a fresh plate containing 2 mL of fixation solution (CLSM = 4 % paraform aldehyde in 50 mM HEPES; SEM = 4 % paraformaldehyde, 2.5 % glutaraldehyde in 50 mM HEPES, pH 7.0) and fixed for a minimum of 48 h at 4 °C.

2.5.4.1 Confocal light scanning microscopy (CLSM)

For CLSM analysis, the fixed beads were washed by dipping carefully in sterile water and then transferred to a fresh 24-well plate containing 1 mL of staining solution. The staining solution was produced as mentioned in table 2.5.1. The samples were incubated in the staining solution for 30 min in the dark. Afterwards, the beads were washed again by carefully dipping in 1:1 DMSO/H_2O.
The beads were placed on glass slides in Attofluor™ Cell Chambers (Thermo Fisher Scientific, MA US) and imaged using a Leica TCS SP8 microscope (Carl Zeiss Microscopy GmbH, Germany). The scanning settings were set to optimize the fluorescent signal and to minimize the background signal. Comparative presentations were examined with identical scanning settings.

Table 2.5.1: Fluorescent dyes used for light microcopy characterisation of biofilms

Target structure	Stain	Wavelength [nm]	Manufacturer	Dilution*
DNA	SYTO™ 9	$485_{Ex}/498_{Em}$	Thermo Fisher Scientific, MA, USA	1:1000
eDNA	BOBO™-3 Iodide	$570_{Ex}/602_{Em}$	Thermo Fisher Scientific, MA, USA	1:100
dead bacteria	Propidium Iodide	$493_{Ex}/636_{Em}$	Thermo Fisher Scientific, MA, USA	1:1000
Protein	SYPRO™ Orange	$470_{Ex}/570_{Em}$	Thermo Fisher Scientific, MA, USA	1:1000
Lipids	NileRed	$554_{Ex}/638_{Em}$	Sigma Aldrich KGaA, Germany	1:1000
Amyloid-like protein structures	Thioflavin T	$348_{Ex}/454_{Em}$	Sigma Aldrich KGaA, Germany	1:1000

* - The stains were diluted in 1:1 DMSO/H_2O

2.5.4.2 Scanning electron microscopy (SEM)

After fixation the samples were dehydrated in a graded ethanol line (30, 50, 70, 90, 95, 100, 100 %) and dried overnight in hexamethyldisilazane. Then the beads were mounted on aluminium stubs and sputter coated with 16 nm gold-palladium.
The beads were analysed in the SEM ZEISS 1530 Gemini microscope (Carl Zeiss Microscopy GmbH, Germany) operating at 3 kV using the in-lens electron detector.

2.6 Expression patterns of *M. chimaera* biofilms

To obtain a reliable data set, the proteome was determined from three biological replicates, each in technical triplicates, and the transcriptome was analysed from five biological replicates, each in technical triplicates. Due to the natural instability of RNA it was especially for the transcriptome data necessary to produce a broad database.
For comparative analysis, the genomes of all four *M. chimaera* isolates were used. The genomes of the isolates FR-41 and UP-11 were taken from the ENA database (table 2.1.2). For the other isolates, *M. chimaera* ZUERICH-1 and FR-35 the genomes were sequenced using nanopore sequencing (section 2.6.2), in order to enhance quality of the genomic data for further data analysis.

2.6.1 DNA isolation for MinION sequencing

For DNA isolation *M. chimaera* ZUERICH-1 and FR-35 were cultivated as described above as planktonic samples (section 2.2).
One ml of well grown culture was transferred to a fresh 2 mL tube and centrifuged at 12,000 rpm for 10 min at 4 °C. The supernatant was discarded and the pellet resuspended in 400 µL of 1xTE-buffer (pH 8.0). The tubes were incubated for 30 min at 80 °C and afterwards slowly cooled to room temperature. Then, 5 µL of lysozyme-solution (150 mg/mL) were added and the mixture incubated at 37 °C overnight.
The next day, 70 µL of SDS (10 % in H_2O) plus 2 µL of proteinase K-solution (50 mg/mL) were added to the mixture and further incubated for 2 h at 65 °C. Then, 100 µL of sodium chloride (5 mM) and 100 µL CTAB buffer[6] were added, mixed well and further incubated for 10 min at 65 °C.
Afterwards, 500 µL of chloroform/isoamylalcohol were added, mixed by pipetting and centrifuged at 12,000 rpm for 15 min at 4 °C. The aquaeous phase was transferred to a fresh tube and mixed with 400 µL of phenol/chloroform/isoamylalcohol and again centrifuged at the above mentioned settings. Again the aquaeous phase was transferred to a fresh tube and 300 µL of isopropanol were added. The mixture was incubated overnight at -80 °C.
After incubation the samples were taken from the freezer and centrifuged at 12,000 rpm for 15 min at 4 °C. The supernatant was discarded and the pellet carefully washed with fresh 70 % ethanol. The tube was centrifuged again at the mentioned settings and the supernatant discarded again. The DNA was resuspended in 50 µL of 1xTE-buffer (pH 8.0) overnight at 4 °C.
The quantity and quality of the DNA was measured using a TECAN microplate reader using a NanoQuant Plate™ following the manufacturers instructions (Tecan Trading AG, Switzerland).

2.6.2 MinION sequencing

Sequencing of the isolated DNA was performed in the MF2 working group of the Robert Koch - Institute.
MinION one-dimensional (1D) libraries were constructed, using the SQK-RBK004 kit (Nanopore technologies, Oxford, UK) and loaded onto a R9.4 flow cell according to the manufacturer's instructions. Quality control of the genomic data was done using the RKI in-house pipeline QCumber (v2.1.1)[7]. The available genomes of *M. avium* and *M. chimaera* at the ENA were used to prepare a genome

[6] 2% cetyl trimethylammonium bromide, 1% polyvinylpyrrolidone, 100 mM Tris-HCl, 1.4 M NaCl, 20 mM EDTA

[7] Gitlab QCumber (v2.1.1)
`www.gitlab.com/RKIBioinformatics/QCumber` - last checked January 11, 2023

database that was used as a reference for the genome assembly of the *M. chimaera* sequences.
The genomes of FR-41 (ERR1464006) and UP-11 (ERR1463918) were downloaded from the ENA database. Based on the available genomes of *M. avium* and *M. chimaera* from the ENA database, the sequenced samples were annotated using PROKKA [137]. Identification of coding sequences was performed based on sequence similarity (min. 70 %) and coverage (min. 90 %). In order to obtain a presence-absence matrix of all genes the genomes were further processed using ROARY with default settings [138].

2.6.3 Proteome

2.6.3.1 Protein isolation

For protein isolation, biofilm, suspension and planktonic samples of *M. chimaera* ZUERICH-1 and FR-35 were cultivated for 21 days as described in section 2.2. The isolation of proteins followed the SPEED protocol published by Döllinger et al. (2020) [139].
For the biofilm samples one bead each was taken from the cultivation plate, washed by dipping in PBS (1x phosphate-buffered saline, pH ∼7.4) and transferred to a fresh tube containing 1 mL of PBS. The beads were sonicated for 20 min. For the suspension samples, a loop of bacteria was scratched from the agar plate and resuspended in a fresh tube containing 1 mL PBS. For planktonic samples 1 mL of the cultivated bacteria was transferred to a tube and centrifuged at 3,000 rpm for 10 min. The supernatant was discarded and the pelleted resuspended in 1 mL of PBS.
All samples were again centrifuged at 3,000 rpm for 5 min at 4 °C and the supernatant carefully discarded. The pellets were resuspended in PBS and washed by pipetting. Then the pellets were again centrifuged at the above mentioned settings and the supernatant was discarded. This was repeated 3 times. After the last step, the samples were resuspended in the 1:4 - 1:8 volume of TFA (triflouracetic acid, v/v) and lysed at room temperature for 20 min followed by a short incubation for 2 min at 70 °C. Thereafter neutralization buffer (10x volume of TFA, composition see [139]) was added. Then alkylation buffer (1.1x volume of TFA, composition see [139]) was added and incubated for 5 min at 95 °C. The samples were then stored at -20 °C overnight.
The next day, the protein quantity was measured by turbidity measurement using UV cuvettes and absorption measurement at 360 nm using a UV-Vis spectrometer. Thereafter the protein concentration was calculated (1AU = 0.79 µg/µL). All samples were adjusted to an equal protein concentration (0.25 µg/µL) using dilution buffer (composition see [139]). Then the samples were diluted again to a ratio of 1:50 using H_2O and trypsin. The mixture was incubated at 600 rpm for 20 h at 37 °C.
After incubation, TFA was added to a final concentration of 2 %. Pepites were desalted using C18-StageTips in several steps of centrifugation (for further information see detailed protocol at [139]). Afterwards the peptides were dried in a SpeedVac and resuspended in 20 µL of 0.1 % TFA. Thereof peptide concentration was determined using a NanoDrop™ (Thermo Fisher Scientific, US).

2.6.3.2 Orbitrap

Further peptide preparation and measurements were performed by the ZB6 working group of the Robert Koch - Institute.
The probes were measured in an EASY-nanoLC 1200 (Thermo Fisher Scientific, US) coupled online to a Q Exactive™ Plus mass spectrometer (Thermo Fisher Scientific, US) as described elsewhere [139]. The spectrographs were further analysed using internal RKI in-house pipeline protocols. Protein

sequences were aligned to the obtained MinION genome data. Finally a matrix of all samples with the corresponding protein count and the level of expression (up- or downregulation) per gene was provided.

2.6.4 Transcriptome

2.6.4.1 RNA isolation

For RNA isolation, biofilm, suspension and planktonic samples of *M. chimaera* ZUERICH-1 and FR-35 were cultivated for 21 days as described in section 2.2.
For biofilm samples 24 beads were collected in a falcon tube containing 25 mL of H_2O. For suspension, five well-grown agar plates were washed off with each 5 mL of H_2O and collected in a flacon tube. From the planktonic samples 25 mL were directly transferred to a falcon tube. All samples were sonicated for 20 min at 100 %. Thereafter the samples were centrifuged at 6,000 rpm for 10 min at 4 °C. The supernatant was discarded, the pellets resuspended in 1 mL of RNA protect (Qiagen, Germany), incubated at room temperature for 10 min and transferred to a fresh 2 mL tube. The samples were centrifuged at the above mentioned settings and the supernatant discarded again. During the following process, samples were constantly put on ice.
The pellets were resuspended in 1 mL of TRIzol™ (Thermo Fisher Scientific, US) and transferred to screw cap tubes containing 0.2 mm glass beads. The tubes were put into a PreCellys® homogenizer (VWR, Germany) and disrupted at 6,500 rpm for 2x 1 min, 30 sec pause. Thereafter 200 µL of 100 % chloroform were added to each sample and mixed carefully. The samples were incubated for 10 min on ice before they were again centrifuged at 12,000 rpm for 5 min at 4 °C. The upper phase was transferred to a fresh tube and 500 µL of 100 % isopropanol were added. The samples were incubated for 48 h at -80 °C.
After incubation the samples were carefully thawed on ice and then centrifuged at 12,000 rpm for 10 min at 4 °C. The supernatant was discarded, the pellet carefully washed with 70 % isopropanol and centrifuged again at the above mentioned settings. The supernatant was discarded again and the samples dried on ice under the fume hood. Thereafter the samples were resuspended in 60 µL of H_2O. After isolation the DNA was digested using the TURBO™ DNase Kit (Thermo Fisher Scientific, US) following the manufacturer's instructions. The digestion was done twice for each sample.
The RNA samples were stored in aliquots at -80 °C. One aliquot per sample was used for prequantification of RNA using Qubit RNA Assay (Thermoe Fisher Scientific, US) and the abscence of any residual DNA was controlled by PCR (section 2.4.2). Quality of RNA was checked using a fragment bioanalyzer for RNA (Bioanalyzer High Sensitivity RNA Analyzer, Agilent, US) following the manufacture's instructions.

2.6.4.2 Illumina Sequencing

Library preparation and sequencing of the isolated RNA was performed in the MF2 working group of the Robert Koch - Institute.
The RNA samples were again quantified and diluted in H_2O to an equal concentration amongst all samples. Thereafter the libraries for sequencing were prepared using the Illumina® Stranded Total RNA Prep and Illumina® RNA UD Indexes Set A (Illumina, US, order numbers 20040529 & 20040553) following the manufacturer's instructions. Sequencing was performed using the HighSeq 2500 System (Illumina, US). The sequences were further analysed using internal RKI in-house pipeline protocols

and aligned to the obtained MinION genomes. Finally, a matrix containing the transcript counts and the expression levels of each gene per sample was provided.

2.6.5 Data Preparation and Evaluation

An overview of the data evaluation workflow is given in figure 2.6.1. The data of both Omics-techniques were analysed equally in order to enable data comparison between both measurements.
The transcript [TPM (Transcripts Per Kilobase Million)] and protein [RUP (Razor + unique Peptides)] counts, respectively, were normalized against the median of all genes/proteins for each isolate and $\log_2$-transformed in order to assign expression levels for each gene/protein. The significance of the expression of each gene/protein was evaluated by ANOVA (FDR = 1 %) and validated by an according post-Hoc test. Transcripts and proteome data were aligned to the genomes of both isolates and marked with UniProt identifiers (Uniprot-IDs). The above mentioned steps were proceeded by the working groups of ZBS6 (J. Döllinger) and Bioinformatics (S. Wolf) of the RKI.
Based on the Uniprot-IDs, the datasets were matched and the FASTA sequences included into the dataset. From these, the coding and non-coding sequences were identified and the latter were excluded from the dataset. Using the FASTA sequences, the COG catageories (Cluster of orthologous groups of proteins) for each gene/protein were annotated using eggNOG Mapper[8]. Those that were not annotatable were assigned automatically with the category 'Function unknown' (S).
The produced dataset contained a total of 4.733 genes/proteins and was further split into subsets that were analysed individually focussing on the corresponding research interest.
For the concretisation and description of the biofilm specific genes in the comparative analysis of transcriptome and proteome, the co-expression of genes was further analysed using STRING[9].

2.6.5.1 Heatmap Analysis

In order to analyse general similarities between the expression of genes/proteins in the cultivation forms, heatmaps were generated by clustering the expression levels of all samples by similarity. Clustering was performed by using standard settings of the `heatmap`-function in R.

2.6.5.2 COG analysis of expression profiles

To analyse the functional background of the different cultivation forms, the genes/proteins that presented significant expression levels were assigned with a COG category (as described above). The number and mean expression of all genes/proteins that belong to a specific COG category were analysed.

2.6.5.3 Cultivation form specific genes/proteins

In order to analyse genes/proteins that presented cultivation forms specific up or downregulated expression. It was analysed whether genes/proteins were only up- or downregulated in one of the three cultivation forms in both isolates and voted as uniquely (cultivation form specific) up- or downregulated.

[8] eggNOG Mapper 2.1.9
`http://eggnog-mapper.embl.de` - last checked January 11, 2023

[9] STRING (Version 11.5) Protein-Protein Interaction Networks Functional Enrichment Analysis
`www.string-db.org` - last checked January 11, 2023

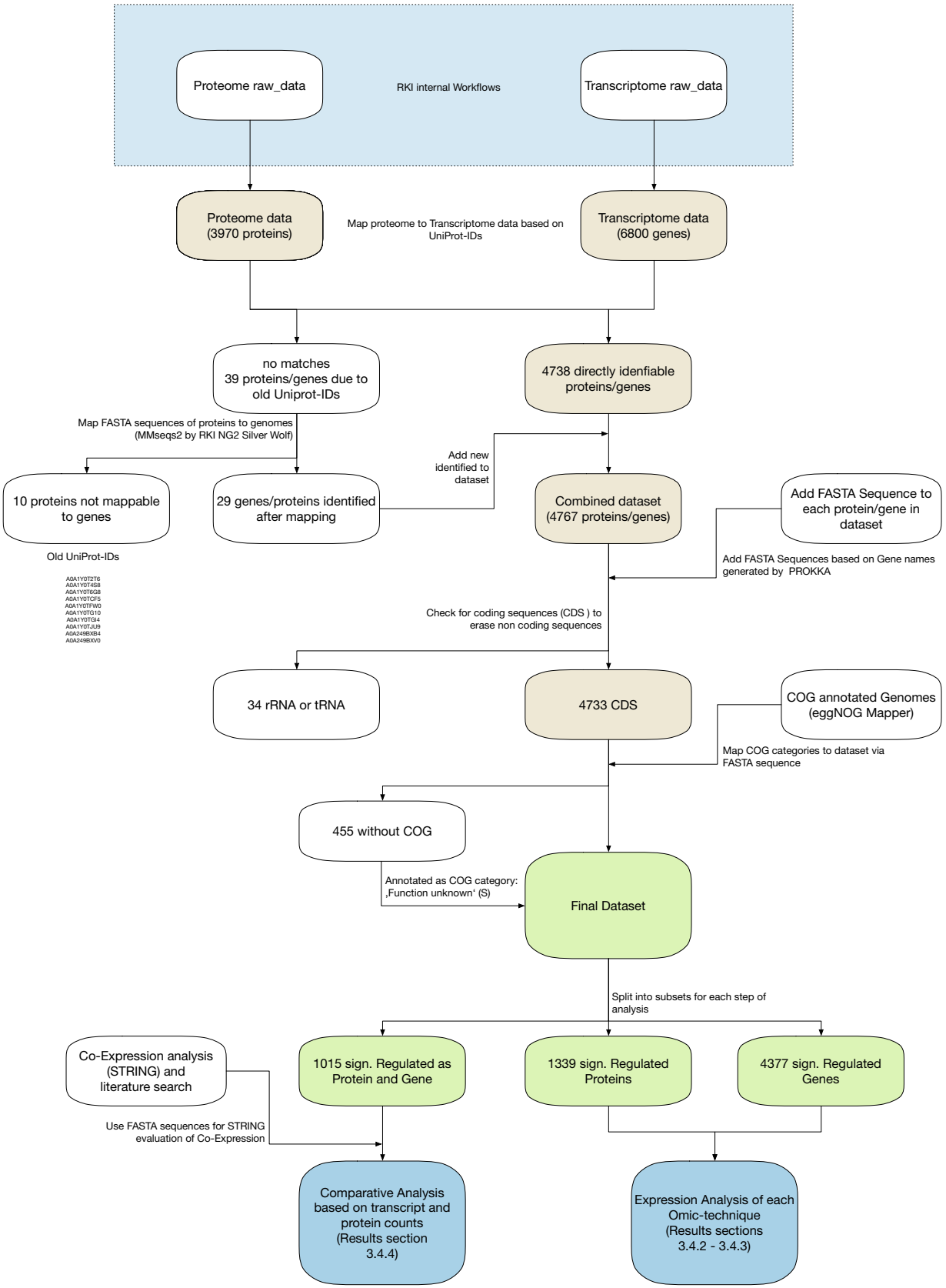

Figure 2.6.1: Workflow for analysis of Omics data.
Displayed is the workflow used for combination and processing of the omics data gained from two separate sources of the RKI. The most important prerequisite was to match as many data as possible. Therefore the datasets were matched according to the assigned UniProt-IDs. In 10 cases a mapping of the UniProt-IDs of the proteome to the transcriptome was not possible. Those concerned are separately mentioned.
Thereafter the FASTA sequences were matched to the dataset based on the gene names generated by PROKKA. Using the PROKKA data, the coding sequences (CDS) and non-coding sequences (e.g. rRNA, tRNA) were extracted from the dataset.
Based on the FASTA sequences, the COG-IDs were extracted from eggNOG and added to the CDS dataset (4,733 genes). To those, that could be annoted via eggNOG with a COG category, the category of 'Function unknown' (S) was assigned and these were reintegrated to generate the final dataset. From this dataset of combined proteome and transcriptome results, the subsets for the individual analysis were produced.

2.7 Disinfectant testing

All disinfectant experiments were performed as previously published by Konrat et al. (2016) [140] with small adaptations to the use of mycobacteria. Three different, common disinfectants were chosen, each in five different concentrations (table 2.7.1).

Table 2.7.1: Used disinfectants and neutralisers

Disinfectant	**Product**	**Conc.*** [% (v/v)]	**Neutraliser**
Glutaraldehyde (GA)	25 % Merck, KGaA, Darmstadt, Germany	0.1 0.5 1 2 5	1 % glycine solution with 0.1 % Tween 80 in water
Chlorine (FCA)	13 % free active chlorine, sodium hypochlorite, Acros Organics, Fisher Scientific, Schwerte Germany	0.1 1 2 3 5	TSH-Thio buffer (1 % Tween 80, 3 % Saponin, 0.1 % L-Histidin, 5 % sodium thio sulfate) in PBS (0.1 M, pH 7)
Peracetic acid (PAA)	Wofasteril 40 %, Kesla Pharma, Wolfen GmbH, Bitterfeld-Wolfen, Germany	0.01 0.05 0.075 0.1 0.5	0.5 % sodium sulfite in PBS (0.1 M, pH 7)

* - only highest concentration was used for neutralising and toxicity testing

2.7.1 Neutralising and toxicity testing

Before disinfectant testing was performed, the efficacy of the neutraliser had to be confirmed and a toxicity of the neutraliser itself needed to be excluded. Therefore the highest concentration of each disinfectant was tested with an according neutraliser using one representative isolate of *M. chimaera* and *M. abscessus*. The neutralising and toxicity testing was performed simultaneously with a negative control. The isolates *M. chimaera* ZUERICH-1 and *M. abscessus* $25/14^{sm}$ were cultivated on agar plates as described before (section 2.2.4). After cultivation five plates of each isolate, respectively, were washed off by adding 5 mL of H_2O + 0.1 % Tween 80 to each plate and resuspending the colonies with a sterile spatula. The resuspended bacteria were transferred to a falcon tube and centrifuged at 3,500 rpm for 15 min. The supernatant was discarded and the pellet washed by adding 25 mL of H_2O + 0.1 % Tween 80 and resuspending the pellet. The washing step was repeated 3 times and afterwards the resulting pellet was resuspended in H_2O + 0.1 % Tween 80 to reach an approximate CFU/mL of 10^3 (bacteria test suspension).

In order to test the neutralising efficacy, three falcon tubes were filled with 8.9 mL of the neutralising agent and pre-warmed for 10 min to 20 °C. Then, 1 mL of the disinfectant was added and mixed shortly by pipetting. Directly after, 0.1 mL of the bacteria test suspension was added and mixed by pipetting. The mixture was incubated again for 20 min at 20 °C. Afterwards the bacteria were quantified as described in section 2.4.1. For testing the toxicity, three falcon tubes ware prepared with 9.9 mL of the neutralising agent and pre-warmed for 10 min to 20 °C. Then 0.1 mL of the bacteria test suspension was added and mixed by pipetting. The tubes were then incubated for 20 min at 20 °C.

Afterwards the bacteria were quantified by plating 100 µL on MB-OADC and incubating it for 7 or 21 days at 37 °C. A negative control was prepared by filling three falcon tubes with 9.9 mL sterile water, pre-warming for 10 min to 20 °C and adding 0.1 mL test suspension. The mix was incubated afterwards for 20 min at 20 °C and then the bacteria were quantified as described in the previous paragraph. The neutralizer was excepted as soon as the numbers of the surviving bacteria in the neutralisation and toxicity testing did not differ from the negative control.

2.7.2 Biofilm

The bacteria were cultivated as biofilm samples as described above (section 2.2.3) in MB-OADC. For disinfectant testing, three tubes per concentration were prepared with 200 µL of the corresponding disinfectant concentration (including the negative control) and preheated for 10 min to 20 °C. Each bead was separately taken from the cultivation plate with sterile tweezers. In order to wash off loose bacteria each bead was twice dipped carefully in 2 mL of sterile water. Directly after, each bead was transferred to the tube containing the disinfectant and incubated for 60 min at 20 °C. After the incubation a total of 1.8 mL neutraliser was added to each tube and mixed by pipetting. Then the tubes were sonicated (20 min at 100 % 40 Hz) in order to detach and homogenise the biofilm associated bacteria. Thereafter the number of bacteria was determined by CFU counting as described in section 2.4.1.

2.7.2.1 Weekly Disinfection

M. chimaera ZUERICH-1 was cultivated as biofilm in either water or MB-OADC for 21 days as described above (section 2.2.3). For the weekly disinfection cycle, three representative concentrations of PAA were chosen (0.045 %, 0.1 %, 0.5 %).
The disinfectant testing was performed in a weekly cycle. Therefore each biofilm bead was separately taken from the cultivation plate with sterile tweezers and directly transferred to a 24-well plate containing 2 mL of the stated PAA concentration. The biofilms were disinfected for 10 min and then directly transferred to a new plate containing 2 mL of sterile water without neutralisation. Thereafter the beads were put in a 24-well plate containing the cultivation medium (water or MB-OADC) and cultivated again as described above until the next disinfection cycle (section 2.2.3). In each week of testing, three beads per concentration per cultivation medium were taken for quantification of the CFU/bead and treated as described in section 2.4.1.

2.7.3 Suspension

The suspension samples were cultivated on MB-OADC agar plates and prepared as described in section 2.2.4. Disinfectant testing was performed according to the DIN 14348. For each tested disinfectant concentration three 2 mL tubes, respectively, were prepared with 900 µL of the corresponding concentration of disinfectant and heated up for 10 min to 20 °C. Afterwards 100 µL of the bacterial test suspension were added and mixed shortly by pipetting. The samples were further incubated for 60 min at 20 °C. After incubation, 100 µL of the suspension-disinfectant mixture was transferred to a fresh 2 mL tube containing 900 µL of the cold corresponding neutralising agent and mixed carefully by pipetting. Thereafter the tubes were sonicated for 20 min at 100 % 40 Hz and then the number of bacteria determined as described above (section 2.4.1).

2.8 Antibiotic susceptibility testing

The susceptibility testing was performed with *M. abscessus* according to the CLSI recommended protocol[10] which is commonly used in the clinical field to determine the susceptibility of NTM. Briefly, the protocol is based on a micro dilution method that enables the testing of multiple specific antibiotics at once and is based on the optical evaluation of 'growth' or 'no growth'.
All experiments were performed in three biological replicates, each in technical triplicates. During the experiment it was ensured that the corresponding biofilm and suspension were treated equally. Therefore the samples of both cultivation forms of each biological replicate were placed and treated in the same 48-well plate.

Prior to the experiment a stock solution of each antibiotic was prepared (amikacin = 256 µg / mL; tigecycline 16 µg / mL). A 48-well plate was prepared with the according antibiotic for the testing of biofilm and suspension simultaneously (supplementary figure S.5). First, all wells except for the highest concentration were filled with 500 µL fresh MH. Then, 1 mL of the antibiotic stock solution was added to the well-row with the highest antibiotic concentration that was to be tested.
From this row, 500 µL were taken and added to the next lower row and mixed by pipetting with the prepared medium. Thereafter, 500 µL were taken from this row and added to the next lower row and so on. To the last row, no antibiotic was added as it served as the negative control. To half of the plate, in which the biofilms were to be tested, 500 µL of fresh medium were added in order to reach a total volume of 1 mL per well.

2.8.1 Biofilm

The biofilm samples were cultivated as described above in MB-OADC for 7 days (section 2.2.3).
Then, each bead was washed by dipping twice in 2 mL of sterile water and transferred to the previously prepared wells of the 48-well plate (see prior paragraph).

Table 2.8.1: Used antibiotics

Antibiotic	**Concentration [µg / mL]**	**negative control**	**mode of action**
Amikacin (AMI)	128 64 32 16 8	water	bactericidal (group aminoglykosides); inhibits bacterial protein biosynthesis by blocking the translocation of tRNA and thereby the initiation of the proteinsynthesis
Tigecycline (TGC)	8 4 2 1 0.5	water	bacteriostatic; binds to the 30S subunit of ribosome, inhibiting protein biosynthesis

[10] CLSI recommendation for susceptibility testing of NTM
www.clsi.org/media

After the corresponding suspension sample was added (see following paragraph), the whole plate was incubated for 5 days in a shaking incubator at 150 rpm and 30 °C.
After the incubation, each bead was taken from the plate, washed by carefully dipping in 2 mL of sterile water and transferred to a fresh 2 mL tube containing 1 mL sterile water. Then the beads were sonicated for 20 min at 100 % 40 Hz and further the CFU/mL determined as described above (section 2.4.1).

2.8.2 Suspension

Prior to the experiment the bacteria were cultivated on MB-OADC and the suspension was prepared as described above using MH (section 2.2.4) and diluted to an approximate number of 10^8 bacteria/mL. From this, 500 µL were added to the corresponding wells of the previously prepared antibiotic test plate (see penultimate paragraph).
The complete loaded test plate was incubated in a shaking incubator (150 rpm) for 5 days at 30 °C.
After incubation, 100 µL were taken from each well containing suspension sample and transferred to a fresh 2 mL tube containing 900 µL of sterile water. The samples were then sonicated for 20 min at 100 % 40 Hz and afterwards the CFU/mL determined as described above (section 2.4.1).

2.9 Statistics and Data Analysis

In general statistic analysis was performed using R[11] in RStudio[12]. Apart from the analysis of the expression profile data, significance testing was performed using Wilcoxon-Rank-Sum test and significance levels were defined as follows: ns = not significant $p \geq 0.05$; * = $p \leq 0.05$; ** = $p \leq 0.01$ and *** = $p \leq 0.01$.

[11] R (4.1.3)
`www.r-project.org` - last checked January 11, 2023

[12] RStudio (2022.02.1-461)
`www.rstudio.com` - last checked January 11, 2023

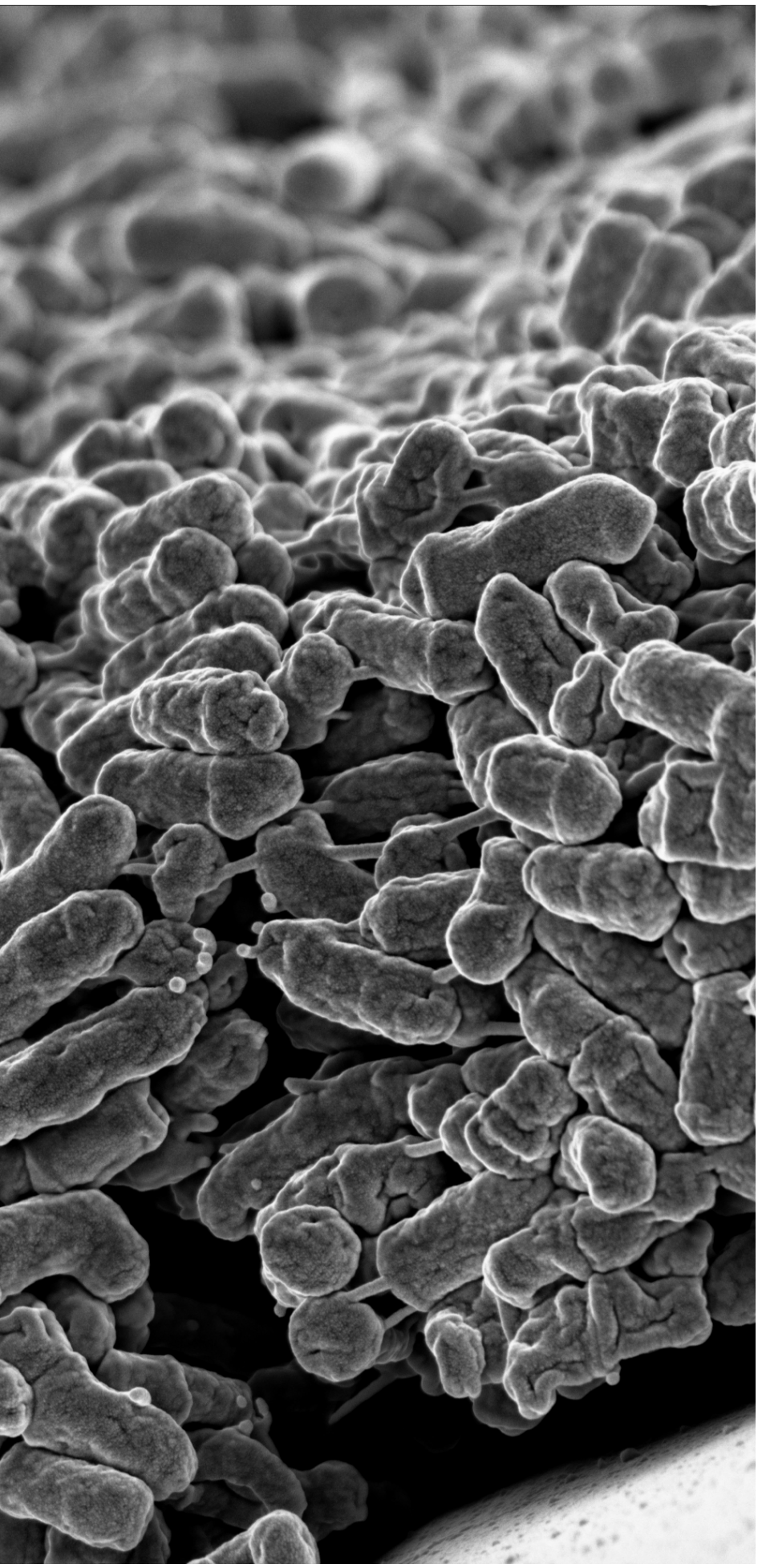

Chapter 3

Results

3.1 Biofilm growth

3.1.1 Substrate Optimization

During the adaptation of the biofilm bead model, different bead types were analysed to guarantee the most optimal substratum for biofilm growth. The isolates *M. abscessus* $25/14^{sm}$ and $35/14^{rg}$ were chosen as representatives. The bacteria were cultivated in MB-OADC on four different bead types that all provide different surface properties.

Both isolates showed the highest number of biofilm associated bacteria when they were cultivated on PGBs ($25/14^{sm}$ = 7.8 $\log_{10}$; $35/14^{rg}$ = 7.1 $\log_{10}$) (figure 3.1.1).

On the other beads, the CFU/mL of both isolates was around 1 – 1.5 $\log_{10}$ less than on PGB. While $25/14^{sm}$ showed the second best biofilm growth on CB, $35/14^{rg}$ displayed the least number of bacteria on this type of beads. A number of minimal 6 $\log_{10}$ CFU/mL is defined as a prerequisite for disinfectant testing, which both isolates only reached when they were cultivated on PGBs. Before any further analysis, the CLSM imaging was used to determine the efficiency of the sonication process (supplementary figure S.8). Thereby it was shown, that after sonication the complete biofilm could be detached from the porous glass beads.

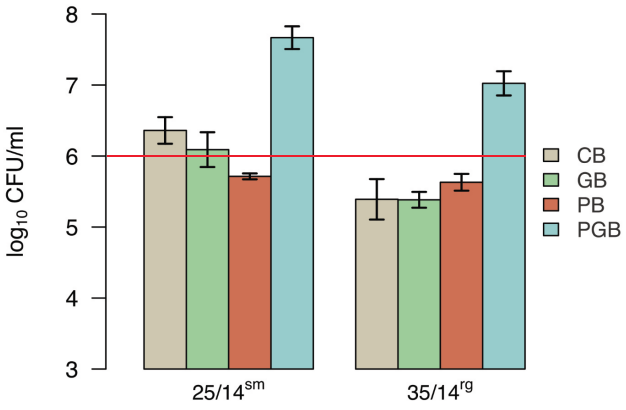

Figure 3.1.1: *M. abscessus* biofilm grown on different substrates

M. abscessus smooth and rough isolates cultivated as biofilm in MB-OADC on different types of beads. Total number of bacteria was analysed by plating (CFU/mL). CB = collagen coated beads; GB = glass beads; PB = Plastic (teflon) beads; PGB = porous glass beads. Displayed are means and standard deviations of five biological replicates. Red line indicates minimal amount of bacteria necessary for susceptibility testing (6 $\log_{10}$).

3.1.2 Reproducibility

An important requirement for reliable disinfectant and susceptibility testing is the reproducibility among individual biological replicates of the tested organism. It was found that all isolates, except *M. chimaera* FR-41, showed a reproducible biofilm growth on PGBs when cultivated in MB-OADC (supplementary figure S.9 & figure S.10).

In five individual repetitions, all isolates displayed a comparable number of bacteria ranging around 7 – 8 $\log_{10}$ by mean. The variability between the means of the experiments needed to be less than 0.5 $\log_{10}$ from the overall mean, which was fulfilled by all isolates except FR-41. The latter displayed an unstable number of bacteria among biological and also technical replicates, which resulted in the exclusion of this isolate from disinfectant testing.

3.1.3 Growth Curves

3.1.3.1 *Mycobacterium abscessus*

M. abscessus was cultivated in MB-OADC and MH. All tested *M. abscessus* isolates grew in both media and obtained a minimal number of 10^6 bacteria per mL after a cultivation time of seven days (figure 3.1.2).

In MB-OADC both smooth and both rough isolates showed an almost identical growth pattern, while the different morphotypes differed by approx. $1-2\log_{10}$ (figure 3.1.2 a). After three days of cultivation, the biofilms reach a stable stationary phase until day 10. The amount of ATP was almost identical in the four tested isolates and presented no differences between the morphological variants.

In MH, all isolates basically presented a similar growth pattern, but less even (figure 3.1.2 b). For the first three days, all isolates displayed an exponential growth. From day three on, the isolates $09/13^{sm}$ and $35/14^{rg}$ showed a slight decrease in CFU/mL. After day seven all isolates presented a decreasing amount of bacteria till day 10. This was almost identical displayed in the measurement of

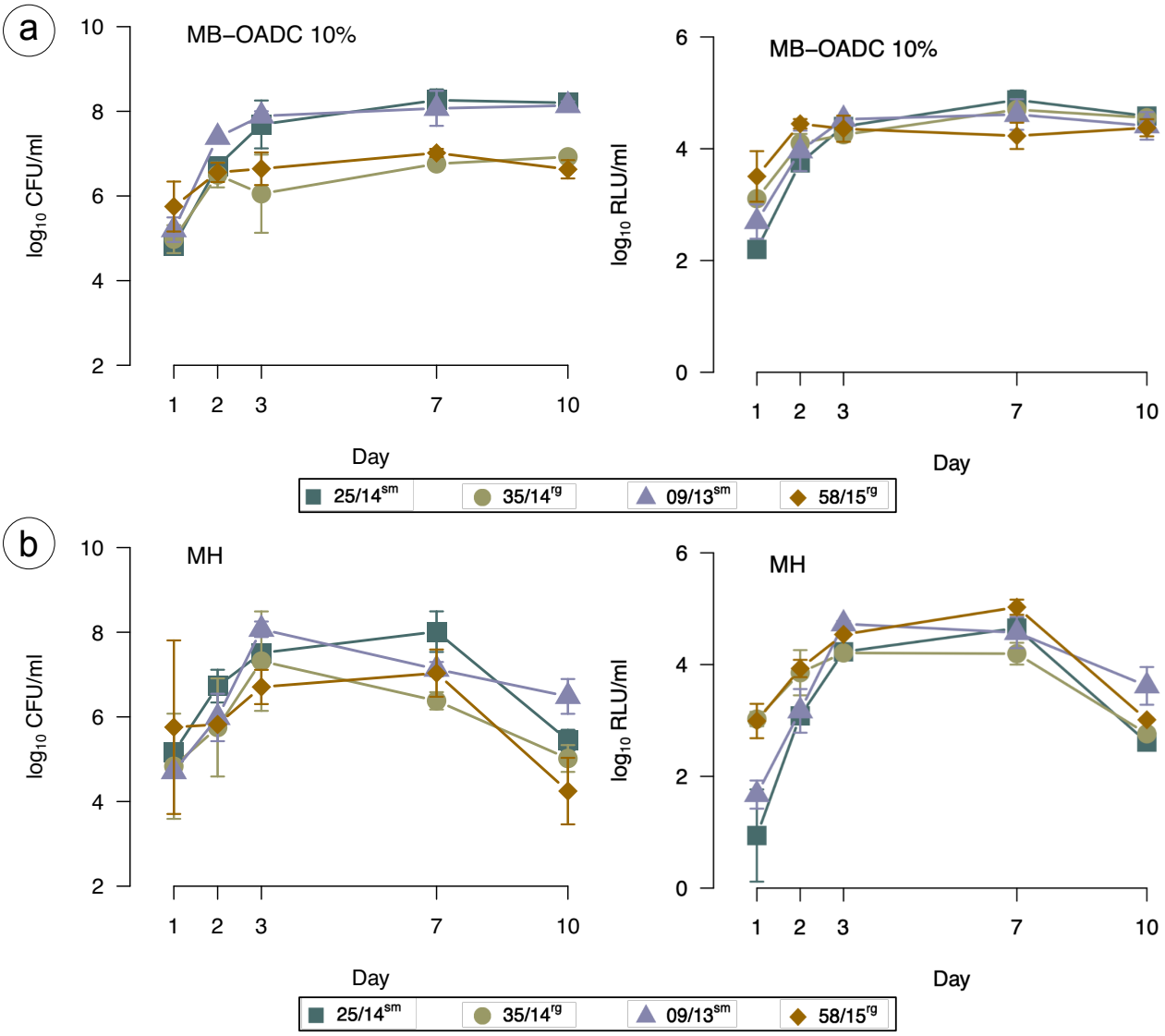

Figure 3.1.2: *M. abscessus* biofilm growth curves

M. abscessus biofilm cultivated in MB-OADC **(a)** and MH **(b)**. Total number of bacteria was analysed by plating (CFU/mL) and the metabolic activity was analysed by ATP-measurement (RLU/mL).
Displayed are means and standard deviations of three individual biological replicates.

the metabolic activity. In general, the differences of the CFU/mL between the isolates was higher in MH, though no distinct difference between smooth and rough isolates was found. In both media, all isolates presented very similar ATP levels.

PMA-qPCR

As rough *M. abscessus* isolates show a strong aggregation of bacteria that affects the CFU/mL counts, the samples were analysed additionally by PMA-qPCR (figure 3.1.3).
This showed that smooth and rough morphotypes contained similar numbers of bacteria in biofilm independent of the used medium. This was comparable to the results gained by the measurement of the metabolic activity. Still, in the time span between day 7 to 10, the GE/mL of the isolates differed between a max of 2 $\log_{10}$ in MB-OADC (figure 3.1.3 a) and 2.5 $\log_{10}$ in MH (figure 3.1.3 b).
Especially for the rough isolates, $35/14^{rg}$ and $58/15^{rg}$, the qPCR analysis showed that the number of bacteria was much higher than counted by CFU/mL. In MH the isolate $09/13^{sm}$ presented a strong increase of GE/mL to a maximum of almost 12 $\log_{10}$.

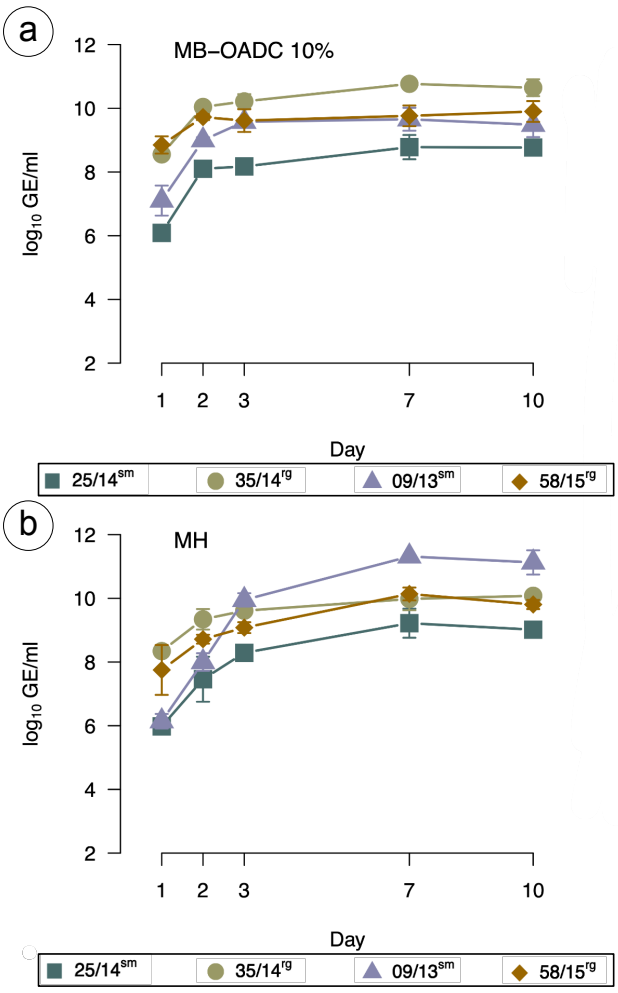

Figure 3.1.3: ***M. abscessus*** **biofilm analysed by PMA-qPCR**

M. abscessus smooth and rough isolates cultivated as biofilm in MB-OADC **(a)** and MH **(b)**. Total number of genome equivalents per mL (GE/mL) was analysed by PMA-qPCR. Displayed are means and standard deviations of three individual biological replicates.

For further susceptibility experiments, the isolates were analysed by CFU/mL as of the costs and expense that PMA-qPCR analysis requires. When more exact numbers of bacteria were required for evaluation, such as for example the ECM analysis, the bacteria were quantified by PMA-qPCR.
Most importantly, all tested isolates were able to form biofilm in a time period needed for susceptibility testing. All isolates grew to a minimal number of 6 $\log_{10}$ CFU/mL, which is necessary for disinfectant testing.

3.1.3.2 *Mycobacterium chimaera*

In MB-OADC, three of the four *M. chimaera* isolates (ZUERICH-1, FR-35, UP-11) grew very similar (figure 3.1.4 a). From day three to day 10, these isolates showed an exponential growth whereafter the amount of biofilm-associated bacteria reached a stationary number.
M. chimaera FR-41 displayed a completely different growth pattern with a decrease of bacteria in the first seven days and afterwards started to grow to a maxiumum of approx. 7.8 $\log_{10}$ CFU/mL at day 28. This pattern was also measurable in the metabolic activity. In both cases the measurements displayed high standard deviations, which showed that the growth of this isolate is very inconsistent in this medium.
The amount of ATP differed over time of cultivation. From day 3 to day 7, the amount of ATP increased in the isolates *M. chimaera* FR-35 and UP-11. The amount of ATP ranged constantly around 4 RLU/mL for the isolate ZUERICH-1. The course of the metabolic activity of the isolate FR-41 was very similar to the CFU measurement. In the first days of cultivation, the amount of ATP decreased

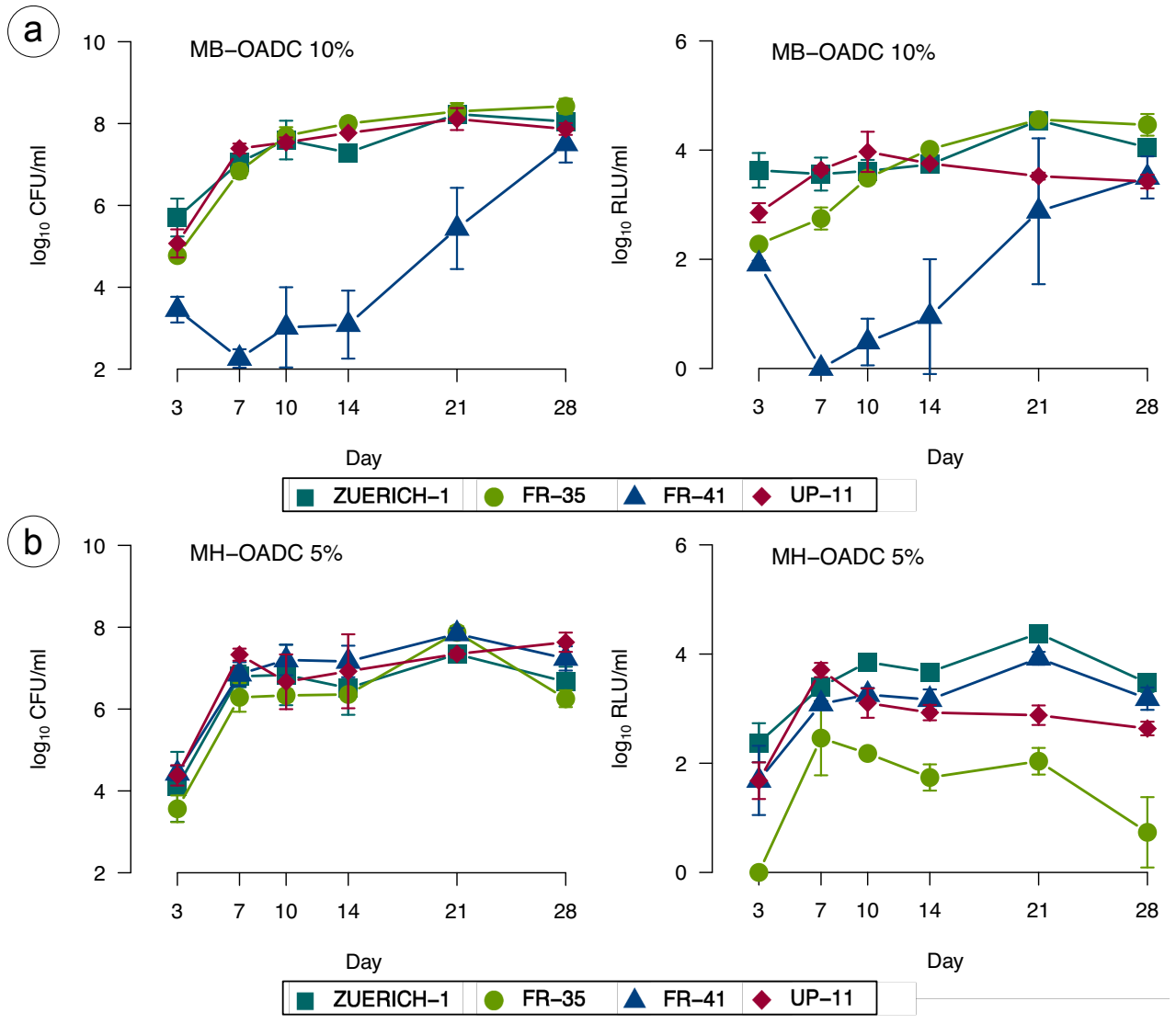

Figure 3.1.4: *M. chimaera* biofilm growth curves

M. chimaera biofilm cultivated in MB-OADC **(a)** and MH-OADC **(b)**. Total number of bacteria was analysed by plating (CFU/mL) and the metabolic activity was analysed by ATP-measurement (RLU/mL). Displayed are means and standard deviations of three individual biological replicates.

to almot 0 RLU/mL. Thereafter, the ATP increased until it reached a similar level as documented for the other isolates at day 28.
In the MH-OADC, the isolate FR-41 grew absolutely similar to the other isolates and did not show any delay in growth. Until day 7 the biofilms showed an exponential growth, staying at stable levels until day 14 after which a slight increase in CFU/mL was documented. Except for UP-11, all isolates showed a slight decrease in numbers after day 14.
The ATP measurement showed similar metabolic behaviour of ZUERICH-1 and FR-41. The metabolic activity of UP-11 increased at first and was stable after day 7. Interestingly, the isolate FR-35 represented the lowest metabolic activity, with a minimum of almost 0.1 RLU/mL at day 3. Thereafter, the metabolic rate increased till day 7 and stayed stable at a level of approx. 2 RLU/mL until day 21, then the metabolic activity decreased again.

In summary, in MB-OADC three out of four isolates grew almost identical, while FR-41 was retarted. In MH-OADC this delay was not occurring and the metabolic activity of the four isolates was less similar than in MB-OADC. As the growth behaviour of FR-41 in MB-OADC medium strongly differed from the other isolates, this isolate was excluded from further analysis of ECM composition and susceptibility testing.
In addition, the isolate *M. avium* ATCC 15769 was used as it is the common reference isolate taken for disinfectant testing. In comparison to the remaining *M. chimaera* isolates, *M. avium* ATCC 15769 showed a very similar growth behaviour in MB-OADC and further the reproducibility between individual repetitions was also tested (supplementary figure S.10).

3.2 Biofilm structure

The microscopic presentation of the biofilm was an important step to get an impression of how the biofilms are structured and composed. Due to the 3-dimensional structure of the porous glass beads, the image recording of CLSM and SEM was limited to two different perspectives, the top and the bottom of the beads (figure 2.5.1).
The presented images reflect a representative selection of all gained microscopic impressions. The images were cropped and the whole images optimized for brightness and contrast using Affinity Photo[1].

3.2.1 *Mycobacterium abscessus*

The biofilms of the two morphotypes of *M. abscessus*, smooth and rough, displayed strong differences in their architecture. While both smooth isolates covered the complete surface of the glass particles in an almost mono-layered film, the rough isolates aggregated in-between the glass particles, attaching only at limited positions to the surface (figure 3.2.1 & figure 3.2.2). In one sample of *M. abscessus* $35/14^{rg}$, the major amount of bacteria aggregated to one macro-colony that reached a diameter of almost 0.5 mm (figure 3.2.1 d). In general, the visible amount of extracellular matrix was similar between the isolates.
The majority of *M. abscessus* $25/14^{sm}$ was evenly distributed as mono-layered biofilm structure over the complete glass surface of the PGBs (figure 3.2.1 a). Partially, the bacteria aggregated in the edges of the glass particles. In-between the bacteria, ECM was visible. It also covered the glass surface as tiny particle structures (figure 3.2.1 c, arrow 1). The same was documented for *M. abscessus* $09/13^{sm}$ for which this observation was even more pronounced (figure 3.2.2 c, arrow 1).
The rough morphotype $35/14^{rg}$ showed strong aggregation of macro colonies in-between the single glass particles of the beads (figure 3.2.1 d). Partially, the bacteria covered the glass surface and thereby attached the macro-colony to the substrate (figure 3.2.1 d, arrow 2). The majority of the bacteria in the biofilm of $35/14^{rg}$ was densely packed and thereby formed a structure that reminds one of dough. The highest resolution images showed, that the bacteria were tightly packed (figure 3.2.1 f).

The structure of the biofilm of $09/13^{sm}$ was similar to $25/14^{sm}$, which indicates that the general structure of the biofilm of smooth *M. abscessus* isolates in this cultivation model can be assumed as a mono-layered biofilm. Still, in the edges of the glass particle this isolate also aggregated with higher amounts of bacteria. The covering of the glass surface of the beads with ECM particles was more obvious than documented for $25/14^{sm}$ (figure 3.2.2 c, arrow 1).
The isolate $58/15^{rg}$ displayed a biofilm architecture that was almost identical to $35/14^{rg}$, largely consisting of macro-colonies of highly-dense packed bacteria. Still, the aggregate showed the construction of indentions which presumably represent water or nutrient tunnels (figure 3.2.1 f, arrow 2).

[1] Affinity Photo [1.10.4; Serif (Europe) Ltd.]
`www.affinity.serif.de/photo` - last checked January 11, 2023

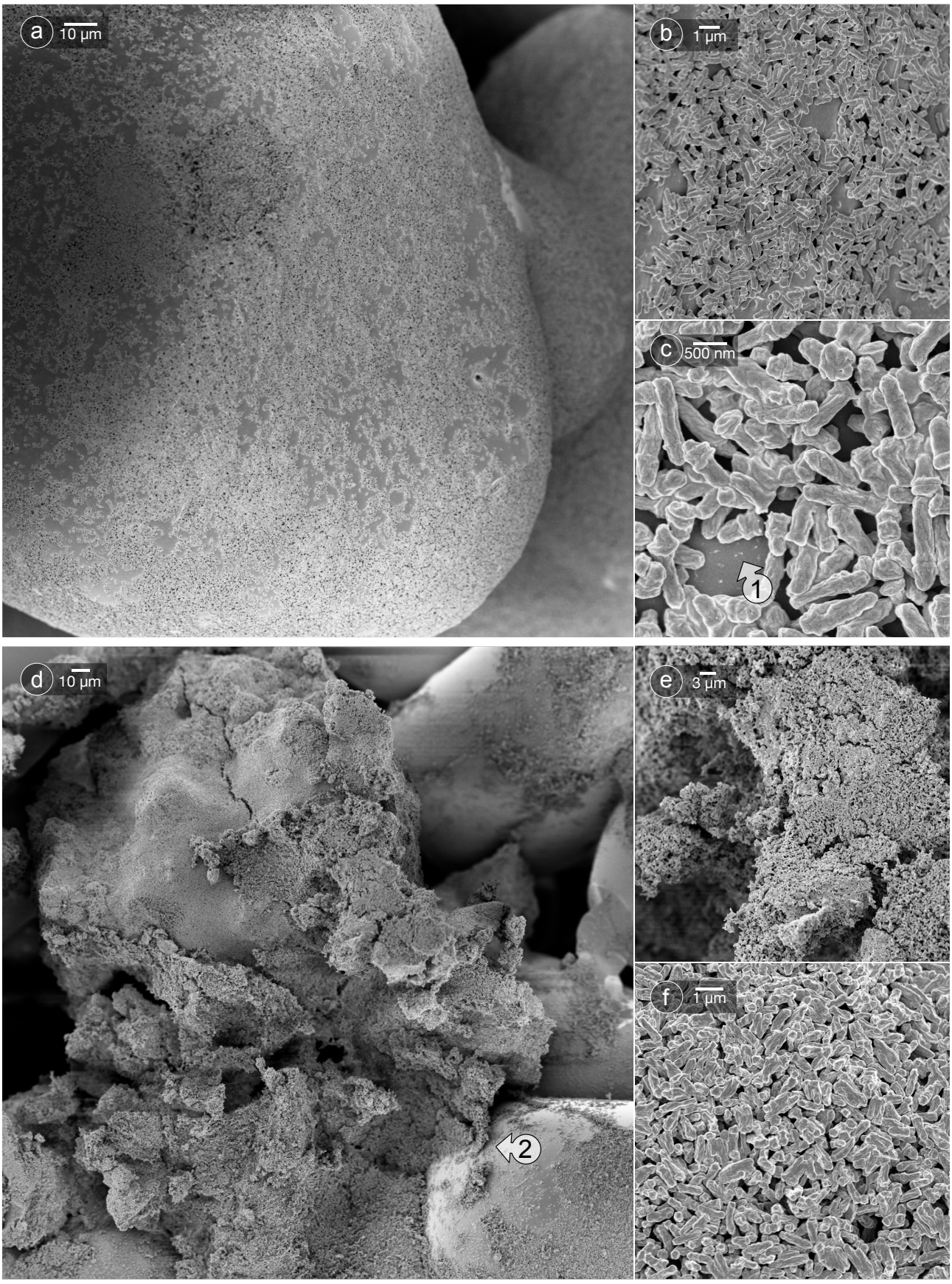

Figure 3.2.1: SEM images of 25/14^{sm} and 35/14^{rg}

Scanning electron microscopy of *M. abscessus* 25/14^{sm} and 35/14^{rg} biofilms cultivated on porous glass beads in MB-OADC. The smooth isolate 25/14^{sm} grew as a mono-layered structure, evenly covering the surface of the glass particles (**a, b, c**). On the surface of the glass, small particles were visible between the bacteria (**arrow 1**).
The rough isolate 35/14^{rg}, grew as a macro-colony formed of highly-dense packed bacteria, (**d, e, f**). Partially the aggregates attached to the glass surface (**arrow 2**).

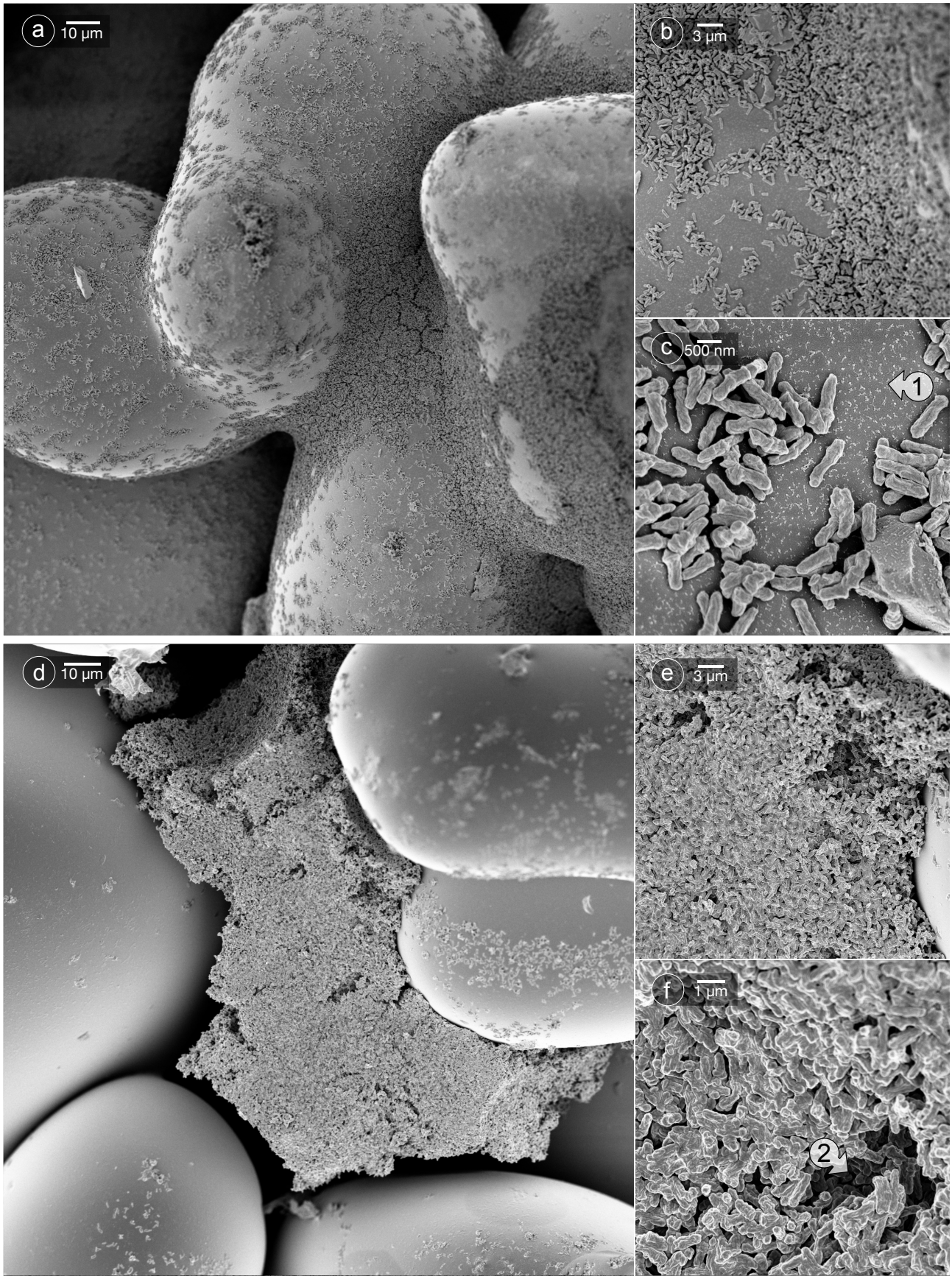

Figure 3.2.2: SEM images of 09/13^{sm} and 58/15^{rg}

Scanning electron microscopy of 09/13^{sm} and 58/15^{rg} biofilms cultivated in MB-OADC on porous glass beads.
The growth behaviour of this pair of morphotypes was similar to the behaviour of the isolates 25/14^{sm} and 35/14^{rg}. 09/13^{sm} grew mostly in a mono-layered structure, aggregating in the edges of glass particles **(a, b, c)**. The surface of the glass was overlayed with small particles (**arrow 1**).
58/15^{rg} formed macro-colonies that settled in-between glass particles with low numbers of bacteria directly attaching to the glass surface **(d, e, f)**. Within the densely packing of bacteria, indentations or tunnels are visible (**arrow 2**).

CLSM

The confocal laser scanning microscopy (CLSM) revealed the distribution of biofilm components in the biofilm structures of the *M. abscessus* isolates.
The analysis of $25/14^{sm}$ and $35/14^{rg}$ displayed the different structures of both phenotypes (figure 3.2.3). While the smooth morphotype ($25/14^{sm}$) showed a cloudy structure, the rough isolate ($35/14^{rg}$) presented a compact packing, which confirmed the results gained by SEM imaging. In both cases, the analysed ECM components did not show any further structural differentiation or uneven distribution within the biofilm. In all observations, a strong correlation of the position of bacteria and the analysed components was recorded.

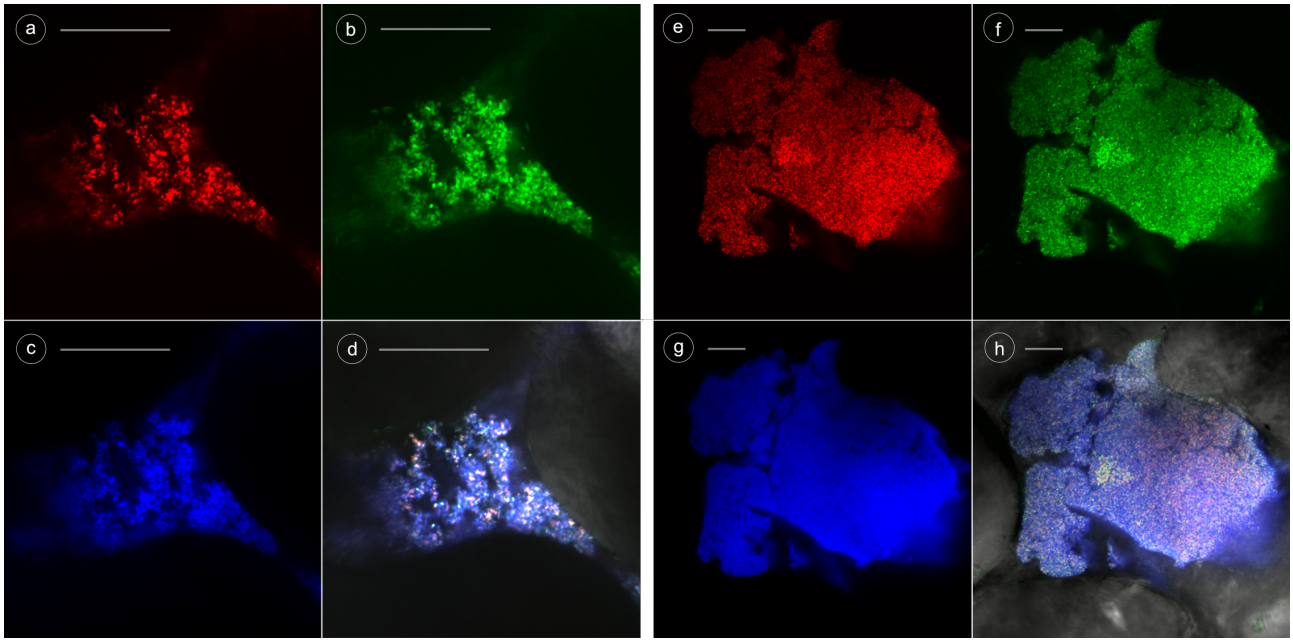

Figure 3.2.3: CLSM images of $25/14^{sm}$ and $35/14^{rg}$ biofilms

The images display the biofilms of *M. abscessus* isolates $25/14^{sm}$ **(a - d)** and $35/14^{rg}$ **(e - h)** on porous glass beads. The scanning was done with a 40x magnitude and a pinhole setting of 1 AU (array unit). The laser settings were optimized for each stain to minimize background and maximize fluorescent signal. Cross signalling of dyes was excluded in separate experiments (data not shown). The settings were identical for both isolates. The bars represent a scale of 10 µm. **a)+ e)** staining of lipids by Nile Red; **b)+ f)** staining of DNA by SYTO 9; **c)+ g)** staining of amyloid protein structures by Thioflavin T; **d)+ h)** merged images with additional transmission light channel.
In both isolates the distribution of the different targeted molecules was very even and corresponded to the biofilm associated bacteria. While $25/14^{sm}$ displayed a cloudy biofilm structure **(a-d)**, $35/14^{rg}$ showed a strong and dense packing of bacteria into a huge aggregate similar to what was documented by SEM imaging **(e-h)**.

3.2.1.1 Cord Formation

When grown as biofilm in MH for seven days, the *M. abscessus* isolates showed an extensive production of biofilm. The same was not documented when the biofilm was cultivated in MB-OADC. This was most pronounced for the isolate 09/13^{sm} which produced a cloudlike biofilm domain (figure 3.2.4 arrow '1') that reached a similar size as the porous glass bead (figure 3.2.4 arrow '2'). The other smooth *M. abscessus* isolate (25/14^{sm}) also showed this biofilm component, though in comparison it was smaller. In both cases, the biofilm domain was still linked to the glass bead or surrounded it. The separate biofilms domain was not documented in the rough strains, though they covered the PGBs with a thick gelatinous structure.
The biofilm domain was stable even after sonication and could only be dissolved when the beads were boiled in H_2O for at least 20 min at 96 °C. It can be assumed that the CFU quantification of bacteria was hampered by that circumstance.
The loosely attached biofilm domain produced by *M. abscessus* 09/13^{sm} was used for further analysis by SEM. Thereby, the bacteria were found to form cords. The whole structure was of a size of approx. 0.5 – 0.8 cm in diameter. The overall structure was a knot of cord-like aggregates of bacteria that aligned parallel to each other forming long cords. In case of 09/13^{sm}, the bacteria were wrapped in an extracellular matrix (figure 3.2.5).

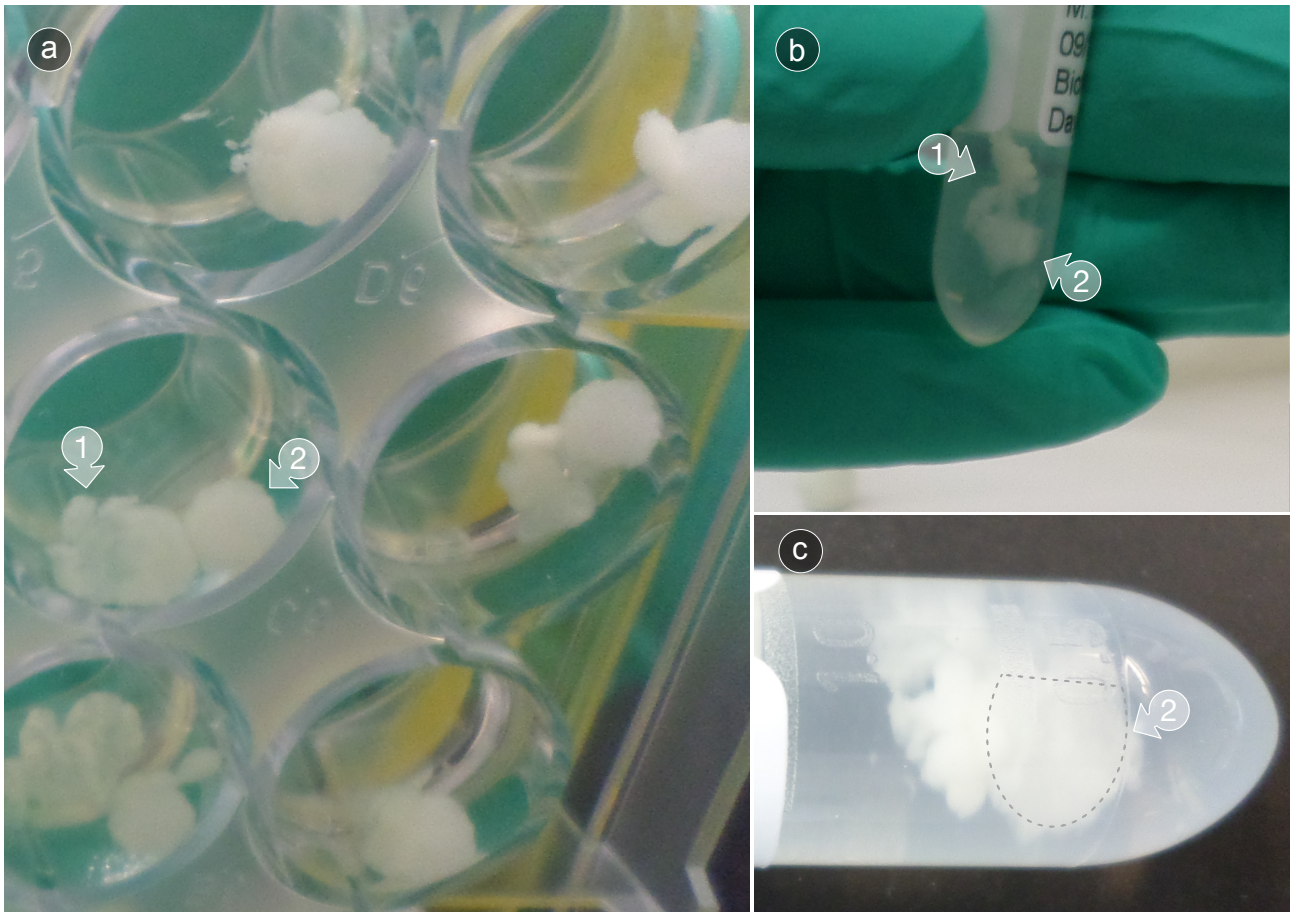

Figure 3.2.4: Cord formation of 09/13^{sm} in a 24-well plate
a) Grown in MH the isolate 09/13^{sm} as well as the isolate 25/14^{sm} (data not shown) displayed the formation of a second biofilm domain (arrow '1') besides or surrounding the porous glass beads (arrow '2'). **b)** The formed biofilm domain with cord formation was in all tested cases linked to the porous glass bead, which was checked by carefully lifting the structure using a pipette. **c)** In most cases the biofilm domain was of comparable size as the PGB (arrow '2').

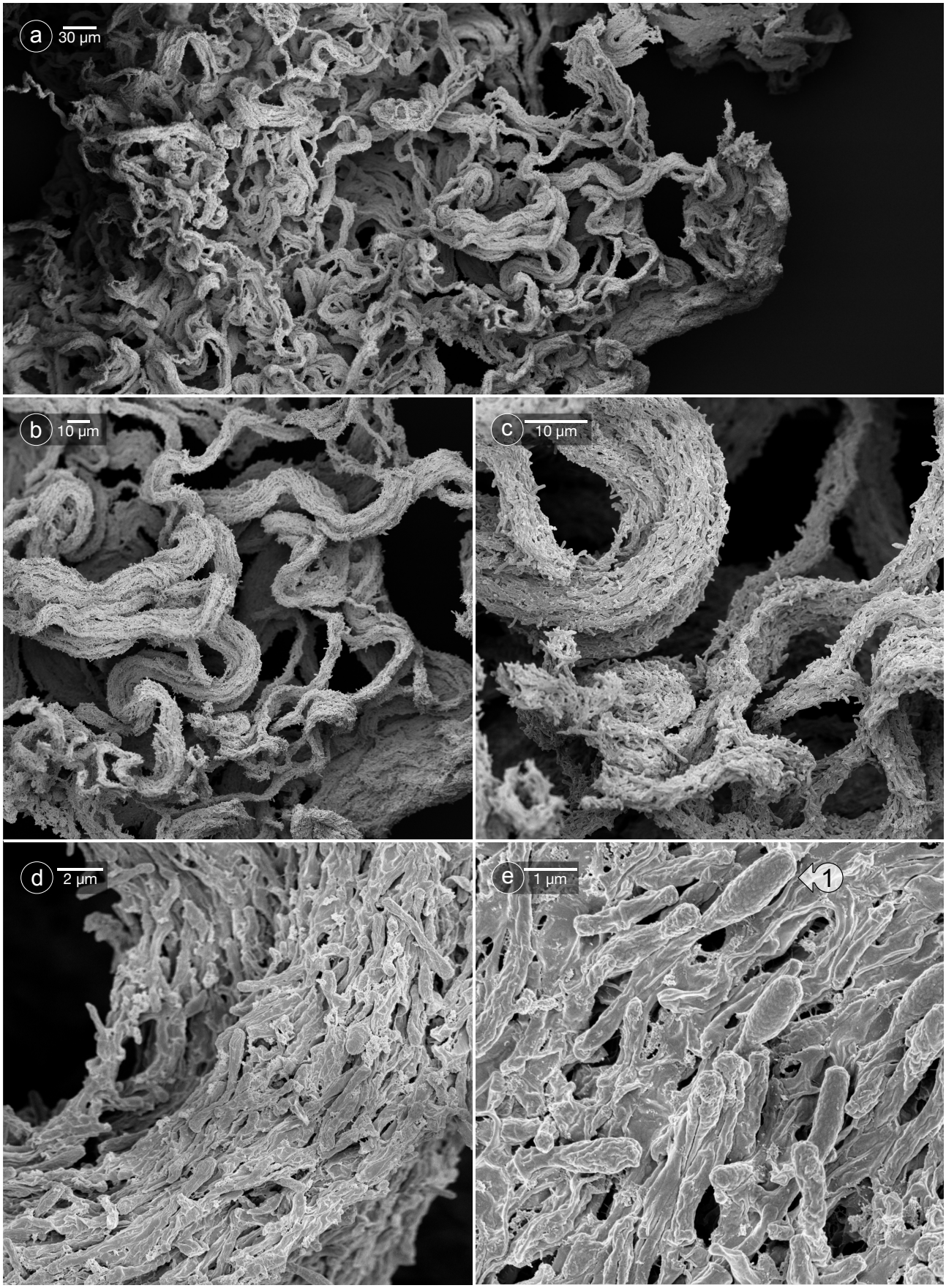

Figure 3.2.5: *M. abscessus* 09/13^{sm} cording phenotype grown in MH.

Upscaled SEM images of the cording phenotype produced by *M. abscessus* 09/13^{sm} when grown as biofilm in MH (**a-e**). Besides the biofilm associated bacteria, that directly attached to the PGB surface, the isolate showed the production of a second cloud-like biofilm domain (figure 3.2.4). While the overall structure was comparable to a cable bundle (**a-c**), the higher magnifications showed the alignment of the bacteria to long cords thickly covered in matrix (**d + e**). The bacteria showed an elongated shape and partially a thickening at the end of the cell (arrow 1).

Interestingly, the single bacteria displayed an elongation when compared to the SEM imaging of biofilm grown in MB-OADC (figure 3.2.2). Moreover, some bacteria presented a thickening of one end of the cell (figure 3.2.5 e, arrow 1).

For the rough morphotype 58/15^{rg} cord formation in a separate biofilm domain was not documented. Though, the growth differed strongly in the two used culture media (figure 3.2.6). While a strong aggregation of bacteria was recorded when the isolate was cultivated in MB-OADC (figure 3.2.6 a-c), in MH, the isolate instead distributed over the whole surface of the glass particles showing no extensive aggregation of bacteria (figure 3.2.6 d-f). The bacteria were elongated and partially thickly embedded in extracellular matrix. Also this isolate displayed an elongation of cells when cultivated in MH.

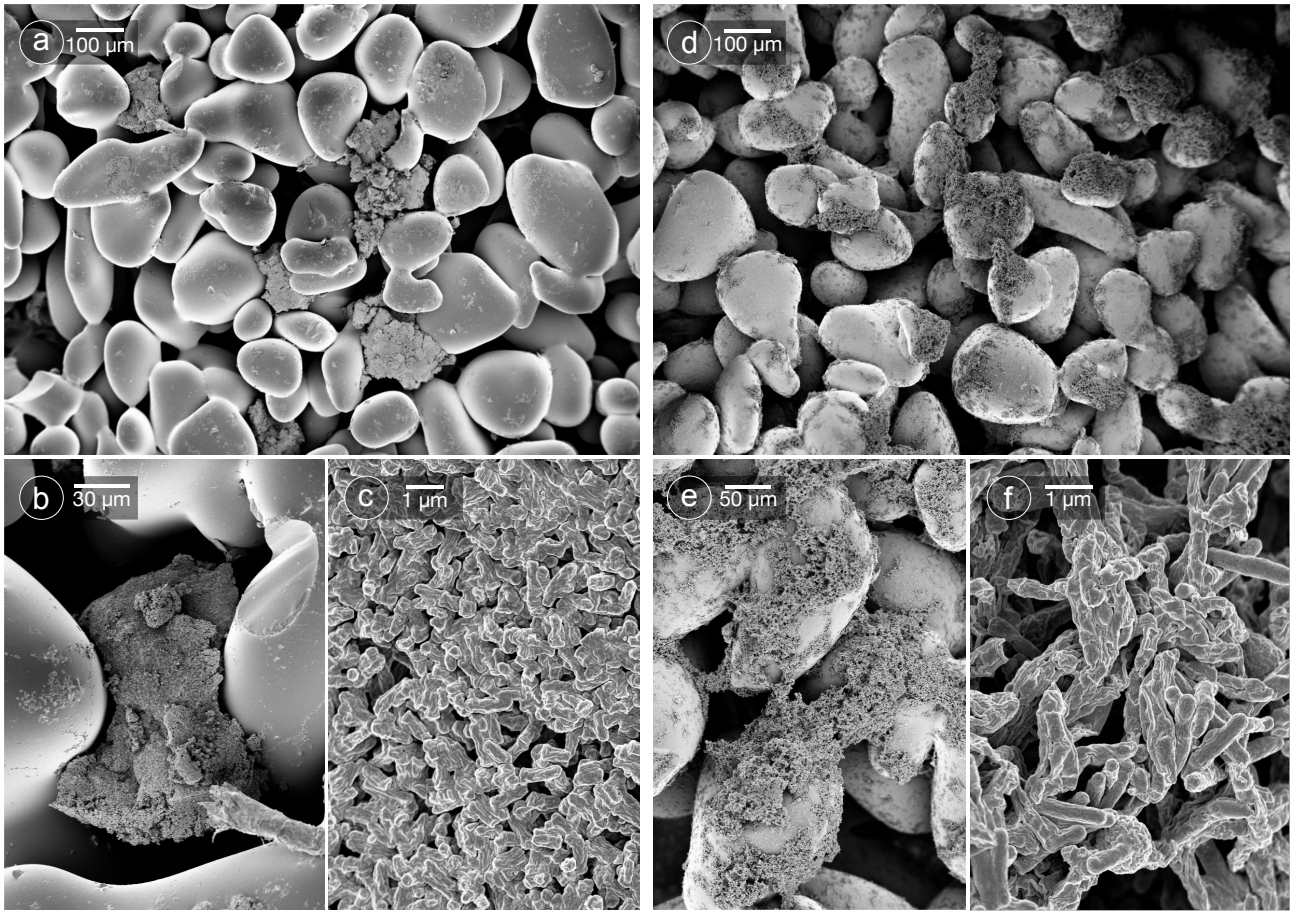

Figure 3.2.6: *M. abscessus* 58/15^{rg} biofilm in MB-OADC (a-c) and MH (d-f) on porous glass beads

Upscaled SEM images of *M. abscessus* 58/15^{rg} grown as biofilm in MB-OADC (**a - c**) and MH (**d - f**) medium in upscaled comparable images.
The isolate grew in MB-OADC as large aggregative biofilm colonies, that settled in-between the glass particle structure (**a - c**). On the contrary, in MH the isolate grew widely distributed over the complete glass surface of the PGBs (**d-f**).
The highest magnification (**c, f**) showed that the density of the aggregates differed in both growth conditions, showing that in MB-OADC the bacteria were more tightly packed. Moreover, in MH (**f**) the single bacteria showed a slightly elongated shape and a more prominent ECM formation.

3.2.2 *Mycobacterium chimaera*

Also the *M. chimaera* isolates formed surface-attached biofilms. The isolates ZUERICH-1, FR-35 and UP-11 formed an adhesive biofilm on the porous glass beads that covered inner and outer parts of the glass particles (figure 3.2.7 a-f & figure 3.2.8 a-c). The aggregates in the inner spaces contained much more bacteria than colonies that attached to the outer glass surface. In comparison to the *M. abscessus* isolates, the presentation of ECM was more pronounced in *M. chimaera*. Although *M. chimaera* formed multi-layered biofilm structures, the density of the packing was less intense as documented for rough *M. abscessus* isolates.
The majority of the biofilm-associated bacteria of ZUERICH-1 settled in inner parts of the PGBs between the cavities of the glass particles (figure 3.2.7 a). The bacteria were embedded in a net-like structure of ECM, which either covered or linked the bacteria (figure 3.2.7 c arrow 1). The overall growth pattern of the biofilm of *M. chimaera* FR-35 was similar to ZUERICH-1. The predominant part of bacteria formed aggregates on the inner parts of the PGBs and attached in smaller aggregates (< 100 bacteria) on the outer surface of the glass particles (figure 3.2.7 d). Comparable to ZUERICH-1, the bacteria were partially embedded in a thick layer of ECM (figure 3.2.7 f arrow 2).
Also the isolate UP-11 showed biofilm growth on the inner and outer parts of the glass particles (figure 3.2.8 a-c). Though, in comparison to the other isolates the colonies of UP-11 that attached to the outer surface presented a special feature. The aggregates were such heavily embedded in a matrix that the identification of single cells was in most cases not possible (figure 3.2.8 c arrow 1). Moreover, the bacteria presented a less elongated shape as documented for ZUERICH-1 and FR-35. This extent of matrix formation was not documented for the other isolates tested. CLSM imaging of UP-11 showed that the ECM, which thickly covered the aggregates, was mostly consisting of eDNA and lipids (data not shown).
Since FR-41 did not reliably form biofilm on PGBs when grown in MB-OADC, multiple beads were analysed by SEM imaging until representative images could be made. It was found that the isolate FR-41 formed huge aggregates similar to those, that have been documented for rough *M. abscessus* morphotypes (figure 3.2.8 d-f). Although, the aggregates of the *M. chimaera* isolate showed more phenotypical diversities in-between the aggregates. In majority, the bacteria were less dense packed, representing a more sponge-like structure showing more tunnels and holes. In a few parts, the bacteria displayed a dense aggregation that was similar to the clumpy structure of the rough *M. abscessus* isolates (figure 3.2.8 d arrow 2). Interestingly, FR-41 showed no additional production or covering with a net-like ECM.

The biofilm structure of the isolate *M. avium* ATCC 15769 was also analysed by SEM (supplementary figure S.11). It presented a similar structure compared to the *M. chimaera* isolates ZUERICH-1 and FR-35. The biofilm aggregates attached to inner and outer parts of the PGBs. Partially the biofilm formed bridge-like connections between glass particles which were not documented neither for the *M. chimaera* nor the *M. abscessus* isolates (supplementary figure S.11 a arrow 1).

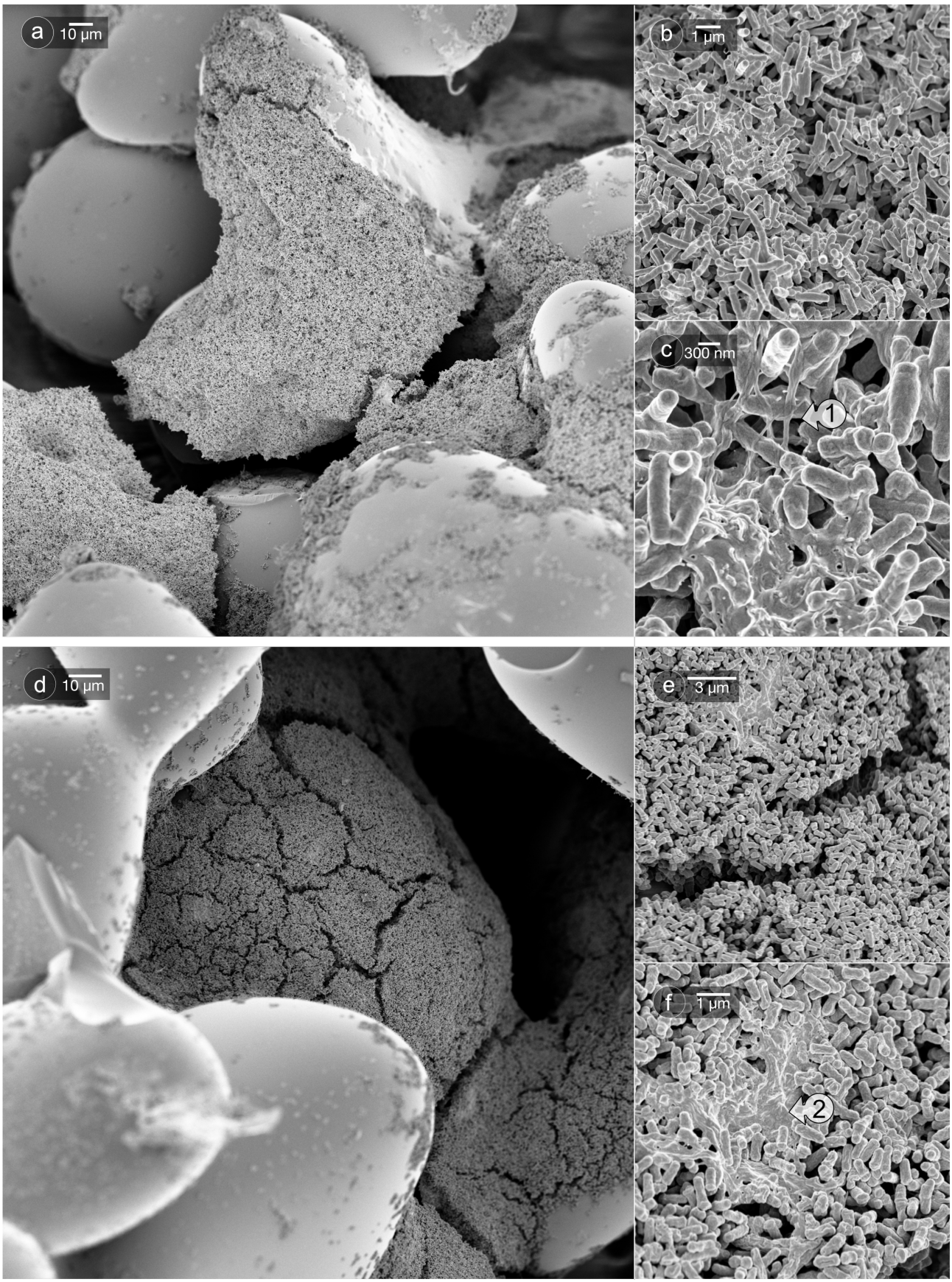

Figure 3.2.7: SEM images of ZUERICH-1 and FR-35 biofilms on porous glass beads

Scanning electron microscopy of ZUERICH-1 (**a-c**) and FR-35 (**d-f**) biofilms cultivated in MB-OADC on porous glass beads. Both isolates displayed biofilm growth on the inner and outer surface of the glass particles.
The highest magnification showed ECM covering the bacteria (**c,f**), while some parts were more densely covered than others.

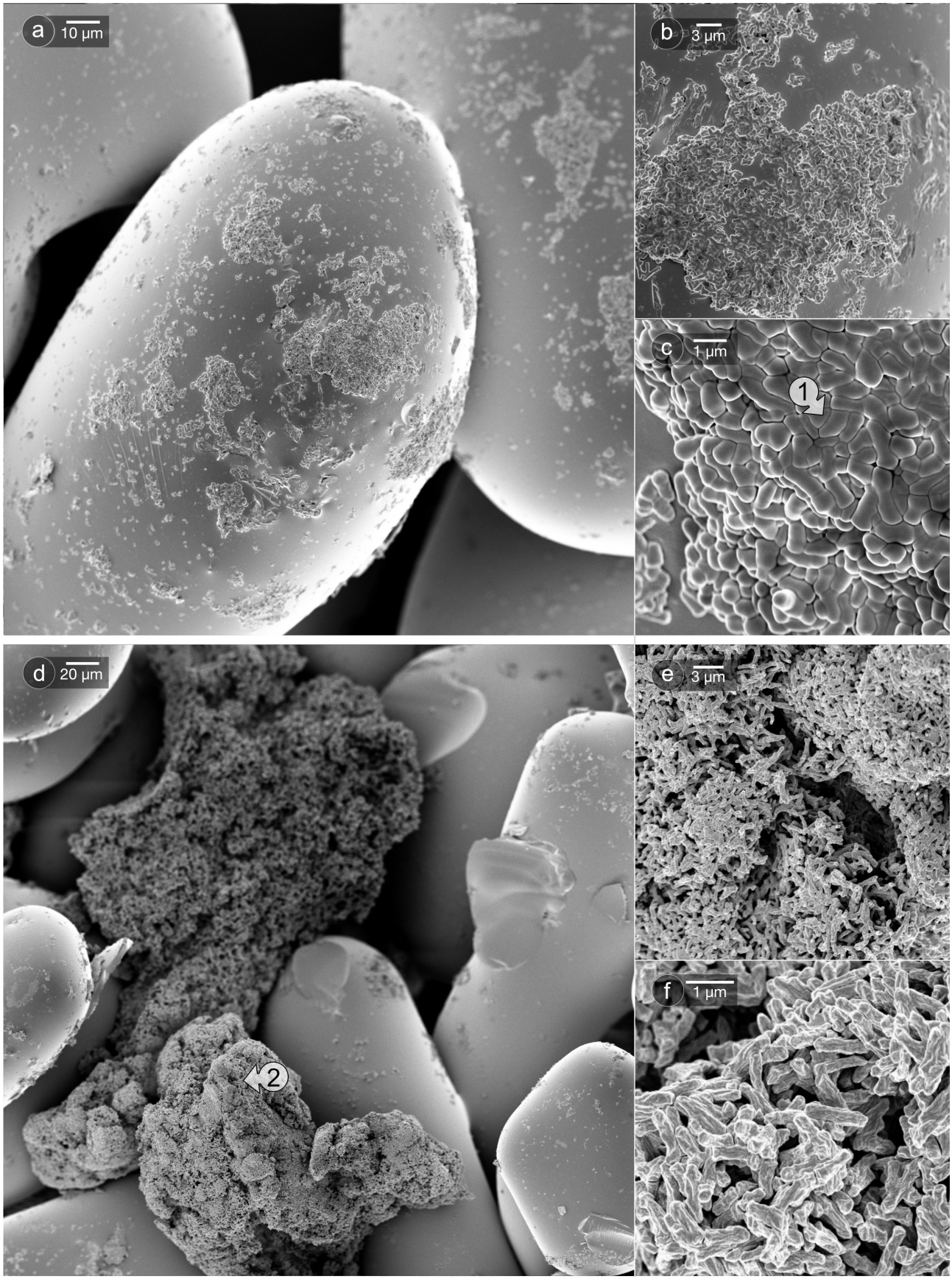

Figure 3.2.8: SEM images of FR-41 and UP-11 biofilms on porous glass beads
The isolates were cultivated as biofilm in MB-OADC on PGBs.
a)-c) UP-11 grew on the outer and inner parts of the PGBs. In comparison to the other isolates (figure 3.2.7) the aggregates on the outer surface of the PGBs were densely packed in ECM (**c**). Due to the massive amount of ECM, the shape of single bacteria was hard to recognize (arrow 1).
d)-f) FR-41 grew completely different in comparison to the other tested *M. chimaera* isolates. FR-41 grew in huge aggregates. Withihn these aggregates the bacteria displayed a strong aggregation (arrow 2).

3.2.2.1 ECM-structure and Nanowires

All four *M. chimaera* isolates showed production of extracellular matrix that - depending on the isolate - was produced to a different extent. Additionally to the SEM analysis, the CLSM imaging confirmed the formation of net-like ECM structures (figure 3.2.9). The fluorescent labelling showed the complete covering of the glass surface with a net-like ECM consisting of proteins, lipids and eDNA. The 3D-imaging showed that the net-like ECM strings not only distributed over the glass surface, but were also sticking out orthogonal (figure 3.2.9 a). Another finding was, that the location of the ECM did not necessarily corresponded to the location of the bacteria. In all cases, the amount of ECM was higher in colonies that attached to the outer surface of the glass particles than aggregates that grew in the inner parts of the beads (data not shown).

The net-like structures were also documented by SEM imaging in which the strings of the ECM net were still visible on the glass surface of the PGBs (figure 3.2.10 a+c arrow 1). ZUERICH-1 produced a net-like matrix that covered most of the bacteria and the surface of the glass particles (figure 3.2.7 c arrow 1 & figure 3.2.9 a-c & figure 3.2.10 a+c arrow 1). The filamentous strings spread over the surface in a fine net. Due to the dehydration process in the preparation for SEM imaging, the ECM-structure partially collapsed. FR-35 also produced net-like ECM comparable to ZUERICH-1 but to a lower extent, in the other isolates this was not documented (data not shown).
The micro-colonies of UP-11, that grew on the outer parts of the glass particles, were most densely

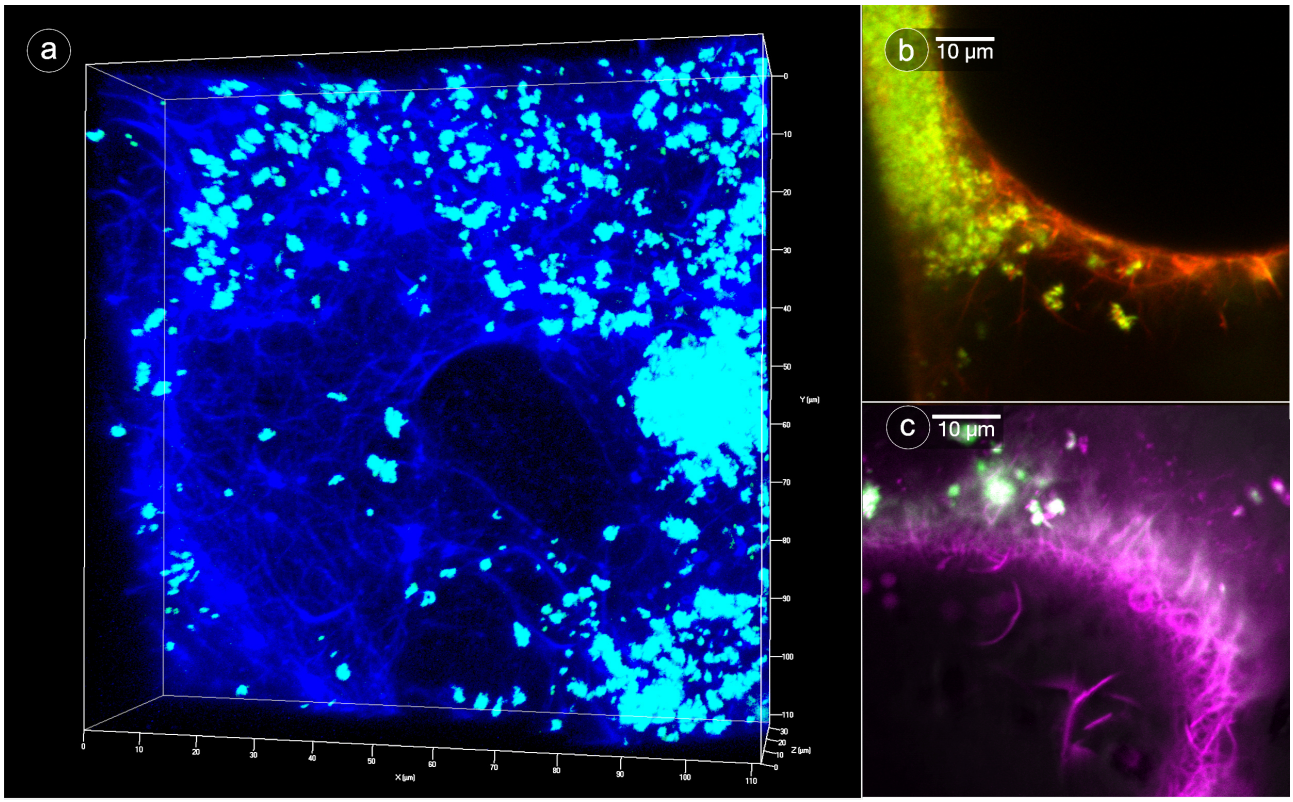

Figure 3.2.9: CLSM images of ZUERICH-1 biofilm

Biofilms of ZUERICH-1 were analysed by CLSM imaging. Thereby the different compartments of the biofilms were stained with different fluorescent labels.
The imaging showed that the glass particles of the PGBs were covered with a net-like structure of ECM. These nets were consisting of proteins (a), lipids (b) and eDNA (c). In all samples the distribution of the bacteria and the ECM were not congruent.
a) The bacteria were stained with Syto9 (DNA; turquoise) and SYPRO Orange (Protein structures; blue).
b) The bacteria were stained with Syto9 (DNA; green) and nilered (Lipids; red).
c) The bacteria were stained with Syto9 (DNA; green) and Bobo-III (eDNA; purple).

packed in matrix. CLSM analysis showed that this ECM was majorly made of eDNA and lipids (data not shown). In comparison, the isolates FR-35 and FR-41 showed less visible amount of extracellular matrix (figure 3.2.7 d-f & figure 3.2.8 d-f).

Detailed SEM-imaging of ZUERICH-1 showed the formation of so-called nanowires between the bacteria (figure 3.2.10 a+b arrow 2). These structures were formed in micro-colonies on the outer surface of the PGBs but also within macro-colonies that were documented in the cavities between the inner glass particles (figure 3.2.10 b arrow 2).
In comparison to the filamentous ECM net (figure 3.2.10 a+c arrow 1), the detected nanowires were a thicker structure, bridging shorter distances between two single bacteria (figure 3.2.10 a+b arrow 2). These nanowires were also documented in high-resolution SEM images of the other isolates tested (data not shown).

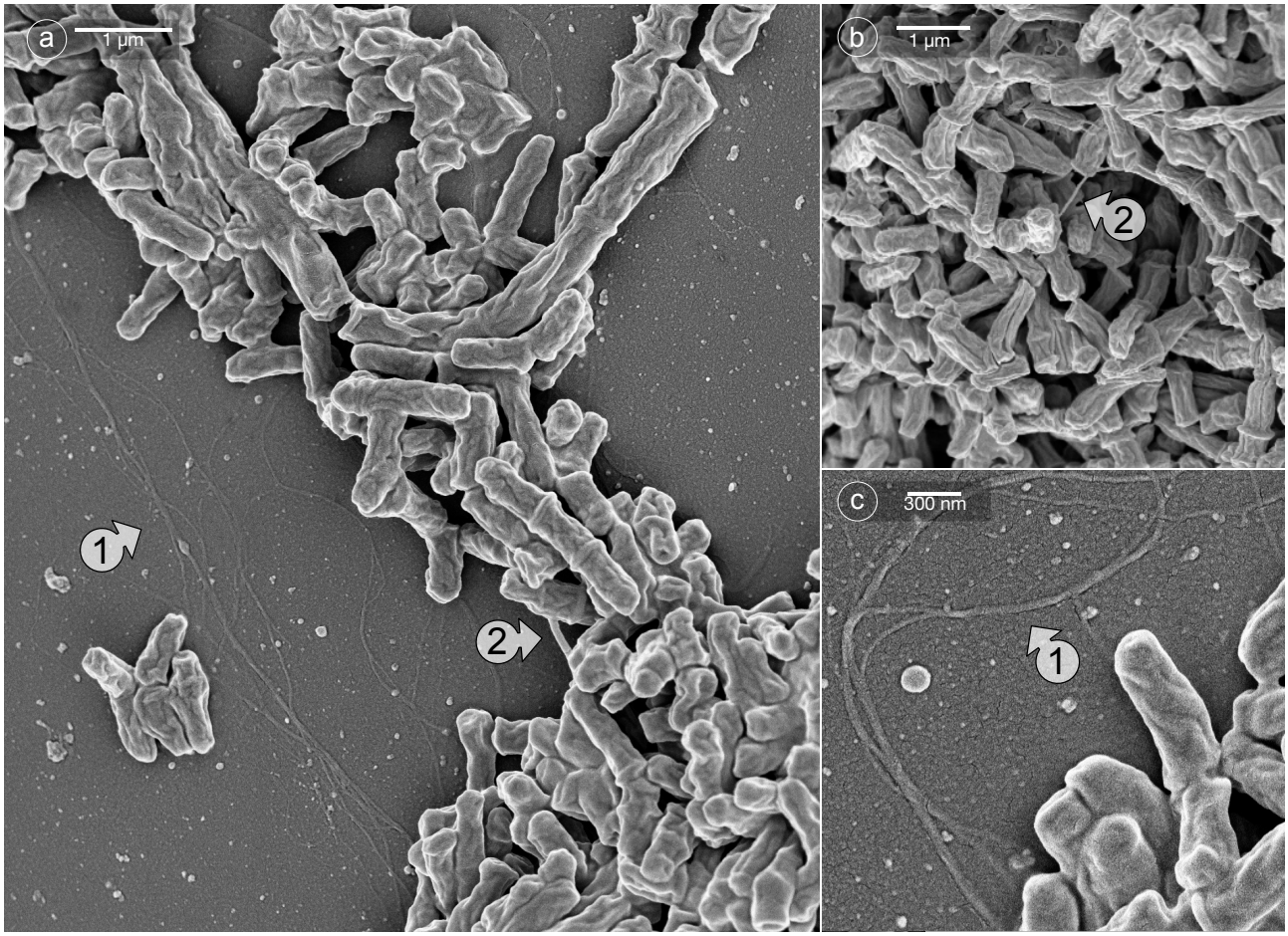

Figure 3.2.10: SEM images of ECM and nanowires formed by ZUERICH-1 biofilm
SEM images of ZUERICH-1 biofilm grown on the surface of the PGBs forming a net-like ECM-structure (arrow 1) and nanowires (arrow 2) between and surrounding the bacteria (**a-c**).

ZUERICH-1 was grown in MB-OADC as biofilm on PGBs for 21 days. Microcolonies of bacteria that attached to the surface of the glass particles showed formation of nanowires and net-like structures of ECM.
Similar to what was documented by CLSM imaging (figure 3.2.9) the bacteria in the biofilm and the surrounding glass surface were covered by a net-like ECM structure. These nets partially covered the glass surface (arrow 1). The nanowire structures (arrow 2) linked single bacteria.

3.3 Biofilm composition

Besides the biofilm structure, the evaluation of the composition of the extracellular matrix was of great interest as it could help to identify components of the biofilm which are influencing the susceptibility against antimicrobials.
In a first approach, the microscopic analysis revealed the occurrence and the distribution of the different matrix components within the biofilm structure (figure 3.2.3 & figure 3.2.9). But in order to analyse the mass relationship, it was aimed to quantify to overall biomass of proteins, DNA and lipids in biofilm and suspension (figure 3.3.1 and figure 3.3.2).

Mycobacterium abscessus

The quantification of the ECM components in *M. abscessus* showed, that in all biofilms, the biomass per bacterium was higher than in suspension (figure 3.3.1 d). The highest difference was found for the isolate 58/15^{rg} while in the corresponding smooth isolate 09/13^{sm} the difference between suspension

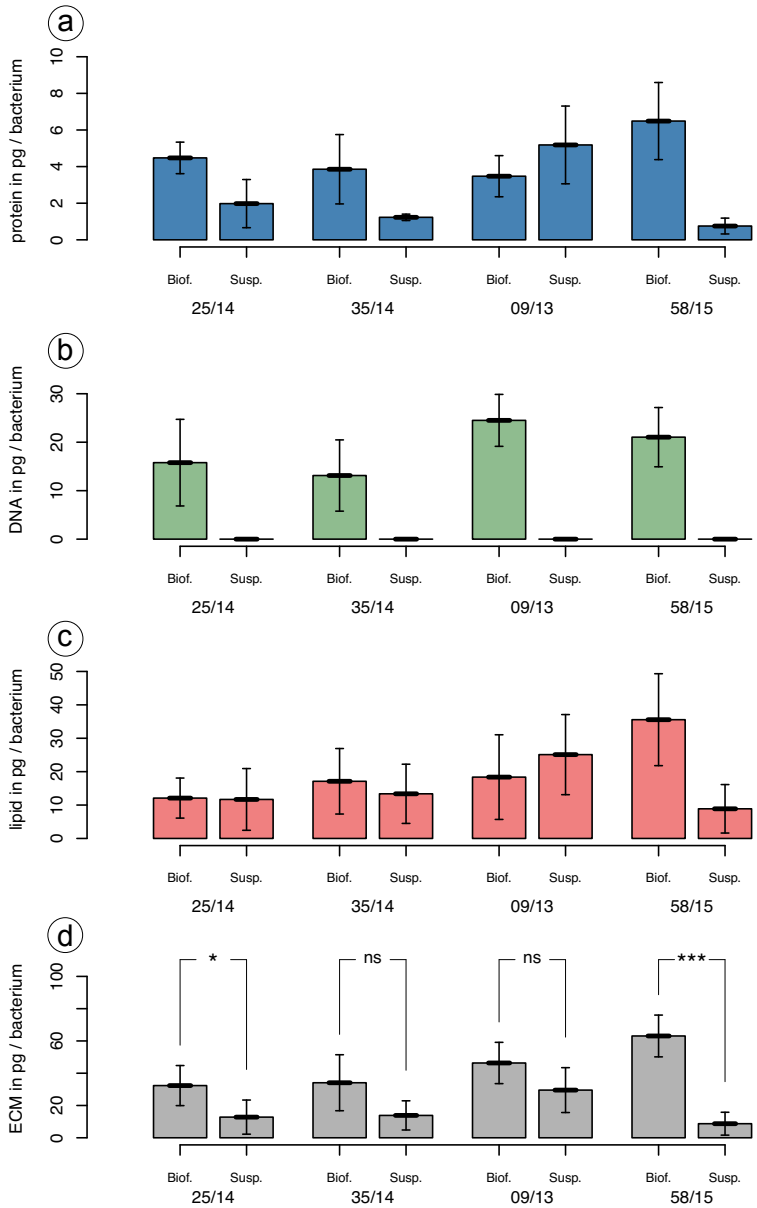

Figure 3.3.1: *M. abscessus* ECM composition

The amount of protein, DNA and lipids per bacterium were analysed for biofilm and suspension of each *M. abscessus* isolate.
a) displaying the amount of protein per bacterium. The evaluations showed that - except for 09/13^{sm} - the biofilm associated bacteria produced more pg protein per bacterium when compared to the corresponding suspension. The difference between biofilm and suspension was most pronounced for 58/15^{rg}.
b) The quantification of DNA per bacterium showed clearly that biofilm associated bacteria have up to the 25-fold of DNA in pg/bacterium when compared to the suspension.
c) The lipid quantification showed that only the isolate 58/15^{rg} displayed clear differences in the amount of lipid in pg/bacterium. For the other isolates no obvious difference was documented.
d) Comparing the overall amount of ECM components between biofilm and suspension showed only for 25/14^{sm} and 58/15^{rg} a significant difference in the amount of quantified ECM components per bacterium. In all isolates, the biofilm contained more biomass than the corresponding suspension.
Bars represent the mean with standard deviation of five biological replicates. Significance was confirmed by unpaired t-test (* $<$ 0.05, ** $<$ 0.01, *** $<$ 0.001, ns = not significant).

and biofilm was not significant. The suspension of 58/15^{rg} displayed only 10 pg/bacterium and the biofilm contained approx. 65 pg/bacterium, which was a highly statistically significant difference (***) (figure 3.3.1 d).

In the biofilms of three out of four isolates the protein biomass was higher than in the corresponding suspension. Only 09/13^{sm} displayed a contrary distribution (figure 3.3.1 a). The pair of morphotype isolates from patient D, 25/14^{sm} and 35/14^{rg}, displayed similar levels of protein in biofilm (4 pg/bacterium) and suspension (2 pg/bacterium). The suspension of 58/15^{rg} displayed only 1 pg/bacterium protein, while in the biofilm this isolate showed approx. 6 pg/bacterium. As an exception, the isolate 09/13^{sm} produced less protein in biofilm (4 pg/bacterium) than in the suspension (5 pg/bacterium).
All *M. abscessus* isolates displayed a much higher amount of pg DNA per bacterium in the biofilm samples. In all suspensions, the amount of DNA ranged between 1 – 1.5 pg/bacterium. Again, the pair of 25/14^{sm} and 35/14^{rg} reached a similar level of DNA in biofilm with approx. 12 – 15 pg/bacterium (figure 3.3.1 b). In case of 09/13^{sm} the biofilm contained up to the 25-fold of DNA when compared to the suspension and the rough morphotype 58/15^{rg} showed approx. 20 pg/bacterium in biofilm.
For 25/14^{sm} and 35/14^{rg} biofilm and suspension showed a lipid amount of approx. 10 – 15 pg/bacterium. In 09/13^{sm}, the suspension (25 pg/bacterium) presented slightly more lipids than the biofilm (20 pg/bacterium). The amount of lipids was in three out of four isolates similar between biofilm and suspension, the biofilm of 58/15^{rg} contained the 4-fold mass of lipids when compared to its suspension (figure 3.3.1 c).

Mycobacterium chimaera

For the slow growing mycobacteria, the analysis showed that the biofilms contained more biomass than the corresponding suspensions in all tested isolates (figure 3.3.2). In ZUERICH-1 the difference between both forms was highest, with 7 times more biomass in biofilm than in suspension. The difference between biofilm and suspension of isolates FR-35 and *M. avium* ATCC 15769 was less clear than for the other two isolates. Still, in three out of four isolates the biofilm contained statistically significantly more biomass than the suspension.
In the overall comparison, including all three tested molecular components, the biofilm of ZUERICH-1 displayed the highest biomass (approx. 75 pg / bacterium) also showing the highest difference in comparison to the suspension (α=**). The difference between both cultivation forms was also statistically significant (α=*) in UP-11 and *M. avium* ATCC 15769 but not in FR-35.

In the quantification of proteins, the outbreak strain ZUERICH-1 displayed a huge difference in comparison to the other isolates (figure 3.3.2 a). In biofilm, ZUERICH-1 produced approx. 15 pg/bacterium protein, while the corresponding suspension displayed approx. 1 pg/bacterium. The other samples ranged in lower levels between 1 – 3 pg/bacterium showing no big difference between biofilm and suspension.
The quantification of DNA showed similar amounts in the biofilms and suspensions in three out of four isolates (figure 3.3.2 b). The biofilms of the isolates ZUERICH-1,UP-11 and *M. avium* ATCC 15769 presented a DNA amount of approx. 6 pg/bacterium and the suspensions approx. 2 – 3 pg/bacterium.

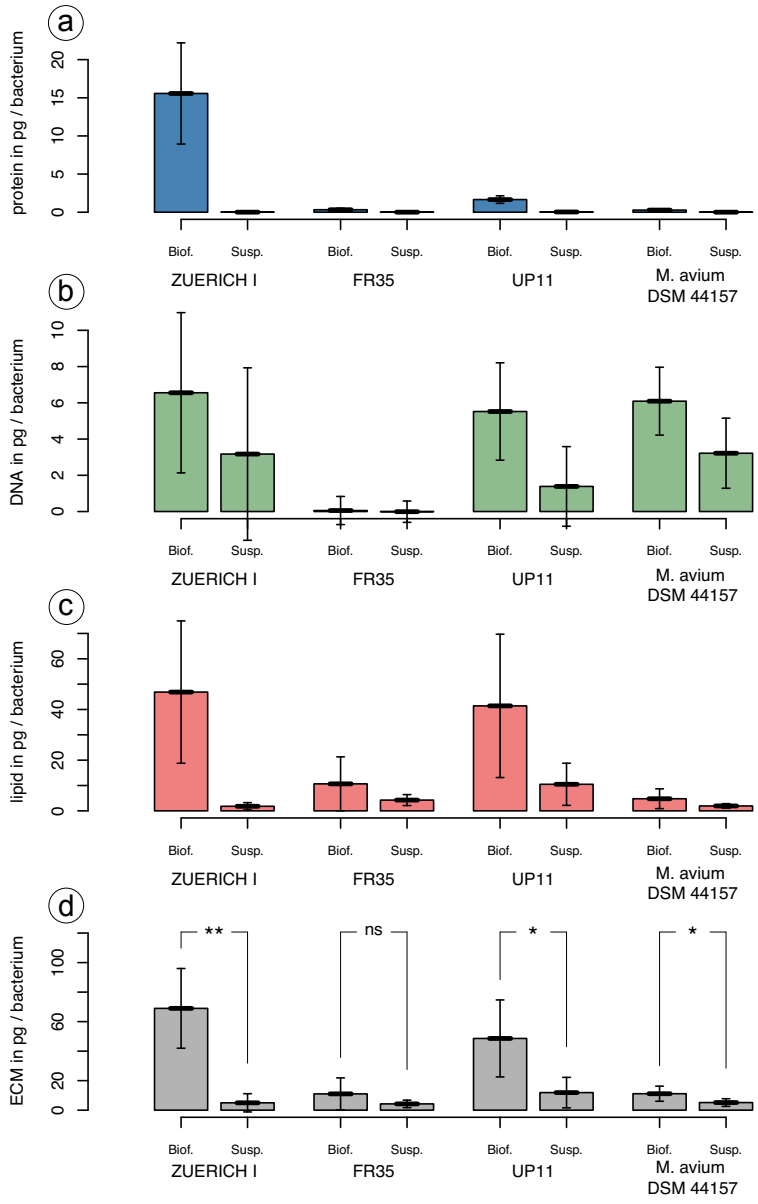

Figure 3.3.2: *M. chimaera* and *M. avium* ECM composition

The amounts of protein, DNA and lipids per bacterium were analysed for biofilm and suspension of three *M. chimaera* isolates and the isolate *M. avium* ATCC 15769.
a) ZUERICH-1 biofilm contained the highest amount of protein per bacterium and was thereby clearly exceeding the levels of the other isolates.
b) The DNA quantifications displayed a higher amount of DNA in all biofilms compared to the suspension. FR-35 had the least amount of DNA while the other isolates showed comparable amounts of DNA.
c) Also the amount of lipids was greater in all biofilm than in suspension. ZUERICH-1 and UP-11 showed similar lipids biomass, such as FR-35 and the *M. avium* isolate.
d) In the biofilm of ZUERICH-1 the measured overall biomass was the highest. Except for FR-35 all isolates showed significantly more biomass in the biofilm than in the corresponding suspension.
Bars represent the mean with standard deviation of five biological replicates. Significance was confirmed by unpaired t-test ($\alpha = 0.05$; * < 0.05, ** < 0.01, *** < 0.001, ns = not significant).

The exception was the isolate FR-35, with around 1 pg/bacterium of DNA in both cultivation forms. The isolates ZUERICH-1 and UP-11 showed highest amounts of lipids in the biofilms (40 pg/bacterium), though, the standard deviation showed that differences between individual repetitions occured (figure 3.3.2 c). The biofilms of FR-35 and *M. avium* ATCC 15769 reached only a level of approx. 8 pg/bacterium of lipids, while all suspensions ranged in lower areas between 1 – 8 pg/bacterium.

3.4 Gene and protein expression analysis of *M. chimaera* biofilms

3.4.1 Genetic background

Prior to the expression analysis, the genetic relationships of the *M. chimaera* isolates were analysed. A total of 7,578 individual genes across all four genomes was identified. The presence or abscence of genes in the MinIon-sequences of ZUERICH-1 and FR-35 and the published ENA sequences of UP-11 and FR-41 were determined. From this, the core and accessory genomes in the group of these four strains were defined.
A majority of 5,127 genes was common among all four *M. chimaera* isolates, representing the core genome and 2,452 genes were identified as parts of the accessory genome (figure 3.4.1). The isolate ZUERICH-1 contained a total of 6,374 genes and the isolate FR-35 a total of 5,945 genes. A percentage of approximately 40 % of the genes was identified as 'hypothetical protein' for which no functional description is available.

M. chimaera FR-35 showed the most accordances to ZUERICH-1 which was also described by the phylogenetic distance calculated by van Ingen et al. (2017) [131]. The analysis showed, that ZUERICH-1 and UP-11 presented similarities in the presence of genes in the accessory genome with the exception of the genes, that belong to the plasmids of ZUERICH-1. The highest difference among the isolates was represented by FR-41. The isolate had a number of 753 genes which were not present in the other isolates, including genes involved in lipid biosynthesis (*lcpA-1, lpgB*).
The outbreak strain ZUERICH-1 showed a total of 513 genes present in only this isolate (supplementary table S.1). These are linked to the presence of five plasmids (14 – 95 kbp). A majority of approximately 80 % of these genes are annotated as 'hypothetical proteins', a few of the residual genes were of special interest. These displayed for example the genes of the type VII secretion systems as well as genes responsible for resistance mechanisms (arsenic or bleomycin resistance genes).

Figure 3.4.1: Phylogenetic comparison of the tested *M. chimaera* isolates.

Graphical presentation of core and accessory genomes of the four *M. chimaera* isolates tested. In the section of the core genome (light blue) a total of 5,127 genes was identified to be common in all four isolates. Genes were voted as equal with a sequence identity of 70 % and a coverage of 90 %.
The accessory genome describes the genes that are different or lacking in at least one of the compared genomes, to which a total number of 2,452 genes belonged.
Accessory genes of ZUERICH-1 (turquoise), FR-35 (green), FR-41 (blue) and UP-11 (red).

3.4.2 Proteome

From the genome data, a total of 5,866 proteins was predicted for ZUERICH-1. Thereof the proteome analysis identified 3,970 proteins (approx. 68 %) from which 1,339 proteins were statistically significant different expressed in comparison of the three cultivation forms planktonic, suspension and biofilm (supplementary table S.2). The clustering analysis of the significantly expressed proteins showed the similarities and differences between the isolates and the tested cultivation forms based on the levels of up- and downregulation of the proteins (figure 3.4.2).
The heatmap of the isolates and cultivation forms showed, that the proteome expression profile was not isolate specific (figure 3.4.2). Still, the expression profiles were also not cultivation form specific as for example the planktonic sample of ZUERICH-1 and the suspension of FR-35 clustered.
Two major clusters were formed, each with two subbranches. In the first cluster, the biofilm and the suspension of *M. chimaera* ZUERICH-1 clustered together showing a high similarity between both cultivation forms. Besides these, the biofilm of FR-35 clustered within this branch.
In the second cluster, the suspension of FR-35 and the planktonic sample of ZUERICH-1 clustered together. Also the planktonic sample of FR-35 belonged to this cluster, while it showed a high difference to the other two samples.

The percentual amount of proteins significantly up and down regulated was equally balanced at around 50 % in all samples.
The comparison showed strong similarities between biofilm and suspension sample of ZUERICH-1. Both forms displayed lower expression values than noted for the other samples. Similarities were also found for the suspension of FR-35 and the planktonic sample of ZUERICH-1.
The proteome of the planktonic sample of FR-35 displayed the highest variances in up- and downregulated proteins in comparison to the other samples. Moreover, in this isolate in this particular cultivation form, a few proteins were uniquely either up or downregulated when compared to the other samples.

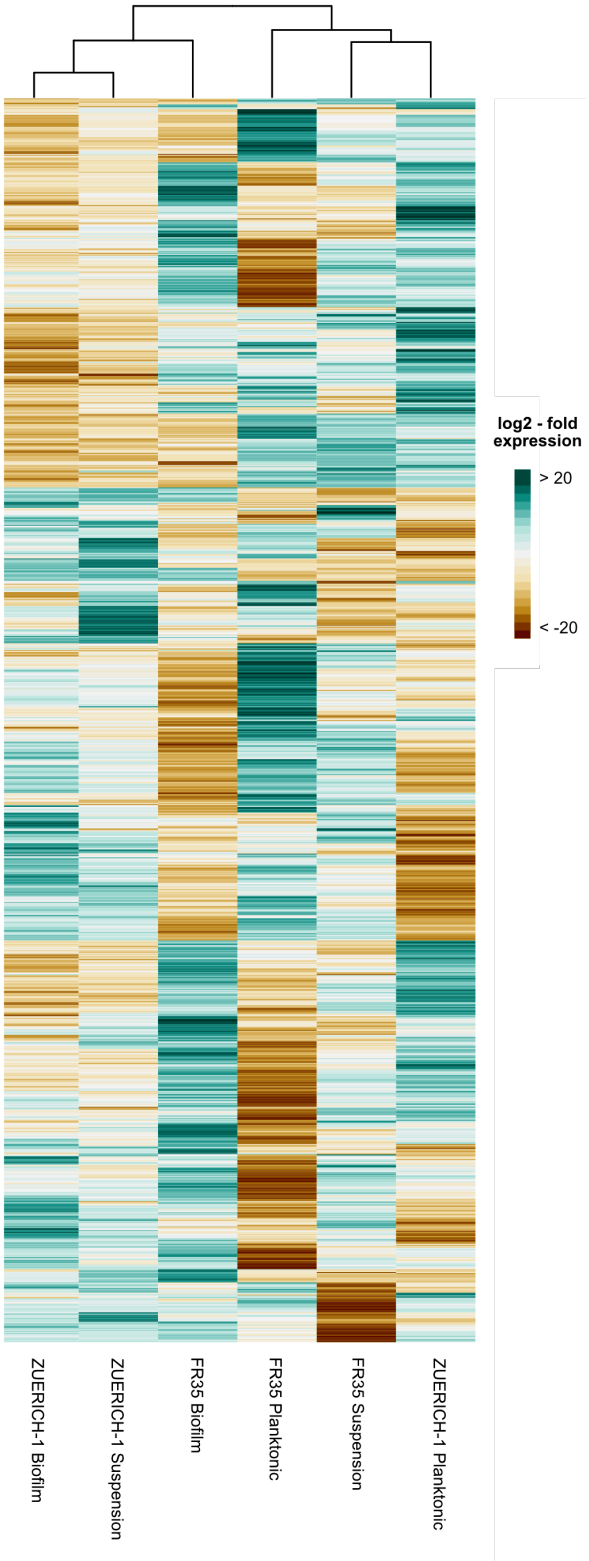

Figure 3.4.2: Heatmap of the proteome analysis of ZUERICH-1 and FR-35

Displayed are the proteome expression profiles of the significantly regulated proteins in all tested cultivation forms of the isolates ZUERICH-1 and FR-35. The data was clustered hierarchical in horizontal and vertical orientation. The clustering showed a strong similarity of the biofilm and the suspension of ZUERICH-1, while the planktonic sample of FR-35 showed the highest differences in comparison to the other samples. The $\log_2$-fold expression of each protein in each sample is indicated by color scale from turquoise (upregulated) to brown (downregulated). Each sample was proceeded in three biological replicates, each in technical triplicates. From the samples, the overall mean expression was calculated and normalized against the median expression of all samples per isolate.

3.4.2.1 COG analysis of the proteome expression profiles

In a further approach the functional background of the significantly regulated proteins was analysed. Therefore, the COG (Cluster of Orthologous Gene) group of each protein was analysed by using eggNOG mapper.

In general it was found that the number of proteins, regulated either up or down, was similar between all three cultivation forms (figure 3.4.3 & figure 3.4.4). Moreover, in most cases, the number of proteins up- or downregulated in each form was balanced. The analysis showed, that the majority of proteins were of 'unknown function' (COG group = S).

In most categories, the number of up- and downregulated proteins ranged between 0 - 40. The major exception displayed the category of 'unknown function' (S) in which approximately over 200 proteins were grouped in each cultivation form. Other groups with slightly higher numbers of proteins were in both isolates 'Energy production and conversion' (C), 'Lipid transport and metabolism' (I) as well as 'Secondary metabolites biosynthesis, transport and catabolism' (Q).

For the isolate ZUERICH-1 it was found, that overall, the mean expression of the proteins was in all COG groups at an equal level either approx. 0.2 $\log_2$ fold (up) or approx. -0.3 $\log_2$ fold (down) (figure 3.4.3).

Only a few COG categories showed specific deviations. For example, while 'cell cycle control, cell division, chromosome partitioning' (COG group = D) and 'posttranslational modification, protein turnover, chaperones' (O) displayed a higher $\log_2$ fold upregulation in the planktonic sample, the opposite was documented for the biofilm in the same COG group.

Similar patterns were documented for FR-35 (figure 3.4.4). In a few cases, the number of proteins was not equal in up- and downregulation, such as 'transcription' (K), 'secondary metabolites biosynthesis, transport and catabolism' (Q) or 'cell wall/membrane/envelope biogenesis' (M). In the mentioned cases, the number of upregulated proteins in the biofilm samples and in the downregulated proteins of the planktonic samples was enhanced. The upregulated proteins of the planktonic sample of ZUERICH-1 displayed in most cases the highest $\log_2$ fold upregulation when compared to the other cultivation forms. This was partially also true for the planktonic sample of FR-35, though it was displayed in fewer COG categories as for ZUERICH-1.

In both isolates, the fewest proteins were sorted to the category of 'intracellular trafficking, secretion and vesicular transport' (U).

Concerning the mean $\log_2$ fold expression, similar results were found for FR-35 as documented for ZUERICH-1. Especially, in the COG groups 'posttranslational modification, protein turnover, chaperones' (O) and 'cell cycle control, cell division, chromosome partitioning' (D) the biofilm and planktonic samples displayed similar expression intensities in both isolates. This indicates that the regulation of proteins in these groups is eventually phenotype specific.

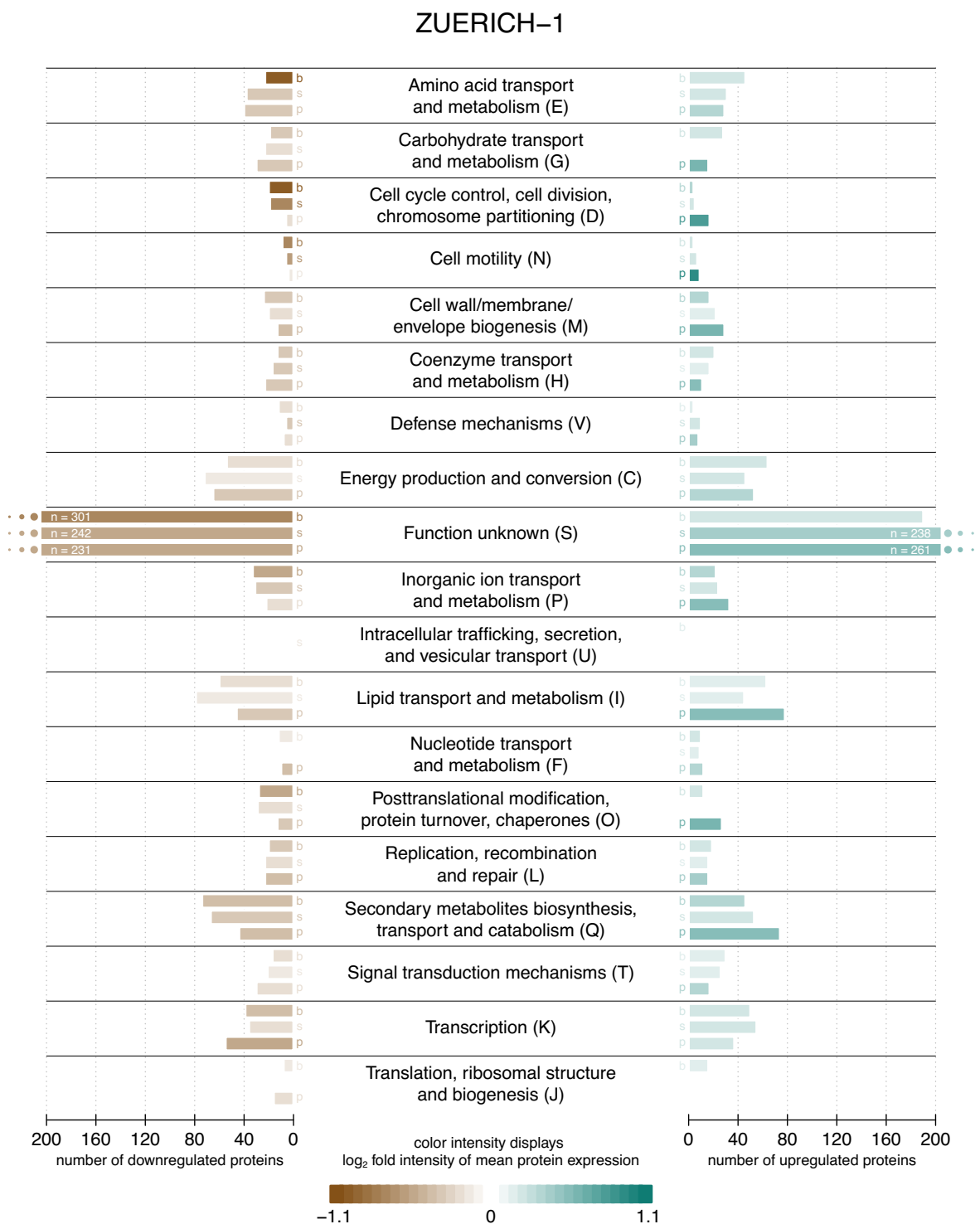

Figure 3.4.3: Distribution of significant differently regulated proteins of ZUERICH-1 in COG groups (Proteome).

Displayed are the protein numbers of up- and downregulated proteins of *M. chimaera* ZUERICH-1 to the assigned COG category. The color intensity displays the mean $\log_2$ fold expression change, while brown represents the downregulated and turquoise represents the upregulated genes. If the number of proteins exceeded the limit of 200, this was indicated by three dots and the actual number was mentioned in the bars.
The analysis showed that the majority of the proteins belonged to the category of 'Function unknown' (S). In the majority of the COG groups, the number of proteins was balanced between all three cultivation forms as well as the $\log_2$ fold expression.
In a few categories, namely 'Amino acid transport and metabolism' (E), 'cell cycle control, cell division, chromosome partitioning' (D) and 'Cell motility' (N), the mean expression of the downregulated proteins was enhanced in the biofilm. In case of the upregulated genes, in almost all categories, the planktonic sample presented the highest upregulation $\log_2$ fold expression change. The majority of the mean expression of up- and downregulation ranged in a similar scale of approx. -0.3 or 0.3 $\log_2$ fold, respectively. In no case, the suspension displayed the highest $\log_2$ fold expression change and was either between or below biofilm and planktonic.

Following COG categories were excluded, since no protein was annotated in any cultivation form:
'Total'; 'Cytoskeleton' (Z); 'Chromatin structure and dynamics' (B); 'RNA processing and modification' (A); 'General function prediction only' (R); 'Extracellular structures' (W); 'Nuclear structure (Y)'

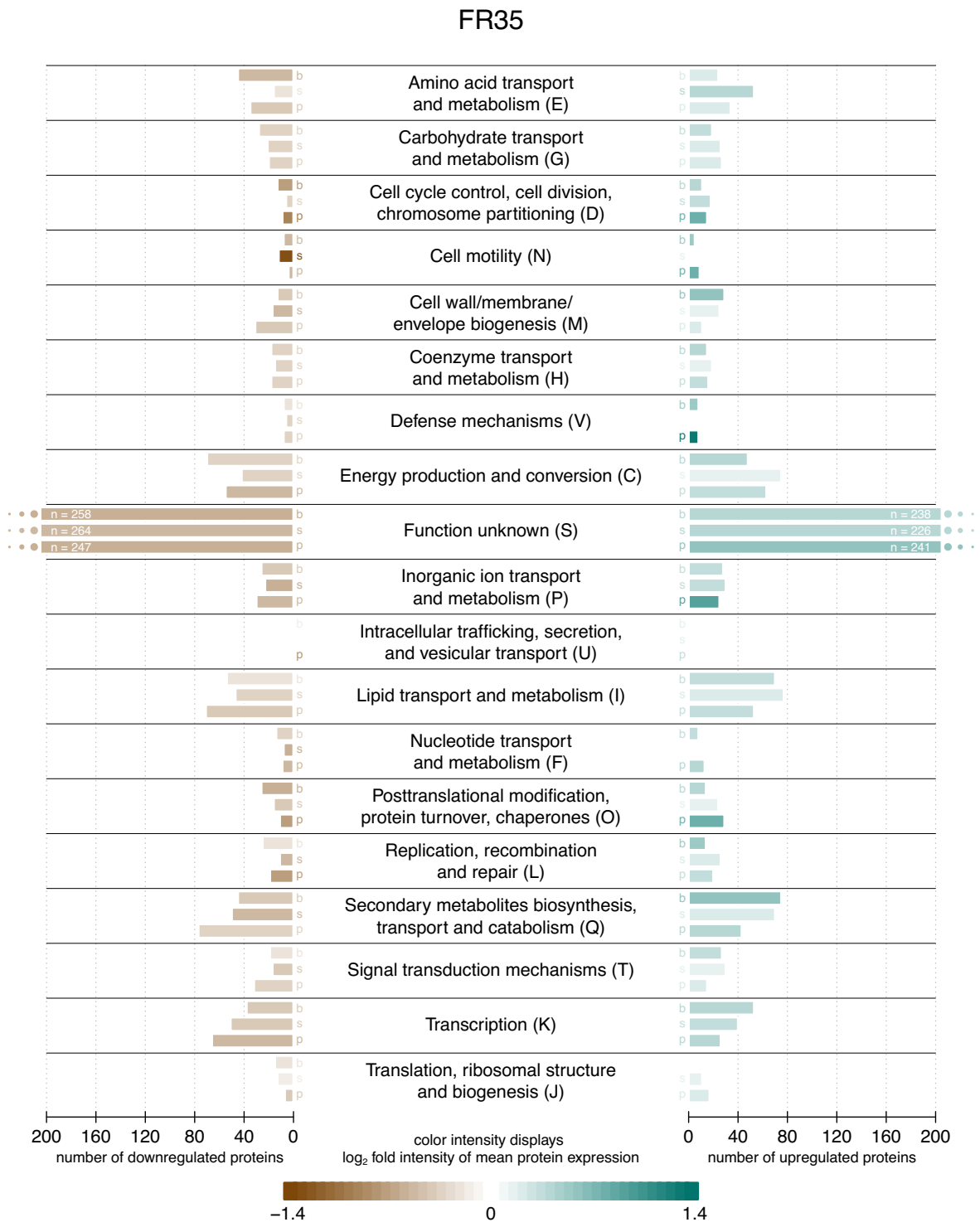

Figure 3.4.4: Distribution of differently significant regulated proteins of FR-35 in COG groups (Proteome).

Displayed are the protein numbers of up- and downregulated proteins of *M. chimaera* FR-35, respectively to the assigned COG category. The color intensity displays the mean $\log_2$ fold expression change, while brown represents the downregulated and turquoise represents the upregulated genes. If the number of proteins exceeded the limit of 200, this was indicated by three dots and the actual number was mentioned in the bars.

Similar to ZUERICH-1, the mean $\log_2$ fold expression of the proteins in the COG categories was similar among all three cultivation forms. In a few cases, the $\log_2$ fold expression change was enhanced in one of the forms. In the category 'Cell motility' (N), for example, the suspension presented an enhanced downregulation of proteins in comparison to biofilm and planktonic. Similar changes were documented for the upregulated proteins of the planktonic sample in the COG groups 'Cell cycle control, cell division, chromosome partitioning' (D), 'Defense mechanisms' (V) and 'Inorganic ion transport and metabolism' (P) as well as 'Posttranslational modification, protein turnover, chaperones' (O). In case of the categories 'D' and 'O' similar findings were made for *M. chimaera* ZUERICH-1. In contrast to the other isolate, the biofilm of FR-35 presented in no category the highest $\log_2$ fold expression change in comparison to the other cultivation forms.

Following COG categories were excluded, since no protein was annotated in any cultivation form:
'Total'; 'Cytoskeleton' (Z); 'Chromatin structure and dynamics' (B); 'RNA processing and modification' (A); 'General function prediction only' (R); 'Extracellular structures' (W); 'Nuclear structure (Y)'

3.4.2.2 Cultivation form specific regulated proteins

In order to analyse cultivation form specific proteins, the proteins, that were either up- or downregulated specifically in one of the three cultivation forms were filtered (table 3.4.1). For example, when a protein was only upregulated in the biofilms of both isolates but not in the suspension and also not in the planktonic samples, the protein was voted as 'uniquely upregulated'.
In the biofilms of both isolates only 9 proteins were found to be uniquely upregulated in this cultivation form and seven proteins were downregulated. Interestingly, in the suspensions, no protein was

Table 3.4.1: Significantly regulated proteins (Proteome).
Listed are the respectively five most up and down regulated proteins of each cultivation form in both isolates.

Form	Reg.*	Ø fold change	Description	COG	Accession
Biofilm	*Up*	1.3	Ring hydroxylating α subunit	Inorganic ion transport and metabolism (P)	WP_042912857
		1.29	SufI - multicopper oxidase family protein	Secondary metabolites biosynthesis, transport and catabolism (Q)	WP_054585729
		1.2	MmpS family transport accessory protein	Function unknown (S)	WP_236595505
		1.19	DivIVA domain-containing protein - interacts with FtsZ, MinD and other proteins	Cell cycle control, cell division, chromosome partitioning (D)	WP_008258949
		1.16	ATP-dependent Clp protease ATP-binding subunit ClpX	Posttranslational modification, protein turnover, chaperones (O)	WP_008255183
	down	-1.28	ornithine cyclodeaminase	Amino acid transport and metabolism (E)	WP_014942259
		-1.49	type VII secretion protein EccB	Function unknown (S)	WP_101953247
		-1.85	sensor domain-containing protein	Function unknown (S)	WP_232538303
		-1.95	cysC; adenylyl-sulfate kinase	Inorganic ion transport and metabolism (P)	WP_008254752
		-2.5	DUF4226 domain-containing protein EspA/EspE family	Function unknown (S)	WP_101953231
Suspension	*Up***				
	*down****	-1.67	YrrM - class I SAM-dependent methyltransferase	Function unknown (S)	WP_042913989
Planktonic	*Up*	4.66	isocitrate lyase	Energy production and conversion (C)	AFC56195
		2.15	metal-sensitive transcriptional regulator	Function unknown (S)	WP_101953457
		2.07	AhpD family - alkyl hydroperoxide reductase	Posttranslational modification, protein turnover, chaperones (O)	WP_042911860
		1.92	HNH endonuclease	Defense mechanisms (V)	WP_042913257
		1.57	SucD - succinate–CoA ligase subunit alpha	Energy production and conversion (C)	WP_008254012
	down	-1.55	AldA - aldehyde dehydrogenase	Energy production and conversion (C)	WP_042911158
		-1.71	AcrR - TetR/AcrR family transcriptional regulator	Transcription (K)	WP_042913814
		-1.73	TadA - nucleoside deaminase	Nucleotide transport and metabolism (F) Translation, ribosomal structure and biogenesis (J)	WP_020821374
		-1.86	cytochrome D ubiquinol oxidase subunit 1	Energy production and conversion (C)	ASL11887
		-2.01	thiolase family protein	Lipid transport and metabolism (I)	WP_042911447

* - Regulation; ** - no protein found; *** only one uniquely downregulated protein found

The NCBI-accession was determined by pBLAST of the FASTA sequences with a coverage of min. 90% and an identity of min. 70%. For results that did not surpass this thresholds the UniProt-ID is mentioned instead.

found to be uniquely upregulated and only one protein was uniquely downregulated in this form. In the planktonic samples, 24 proteins were found to be uniquely downregulated. On the opposite, a total of 25 proteins was upregulated in this cultivation form (table 3.4.1).
The range of the five most upregulated proteins in biofilm was rather small (1.3 – 1.16 fold expression change; table 3.4.1). The majority of these identified five proteins is involved in metabolic and cell division processes (SufI; DivIVA containing protein, ATP dependent Clp protease, ring hydroxylating α subunit), one protein was found that is of 'unknown function' (COG category = S; MmpS family transport accessory protein). In the suspension no protein was found that was uniquely upregulated in this cultivation form and only one protein (YrrM) was found on the downregulated side (table 3.4.1). The function of this protein remains unknown.
In case of the planktonic samples, four proteins were found that are functionally involved in 'energy production and conversion' (C) while two were either up- (isocitrate lyase, SucD) or downregulated (AldA, cytochrome D ubiquinol oxidase subunit 1). The most upregulated protein (isocitrate lyase) showed the highest value of fold change (4.66x). The other proteins were in a similar range as it was documented in the biofilm. The detailed analysis showed no clear functional pattern or dependency of the proteins documented (table 3.4.1).
Two of the most upregulated proteins in biofilm (DivIVA and Clp protease) are involved in cell division processes and interact with the same genomic counterparts (FtsZ). The most downregulated protein in biofilm was a DUF protein (domain of unknown function) of the the EspA/EspE family, which is described to be involved in blocking parts of the type VII secretion system to which also EccB belongs, one of the other five most downregulated proteins.

3.4.3 Transcriptome

A total of 4,377 genes was found to be significantly regulated in the transcriptome analysis (supplementary table S.3). That displays approximately 64 % of genes that were annotated. In contrast to the results gained by the proteome analysis, the heatmap of the significant regulated genes from the transcriptome analysis showed a isolate specific expression. In the overall comparison, the $\log_2$ fold expression was lower in the transcriptome as in the proteome.
In case of ZUERICH-1, more genes were found to be significantly regulated. These belong to the plasmids, that are lacking in FR-35. All of these genes were downregulated in ZUERICH-1.
Similar to the proteome, the samples clustered in two major branches. In one branch, planktonic and biofilm of FR-35 clustered together while the other four samples clustered in the other branch. In this second branch, the suspension of FR-35 was separated from the other three samples. The biofilm and the planktonic samples of ZUERICH-1 clustered closely together, while the suspension of ZUERICH-1 was also separated.

While the biofilm and the planktonic sample of ZUERICH-1 presented a relatively similar overall pattern of up- and downregulated genes, the suspension of this isolate displayed a deviating regulation. In comparison to the other two cultivation forms, a higher percentage of the genes in suspension showed higher $\log_2$ fold expression levels.
Also in FR-35, the biofilm and the planktonic sample clustered together, though the forms presented higher differences in comparison to ZUERICH-1. The planktonic sample of FR-35 showed many genes with strong upregulation when compared to the other two forms. Like in ZUERICH-1, the suspension of FR-35 presented the highest difference to the other two cultivation forms. The majority of the genes was downregulated in this form.

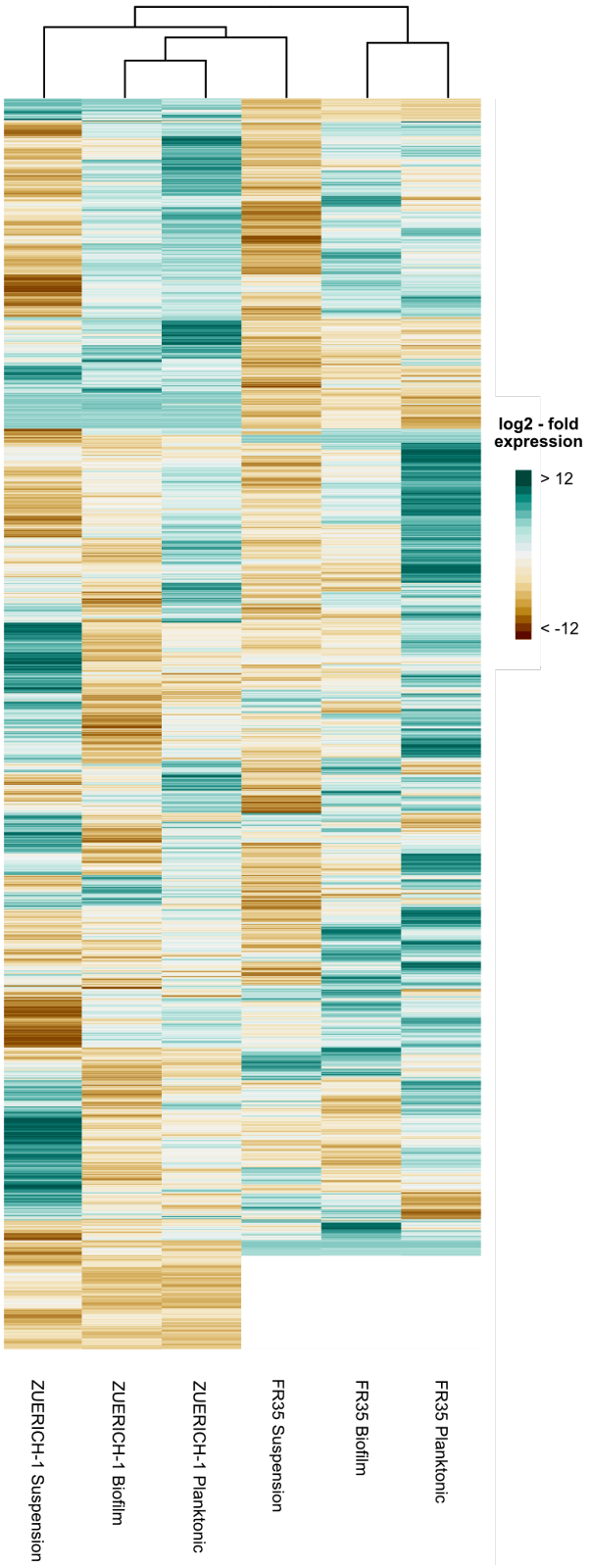

Figure 3.4.5: Heatmap of the transcriptome analysis of ZUERICH-1 and FR-35

Displayed are the transcriptome expression profiles of the significantly regulated genes in all tested cultivation forms of the isolates ZUERICH-1 and FR-35. The data was clustered hierarchical in horizontal and vertical orientation. The analysis showed a clustering of the cultivation forms in the individual isolates, while in both cases the biofilm clustered more with the planktonic sample than with the suspension. The $\log_2$-fold expression of each protein in each sample is indicated by color scale from turquoise (upregulated) to brown (downregulated). Each sample was proceeded in five biological replicates, each in technical triplicates. The overall expression per sample was normalized against the median expression of all samples per isolate.

3.4.3.1 COG analysis of the transcriptome expression profiles

Similar to what was documented for the proteome, the majority of genes belonged to the COG category of 'unknown function' (S), though the numbers differed between the forms. While in the biofilm of FR-35 for example, a total of 209 genes (upregulated) was grouped in this COG category, the biofilm of ZUERICH-1 displayed over 900 genes (downregulated). This showed that the variability between the samples was much higher than in the proteome sample. Moreover, in contrary to the results of the proteome, the numbers of genes up- or downregulated were not similar among the cultivation forms. In general, the results of the COG analysis gained for transcriptome and proteome differed mostly.
In contrary to the proteome analysis, the numbers of genes differed strongly in the separate COG categories. While in the proteome the numbers ranged between 0 - 40 in most cases, the distribution of the genes displayed no such stability.
For ZUERICH-1, in most categories, the number of genes downregulated was highest in the biofilm sample and lowest in the planktonic sample. The opposite finding was documented for the upregulated genes (figure 3.4.6). The mean expression in most COG groups was highest in the suspension sample, for upregulated as well as for downregulated genes. Especially in the groups of 'cell cycle control, cell division, chromosome partitioning' (D), 'cell motility' (N), 'posttranslational modification, proteins turnover, chaperones' (O) and 'defense mechanisms' (V), the suspension of ZUERICH-1 represented enhanced $\log_2$ fold expression levels. The biofilm displayed enhanced expression in the upregulated genes in the COG groups of 'intracellular trafficking, secretion and vesicular transport' (U) and 'replication, recombination and repair' (L) which was different to what was documented for the proteome. In the category of 'Cell motility' (N), the suspension of ZUERICH-1 displayed higher mean $\log_2$ fold expression than the other two forms.
The general, the observations made for ZUERICH-1 were not displayed equally in FR-35 (figure 3.4.7). The suspension represented in all COG categories the highest number of genes in the downregulated. In most cases the mean $\log_2$ fold expression did not vary strongly between the cultivation forms, which differed from what was documented for ZUERICH-1.
The numbers of genes up- or downregulated were similar between biofilm and planktonic. While the mean expression between both cultivation was majorly balanced, in the categories 'cell motility' (N) and 'defense mechanisms' (V) the biofilm displayed slightly higher $\log_2$ fold expression in the upregulated genes.
Interestingly the differences between both isolates were more displayed in the transcriptome than in the proteome analysis. Thereof it was not possible to find much similarities in the COG category analysis of both omics-analysis.

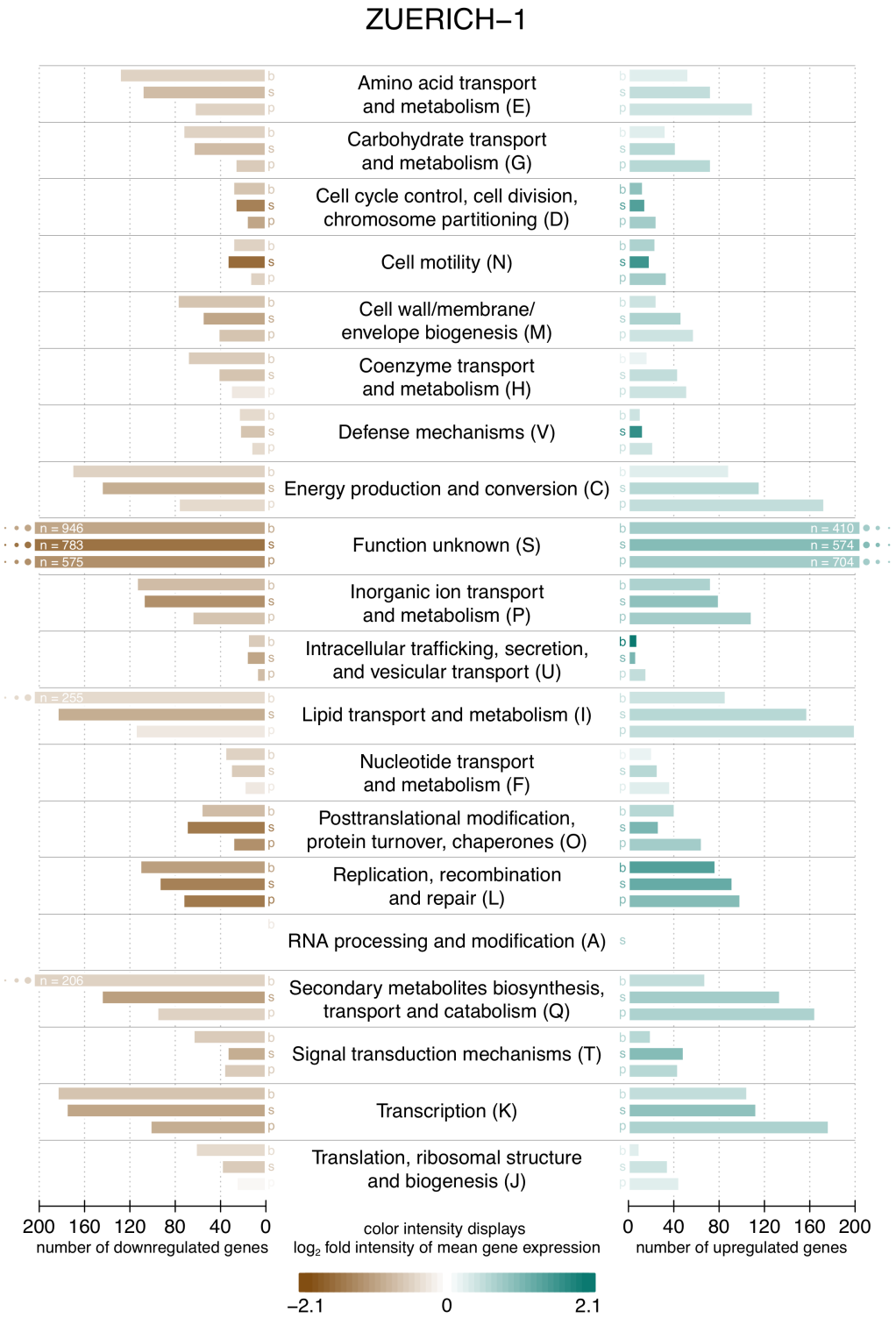

Figure 3.4.6: Distribution of significant regulated genes of ZUERICH-1 in COG groups (Transcriptome).

Displayed are the numbers of up- and downregulated genes of *M. chimaera* ZUERICH-1, respectively to the assigned COG category. The color intensity displays the mean $\log_2$ fold expression change, while brown represents the downregulated and turquoise represents the upregulated genes. If the number of proteins exceeded the limit of 200, this was indicated by three dots and the actual number was mentioned in the bars.
In almost all categories, the number of proteins downregulated was highest in the biofilm and lowest in the planktonic sample. The opposite was documented for the upregulated proteins. Similar to the proteome analysis, the $\log_2$ fold expression was in most cases balanced among all three cultivation forms, with a few exceptions. In the categories 'cell cycle control, cell division, chromosome partitioning' (D), 'cell motility' (N) and 'posttranslational modification, protein turnover and chaperones' (O), the suspension displayed enhanced mean $\log_2$ fold expression which differed from the findings of the proteome analysis. The mean expression of the biofilm was enhanced in the upregulated genes of the COG group of 'intracellular trafficking, secretion and vesicular transport' (U) as well as in 'replication, recombination and repair' (L).

Following COG categories were excluded, since no protein was annotated in any cultivation form:
'Total'; 'Cytoskeleton' (Z); 'Chromatin structure and dynamics' (B); 'General function prediction only' (R); 'Extracellular structures' (W); 'Nuclear structure (Y)'

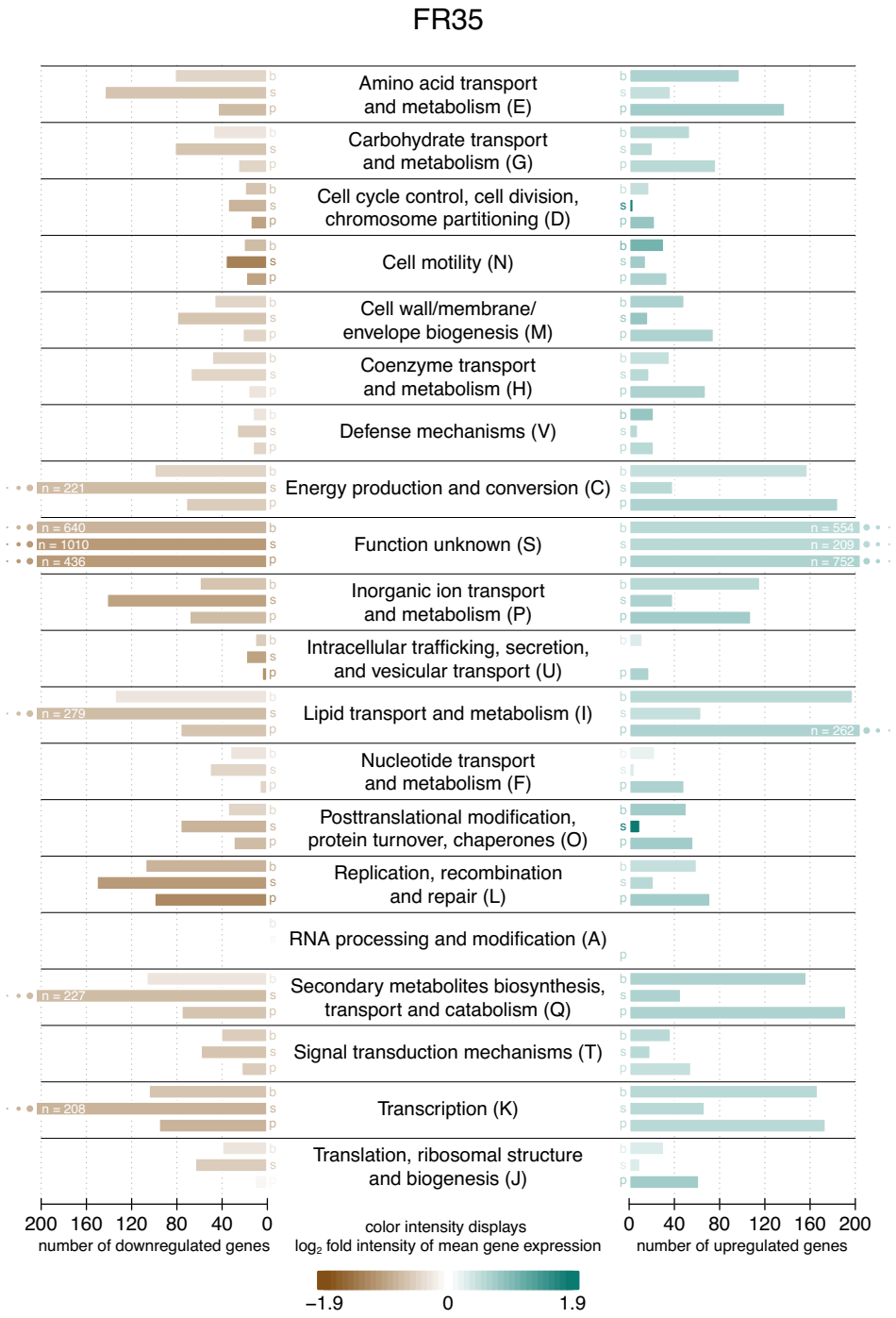

Figure 3.4.7: Distribution of significant regulated genes of FR-35 in COG groups (Transcriptome).

Displayed are the numbers of up- and downregulated genes of *M. chimaera* FR-35, respectively to the assigned COG category. The color intensity displays the mean $\log_2$ fold expression change, while brown represents the downregulated and turquoise represents the upregulated genes. If the number of proteins exceeded the limit of 200, this was indicated by three dots and the actual number was mentioned in the bars.
Similar to ZUERICH-1, the mean $\log_2$ fold expression was balanced between the cultivation forms in the majority of the COG groups. Interestingly, in all categories, the number of genes downregulated was highest and the number of genes upregulated was lowest in the suspension sample. The mean expression of the suspension was enhanced in the downregulated genes in the category 'cell motility' (N) which was also documented for ZUERICH-1.

Following COG categories were excluded, since no protein was annotated in any cultivation form:
'Total'; 'Cytoskeleton' (Z); 'Chromatin structure and dynamics' (B); 'General function prediction only' (R); 'Extracellular structures' (W); 'Nuclear structure (Y)'

3.4.3.2 Cultivation form specific regulated genes

The detailed analysis of the five most up- and most downregulated genes, showed that the expression levels ranged in max. around 2 - 3 fold change in biofilm and planktonic (table 3.4.2). In suspension, the expression levels were much higher than documented in the other cultivation forms (upregulated up to 21.9 x; downregulated down to -40.8 x).
In comparison to the proteome analysis, a similar amount of genes was uniquely regulated in the cultivation forms. In the biofilms of both isolates, 46 genes were uniquely up- and 34 genes were uniquely downregulated, which is a comparable number to what was investigated for the proteome analysis. The suspension samples displayed with 118 upregulated and 387 downregulated genes the

Table 3.4.2: Significantly regulated genes (Transcriptome).
Listed are the respectively five most up and down regulated genes of each cultivation form of both isolates.

Form	Reg.*	Ø fold change	Description	COG	Accession
Biofilm	*Up*	2.9	PPE-repeat protein	Cell motility (N)	WP_054585265
		2.5	PPE-repeat protein	Cell motility (N)	WP_042910820
		2.0	Sulfotransferase	Function unknown (S)	WP_042911290
		1.8	type VII secretion protein EccB	Function unknown (S)	WP_042913755
		1.8	DNA-binding transcriptional regulator, AcrR family	Transcription (K)	WP_042910305
	down	-1.8	R2-like ligand-binding oxidase	Nucleotide transport and metabolism (F)	WP_008261828
		-2.0	HAD family hydrolase	Function unknown (S)	WP_042910536
		-2.3	Putative hydrophobic ligand-binding SRPBCC domain	Function unknown (S)	WP_020822560
		-2.8	MmgE/PrpD family protein	Function unknown (S)	WP_014383663
		-3	TIGR00730 family Rossman fold protein	Function unknown (S)	WP_232525692
Suspension	*Up*	21.9	SDR family NAD(P)-dependent oxidoreductase	Function unknown (S)	WP_042913104
		6.9	DNA starvation/stationary phase protection protein	Inorganic ion transport and metabolism (P)	WP_080691222
		6.6	hypothetical protein	Function unknown (S)	WP_042912643
		5.4	UbiX family flavin prenyltransferase	Coenzyme transport and metabolism (H)	WP_042912986
		4.4	Predicted flavoprotein CzcO associated with the cation diffusion facilitator CzcD	Inorganic ion transport and metabolism (P)	WP_009955494
	down	-22.7	NADPH-dependent 2,4-dienoyl-CoA reductase, sulfur reductase, or a related oxidoreductase	Function unknown (S)	WP_042910276
		-25.4	-	Function unknown (S)	A0A249C7L2
		-27.1	Transcriptional regulator CsoR (copper-sensitive operon repressor)	Function unknown (S)	WP_042910276
		-33.4	30S ribosomal protein S18	Translation, ribosomal structure and biogenesis (J)	WP_009952527
		-40.8	hypothetical protein	Function unknown (S)	WP_167544946
Planktonic	*Up*	3.6	nuclear transport factor 2 family protein	Function unknown (S)	WP_042911918
		2.7	trans-aconitate 2-methyltransferase	Translation, ribosomal structure and biogenesis (J)	WP_009955670
		2.2	citrate synthase 2	Energy production and conversion (C)	WP_008253892
		2.1	chaperonin GroEL	Posttranslational modification, protein turnover, chaperones (O)	WP_042913297
		2.0	wax ester/triacylglycerol synthase family O-acyltransferase	Lipid transport and metabolism (I)	WP_065500793
	*down***	-1.6	DNA-binding transcriptional regulator, AcrR family	Transcription (K)	WP_042910276

* - Regulation; ** - only one unique gene found for the planktonic sample

The NCBI-accession was determined by pBLAST of the FASTA sequences with a coverage of min. 90% and an identity of min. 70%. For results that did not surpass this thresholds the UniProt-ID is mentioned instead.

highest number of uniquely regulated genes in the comparison of the three cultivation forms. This was completely contrary to what was documented in the proteome analysis. In the planktonic samples only one gene was found to be downregulated while a total of 36 genes was upregulated.
An interesting finding was, that three of five of the most upregulated genes in biofilm belong or contribute to the type VII secretion systems (T7SS; namely ESX 1-5). The PPE-repeat proteins, which are grouped in the category of 'cell motility' (N), are known to interact with ESX proteins and are essential participants in infection and host-pathogen interaction. On the other hand, the majority of the identified downregulated genes was categorised with 'unknown function' (S).
Also in the suspension, four of the five most downregulated genes belonged to the group of 'unknown function' (S). One of these genes was not to be annotated with NCBI pBLAST with the set limitations, why it was not possible to add an NCBI accession number or gene name. In case of the upregulated genes in suspension, two out of five genes belonged to the COG group of 'Inorganic ion transport and metabolism' (P). One of these genes was annotated as a DNA starvation or stationary phase protection protein (WP_080691222; no concrete gene name available).
In the planktonic sample only one gene was found to be uniquely downregulated. It was annotated as a DNA-binding transcriptional regulator (AcR family) belonging to the COG category 'transcription' (K). The upregulated genes of the planktonic form displayed the highest functional variability, though the highest upregulated gene was also of 'unknown function' (S). Most interestingly, in these five most upregulated genes the chaperonin GroEL was documented. In many bacteria this protein is necessary for proper protein folding and was related to biofilm formation.

3.4.4 Integrative analysis of Proteome and Transcriptome expression patterns

3.4.4.1 Count correlation

The correlation of transcript and proteome counts is a possiblility to identify genes which are of special interest when high numbers occur in both omics-techniques. In the present study, no linear or

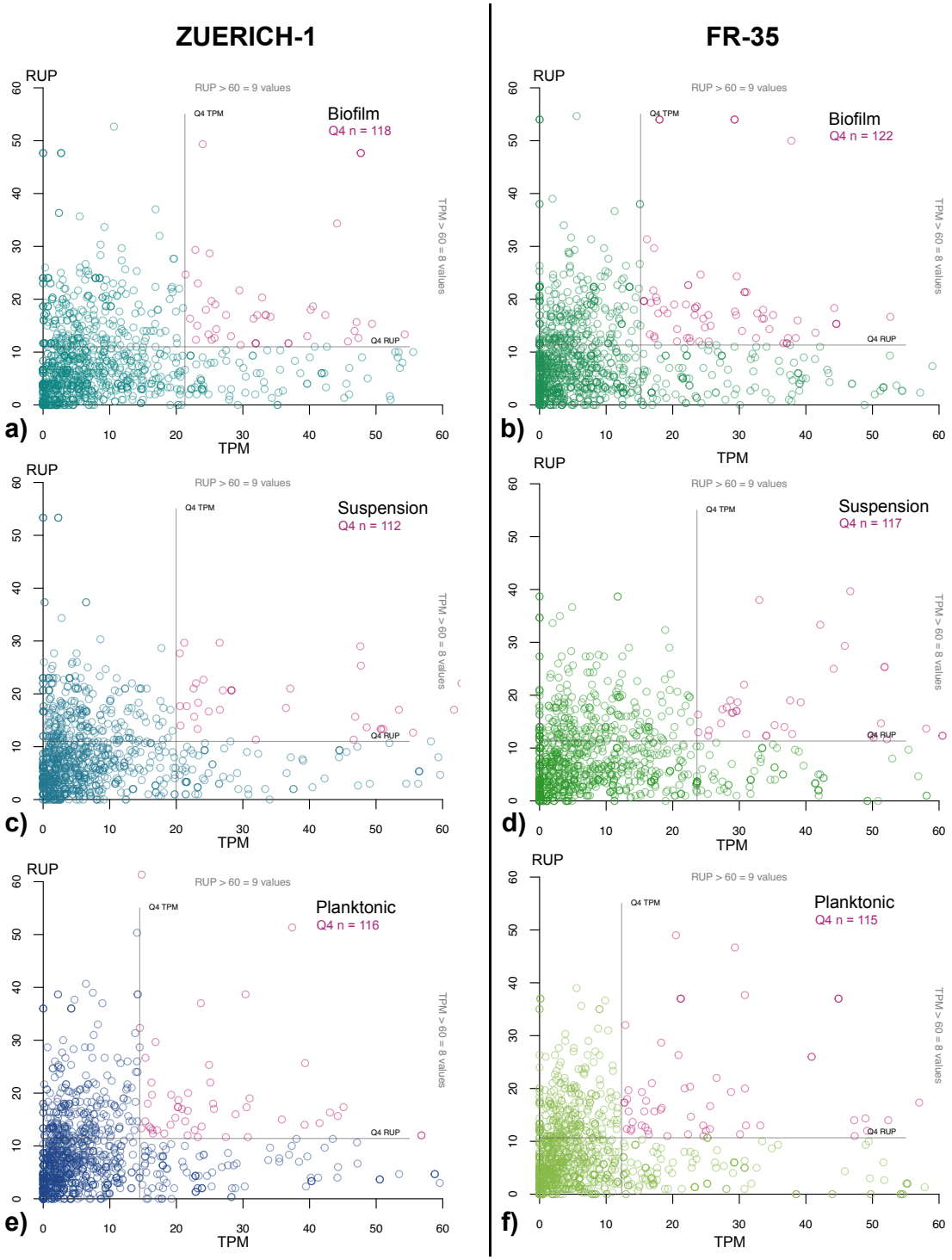

Figure 3.4.8: Comparison of protein and transcript counts of ZUERICH-1 (a,c,e) and FR-35 (b,d,f)

Displayed are the mean counts of each gene in transcriptome (TPM = transcripts per million) and proteome (RUP = razor unique peptides) for each cultivation form per isolate (**a** = ZUERICH-1; **b** = FR-35). The genes, which displayd the fourth quartile (Q4; values > 75 %) of both, transcript and protein counts, are marked in pink. The borders of the quartiles are displayed (Q4 TPM [transcript counts] & Q4 RUP [protein counts]).

proportional correlation of the transcript and protein counts was found in any of the cultivation forms tested (figure 3.4.8). In all cases, the number of transcript counts was higher as the corresponding protein count and the overall distribution was similar among all samples. The majority (approx. 60 %) of the genes clustered in the range of 0 – 10 million counts.
In order to identify genes, which present high counts in both omis techniques, the upper quartile (Q4; > 75 %) of each dataset was calculated. Genes that are represented in the fourth quartile of both datasets were identified and used for further analysis (supplementary table S.4). The number of identified genes (Q4 n) was similar in all samples ranging between 112 to 122 (figure 3.4.8 pink circles).

3.4.4.2 Biofilm specific genes

In the Q4 subset of the biofilms of ZUERICH-1 and FR-35, six genes were identified in both isolates that were not present in the other cultivation forms. These genes were further analysed in a literature

Table 3.4.3: Biofilm specific genes
Listed are the genes that were only present in the fourth quartiles of transcript and protein counts of the biofilm samples of both isolates.

Name	Presumed Function	Co-Expression*	NCBI/UniProt Accession
Aminopeptidase N *pepN*	highly conserved in pathogenic and non-pathogenic mycobacteria; required for modulating virulence *in vivo* (MTB) and essential for growth *in vitro* (*M. smegmatis*) [141]	*pepA, glyA, truB*	WP_042911201 A0A220Y9H2
Aldehyde Dehydrogenase AldA-like (Rv0768)	expressed under oxygen starvation and putative stress protection protein (*M. smegmatis*) [142]; ALDHs are in general linked to oxidative stress in cells [143]	*ackA, purQ*	WP_042913909 A0A1Y0THM4
phosphoglucosamine mutase *glmM*	key enzyme for cell wall biosynthesis [144], essential for growth and biofilm formation (*M. smegmatis*) [145], potential drug target [144, 146]	*glmU, glmS, murA rpsI*	WP_014385767 A0A220YI14
Fatty acyl-AMP ligase (FAAL)	lipid biosynthesis [147]	-	WP_042912964 A0A1Y0T9D6
glycogen debranching protein *glgX*	involved in starch and sucrose metabolism and required for optimal growth (*M. smegmatis*) [148]; important for adaptation to hyperosmotic stress (*Corynebacterium glutamicum*) [149]	*glgB, glgC*	WP_042912951 A0A1Y0TCK4
succinate–CoA ligase subunit beta *sucC*	persumed to play an important role in biofilm formation (MTB) [150]	*sucD, mdh, sdhC, acsA, kgd*	WP_009957827 A0A220Y7W6

* - Co-Expression as noted by STRING (Version 11.5) Protein-Protein Interaction Networks Functional Enrichment Analysis www.string-db.org only annotated genes mentioned

search and co-expression analysis using STRING (table 3.4.3).
From these six genes, two were mentioned in the literature to be involved in biofilm formation of *M. smegmatis* or MTB (*glmM, sucC*). *glmM* is involved in cell wall biosynthesis and is co-expressed with *glmU, glmS, murA* and *rpsI*. In MTB, the genes *glmU, glmS* and *glmM* are identified as possible drug targets. The second gene, *sucC*, is not well described yet. It is supposed to be importantly involved in biofilm formation of *M. smegmatis*.
Of the other genes, two were presumed to be required for optimal growth in mycobacteria (*pepN, glgX*). One gene was linked to oxidative stress (AldA-like aldehyde dehyrdogenase) and the last one was annotated to be involved in lipid biosynthesis, a fatty acyl-AMP ligase (FAAL) for which no further information was found (table 3.4.3).

3.4.4.3 Further cultivation form specific genes

For the suspension, three genes were found to be present in this cultivation form but not the others (data not shown), namely EccC (a type VII secretion protein), an iron-sulfur cluster assembly protein (genome region name ParA) and a DivIVA domain-containing protein. Interestingly, the latter is exact the same protein, that was documented in the proteome analysis within the five most upregulated proteins of the biofilm.
In the planktonic samples, a total of five genes was found to be unique for this cultivation form, namely a MCE family protein, cytochrome P45, an arylsulfatase, PhoE (phosphoglycerate mutase family protein) and FlhG (MinD/ParA family protein).

3.5 Susceptibility

An important advantage of biofilm formation is the enhancement of tolerance towards antimicrobials. Therefore, the susceptibility of *M. abscessus* and *M. chimaera* against antibiotics and disinfectants in biofilms was an important part of the present study. As the isolate *M. chimaera* FR-41 did not show reliable growth in MB-OADC, it was not possible to proceed disinfectant testing with this isolate. The disinfectant testing was additionally performed with *M. avium* ATCC 15769. The strain is recommended by the DIN 14348 as reference isolate for disinfectant testing of mycobacteria. Disinfection was only performed with biofilm and suspension samples.
Prior to disinfectant testing all neutralizers were tested. The tested neutralizers displayed no toxicicty against the bacteria and were found to sufficiently neutralize the highest concentration of the corresponding disinfectant (data not shown).

3.5.1 Disinfection

In summary, the disinfectant testing showed that the biofilm samples were in most cases more tolerant than the corresponding suspension. In case of sodium hypochlorite (FAC), the suspension samples of *M. chimaera* displayed a higher tolerance towards the disinfectant than the biofilm. The commonly recommended concentrations of the chosen disinfectants were in most cases not effective against the biofilm samples (table 3.5.1). While the concentration of 0.1 % FAC did not sufficiently disinfect neither biofilm nor suspension, the other disinfectants sufficiently eradicated all suspensions tested with the exception of *M. avium* ATCC 15769. In comparison, the concentration of 0.1 % PAA was

Table 3.5.1: Efficacy of commonly used disinfectant concentrations
Displayed is the efficacy of common disinfectant concentrations used for decontamination of medical devices (e.g. HCUs). A positive reduction (+) was evaluated when the reductions threshold of 4 $\log_{10}$ was reached in disinfectant testing. An unsufficient reduction is indicated by −. The results present a summary of the detailed experiments documented in figures 3.5.1 to 3.5.6.

Isolate	Form	2 % GA [1]	0.1 % FAC [2]	0.1 % PAA [2]
M. chimaera ZUERICH-1	Biofilm	−	−	−
	Suspension	+	−	+
M. chimaera FR-35	Biofilm	+	−	+
	Suspension	+	−	+
M. chimaera UP-11	Biofilm	−	−	+
	Suspension	+	−	+
M. avium ATCC 15769	Biofilm	−	−	−
	Suspension	−	−	+
M. abscessus $25/14^{sm}$	Biofilm	−	−	+
	Suspension	+	−	+
M. abscessus $35/14^{rg}$	Biofilm	−	−	+
	Suspension	+	−	+
M. abscessus $09/13^{sm}$	Biofilm	+	−	−
	Suspension	+	−	+
M. abscessus $58/15^{rg}$	Biofilm	+	−	−
	Suspension	+	−	+

[1] - concentration of 2 % glutaraldehyde is commonly used for instrumental disinfection (e.g. endoscopes)
[2] - recommended concentration used for decontamination of HCUs

the most efficient. Only the biofilm samples of ZUERICH-1, *M. avium* ATCC 15769, *M. abscessus* 09/13^{sm} and 58/15^{rg} were not sufficiently disinfected by this PAA concentration.

3.5.1.1 *Mycobacterium abscessus*

Glutaraldehyde

In the most cases, the biofilms of the tested *M. abscessus* isolates were more tolerant towards GA than the corresponding suspension. In the higher concentrations of GA ($\geq$ 1 %), the tested suspensions were completely eradicated while the biofilms still showed survival of bacteria. The differences between biofilm and suspension of the smooth isolates were in most cases statistically significant but not for the rough isolates (figure 3.5.1).

In *M. abscessus* 25/14^{sm}, biofilm and suspension surpassed the reduction threshold of 4 $\log_{10}$ at 0.5 % GA. But while the suspension was completely killed at concentrations $\geq$ 1 % GA, the biofilm still showed survival of bacteria (figure 3.5.1 a). Though it already surpassed the reduction threshold in concentrations between 0.5 – 1 % GA, the biofilm of 25/14^{sm} was not sufficiently reduced at a concentration of 2 % GA, although high differences between biological replicates occured.

In comparison to its smooth counterpart 25/14^{sm}, the rough isolate 35/14^{rg} showd a higher tolerance of

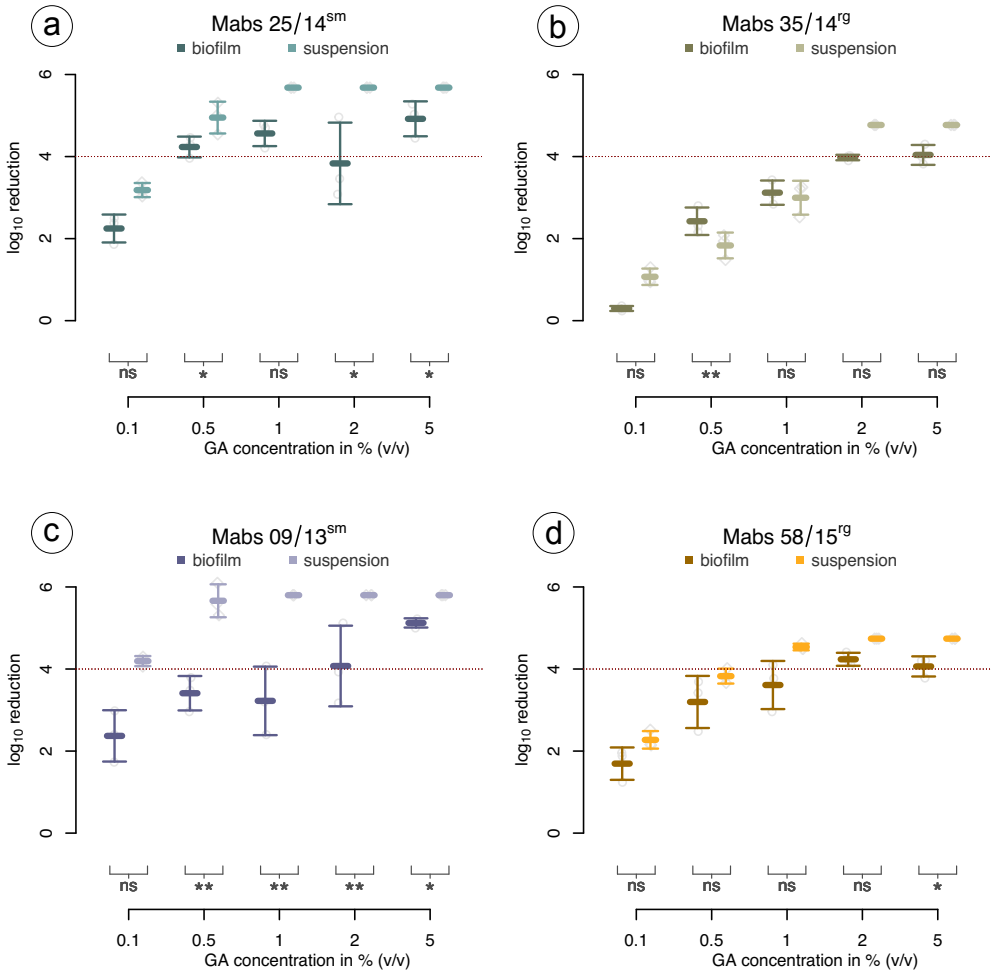

Figure 3.5.1: Disinfectant testing of *M. abscessus* using glutaraldehyde (GA)
Displayed is the $\log_{10}$ reduction against the according GA concentration. While for the rough isolates biofilm and suspension showed similar tolerance towards GA (**b & d**), the biofilm formation of the smooth isolates strongly decreased the efficacy of the disinfectant when compared to the corresponding suspension (**a & c**). Each experiment was performed as biological triplicates, the bars represent the overall mean with standard deviation. The red dotted line displays the minimal reduction factor of 4 $\log_{10}$. The statically significant difference is displayed as follows: ns = not significant, * $\leq$ 0.05, ** $\leq$ 0.01, *** $\leq$ 0.001.

biofilm and suspension (figure 3.5.1 b). Neither the suspension nor the biofilm were sufficiently reduced at concentrations ≤ 1 % GA. At 2 % GA, the suspension of 35/14^{rg} was completely killed while the biofilm did not surpass the reduction threshold of 4 $\log_{10}$. At the highest tested concentration (5 % GA), the biofilm of 35/14^{rg} slightly surpassed the reduction threshold.
The suspension of the isolate 09/13^{sm} showed the same tolerance pattern as reported for the suspension of 25/14^{sm}. The biofilm of 09/13^{sm} was more tolerant to GA (figure 3.5.1 c). It was first sufficiently reduced at 2 % GA, although the standard deviation showed, that this result was not gained in all biological replicates.
The isolate 58/15^{rg} showed high similarities between the biofilm and the suspension (figure 3.5.1 d). In concentrations between 0.1 – 1 % GA, it was stronger reduced than 35/14^{rg}. The suspension was sufficiently reduced at ≥ 1 % GA and the biofilm at ≥ 2 % GA, though it only surpassed the reduction threshold slightly.

Sodium Hypochlorite

In most cases, the differences between biofilm and suspension were less distinct as documented for the other disinfectants. Still, the biofilms of the smooth isolates presented a higher tolerance to FAC

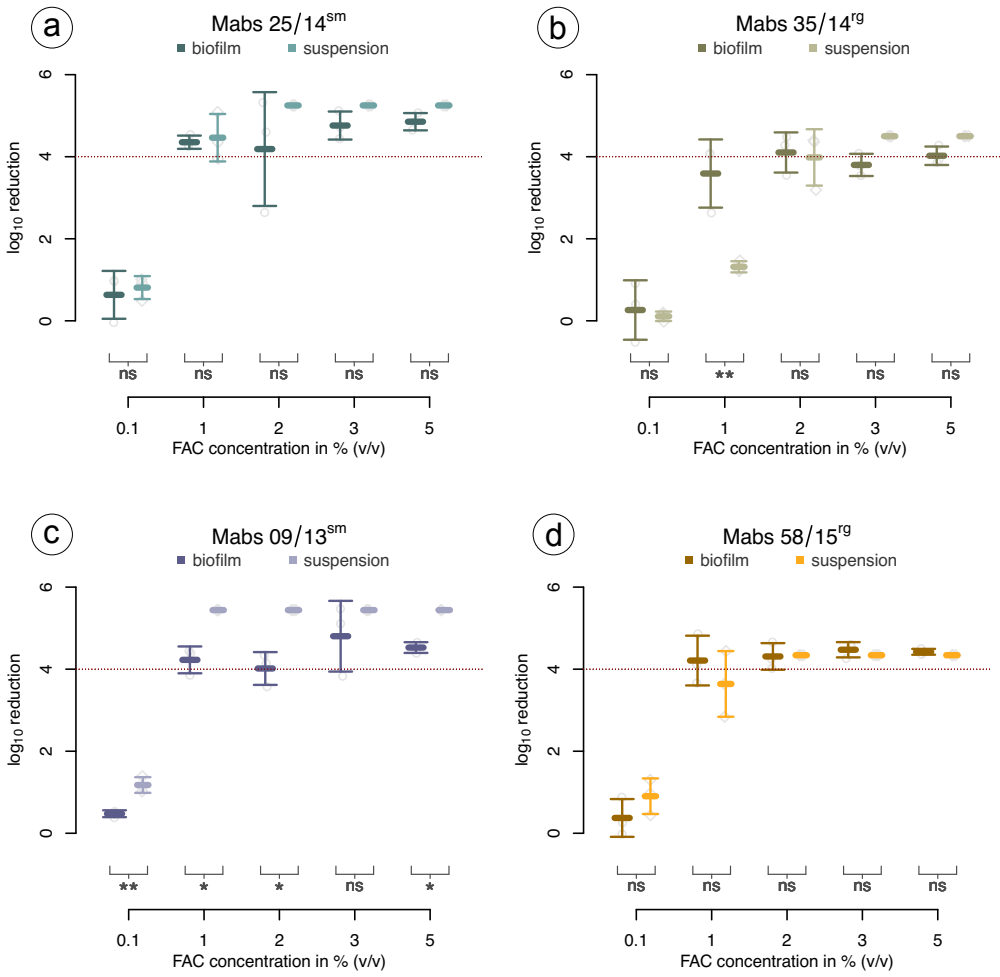

Figure 3.5.2: Disinfectant testing of *M. abscessus* using free active chlorine (FAC)
Displayed is the $\log_{10}$ reduction against the according FAC concentration. The biofilms of the smooth isolates 25/14^{sm} and 09/13^{sm} were in all concentrations more tolerant towards FAC than the corresponding suspension (**a & c**), while the rough isolates showed similar reduction in both cultivation forms. At 1 % FAC both rough isolates showed a reduced tolerance for the biofilms compared to the suspension (**b & d**). Each experiment was performed as biological triplicates, the bars represent the overall mean with standard deviation. The red dotted line displays the minimal reduction factor of 4 $\log_{10}$. The statically significant difference is displayed as follows: ns = not significant, * ≤ 0.05, ** ≤ 0.01, *** ≤ 0.001.

than the suspensions (figure 3.5.2). Interestingly, the biofilms of the rough isolates were less tolerant to FAC in the intermediate concentrations (1 – 2 %).
In case of FAC, biofilm and suspension of *M. abscessus* $25/14^{sm}$ showed at no concentration tested a statistically significant difference in tolerance. Both cultivation forms were sufficiently reduced at 1 % FAC (figure 3.5.2 a). In the higher concentrations $\geq$ 2 % FAC, the suspension was completely killed while the biofilm still showed survival of bacteria up the 5 % FAC.
In contrary to its smooth counterpart ($25/14^{sm}$), the rough morphotype $35/14^{rg}$ showed a higher tolerance of the suspension to FAC than the biofilm at least in concentrations up to 3 % FAC (figure 3.5.2 b). While the suspension was reduced approx. 1.5 $\log_{10}$ at 1 % FAC, the biofilm was reduced approx. 3.5 $\log_{10}$. In the concentrations $\geq$ 3 % FAC the suspension was completely eradicated but the biofilm still showed survival and ranged around the reduction threshold of 4 $\log_{10}$.
The other smooth isolate $09/13^{sm}$ presented an enhanced tolerance of the biofilm to FAC which in most concentrations was statistically significant (figure 3.5.2 c). The suspension of this isolate was completely killed at 1 % FAC while the biofilm showed survival up the 5 % FAC. Though, the biofilm surpassed the reductions threshold in all tested concentrations $\geq$ 1 % FAC.
In $58/15^{rg}$ biofilm and suspension presented almost no difference in tolerance to FAC (figure 3.5.2 d). At 1 % FAC, the biofilm was slightly less tolerant to the disinfectant than the corresponding suspension. This is similar to what was documented for $35/14^{rg}$. In concentrations $\geq$ 2 % FAC both cultivation forms were sufficiently reduced.

Peracetic Acid

In comparison to the other disinfectants, the differences in tolerance were the most pronounced in the disinfectant testing of PAA. In all concentrations, the biofilms of the *M. abscessus* isolates was more tolerant than the suspensions (figure 3.5.3).
In disinfection testing with PAA the isolate *M. abscessus* $25/14^{sm}$ presented a much higher tolerance in biofilm than in suspension (figure 3.5.3 a). The suspension was completely eradicated at 0.05 % PAA while the biofilm was only reduced approx. 1 $\log_{10}$. The biofilm of $25/14^{sm}$ was first sufficiently reduced at a concentrations of 0.1 % PAA though it showed survival of bacteria up the 0.5 % PAA.
In $35/14^{rg}$ the tolerance behaviour of biofilm and suspension were similar to what was documented for $25/14^{sm}$ (figure 3.5.3 b). In contrary, the suspension was first sufficicently reduced at 0.075 % PAA. Also the biofilm of $35/14^{rg}$ presented survival in biofilm associated bacteria up to a concentrations of 0.5 % PAA.
Similar to $25/14^{sm}$ the suspension of the other smooth isolate $09/13^{sm}$ was completely killed at concentrations $\geq$ 0.05 % PAA (figure 3.5.3 c). The biofilm of this isolate was more tolerant than documented for the other two mentioned isolates. In concentrations of $\leq$ 0.1 % PAA, the biofilm of $09/13^{sm}$ was not sufficiently reduced. First at the highest tested concentration of 0.5 % PAA, the biofilm surpassed the reduction threshold but also this isolate showed survival of bacteria.
The rough morphotype $58/15^{rg}$ also showed a higher tolerance in biofilm than in suspension though the difference was less pronounced than in its' smooth counterpart $09/13^{sm}$ (figure 3.5.3 d). The suspension was completely killed at concentrations $\geq$ 0.05 % PAA while the biofilm did not surpass the reduction threshold of 4 $\log_{10}$ up the concentration of 0.1 %. At 0.5 % PAA the biofilm of this isolate was sufficiently reduced.

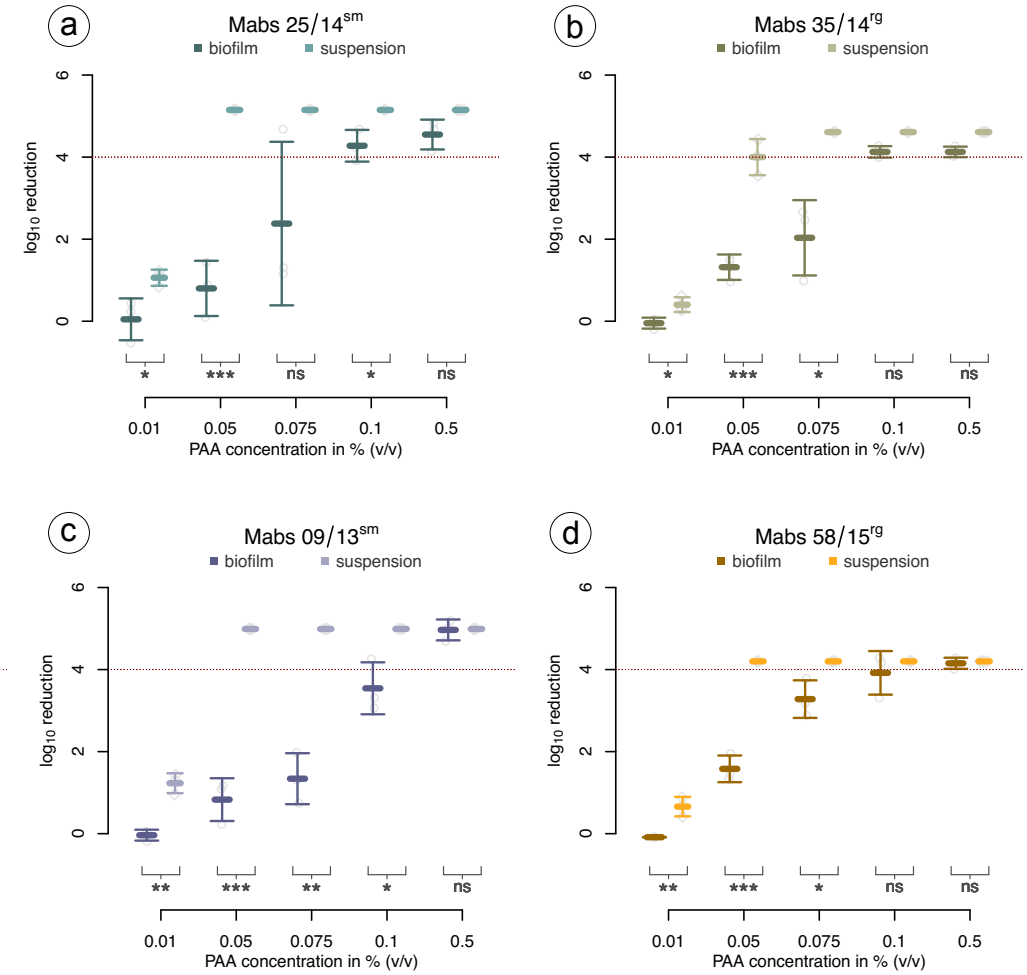

Figure 3.5.3: Disinfectant testing of *M. abscessus* using peracetic acid (PAA)
Displayed is the $\log_{10}$ reduction against the according PAA concentration. In all isolates the formation of biofilm strongly enhanced the tolerance towards PAA, while for the rough isolates (**b** & **d**) the difference to the suspension samples was less pronounced than in the smooth isolates (**a** & **c**). Each experiment was performed as biological triplicates, the bars represent the overall mean with standard deviation. The red dotted line displays the minimal reduction factor of 4 $\log_{10}$. The statically significant difference is displayed as follows: ns = not significant, * $\leq$ 0.05, ** $\leq$ 0.01, *** $\leq$ 0.001.

3.5.1.2 *Mycobacterium chimaera*

Glutaraldehyde

Especially in the higher concentrations of GA tested ($\geq$ 2 %) the biofilm was more tolerant towards the disinfectant than the corresponding suspension. In the lower and intermediate concentrations both cultivation forms presented similar tolerance (figure 3.5.4).

Up to a concentration of 1 % GA, biofilm and suspension of *M. chimaera* ZUERICH-1 showed no statistically significant difference in tolerance (figure 3.5.4 a). First at concentrations $\geq$ 2 % GA, both cultivation forms displayed significant differences. While the supension was sufficiently reduced at 2 % GA, the biofilm was not. At the highest tested concentration of 5 % GA, both forms surpassed the reduction threshold of 4 $\log_{10}$, though, both also showed survival of bacteria. The isolate FR-35 was the most sensitive to GA in comparison to the other *M. chimaera* isolates (figure 3.5.4 b). In the intermediate concentations between 0.5 – 1 % GA the biofilm was more tolerant than the suspension. The latter was fully killed at concentrations $\geq$ 1 % GA and the biofilm surpassed the reduction threshold first at a concentration of 2 % GA. Also in FR-35, the biofilm presented survival of bacteria in biofilm at the highest tested concentration of 5 % GA.

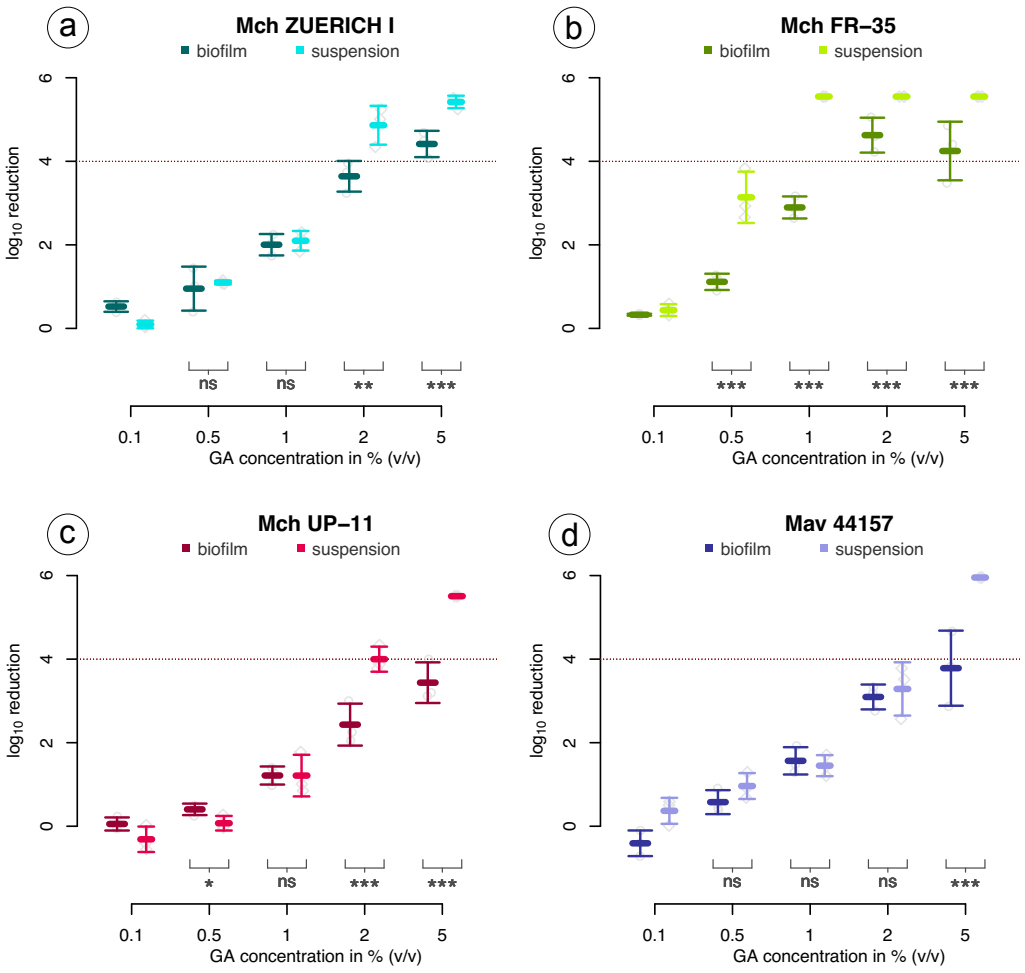

Figure 3.5.4: Disinfectant testing of *M. chimaera* using glutaraldehyde (GA)
Displayed is the tolerance of *M. chimaera* (Mch) and *M. avium* (Mav) against GA. All isolates displayed a significant difference in tolerance between biofilm and suspension above 2 % GA. In the higher concentrations (> 1 % GA) the biofilm was more tolerant than the corresponding suspension. Each experiment was performed as biological triplicates, the bars represent the overall mean with standard deviation. The red dotted line displays the minimal reduction factor of 4 $\log_{10}$. The statically significant difference is displayed as follows: ns = not significant, * $\leq$ 0.05, ** $\leq$ 0.01, *** $\leq$ 0.001.

M. chimaera UP-11 displayed the highest tolerance towards GA when compared to the other *M. chimaera* isolates (figure 3.5.4 c). In concentrations between 0.1 – 1 % GA, both cultivation forms displayed similar tolerance. From 2 % GA on, the biofilm was more tolerant to the disinfectant than the suspension. While the suspension surpassed the reduction threshold at 5 % GA, the biofilm was at no tested concentration sufficiently reduced.
The isolate *M. avium* ATCC 15769 showed similar tolerance of biofilm and suspension in all concentrations ≤ 2 % GA (figure 3.5.4 d). The difference between both forms was not statistically significant. At 5 % GA, the suspension of this isolate was completely eradicated while the biofilm did not surpass the reduction threshold of 4 $\log_{10}$.

Sodium Hypochlorite

The disinfectant testing with FAC resulted in a very unexpected pattern - in all tested isolates was the suspension more tolerant towards FAC than the corresponding biofilm (figure 3.5.5).
In the lowest (0.1 %) and the highest (5 %) concentrations of FAC tested, the biofilm and the suspension of *M. chimaera* ZUERICH-1 presented similar reduction levels (figure 3.5.5 a). In the intermediate concentrations between 1 – 3 % FAC, the suspension was more tolerant to the disinfectant than the

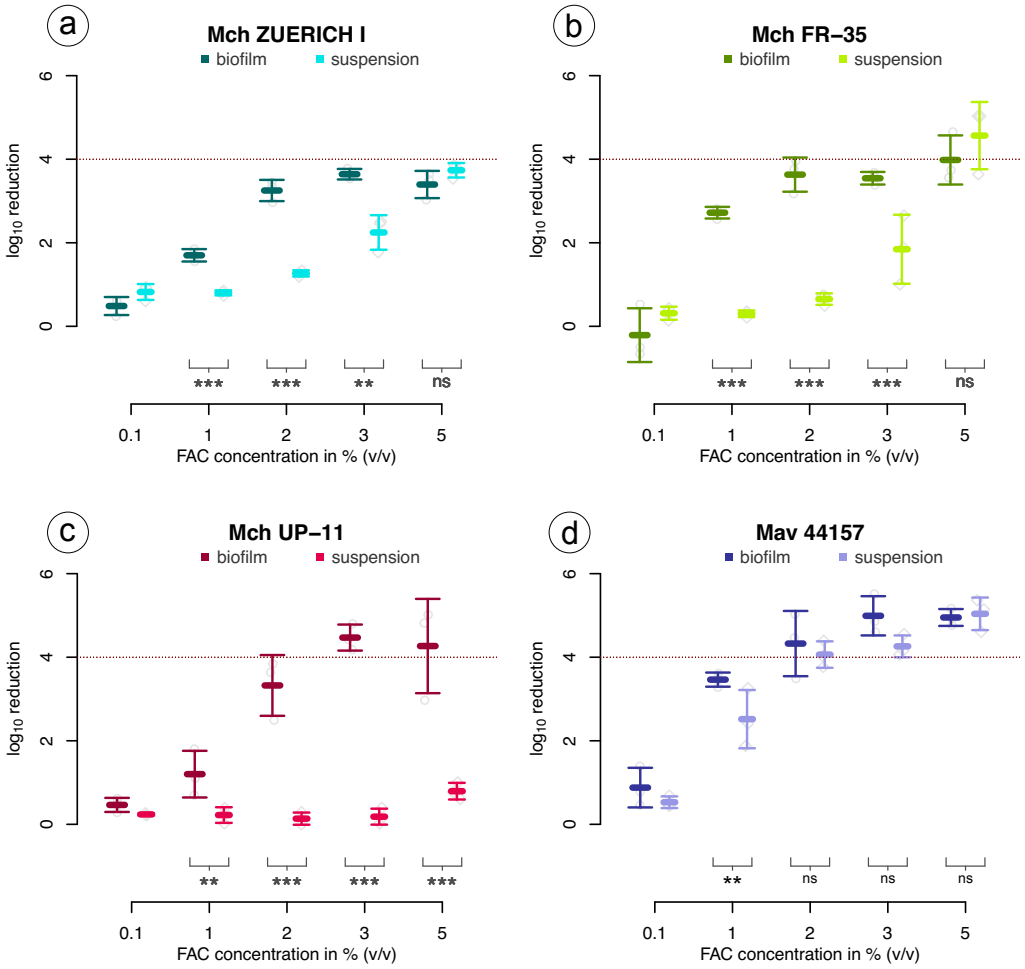

Figure 3.5.5: Disinfectant testing of *M. chimaera* using free active chlorine (FAC)
Displayed is the disinfectant testing of biofilm and suspension of *M. chimaera* (Mch) and *M. avium* (Mav) with FAC. Especially for the *M. chimaera* isolates, the suspension displayed a much higher tolerance against FAC than the biofilm. Each experiment was performed as biological triplicates, the bars represent the overall mean with standard deviation. The red dotted line displays the minimal reduction factor of 4 $\log_{10}$. The statically significant difference is displayed as follows: ns = not significant, * ≤ 0.05, ** ≤ 0.01, *** ≤ 0.001.

biofilm. At 2 % FAC the cultivation forms presented a difference of approx. 2 $\log_{10}$ steps. At all tested concentrations, neither the biofilm nor the suspension were sufficiently reduced. The isolate FR-35 presented a similar toelerance pattern as documented for ZUERICH-1 (figure 3.5.5 b). In contraray to ZUERICH-1, the suspension of FR-35 surpassed the redudction threshold at a concentration of 5 % FAC. In case of *M. chimaera* UP-11, the differences between biofilm and suspension were most pronounced when compared to the other isolates (figure 3.5.5 c). While the suspension was not reduced more than 1.5 $\log_{10}$ at the highest tested concentration of 5 % FAC, the biofilm of this isolate surpassed the reduction threshold of 4 $\log_{10}$ at a concentration of $\geq$ 3 % FAC.
In contrast to the mch isolates, *M. avium* ATCC 15769 presented a lower tolerance in suspension and biofilm to FAC and a much lower difference between both cultivation forms (figure 3.5.5 d). Overall, biofilm and suspension of *M. avium* ATCC 15769 showed similar levels of reduction while the suspension was slightly more tolerant in most cases. Both cultivation forms of this isolate were sufficiently reduced at concentrations $\geq$ 2 % FAC.

Peracetic Acid

In case of PAA, all biofilms samples of the tested *M. chimaera* and *M. avium* isolates displayed a

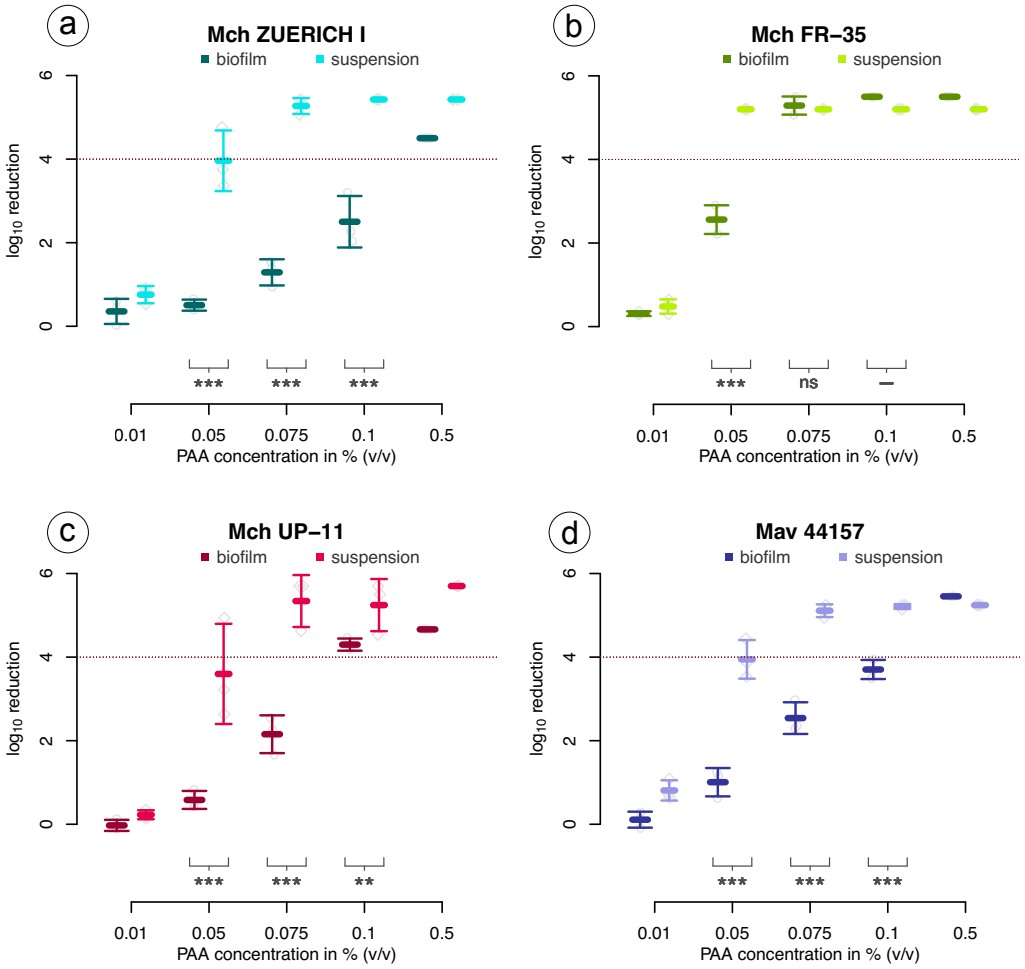

Figure 3.5.6: Disinfectant testing of *M. chimaera* using peracetic acid (PAA)
Displayed is the tolerance of biofilm and suspension samples of *M. chimaera* (Mch) and *M. avium* (Mav) against PAA. For all tested isolates, the biofilm samples were more tolerant than the suspension at the same concentration. Each experiment was performed as biological triplicates, the bars represent the overall mean with standard deviation. The red dotted line displays the minimal reduction factor of 4 $\log_{10}$. The statically significant difference is displayed as follows: ns = not significant, * $\leq$ 0.05, ** $\leq$ 0.01, *** $\leq$ 0.001.

higher tolerance than the corresponding suspension (figure 3.5.6). In case of ZUERICH-1 the suspension reached the reduction threshold of 4 $\log_{10}$ already at a concentration of 0.05 % PAA, the biofilm was first sufficiently reduced at the highest tested concentration (0.5 % PAA) (figure 3.5.6 a). The differences between both forms were highly statistically significant (***) in the intermediate concentrations (0.05 – 0.1 % PAA). In comparison to the other *M. chimaera* isolates, the biofilm of ZUERICH-1 was the most tolerant to PAA.
The isolate FR-35 displayed the most sensitive tolerance pattern when compared to the other isolates (figure 3.5.6 b). The suspension of this isolate was completely killed at a concentration of 0.05 %. The biofilm was more tolerant than the suspension, though it was sufficiently reduced at a concentration of 0.075 % PAA and in the concentrations $\geq$ 0.1 % both forms displayed no survival of bacteria.
Similar to ZUERICH-1, the differences between biofilm and suspension of UP-11 were statistically siginificant in the intermediate concentrations of PAA (0.05 – 0.1 %) (figure 3.5.6 c). In these concentrations, the biofilm was more tolerant towards the disinfecant than the suspension. The suspension of *M. chimaera* UP-11 was sufficiently reduced at a concentration of 0.075 % PAA. The biofilm surpassed the reduction threshold at a concentration of 0.1 % PAA. Like noted for *M. chimaera* ZUERICH-1, both cultivation forms of UP-11 were completely eradicated at a concentration of 0.5 % PAA.
Also the isolate *M. avium* ATCC 15769 presented a higher tolerance of the biofilm to PAA when compared to the suspension (figure 3.5.6 d). Similar to *M. chimaera* ZUERICH-1, the suspension of *M. avium* ATCC 15769 reached the reduction threshold at 0.05 % PAA. The biofilm was more tolerant and was first sufficiently reduced at 0.5 % PAA. Corresponding to the results gained for the *M. chimaera* isolates, both cultivation forms were completely killed at this concentration.

3.5.1.3 Weekly disinfection

The outbreak strain ZUERICH-1 was further tested in a weekly disinfection procedure using different concentrations of PAA. Therefore, the bacteria were either cultivated in water or MB-OADC. Both were inoculated with the identical number of bacteria. The biofilms cultivated in water grew to a CFU/bead of 5 $\log_{10}$ after 21 days and the bacteria cultivated in MB-OADC grew to a number of 9.5 $\log_{10}$ CFU/bead in the same time (figure 3.5.7).

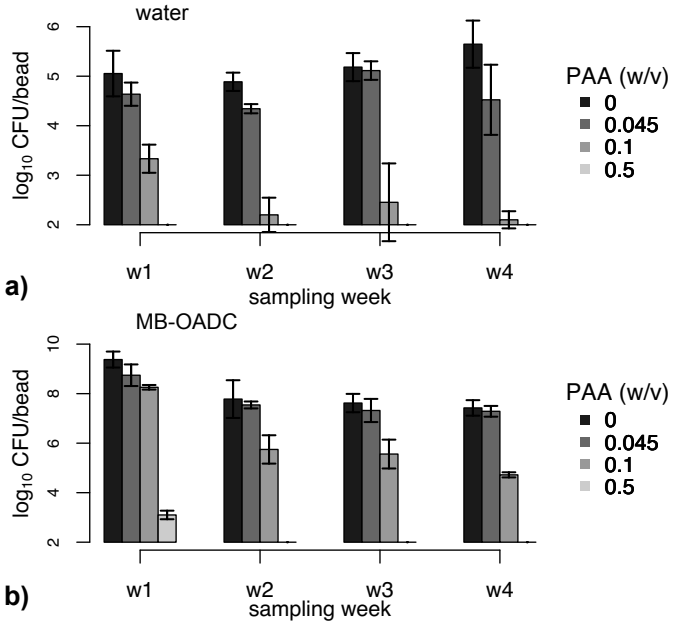

Figure 3.5.7: Weekly disinfection of ZUERICH-1

Biofilm samples of the outbreak strain ZUERICH-1 were cultivated in either water **(a)** or MB-OADC **(b)** for 21 days. Afterwards the biofilms were disinfected for 10 min in a weekly cycle with different concentrations PAA and afterwards again cultivated in water or medium.
In both variants, the commonly used concentrations of 0.045 % and 0.1 % PAA were not sufficient to eradicate the bacteria. After 4 weeks of weekly disinfection, surviving bacteria were still detected. Only a concentration of 0.5 % PAA was sufficient to completely kill the bacteria.

Independent from the cultivation medium, neither of the recommended concentrations of PAA (0.045 % and 0.1 %) were sufficient to eradicate the biofilm after 4 weeks (figure 3.5.7). The biofilms cultivated in water that were not disinfected, kept growing during the time of the experiment. The bacteria that were grown in MB-OADC without disinfectant showed a slight reduction of CFU/mL after the first week and thereafter kept a stationary number of bacteria (approx. 7.5 $\log_{10}$).
Independent of the growth medium, the biofilms that were disinfected with a concentration of 0.045 % PAA kept an almost consistent number of bacteria during the four weeks of weekly disinfection, which in case of the MB-OADC cultivated bacteria was similar to the negative control. In case of the water cultivated biofilms, the numbers were lower than in the negative control and less constant during the time of the experiment.
The disinfection with 0.1 % PAA resulted in a reduction of the biofilms cultivated in water in the first week to a number of approx. 3.5 $\log_{10}$ CFU/bead (figure 3.5.7 a). In the second week the biofilms cultivated in water were further reduced to a CFU/bead of approx. 2 $\log_{10}$ which remained constant during the residual weeks of testing. The biofilms cultivated in MB-OADC were reduced after the second week to a CFU/bead of approx. 6 $\log_{10}$ that remained constant during the experiment (figure 3.5.7 b).
Only with 0.5 % PAA the bacteria were completely eradicated. The biofilms that were cultivated in water were killed in the first week, while the biofilms grown in MB-OADC were strongly reduced in the first and completely killed in the second week of testing.
It can be summarized that the recommended concentrations of 0.045 % and 0.1 % PAA, were both not able to completely eradicate the biofilm of *M. chimaera* ZUERICH-1 in a weekly disinfection cycle over four weeks (figure 3.5.7).

3.5.2 Antibiotic Susceptibility of *M. abscessus*

Antibiotic susceptibility testing was focussed on *M. abscessus*. Two antibiotics were selected that are part of current therapy regimens and target different cell functions of the bacteria. Amikacin is able to show bacteriocidal effects against the bacteria in the used concentrations, while tigecycline is only having bacteriostatic effects. The experimental protocol was inspired by common laboratory susceptibility testing procedures that majorly base on micro-dilution.

3.5.2.1 Amikacin

The susceptibility testing with amikacin (AMI) showed a dramatically higher tolerance of the biofilms of all tested *M. abscessus* isolates in comparison to the corresponding suspension (figure 3.5.8). The differences between both cultivation forms were more pronounced in the higher concentrations of the antibiotic ($\geq$ 32 µg/mL). In all tested concentrations, the number of bacteria in the biofilm samples remained almost constant with the exception of 35/14^{rg}. The number of bacteria in the suspensions on the other hand decreased continually in all isolates.
The biofilm samples of the isolate 25/14^{sm} ranged around a CFU/mL of about 8 $\log_{10}$ at all tested AMI concentrations while the suspension showed a decrease in bacterial numbers at an AMI concentration of $\geq$ 8 µg/mL (figure 3.5.8 a). At 16 µg/mL of AMI, the number of bacteria in suspension was reduced more than the half in comparison to the initial quantity. In the higher concentrations ($\geq$ 32 µg/mL) the number of bacteria in suspension was reduced below the detection limit of 3 $\log_{10}$ CFU/mL.

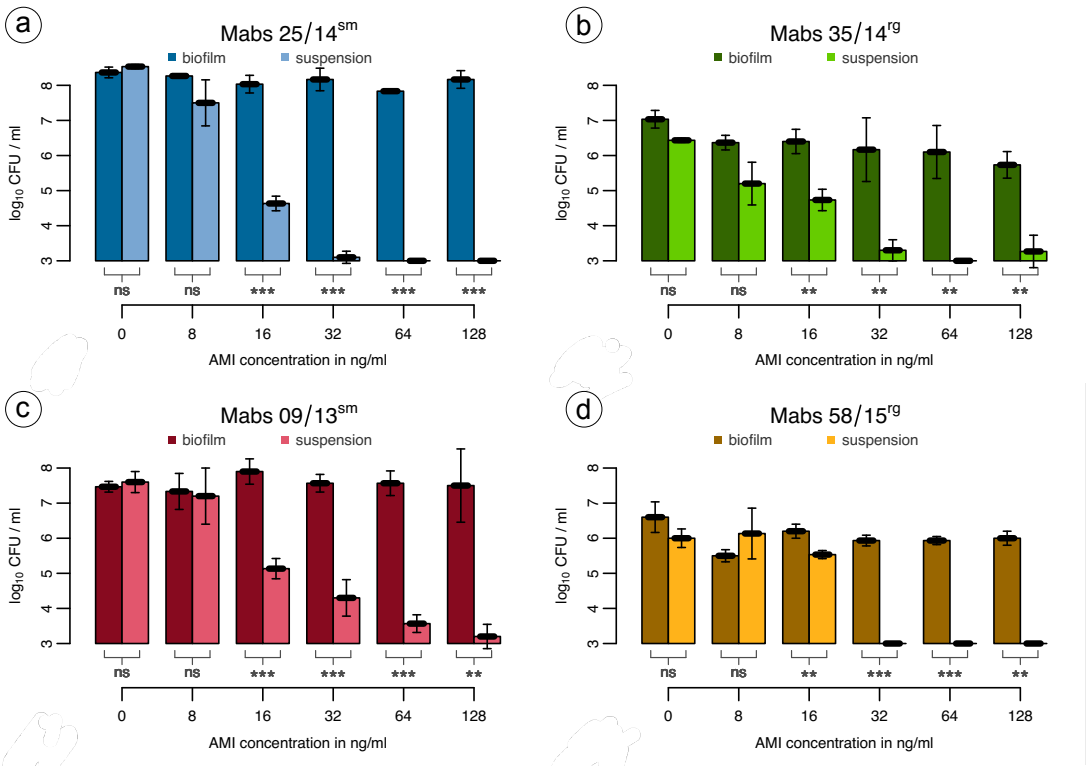

Figure 3.5.8: Susceptibility of *M. abscessus* towards amikacin

The susceptibility against amikacin (AMI) of *M. abscessus* smooth and rough isolates was tested with biofilm and suspension. All biofilms presented a dramatically higher tolerance towards the antibiotic when compared to the corresponding suspension. The bacteria in the suspension samples of the isolates 25/14^{sm} 35/14^{rg} and 09/13^{sm} were distinctly reduced at AMI concentrations $\geq$ 8 µg/mL. The suspension of 58/15^{rg} was stable until a concentration of 32 µg/mL.
Bars represent mean and standard deviation of three individual biological replicates. The statically significant difference is displayed as follows: ns = not significant, * $\leq$ 0.05, ** $\leq$ 0.01, *** $\leq$ 0.001.

The rough isolate 35/14^{rg} displayed a slight reduction of bacteria in biofilm from 7 $\log_{10}$ in the negative control to approx. 6 $\log_{10}$ at the highest concentration AMI tested (128 µg/mL). The suspension samples were continually reduced with increasing concentration of AMI. Although, even at the highest concentration tested (128 µg/mL), the suspension still contained surviving bacteria (figure 3.5.8 b).
The other smooth isolate, 09/13^{sm}, displayed a higher tolerance towards the increasing concentration of AMI in suspension when compared to 25/14^{sm} (figure 3.5.8 c). Even when tested with 128 µg/mL AMI, survival of bacteria was documented. The biofilm of this isolate showed a constant number of bacteria, that seemed to increase slightly in comparison to the negative control at AMI concentrations $\geq$ 16 µg/mL.
The isolate 58/15^{rg} displayed a slight reduction of bacteria in the biofilm samples treated with AMI when compared to the negative control (figure 3.5.8 d). Independent from the concentration, the number of bacteria in biofilm was relatively constant. In concentrations $\leq$ 16 µg/mL of AMI, the suspension samples presented only a small reduction. At higher concentrations ($\geq$ 32 µg/mL) there was no survival above the detection limit documented for the suspension.

3.5.2.2 Tigecycline

The effects documented for susceptibility testing with TGC were less striking in comparison to the results gained with AMI. All biofilm samples presented a higher tolerance towards the antibiotic treatment when compared to the corresponding suspension (figure 3.5.9). In contrast to AMI susceptibility testing, the suspension showed only slight reduction in the increasing concentrations of TGC.

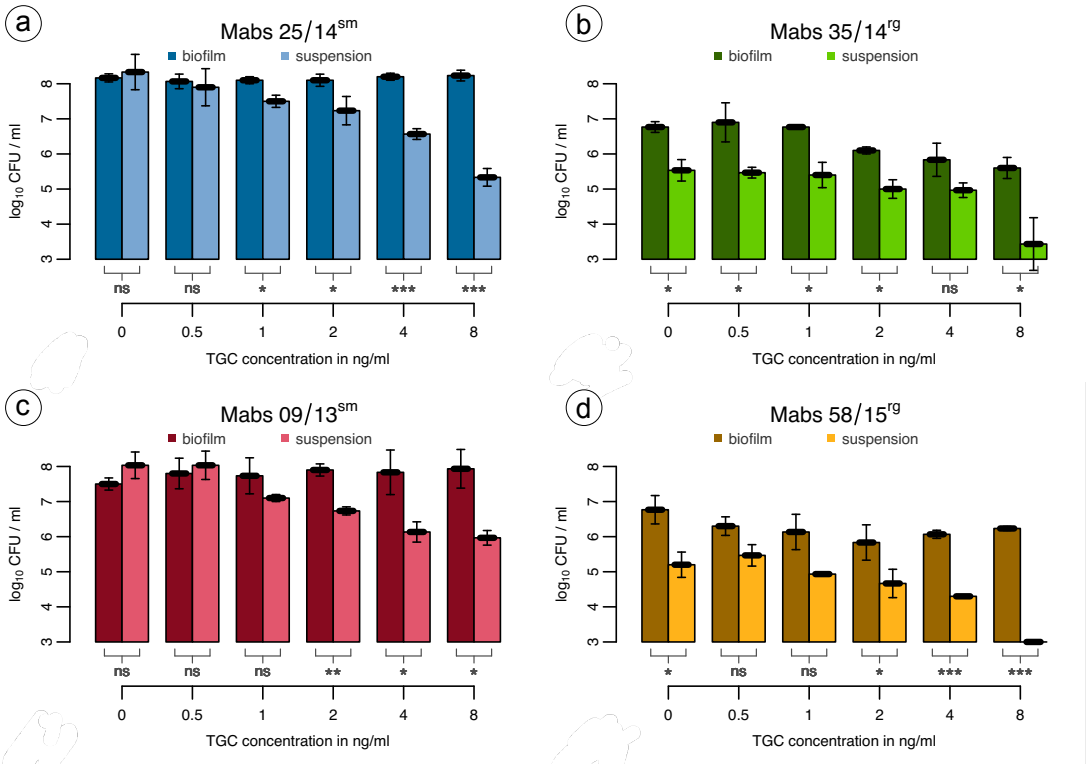

Figure 3.5.9: Susceptibility of *M. abscessus* towards tigecycline

The susceptibility against tigecycline (TGC) of *M. abscessus* smooth and rough isolates was tested with biofilm and suspension. In general the tested biofilms presented a higher tolerance towards TGC when compared to the suspension.
Bars represent mean and standard deviation of three individual biological replicates. The statically significant difference is displayed as follows: ns = not significant, * $\leq$ 0.05, ** $\leq$ 0.01, *** $\leq$ 0.001.

The number of biofilm-associated bacteria was constant in both smooth isolates, while the rough counterparts displayed slight reductions.
With increasing concentration of TGC, the biofilm of the isolate $25/14^{sm}$ showed no reduction. Instead, the number of bacteria remained constant at a number of approx. 8 $\log_{10}$ CFU/mL. The number of bacteria in suspension continually decreased with increasing antibiotic concentration to a number of approx. 5 $\log_{10}$ CFU/bead (figure 3.5.9 a). At 8 µg/mL TGC the suspension displayed a survival of approximately 50 % when compared to the negative control.
The isolate $35/14^{rg}$ presented a a slight reduction of bacteria in both cultivation forms, though the total number of bacteria in suspension was lower from the beginning. Both cultivation forms retained a constant number of bacteria up to a concentration of $\leq$ 1 µg/mL TGC (figure 3.5.9 b). Thereafter, a slight decrease in numbers was noted. Only at a concentration of 8 µg/mL, a clear reduction was found for the suspension sample while the number of bacteria in biofilm was only slightly reduced.
Similar to the other smooth isolate, the biofilm samples of $09/13^{sm}$ displayed an increase in bacterial numbers with increasing concentration of TGC, while the suspension displayed a constant decrease (figure 3.5.9 c). The treatment with 0.5 µg/mL TGC showed no effect on the suspension but in concentrations $\geq$ 1 µg/ml, the CFU/ml reduced continually. In comparison to $25/14^{sm}$, the bacteria in suspension were less reduced in the higher concentrations of TGC.
The other rough isolate $58/15^{rg}$ also presented a higher tolerance of the biofilm towards the antibiotic when compared to its suspension samples (figure 3.5.9 d). Similar to $35/14^{rg}$ the initial number of bacteria was lower in the suspension samples. In the intermediate concentration of TGC used (2 µg/mL) the biofilm showed a slight decrease in CFU/mL counts and in higher concentrations again a small increase. In comparison to the negative control, the number of bacteria in suspension samples increased at 0.5 µg/mL TGC and decreased continually in the higher concentrations. At 8 µg/mL TGC no survival of the suspension above the detection limit was documented.

In summary, all biofilm samples displayed almost no or only very little reaction to the antibiotic treatment in neither case of AMI or TGC. The corresponding suspensions showed a higher susceptibility, especially to higher concentrations of each of the antibiotics, but not all were completely eradicated even at the highest concentration tested.

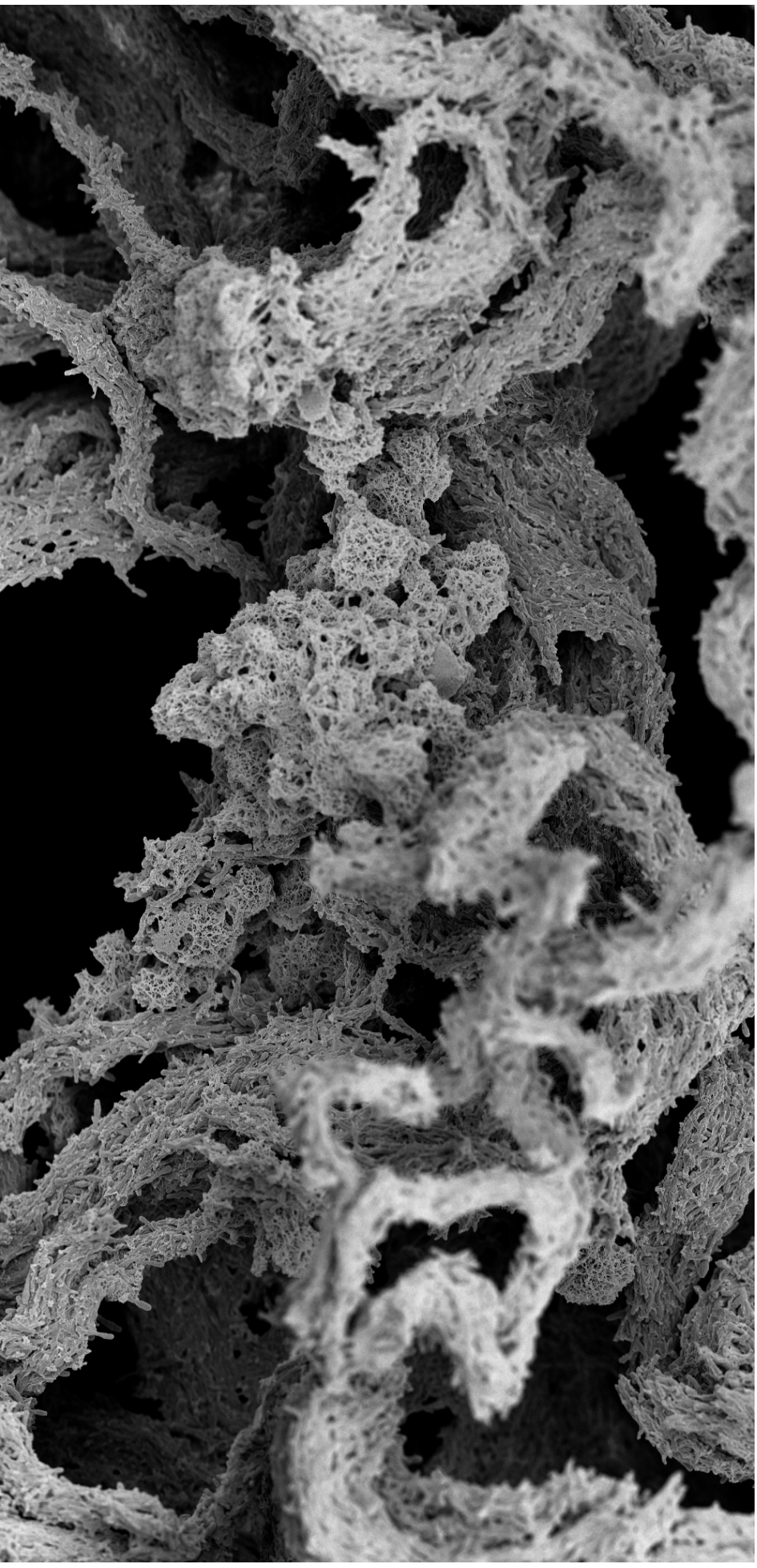

Chapter 4

Discussion

4.1 NTM biofilms

The standardized laboratory cultivation of biofilms has become more and more important in the past decades as they represent the most common natural lifestyle of bacteria [111, 113, 114]. Meanwhile, a broad range of biofilm cultivation methods was established and evaluated focussing on practicability, handling, suitability for different applications, time and resource expense. Overall, each method has its specific advantages and limitations and should be chosen depending on the individual research question [151].
Mycobacterial biofilms are commonly cultivated as air-liquid interface pellicle biofilms. On top of broth medium, the bacteria form floating pellicle structures ('scum skin') which contain the majority of bacteria embedded in an ECM [115]. These pellicles are used in variable approaches as for example susceptibility testing [101]. The limitation of this biofilm cultivation model is quite obvious: The formed pellicles can not easily be moved or transferred from the medium. As a result, the cultivated biofilms are hardly to be analysed with further experimental techniques.
Other methods use floating chambers in which the bacteria attach to pegs. These pegs can be made of several different materials and the experimental design enables the testing of different cultivation conditions [151]. The major 'problems' of this method are the high shear forces to which the bacteria are exposed as well as the price and resource expense. Due to high shear forces, the formation of biofilm of rough *M. abscessus* isolates is hindered which in result led to the assumption in previous studies that these morphotypes are not able to form biofilms at all [76, 77].
Though the assumption that rough isolates are not able to produce biofilms was disproved meanwhile, it was not possible to cultivate surface attached biofilms of these morphological variants yet [101]. The cultivation of surface attached biofilms of NTM is a major approach of this work. This observation is of great importance as it tackles the common assumptions of certain NTM to form biofilms and helps to correct previous wrong interpretations.

4.1.1 PGBs as a reliable substrate for NTM biofilm cultivation

This study focussed on a cultivation method using a cost-efficient biofilm bead assay that was established for the use in disinfectant testing at the Robert Koch - Institute [140]. The system bases on biofilm grown on the surface of beads which can further be used as a transferable substrate for various analysis methods.
The original assay used round glass beads with a smooth surface. These have two major disadvantages; first, they have a high level of abrasion of multilayered biofilm and second, they have a limited surface to which the biofilm can attach [140]. Because of this, different substrates were tested in the present study in order to find the most appropriate for NTM biofilm cultivation. Porous glass beads (PGB) were identified to be the most efficient substrate exhibiting the highest numbers of bacteria compared to the other tested materials and moreover, they enabled the formation of surfaced attached biofilms by rough *M. abscessus* isolates. This is presumably based on the enlarged surface of the PGBs resulting from the sintered glass particles, that form cavities and edges in which shear forces are less intensive.
The bead assay using PGBs provided also high levels of reproducibility among multiple trials. As a prerequisite for antimicrobial susceptibility testing, the amount of bacteria is necessary to be constant in all samples otherwise the results loose reliability. Only a few biofilm susceptibility testing methods can enable constant and reproducible growth of biofilm [140, 151].

Another advantage of the PGB model in comparison to other established biofilm cultivation methods is the easy application to variable subsequent analysis techniques. In this study, the cultivated biofilms were used for growth analysis, microscopy, ECM-composition analysis, proteome and transcriptome as well as different susceptibility testing protocols. This variability of the cultivation system enabled to analyse the NTM biofilms from different research perspectives and provided important insights into the biofilm formation of *M. chimaera* and *M. abscessus*.

4.1.2 Lipids influence the biofilm structure

A remarkable finding was the difference that appeared in the biofilm structure between smooth and rough *M. abscessus* isolates as well as the biofilm structure of *M. chimaera* FR-41 in comparison to the other *M. chimaera* isolates.
The rough *M. abscessus* isolates and *M. chimaera* FR-41 displayed a strong aggregation of bacteria and less attachment to the surface of the glass particles than the other analysed isolates. Further analysis showed that these aggregative isolates display certain differences in the lipid expression profiles. The influence of GPL on the ability of mycobacteria to form biofilms has been documented before [116]. The rough *M. abscessus* isolates of the present study are lacking GPL expression due to genetic variations in the *mps2* gene [73] which influences their specific lipid profile on the cell surface. It was stated that rough isolates of *M. abscessus* in general are not able to grow as biofilms [76]. In contrary, the present study shows that they can grow as adhesive biofilm, though, the extend of surface attachment is reduced when compared to their smooth counterparts. Therefore, the aggregation of bacteria dominates in the biofilm.
In comparison to the rough *M. abscessus* morphotypes, the isolate *M. chimaera* FR-41 grew in variable but smooth colonies on agar plates that did not present a rough appearance which indicates that GPL expression is not altered in this isolate. Still, the isolate FR-41 shows a more yellowish coloration of the colonies on agar plate in comparison to the other *M. chimaera* isolates. The TLC analysis showed, that FR-41 presented a different lipid profile when compared to the other *M. chimaera* isolates. The comparison of the genomes of FR-41 and the other *M. chimaera* isolates showed that FR-41 is missing 75 genes which were found in the proteome analysis to be significantly different expressed in biofilm (data not shown). Two of these genes, *lcpA-1* and *lpgB*, are of special interest with regard to the lipid expression. The gene *lcpA_1* encodes for LytR, a transcriptional regulator that is involved in cell wall biosynthesis [152]. The gene *lpgB* is genetically similar to the gene *lpqB* from MTB and *M. smegmatis*. LpqB mutants from *M. smegmatis* display increased cell-to-cell adhesion and severe defects in surface attachment of biofilm associated bacteria [153]. Moreover, LpqB has been found to influence the multidrug resistance of *M. smegmatis*. The characteristics described for *M. smegmatis* mutants lacking *lpqB* are overlapping with what was documented in this study for FR-41.
Another finding was, that the biofilm growth of FR-41 in MB-OADC was swaying as represented by the inconsistent number of bacteria documented in reproducibility testing. This was also shown for biofilms of *M. smegmatis* LpqB mutants by Nguyen et al. 2010 [153]. On the other hand, *M. chimaera* FR-41 showed no problems of biofilm growth in MH-OADC. It was shown before, that in low-nutrient environments bacteria majorly attach to preferable substrates which could be an explanaition for the different growth patterns of *M. chimaera* FR-41 in the two used media [111, 112]. Further research should focus on the influence of the cultivation medium on the numbers of bacteria and the structure of the biofilms in order to standardise methods and to improve comparability among experiments.

4.1.3 Biofilm structure highly depends on the cultivation medium

The structure and composition of biofilms indisputably depends on environmental conditions [113, 128]. The experiments presented in the current study underline this statement comprehensively.
In general, NTM are cultivated in MB-OADC which is also the standard medium used for cultivation prior to disinfectant testing. Due to its composition, it provides optimal growth conditions and nutrient supply for NTM. On the opposite, the here used medium MH/MH-OADC is recommended for susceptibility testing of NTM. It is a broth with reduced ingredients, enabling growth of NTM but does not provide optimal nutrient conditions.
In MB-OADC the smooth isolates of *M. abscessus* presented a mono-layered biofilm structure covering almost the complete surface of the glass particles. The rough isolates showed extreme aggregation and limited attachment to the glass surface. A completely different behaviour was displayed when *M. abscessus* isolates were cultivated in MH. The smooth isolates still displayed complete coverage of the PGB surface but they also presented cording in a separate biofilm domain. The corded structure was of a similar size as the PGB. The rough isolates on the other hand showed no separate biofilm domain, though the PGBs were thickly covered in a slimy structure. The microscopic evaluation showed that in contrary to the cultivation in MB-OADC, the bacteria did not predominantly form aggregates, instead they distributed over to complete glass surface showing no attachment delays.
A possible explanation is, that the admixed oleic acid in the MB-OADC medium is catabolised by the mycobacteria to a substance called Tween 80 or polysorbat 80 [154]. It is commonly used as a detergent added to the cultivation medium for mycobacteria as it is meant to inhibit the strong aggregation of the bacteria for improving cultivation and plating. Tween 80 presumably influences the structure of the biofilms and could be the reason, why cording was not documented when the bacteria were cultivated in MB-OADC and why rough *M. abscessus* isolates show reduced surface attachement.
Besides *M. abscessus*, also the biofilm growth of the isolate *M. chimaera* FR-41 was majorly influenced by the medium. While in MB-OADC the biofilm growth of this isolate was retarted, it did not show any delay in growth when cultivated in MH-OADC. In this case, it can not be explained by hindered surface attachement due to Tween 80 since oleic acids was admixed in both media. Therefore the reason for this changed growth behaviour stays presumably in relation to other ingredients in the medium.

4.1.3.1 Cording of *M. abscessus* is medium specific

Mycobacterium tuberculosis is adapted to the conditions in the sputum and the survival in the human's lung. The cord formation within the patient is thereby directly linked to virulence and pathogenesis. In MTB the cording is directly linked to the expression of TDM (trehalose dimycolate). Meanwhile, the cording phenotype was also documented *in vitro* in different NTM including *M. abscessus* [87, 88, 89, 90]. For further research it would be of great interest to analyse whether *M. abscessus* is also forming cords during the infection of the patients lung. In the present study, cording was documented when *M. abscessus* was cultivated in MH, though the expression of TDM was not investigated due to time restrictions. Therefore it can not finally be proven in this work, that the documented cording results from the same molecular structure that is responsible for this phenotype in MTB.
Another interesting finding of the cording phenotype of *M. abscessus* was the documented elongation of cells and in case of *M. abscessus* $09/13^{sm}$, the thickening of one end of the cell within the cording

structure. Since this phenotype was not yet described for mycobacteria, it remains unclear to which mechanisms or functions this cell shape contributes.
In a further approach of the present study, the cultivation of *M. abscessus* biofilms in artifical sputum medium (ASM) was tested. As the name indicates, ASM provides conditions similar to what is biochemically present within the patients lung. Biofilms of *M. abscessus* were cultivated in ASM, showing a similar appearance as it was documented for the cultivation in MH (personal communication RKI). Till now it has not yet been analysed whether these biofilms also displayed cord formation. Hunt et al. (2019) showed the cord formation of *M. abscessus* when it was cultivated in ASM including the expression of TDM [90]. It was suggested that - similar to MTB - the cording of *M. abscessus* is a virulence or infection phenotype [90]. The major components of MH - casein and bovine extract - provide a high level of amino acids which are also significant ingredients of ASM and are of course present in the sputum of the patient. A link between amino acids and the expression of cord factor has not yet been documented but could be an interesting focus for future research.

4.1.4 ECM composition - general and particular patterns

In general it was documented, that the biofilms of all tested isolates in both species produce more biomass of protein, lipids and DNA than the corresponding suspension. This was in most cases statistically significant.
The composition of the biofilm is of high interest as the ECM majorly contributes to survival against antimicrobials [129]. The biofilm matrix is composed of a huge variety of molecules and structures and many efforts have been made to investigate the biofilms distinct composition [155]. A common approach is to separate the ECM from the bacteria by centrifugation or by fluorescent labelling [130, 156, 157]. The imaging approach is limited to the analysis of structure and distribution but does not enable to quantify ECM components reliably or to differentiate between specific molecules yet. The other method using centrifugation makes it possible to analyse the composition in detail as for example by mass spectroscopy or NMR. Taking in consideration that the ECM is tightly linked to the bacteria, it can not be proven that the ECM is completely detached from the bacteria by centrifugation. Thereby it is likely that by this approach, not the complete ECM is to be analysed and/or mixed with residual bacteria.
Since in this study, the major questions regarding the ECM was not to investigate single molecules in the biofilm but to analyse the overall composition, a new approach was established to determine the biomass of different general components (DNA, protein, lipids). This enabled to give first impressions of the differences or similarities in the ECM of species and/or isolates.

4.1.4.1 *M. abscessus* biofilms display increased amounts of eDNA

All tested *M. abscessus* isolates displayed a distinct increase in DNA per bacterium when cultivated as biofilm. The biofilm of *M. abscessus* $09/13^{sm}$ thereby displayed the highest increase showing the approx. 25-fold amount of DNA when compared to its suspension. Though, the established quantification method also includes the measurement of dead bacteria, it can be suggested that the here shown DNA amount represents eDNA in majority.
While in this study the amount DNA was evaluated using qPCR and PMA-qPCR, many other studies focus on staining and microscopy for determining the eDNA quantity in the biofilm [158, 159, 160]. A similar approach was also tested in the present study (data not shown). Different stains (Propidium Iodide, Bobo-III) commonly taken for eDNA labelling were used and quantified using a TECAN

reader. This did not lead to reliable results as the measurements showed very high fluctuations (data not shown). Especially when establishing a DNA standard for this method the RLU (relative light units) of the standard concentrations were not consistent even within the same test plate.

eDNA highly contributes to biofilm formation of many bacteria as it for example supports the attachment process and stabilizes the overall ECM [161]. Tang et al (2013) showed for four different species (*Pseudomonas, Rheinheimera, Serratia, Microbacterium*) the correlation of growth and eDNA expression in biofilm [158]. While in all planktonic cultures an increase of eDNA was measured in the late exponential growth phase, the amount of eDNA in the biofilms did not correlate with the growth phases, though, the removal of eDNA directly affected the attachment process in the biofilms of all species [158]. Reflecting the concentration of eDNA over time, it was shown that, as further the biofilm grows, the more eDNA is released. This indicates that the initial eDNA production does not exclusively influence the attachement process but is also necessary for keeping stability and providing protection [159].
Since *M. abscessus* displays great differenes in the amount of DNA in biofilm and suspension, it can be assumed that eDNA is an essential component of the *M. abscessus* biofilm. It was shown previously that the addition of DNase enhances the susceptibility of *M. abscessus* isolates to antibiotics. Therefore it was further used for treatment of patients [162, 163]. Preliminary results gained in a further approach of the present study showed that the amount of eDNA was even more increased when *M. abscessus* biofilms were cultivated in MH instead of MB-OADC. Specifically the cording domain of the biofilm of *M. abscessus* $09/13^{sm}$ presented a four times higher amount of eDNA than the biofilm attached to the surface of the bead (preliminary data not shown). Assuming that the cording phenotype is similar to the biofilms produced by *M. abscessus* in the lung of patients, it is reasonable that the additional treatment with DNAse could support the effects of antibiotic treatment. Though it remains still unknown whether *M. abscessus* also produces a cording phenotype during the infection. This is a very important question for future research as it could help to provide better understanding of the infection process and enable to adapt treatment and testing methods. Using the presented susceptibility testing method of *M. abscessus* biofilms, it could be analysed how and to which extent the addition of DNase supports the efficacy of the antibiotics and thereby, perhaps enables to improve treatment recommendations.

4.1.4.2 ZUERICH-1 biofilm is composed of outstanding amounts of proteins

In comparison to its suspension, the biofilm of *M. chimaera* ZUERICH-1 showed an enhanced production of ECM which contained an above-average amount of proteins. The majority of the biofilm was composed of lipids, which was a common finding in all SGM biofilms tested. While all biofilms of the SGM isolates tested presented a similar percentual composition of the ECM components, the high amount of proteins in the biofilm of ZUERICH-1 was outstanding.
Proteins play a very important part in biofilm formation, as they incorporate a huge amount of different molecular structures and functions. A well-known representative is the Bap (biofilm associated protein) protein in *Staphylococcus aureus*, that was found to be essential for adherence on abiotic surfaces [164, 165]. Interestingly, the absence of a functioning *bap* gene resulted in the transformation from rough to smooth colony morphotypes, displaying the link between biofilm formation and colony morphology, which is also playing a big role in the present study.
Other prominent proteins that contribute to biofilm formation are for example the curli fimbriae of

E. coli [166, 167] or the Lap-proteins of *P. aeruginosa* [168, 169]. Though some proteins are more often reported and may contribute more to the biofilm formation and its conservation, a huge variety of proteins and other molecules was meanwhile described to be individually involved in biofilm building processes. The majority of these proteins is usually involved in surface attachment (adhesins) [164, 169, 170] and in maintaining the biofilm structure [166, 168, 171].

Since in the present study, the detailed composition of the ECM on molecular basis was not to be analyzed, it can only be speculated which proteins contributed to the enhanced biomass of proteins in *M. chimaera* ZUERICH-1 biofilm. The microscopic analysis suggests that the net-like ECM structure found, primarily consisted of proteins since these structures were not found to this extent in the other *M. chimaera* isolates. Considering this, it is likely that the major function of the expressed proteins lays in the area of surface attachment of bacteria and/or the further distribution of the biofilm.
Another benefit of an extensive production of proteins could be the increase in protection. Especially in disinfectant testing, additional protein (e.g. albumin) is used as an organic load in the experimental design (e.g. DIN 13727, DIN EN 14348). Usually, the efficacy of the disinfectant is negatively influenced by this protein burden. It could be likely, that the isolate ZUERICH-1 which was regularly disinfected with sublethal concentrations of disinfectants in the HCUs, adapted to this stress and responded with enhanced protein production in the ECM of the biofilm.
The gain of adaptations to environmental stress is a common mechanism in mycobacteria usually seen for antibiotics [172] to which the bacteria react for example with enhanced expression of efflux-pumps. de Carvalho et al. (2020) showed that *Mycobacterium vaccae* reacts to disinfectants commonly used in hand sanitizers with an adaptation of the lipid profile [173]. The mentioned study focussed on alcohol containing disinfectants and the lipid profile of this species, but the overall message is, that mycobacteria are able to adapt to environmental stress including disinfectants.
Further research reflecting the amount of proteins in the biofilms' ECM during repeated disinfection with sublethal concentrations could clarify whether the enhanced production of proteins in ZUERICH-1 is an adaptation or a natural advantage of this isolate.

4.2 Proteome and transcriptome of *M. chimaera*

Since the biofilm genotype is not yet well described in NTM, a major approach of the present study was to analyse the differences and similarities of the different cultivation forms used. Another goal was to identify genes, which could be biofilm specific and thereby probable drug targets. By including two different *M. chimaera* isolates in the expression analysis, it was possible to identify genes, that presumably contribute to biofilm formation of this species.
In general, the comparison of proteome and transcriptome data was rather difficult. The transcriptome presents the expression profile of genes that are transcribed right at the moment the RNA is extracted. The proteome on the other hand, includes proteins that were synthesized before the extraction. The abundance of specific proteins is influenced by protein stability and turn-over as well as post-translational modifications [174]. Due to these factors, the number of transcripts is usually not directly proportional to the number of proteins measured in proteome analysis [174]. Nevertheless, the identification of some genes contributing to biofilm formation was, however, possible by comparative analysis of both omics techniques.

4.2.1 Expression profiles of cultivation forms

While in the transcriptome analysis, the samples clustered by isolate, the proteome did not show a isolate specific clustering. Instead, the planktonic sample of ZUERICH-1 showed the widest distance in this comparison to the biofilm and the suspension of this isolate. On the other hand, biofilm and suspension of ZUERICH-1 displayed very similar expression patterns. In the biofilm research field, it is still under discussion whether the colony grown on agar plate is also a sort of biofilm. The bacteria grown between two physical layers (solid and air), attach to a surface and cover themselves in a matrix. The similarities found in the proteome of ZUERICH-1 between biofilm and suspension also support the assumption that both cultivation forms are at least very similar. On the other hand, the biofilm and the suspension of FR-35 showed no such strong similarities. A clear answer to this question can only be gained when a distinct biofilm genomic expression pattern is defined, which was not possible for mycobacteria yet.
In the transcriptome, the biofilm of ZUERICH-1 displayed an expression pattern more similar to its planktonic counterpart. It is possible, that the biofilm grown on PGBs displays an intermediate cultivation form between suspension and planktonic. On the one hand the bacteria are attached to a surface - similar to the suspension - but they are also cultivated in a liquid medium - such as the planktonic bacteria.
Though the numbers of up- and downregulated proteins and genes were similar among all three cultivation forms, the analysis of the functional expression profiles including the COG categories showed that in general, the expression of upregulated proteins or genes was the highest in the planktonic samples. Especially the enhanced upregulation in the category of 'cell cycle control, cell division and chromosome partitioning' (D) indicates that the bacteria in this cultivation form are actively growing. On the opposite, the biofilm and the suspension displayed in most cases a higher down- than upregulation indicating that reduced growth or persistence is desired. It is possible that biofilm embedded cells change to a stationary or persistence metabolic state presumably due to starvation and loss of nutrients in the lower biofilm layers [115]. Persisting cells on the other hand provide a better protection to antibiotic treatment since antibiotics often interfere during growth or metabolic processes [175, 176].

4.2.1.1 Two methods, two meanings?

Since the majority of proteins and genes was annotated in the COG category of unknown function, it can be assumed, that interesting candidates are underrepresented in the analysis of functional expression patterns. Therefore, the genes and proteins which were up- or downregulated in each cultivation form were more specifically analysed.
The proteome revealed only one protein that was downregulated in the suspension of both isolates (YrrM, class I SAM-dependent methyltransferase). Interestingly, in the transcriptome the suspension showed the highest log expression fold change compared to the biofilm or planktonic culture. In the upregulated fraction, two of five genes are related to the COG category of 'Inorganic ion transport and metabolism' (P) with one of them being a DNA starvation or stationary phase protection protein. In the other two forms, the level of expression fold change was similar between proteome and transcriptome. It remains unclear, why the suspension displays such a different pattern in comparison to the other two forms and among both expression analyis techniques.
In the transcriptome of the biofilm, three of the five most upregulated genes are related to the type VII secretion systems (two PPE-repeat proteins and EccB). Interestingly in the proteome analysis, the EccB protein was found in the five most downregulated proteins of the biofilm. A possible explanation could be, that the transcriptome represents a reaction to the low levels of this protein measured in the proteome to maintain a constant amount of EccB in the biofilm. Since this was not documented for any other gene or protein, this can only be speculated.
Though in majority the genes/proteins that were identified in the separate omics methods differed, one similarity was found in both: In proteome and transcriptome of the planktonic samples of both isolates, a transcriptional regulator of the AcrR family was in the group of the five most downregulated. Moreover, another AcrR family transcriptional regulator was in the five most upregulated genes of the biofilm. The TetR transcriptional regulators mediates the transcription of a huge variety of different structures. Nevertheless, AcrR/TetR transcriptional regulators have been associated with drug resistance mechanisms in mycobacteria and mentioned as potential drug targets [177, 178, 179]. A further analysis of the identified AcrR/TetR family transcriptional regulators found in the present study could perhaps clarify why they are differently expressed in biofilm and planktonic sample and which underlying functions they fulfil.

4.2.2 Upregulation of type VII secretion system components in the biofilm.

Another interesting finding was, that in the biofilms of both isolates the type VII secretion protein EccB was in the fraction of the five most downregulated proteins and reappeared in the five most upregulated genes of the transcriptome. The type VII secretion systems (ESX1-5) of mycobacteria consist of multiple proteins that enable the secretion of effector proteins through the mycobacterial cell envelope into the environment and/or the host cell [180, 181]. Thereby they majorly contribute to the pathogeny of mycobacteria. The EccB is mentioned as a core component of these systems by providing energy for the transport of virulence factors across the type VII secretion apparatus [182].
The two most upregulated genes in the biofilm display two PPE-repeat proteins that are, by annotation, involved in 'cell motility' (N) functions. Interestingly, PE and PPE-family proteins belong to the class of substrates secreted by the type VII secretion systems and are directly linked to virulence and drug resistance in NTM [183, 184, 185]. Though, the specific functions of the identified PE and PPE-family proteins remain unclear. Still, these findings indicate that the biofilm phenotype of

M. chimaera is also potentially linked to virulence in this species.
It has been documented before, that the type VII secretion systems play an important role in the biofilms of mycobacteria [186, 187]. By screening *M. marinum* mutants, Lai et al. (2018) showed, that the a functional ESX-1 secretion system is crucial for biofilm formation and sliding motility [186]. In accordance with other research, the results of the present study indicate, that type VII secretion systems and their counterparts contribute to the biofilm phenotype of *M. chimaera*. Further investigations, as for example the generation of type VII secretion system deficient mutants, could clarify how and which specific components of the type VII secretion systems are involved in biofilm formation.

4.2.3 Hints on potential biofilm specific genes

The comparative analysis of transcriptome and proteome showed no direct proportional or linear correlation of transcript and protein counts. Still, genes in biofilm could be identified that displayed enhanced transcript and protein counts in comparison to the other cultivation forms. A total of six genes was identified in both isolates which could be possible biofilm-specific genes.
From these, two genes were found that are already linked to biofilm formation in literature. The first is *glmM*, a phosphoglucosamine mutase, that is essential for cell wall biosynthesis in MTB [144] and is crucial for growth and biofilm formation in *M. smegmatis* [145]. It was described as a potential drug target. The protein GlmM is involved in the biosynthesis of peptidoglycan, an important part of the mycobacterial cell envelope.
The other gene identified was *sucC*, a succinate-CoA ligase, which was proclaimed to play an important role in biofilm formation of MTB [150]. SucC is not yet further investigated with regard to biofilm formation. The identified co-expressed genes of *sucC* were also not yet mentioned with respect to biofilm formation in literature.
Two more genes were identified that were directly linked to growth and - in one case - also to virulence. The gene *pepN* is highly conserved in both, pathogenic and non-pathogenic mycobacteria. It is essential for *in vitro* growth of *M. smegmatis* and is required to modulate the virulence of MTB *in vivo* [141]. *pepN* encodes for the aminopeptidase N, for which a homologue is also found in human. It is co-expressed in *M. chimaera* with *truB, glyA* and *pepA* which, according to the literature, are also linked to the virulence of MTB [188].
The gene *glgX*, a glycogen debranching protein, was also found in the subset of biofilm specific genes. It was described before to be involved in the starch and sucrose metabolism of *M. smegmatis* and *glgX*-deficient mutants display reduced growth [149]. A further characterization of this gene in mycobacteria has not yet been done, but in *Corynebacterium glutamicum* a homologue was found to be majorly involved in the adaptation to hyperosmotic stress [149], a circumstance that is also typically noted in biofilms.
Another gene was found that is linked to stress protection and starvation, an AldA-like aldehyde dehydrogenase (ALDH). In general, ALDHs are linked to oxidative stress in cells [143] and it was found that AldA-like ALDHs are expressed in *M. smegmatis* under oxygen starvation [142] which is typically described for inner cells of biofilm communities and could therefore by a reasonable explanation why it was also expressed in the biofilms of the *M. chimaera* isolates.

Many of the above mentioned genes are related to a mycobacterial biofilm phenotype. While some genes are directly mentioned to be involved in biofilm formation (*glmM* and *sucC*), the other genes found are rather related to biofilm characteristics, such as the adaptation to oxidative stress. The genes

glgX and the AldA-like ALDH, are commonly linked to stress as for example oxidative stress which is naturally occurring in the inner parts of the biofilm. In a further approach it would be necessary to quantify the expression of these genes in the biofilms of other *M. chimaera* isolates or even other NTM species such as *M. abscessus*. Thereby it could be possible to describe a biofilm genotype in multiple NTM species. This could finally lead to potential drug targets that in the future, might help to prevent biofilm formation of NTM in the hospital environment and enhance treatment success.

4.3 Biofilm formation enhances tolerance against antimicrobials

The results of the current work display that biofilm formation results in an enhanced tolerance of the tested NTM species towards antimicrobials when compared to suspension samples.
The susceptibility testing of *M. abscessus* proved that well grown biofilms are almost not affected by the antibiotics tested while the corresponding suspension were continuously killed. Also the disinfectant testing showed a clear trend towards increased tolerance of biofilm compared to suspension, with one - surprising - finding:
The biofilms of the *M. chimaera* isolates were far less tolerant to FAC than the corresponding suspensions. This effect was most pronounced in *M. chimaera* UP-11, whose suspension was reduced by less than 1 $\log_{10}$ even at the highest concentration tested (5 % FAC for 60 min).

4.3.1 Enhanced tolerance of *M. chimaera* suspensions towards FAC could depend on oxygen-levels in the cultivation environment

Mycobacteria are naturally resistant to a wide range of disinfectants and present an enhanced tolerance to sodium hypochlorite [23, 55, 56, 57]. A reasonable explanation is, that NTM often inhabit waterborne environments for which the decontamination with FAC is a common procedure. In the US for example, the water drinking system is regularly treated with very low concentrations of FAC (approx. 0.0004 %)[1]. These sublethal concentrations have presumably triggered a positive selection of mycobacteria in the US drinking water systems [56].
Though it is commonly assumed, that biofilm formation increases the tolerance towards antimicrobials, the disinfectant testing with FAC showed the opposite. The experiments of the present study showed that the tested suspensions were more tolerant towards FAC than the corresponding biofilms. Interestingly, this effect was more pronounced in *M. chimaera* than in *M. abscessus*.
Since it was out of the research focus, It was not possible to analyse the background of this effect further within this study. A possible reason suggested by the literature could be, that the oxygen level in the cultivation environment influences the tolerance towards FAC indirectly. Falkinham et al. (2003) presented that different factors, including the cultivation at low oxygen levels, influence the susceptibility of different MAC species to chlorine disinfection [189]. They were able to show that a reduced oxygen level (approx. 6 %) enhanced the susceptibility of the tested isolates to chlorine when compared to samples grown under normal oxygen-conditions.
It can be assumed that this effect might have also affected the resistance of the suspension and the biofilm in the present work. While the bacteria grown as suspension on agar plate are largely well supplied with oxygen, bacteria in biofilm often face hypoxia, especially those at in the inner parts of larger aggregates. The comparative analysis of transcriptome and proteome showed, that also in the biofilm of *M. chimaera*, a response to oxygen starvation is probable. The analysis of the biofilms pointed at a AldA-like aldehyde dehydrogenase which was found to be expressed under oxygen starvation conditions in *M. smegmatis* [142]. Thus it is likely, that the oxygen level in the cultivation environment directly influences the susceptibility towards FAC - also in *M. chimaera*. It is commonly observed in biofilms of other bacteria, that the expression of genes linked to hypoxia is enhanced [36, 190, 191]. In *M. avium*, incubation under anaerobic conditions resulted in an enrichment and

[1] CDC recommendations for water chlorination
`cdc.gov/drinking/public/water_disinfection` - last checked January 11, 2023

downregulation of different proteins and metabolic pathways (pantothenate and CoA biosynthesis, glycerolipid metabolism, nitrogen metabolism and chloroalkene degradation) linked to oxygen consumption [192].

Interestingly, it was also shown for MTB, that oxydative stress increases the susceptibility to isoniazid [193], an antibiotic commonly used in combination with rifampicin for treatment of tuberculosis. This shows that oxygen starvation has an important and widespread influence on the tolerance of mycobacteria to various antimicrobials. Further analysis is needed to investigate which further genetic or metabolic processes in mycobacteria are affected by low oxygen levels and thereby enable to find potential treatment or eradication targets.

4.3.2 How to become an outbreak strain - ZUERICH-1 survives 4 weeks of disinfection

Another important question of the present work was, whether *M. chimaera* ZUERICH-1 shows any properties that could have supported its success as a global outbreak strain. It was found that ZUERICH-1 presents an increased tolerance to PAA when compared to the other *M. chimaera* isolates. This increase in tolerance could have resulted from an adaptation to a repeated or continuous sublethal disinfection with PAA in the heater-cooler unit (HCU). It has been shown in previous studies that adaptation to disinfectants is possible in NTM [56].
In the present study it was possible to show, that ZUERICH-1 survives over 4 weeks of a weekly disinfection cycle with recommended concentrations of PAA used in HCUs, although the bacteria were only cultivated in sterile water. The applied cycle of disinfection in the experiment was even shorter than it is usually recommended. In the actual disinfection protocol of the HCUs from LivaNova, a 14-day cycle of disinfection is recommended [2]. From the presented results it can be assumed that the recommended disinfection protocols of the HCU will presumably never be sufficient to eradicate ZUERICH-1 from those machines. Still, it has to be taken in account that other measures were taken to clean the HCUs after the global outbreak was identified. These measures include for example mechanical disruption of the biofilms within the HCUs, but also this did not prevent the reemergence of ZUERICH-1 in the machines [110].

Though, it was found that ZUERICH-1 shows an enhanced resistance to the used disinfectants, this isolate was not the one originally isolated from the contaminated HCU. Instead it was isolated from the first patient linked to global outbreak. It would be very interesting to analyse the tolerance of the isolate *M. chimaera* ZUERICH-2, which is the corresponding isolate to ZUERICH-1, that was directly taken from the water tanks of the contaminated HCU.
From the phylogenetic analysis made by van Ingen et al. (2017) it was shown that both isolates differ by their number of plasmids and the insertion of several mobile genetic elements including two large genomic islands that were integrated in the genome of ZUERICH-1 [131]. *M. chimaera* ZUERICH-2 also harboured several plasmids, from which one (154 kbp) did not show homology to any of the five plasmids of ZUERICH-1. It is reasonable that genetical differences of both isolates also result in different tolerance patterns. The comparison of both isolates in a further approach would allow to analyse which genetic mechanisms are changing or adapted during the process of infection.

[2] Heater-cooler system 3T operating instructions. Version 02/2020. LivaNova `livanova.com/T3/productsite` - last checked January 11, 2023

4.3.3 Biofilm formation is more beneficial for smooth *M. abscessus* morphotypes

M. abscessus belongs to the NTM species with the highest natural resistances against antibiotics [10, 71, 77]. Antibiotic susceptibility testing of *M. abscessus* is required to support the clinical treatment. In *M. abscessus* pulmonary disease (MAB-PD) the treatment success goes not always in line with the susceptibility previously investigated in the laboratory [12, 17]. The common laboratory test methods are based on the use of suspended bacteria, though, it was shown that *M. abscessus* forms biofilms within the patients lung cavities [95]. It is assumed that the biofilm formation is the major reason why the treatment of MAB-PD fails [13].

The present study shows that biofilm formation of *M. abscessus* results in an enhanced tolerance to the commonly used antibiotics amikacin and tigecycline. Similar results were also documented in other studies which included air-liquid interface biofilms [101]. The hereby presented results show that smooth *M. abscessus* isolates benefit more from biofilm formation than their rough counterparts. Comparing the susceptibility of the biofilm and the suspension of smooth *M. abscessus* isolates, the differences are much more pronounced than in the rough morphotypes. Since the amount of ECM components was similar in both morphotypes or even higher in the rough isolate (e.g. *M. abscessus* $58/15^{rg}$), it can be assumed, that the amount of ECM does not directly influence the tolerance. Also the composition of the ECM with respect to the amounts of protein, DNA and lipids was comparable between the smooth and the rough isolates. Therefore, other properties of the biofilm seem to contribute to the enhanced tolerance of the smooth isolates when grown as biofilm.

It is known that autoaggregation or autoagglutination of bacteria is, such as surface adherence, one of the first steps leading to biofilm formation and influencing the susceptibility to antimicrobials [194]. Bohrerova & Linden (2006) showed that the aggregation of *Mycobacterium terrae* enhances the tolerance of the bacteria to chlorine and ultraviolet disinfection [195]. It can be assumed that the natural aggregation of bacteria in biofilm results in an enhanced tolerance of the smooth *M. abscessus* isolates when compared to the corresponding suspension. Another indicator is, that disrupted biofilms present a lower tolerance to antimicrobials. Kolpen et al. (2020) showed that the disruption of smooth *M. abscessus* biofilm results in an enhanced susceptibility towards several common antibiotics [196].

Rough *M. abscessus* morphotypes display a strong aggregation also in suspension. Therefore it is reasonalbe that the differences between both cultivation forms are less pronounced in the rough compared to the smooth isolates. Still, an aggregation in biofilms of smooth *M. abscessus* morphotypes was only documented in-between the glass particles where multi-layered structures were formed. This indicates that also other mechanisms may contribute to the enhanced tolerance of the smooth *M. abscessus* biofilms against antibiotics.

4.4 Further research and outlook

4.4.1 Multi-species biofilms and cultivation in ASM

Due to time restriction it was not possible to adjust the presented PGB biofilm model to the use with multiple species, although this is an important aspect that needs a special focus in the future.
Usually, biofilms in the environment are not formed by one species but consist of a variety of different microorganisms that together form a biofilm [111, 113]. These multi-species biofilms provide very different properties, influencing the outcome of susceptibility testing. Meanwhile, multi-species biofilm models were established, also using mycobacteria [44, 197]. In the lung of patients, *M. abscessus* is settling in a community with other species as for example *Pseudomonas aerigunosa*. Rodriguez-Sevilla et al. (2018) invented a dual species biofilm model using *M. abscessus* and *P. aerigunosa*. The species were cultivated together on polycarbonate membranes and the amount of each was screened over time, finding that the presence of *P. aerigunosa* had a negative effect on the growth of *M. abscessus*. The balance of the different species in a biofilm can affect the complete structure and composition of the biofilm and ECM and therefore change the tolerance to antimicrobials.
Following the present work, the PGB biofilm model was used at the RKI for co-cultivation of *M. abscessus* and the fungus *Exophiala dermatitidis* in mixed biofilms. The fungus is also a common co-cultivator during MAB-PD. It was shown that both species co-existed in the biofilm and each influenced the amount of the other species. Thus, *M. abscessus* had a positive effect on the growth of *E. dermatitidis* in the biofilm while *M. abscessus* was inhibited by *E. dermatitidis* (Bachelor thesis Hoda Yousof). This showed that the PGB biofilm model is also adaptable to the use with multiple species, including fungi.

Also as follow-up of the present study, the PGB biofilm model was modified to use artificial sputum medium (ASM) allowing the cultivation of *M. abscessus* under conditions similar to what is given in the patients lung. It was possible to show that the structure of the biofilms formed in ASM were similar to the cording phenotype documented in the present study when *M. abscessus* was cultivated in MH.
A further approach will be the cultivation the mixture of bacteria and fungi directly from sputum samples of CF-patients, to investigate the role of NTM in this microbial community and to analyse the antibiotic susceptibility of these multi-species biofilms. It enables to test the efficacy of antibiotics directly using biofilms generated by use of the complete sputum microflora which will be a great leap forward by hopefully increasing the treatment success.

4.4.2 Adapting current antimicrobial testing to biofilms

It will be necessary to adjust the common disinfectant and antibiotic testing methods. The present study shows that NTM biofilms usually dispose of a higher tolerance towards antimicrobials than the corresponding suspension. This finding was also congruent with multiple experiments performed with various species at the FG14 of the RKI using other species (*P. aeruginosa, Klebsiella pneumoniae*). Taking into account, that biofilms are the most natural form bacteria grow in, it is obvious that the common methods of resistance testing need to be adapted. Since NTM were shown to be present within biofilms in the lung cavities of patients [95, 198], an adaptation of test procedures regards to both, disinfectant and antibiotic testing.

The bead assay for biofilms was invented by Konrat et al. (2016) especially for disinfectant testing [140] and was adapted in the present study for antibiotic susceptibility testing. Since there is no approved biofilm model yet which is recommended for regular disinfectant testing, it is envisaged to get a DIN standard admission of the biofilm bead assay invented at the RKI (personal communication). In the future, the use of an approved biofilm model for antimicrobial testing will improve the recommendations for standard testing procedures, treatment and eradication.

4.5 Conclusion

The present study showed that the PGB bead model is a suitable system for the cultivation of biofilms of slow and rapid growing NTM species. It was shown that the model can be used for further experimental protocols such as microscopy, ECM analysis, Omics-techniques or susceptibility testing.

In this work, the differences and similarities of the structure and composition of biofilms from *M. abscessus* and *M. chimaera* were analysed. Moreover, this study was the first to present a biofilm cultivation model in which rough *M. abscessus* isolates show surface adhesion of biofilms - a finding that will change common assumptions in this research field. Interestingly, one *M. chimaera* isolate was found, that presented a different biofilm morphotype than the other *M. chimaera* isolates. It was proposed that this specific morphologic variant arises from changes in the lipid biosynthesis pathway by the loss of the genes *lcpA_1* and *lpgB*. Thereby this work demonstrated for both species, that the lipid profile could have a major impact on the biofilm formation.
Another interesting finding was the cording phenotype of smooth *M. abscessus* isolates when they were cultivated in MH. The cording is linked to a virulence phenotype in MTB. The phenotypical difference of the biofilms of *M. abscessus* in different media rises the question which of the diverse media for NTM cultivation is the most appropriate for biofilm formation. The choice of media will also depend on the further use of the biofilms. For antibiotic resistance testing ASM may be most suitable, while for disinfectant testing other media like MB-OADC should be preferred.
In general, the biofilms of *M. chimaera* and *M. abscessus* showed an enhanced amount of ECM when compared to their suspensions. In *M. abscessus*, the biofilm presented a distinct increase in DNA biomass when compared to the corresponding suspension. Though an increase of DNA biomass was also found in *M. chimaera* biofilms, a more interesting result was the increased production of protein in the ECM of the outbreak strain *M. chimaera* ZUERICH-1. In comparison to the other isolates, ZUERICH-1 showed an enhanced protein biomass in the biofilm which may contribute to its enhanced tolerance towards certain disinfectants and its success as an outbreak strain.
Using the proteome and transcriptome analysis it was possible to identify genes that presumably contribute to biofilm formation in mycobacteria. By using omics techniques, a contribution of the type VII secretion system to the biofilm phenotype of *M. chimaera* was identified. The type VII secretion systems of mycobacteria are important for virulence and pathogenicity, showing that biofilms of *M. chimaera* are presumably linked to virulence phenotypes. The proteome and transcriptome analysis revealed potential anti-biofilm drug targets. Especially the gene *glmM* was already described as a key enzyme essential for cell wall biosynthesis and thereby being relevant for biofilm formation in *M. smegmatis*. Further investigations by mutagenesis and phenotype analysis will be needed to confirm the importance of this and the other identified genes on the biofilm formation of *M. chimaera* and also other mycobacteria.

Finally, it was shown that the biofilm phenotype provides to both species, *M. chimaera* and *M. abscessus*, an enhanced tolerance towards disinfectants and antibiotics. Moreover, it was shown that commonly used concentrations of disinfectants fail to sufficiently reduce the mycobacteria in biofilm. It was also demonstrated that *M. chimaera* ZUERICH-1 survives four weeks of disinfection using the recommended concentrations of PAA. This shows the severity of the problematic to further adapt common recommendations.
An interesting finding was that the suspensions of the *M. chimaera* isolates were more tolerant to FAC than the corresponding biofilm. A potential explanation is that the oxygen levels in the cultivation environment influence the susceptibility of *M. chimaera* towards FAC.
The antibiotic testing of *M. abscessus* also revealed a higher tolerance of the biofilms compared to the suspensions, while the effect was more pronounced in AMI (bactericidal) than in TGC (bacteriostatic). Since suspension is commonly used for susceptibility testing of *M. abscessus* in the clinical field this is a major problem and a possible explanation why the outcome of the laboratory susceptibility testing does not correlate with treatment success.

Overall, the presented work raised a variety of new and interesting questions for future research. Still it was possible to present a reliable cultivation method for NTM biofilms and to give insights into the structure, composition, expression profiles and tolerance behaviour. Future projects should focus on the contribution of the media and the culturing conditions on the biofilm of *M. abscessus* and *M. chimaera*. With this, the cording phenotype of *M. abscessus*, surprisingly documented in this study, should be further investigated. Another important topic for future investigation is the potential of the identified biofilm-specific genes as drug targets. Also the presence of these genes in other NTM biofilms needs clarification.

Bibliography

[1] Enrico Tortoli. Microbiological features and clinical relevance of new species of the genus mycobacterium. *Clinical microbiology reviews*, 27(4):727–752, 2014.

[2] Chung-Jong Kim, Nak-Hyun Kim, Kyoung-Ho Song, Pyoeng Gyun Choe, Eu Suk Kim, Sang Won Park, Hong-Bin Kim, Nam-Joong Kim, Eui-Chong Kim, Wan Beom Park, et al. Differentiating rapid-and slow-growing mycobacteria by difference in time to growth detection in liquid media. *Diagnostic microbiology and infectious disease*, 75(1):73–76, 2013.

[3] Joseph O Falkinham III. The biology of environmental mycobacteria. *Environmental Microbiology Reports*, 1(6):477–487, 2009.

[4] Enrico Tortoli, Tarcisio Fedrizzi, Conor J. Meehan, Alberto Trovato, Antonella Grottola, Elisabetta Giacobazzi, Giulia Fregni Serpini, Sara Tagliazucchi, Anna Fabio, Clotilde Bettua, Roberto Bertorelli, Francesca Frascaro, Veronica De Sanctis, Monica Pecorari, Olivier Jousson, Nicola Segata, and Daniela M. Cirillo. The new phylogeny of the genus mycobacterium: The old and the news. *Infection, Genetics and Evolution*, 56:19–25, 2017.

[5] Radhey S. Gupta, Brian Lo, and Jeen Son. Phylogenomics and comparative genomic studies robustly support division of the genus mycobacterium into an emended genus mycobacterium and four novel genera. *Frontiers in Microbiology*, 9:67, 2018.

[6] Aharon Oren and George M Garrity. List of new names and new combinations previously effectively, but not validly, published. *Int J Syst Evol Microbiol*, 68(11):3379–3393, Nov 2018.

[7] Enrico Tortoli, Barbara A. Brown-Elliott, James D. Chalmers, Daniela M. Cirillo, Charles L. Daley, Stefan Emler, R. Andres Floto, Maria J. Garcia, Wouter Hoefsloot, Won-Jung Koh, Christoph Lange, Michael Loebinger, Florian P. Maurer, Kozo Morimoto, Stefan Niemann, Elvira Richter, Christine Y. Turenne, Ravikiran Vasireddy, Sruthi Vasireddy, Dirk Wagner, Richard J. Wallace, Nancy Wengenack, and Jakko van Ingen. Same meat, different gravy: ignore the new names of mycobacteria. *European Respiratory Journal*, 54(1), 2019.

[8] Radha Gopalaswamy, Sivakumar Shanmugam, Rajesh Mondal, and Selvakumar Subbian. Of tuberculosis and non-tuberculous mycobacterial infections–a comparative analysis of epidemiology, diagnosis and treatment. *Journal of biomedical science*, 27(1):1–17, 2020.

[9] Lars-Olof. Larsson, Rutger Bennet, Margareta Eriksson, Bodil Jönsson, and Malin Ridell. *Nontuberculous Mycobacteria (NTM) Microbiological, Clinical and Geographical Distribution. Chapter 5 - Nontuberculous Mycobacterial Diseases in Humans.* Academic Press, 2019.

[10] Laura Victoria, Amolika Gupta, Jose Luis Gómez, and Jaime Robledo. Mycobacterium abscessus complex: a review of recent developments in an emerging pathogen. *Frontiers in Cellular and Infection Microbiology*, 11:659997, 2021.

[11] Roland Diel, Marc Lipman, and Wouter Hoefsloot. High mortality in patients with mycobacterium avium complex lung disease: a systematic review. *BMC infectious diseases*, 18(1):1–10, 2018.

[12] Kyeongman Jeon, O Jung Kwon, Nam Yong Lee, Bum-Joon Kim, Yoon-Hoh Kook, Seung-Heon Lee, Young Kil Park, Chang Ki Kim, and Won-Jung Koh. Antibiotic treatment of mycobacterium abscessus lung disease: a retrospective analysis of 65 patients. *American journal of respiratory and critical care medicine*, 180(9):896–902, 2009.

[13] Julie Jarand, Adrah Levin, Lening Zhang, Gwen Huitt, John D Mitchell, and Charles L Daley. Clinical and microbiologic outcomes in patients receiving treatment for mycobacterium abscessus pulmonary disease. *Clinical Infectious Diseases*, 52(5):565–571, 2011.

[14] Won-Jung Koh, Byeong-Ho Jeong, Su-Young Kim, Kyeongman Jeon, Kyoung Un Park, Byung Woo Jhun, Hyun Lee, Hye Yun Park, Dae Hun Kim, Hee Jae Huh, et al. Mycobacterial characteristics and treatment outcomes in mycobacterium abscessus lung disease. *Clinical infectious diseases*, 64(3):309–316, 2017.

[15] Richard J Wallace Jr, Barbara A Brown-Elliott, Steven McNulty, Julie V Philley, Jessica Killingley, Rebecca W Wilson, Deanna S York, Sara Shepherd, and David E Griffith. Macrolide/azalide therapy for nodular/bronchiectatic mycobacterium avium complex lung disease. *Chest*, 146(2):276–282, 2014.

[16] Sanne Zweijpfenning, Stephan Kops, Cecile Magis-Escurra, Martin J Boeree, Jakko van Ingen, and Wouter Hoefsloot. Treatment and outcome of non-tuberculous mycobacterial pulmonary disease in a predominantly fibro-cavitary disease cohort. *Respiratory Medicine*, 131:220–224, 2017.

[17] Won-Jung Koh, Seong Mi Moon, Su-Young Kim, Min-Ah Woo, Seonwoo Kim, Byung Woo Jhun, Hye Yun Park, Kyeongman Jeon, Hee Jae Huh, Chang-Seok Ki, et al. Outcomes of mycobacterium avium complex lung disease based on clinical phenotype. *European Respiratory Journal*, 50(3), 2017.

[18] Yon Ju Ryu, Won-Jung Koh, and Charles L Daley. Diagnosis and treatment of nontuberculous mycobacterial lung disease: clinicians' perspectives. *Tuberculosis and respiratory diseases*, 79(2):74–84, 2016.

[19] Abdolrazagh Hashemi Shahraki and Mehdi Mirsaeidi. Phage therapy for mycobacterium abscessus and strategies to improve outcomes. *Microorganisms*, 9(3):596, 2021.

[20] Wouter Hoefsloot, Jakko Van Ingen, Claire Andrejak, Kristian Ängeby, Rosine Bauriaud, Pascale Bemer, Natalie Beylis, Martin Boeree, J. Cacho, Violet Chihota, Erica Chimara, Gavin Churchyard, Raquel Cias, R. Dasa, Charles Daley, P Dekhuijzen, Diego Domingo, Francis Drobniewski, Jaime Esteban, and for (www.ntm net.org. The geographic diversity of nontuberculous mycobacteria isolated from pulmonary samples: A ntm-net collaborative study. *European Respiratory Journal*, 42, 04 2013.

[21] C Robert Horsburgh Jr. Epidemiology of disease caused by nontuberculous mycobacteria. In *Seminars in respiratory infections*, volume 11, pages 244–251, 1996.

[22] A Lahiri, J Kneisel, I Kloster, E Kamal, and A Lewin. Abundance of m ycobacterium avium ssp. hominissuis in soil and dust in germany–implications for the infection route. *Letters in Applied Microbiology*, 59(1):65–70, 2014.

[23] Joseph O Falkinham. Nontuberculous mycobacteria in the environment. *Clinics in chest medicine*, 23(3):529–551, 2002.

[24] Yannick Vande Weygaerde, Nina Cardinaels, Peter Bomans, Taeyang Chin, Jerina Boelens, Emmanuel André, Eva Van Braeckel, and Natalie Lorent. Clinical relevance of pulmonary non-tuberculous mycobacterial isolates in three reference centres in belgium: a multicentre retrospective analysis. *BMC Infectious Diseases*, 19(1):1–10, 2019.

[25] Theodore K Marras and Charles L Daley. Epidemiology of human pulmonary infection with nontuberculous mycobacteria. *Clinics in chest medicine*, 23(3):553–568, 2002.

[26] Won-Jung Koh, O Jung Kwon, Kyeongman Jeon, Tae Sung Kim, Kyung Soo Lee, Young Kil Park, and Gill Han Bai. Clinical significance of nontuberculous mycobacteria isolated from respiratory specimens in korea. *Chest*, 129(2):341–348, 2006.

[27] Sami Simons, Jakko Van Ingen, Po-Ren Hsueh, Nguyen Van Hung, PN Richard Dekhuijzen, Martin J Boeree, and Dick Van Soolingen. Nontuberculous mycobacteria in respiratory tract infections, eastern asia. *Emerging infectious diseases*, 17(3):343, 2011.

[28] Juan He, Xujun Guo, Chunfang Lv, Yuzheng Fan, Yao Huang, Liuzhu Lu, Amel Kevin Alame Emane, Howard Eugene Takiff, and Shengyuan Liu. Prevalence and risk factors of nontuberculous mycobacterial infection in a coastal area, southern china. 2022.

[29] David E Griffith, Timothy Aksamit, Barbara A Brown-Elliott, Antonino Catanzaro, Charles Daley, Fred Gordin, Steven M Holland, Robert Horsburgh, Gwen Huitt, Michael F Iademarco, et al. An official ats/idsa statement: diagnosis, treatment, and prevention of nontuberculous mycobacterial diseases. *American journal of respiratory and critical care medicine*, 175(4):367–416, 2007.

[30] P Maureen Cassidy, Katrina Hedberg, Ashlen Saulson, Erin McNelly, and Kevin L Winthrop. Nontuberculous mycobacterial disease prevalence and risk factors: a changing epidemiology. *Clinical Infectious Diseases*, 49(12):e124–e129, 2009.

[31] Rachel M Thomson, Queensland Mycobacterial Reference Laboratory, et al. Changing epidemiology of pulmonary nontuberculous mycobacteria infections. *Emerging infectious diseases*, 16(10):1576, 2010.

[32] Won-Jung Koh, Boksoon Chang, Byeong-Ho Jeong, Kyeongman Jeon, Su-Young Kim, Nam Yong Lee, Chang-Seok Ki, and O Jung Kwon. Increasing recovery of nontuberculous mycobacteria from respiratory specimens over a 10-year period in a tertiary referral hospital in south korea. *Tuberculosis and respiratory diseases*, 75(5):199–204, 2013.

[33] D Rebecca Prevots and Theodore K Marras. Epidemiology of human pulmonary infection with nontuberculous mycobacteria: a review. *Clinics in chest medicine*, 36(1):13–34, 2015.

[34] Jason E Stout, Won-Jung Koh, and Wing Wai Yew. Update on pulmonary disease due to non-tuberculous mycobacteria. *International Journal of Infectious Diseases*, 45:123–134, 2016.

[35] Kevin L Winthrop, Theodore K Marras, Jennifer Adjemian, Haixin Zhang, Ping Wang, and Quanwu Zhang. Incidence and prevalence of nontuberculous mycobacterial lung disease in a large us managed care health plan, 2008–2015. *Annals of the American Thoracic Society*, 17(2):178–185, 2020.

[36] Yilin Wu, Isaac Klapper, and Philip S Stewart. Hypoxia arising from concerted oxygen consumption by neutrophils and microorganisms in biofilms. *Pathogens and disease*, 76(4):fty043, 2018.

[37] Neeraj M Shah, Jennifer A Davidson, Laura F Anderson, Maeve K Lalor, Jusang Kim, H Lucy Thomas, Marc Lipman, and Ibrahim Abubakar. Pulmonary mycobacterium avium-intracellulare is the main driver of the rise in non-tuberculous mycobacteria incidence in england, wales and northern ireland, 2007–2012. *BMC infectious diseases*, 16(1):1–6, 2016.

[38] JC Mgogwe, HH Semvua, F Tenu, JO Chilongola, and BM Nyombi. Prevalence and drug susceptibility of non-tuberculous mycobacteria among presumptive mdr-tb patients admitted at kidh in kilimanjaro, tanzania. *nternational Journal of Medical Science and Health Research*, 6(3), 2022.

[39] Benjamin D Thumamo Pokam, D Yeboah-Manu, Stephen Ofori, PW Guemdjom, PM Teyim, L Lawson, Daniel Amiteye, Nchawa Yangkam Yhiler, Ingrid Cecile Djuikoue, and Anne E Asuquo. Prevalence of non tuberculous mycobacteria among previously treated tb patients in the gulf of guinea-africa. *IJID Regions*, 2022.

[40] Micheska Epola Dibamba Ndanga, Jabar Babatundé Pacome Achimi Agbo Abdul, Jean Ronald Edoa, Rhett Chester Mevyann, Bayodé Romeo Adegbite, Arnault Mfoumbi, Christopher Mebiame Biyogho, Romual Beh Mba, Jocelyn Mahoumbou, Matthew BB McCall, et al. Non-tuberculous mycobacteria isolation from presumptive tuberculosis patients in lambaréné, gabon. *Tropical Medicine & International Health*, 27(4):438–444, 2022.

[41] Abdolrazagh Hashemi Shahraki, Parvin Heidarieh, Saeed Zaker Bostanabad, Azar Dokht Khosravi, Mohammad Hashemzadeh, Solmaz Khandan, Maryam Biranvand, Dean E Schraufnagel, and Mehdi Mirsaeidi. "multidrug-resistant tuberculosis" may be nontuberculous mycobacteria. *European journal of internal medicine*, 26(4):279–284, 2015.

[42] Charles L Daley and Jeffrey Glassroth. Treatment of pulmonary nontuberculous mycobacterial infections: many questions remain, 2014.

[43] Jakko van Ingen and Ed J Kuijper. Drug susceptibility testing of nontuberculous mycobacteria. *Future microbiology*, 9(9):1095–1110, 2014.

[44] Graciela Rodríguez-Sevilla, Marta García-Coca, David Romera-García, John Jairo Aguilera-Correa, Ignacio Mahíllo-Fernández, Jaime Esteban, and Concepción Pérez-Jorge. Non-tuberculous mycobacteria multispecies biofilms in cystic fibrosis: Development of an in vitro mycobacterium abscessus and pseudomonas aeruginosa dual species biofilm model. *International Journal of Medical Microbiology*, 308(3):413–423, 2018.

[45] Richard J Wallace Jr, Gary Dukart, Barbara A Brown-Elliott, David E Griffith, Ernesto G Scerpella, and Bonnie Marshall. Clinical experience in 52 patients with tigecycline-containing regimens for salvage treatment of mycobacterium abscessus and mycobacterium chelonae infections. *Journal of Antimicrobial Chemotherapy*, 69(7):1945–1953, 2014.

[46] Christian Dupont, Albertus Viljoen, Sangeeta Thomas, Françoise Roquet-Banères, Jean-Louis Herrmann, Kevin Pethe, and Laurent Kremer. Bedaquiline inhibits the atp synthase in mycobacterium abscessus and is effective in infected zebrafish. *Antimicrobial agents and chemotherapy*, 61(11):e01225–17, 2017.

[47] Nacer Lounis, Tom Gevers, Joke Van Den Berg, Luc Vranckx, and Koen Andries. Atp synthase inhibition of mycobacterium avium is not bactericidal. *Antimicrobial agents and chemotherapy*, 53(11):4927–4929, 2009.

[48] David C Alexander, Ravikiran Vasireddy, Sruthi Vasireddy, Julie V Philley, Barbara A Brown-Elliott, Benjamin J Perry, David E Griffith, Jeana L Benwill, Andrew DS Cameron, and Richard J Wallace Jr. Emergence of mmpt5 variants during bedaquiline treatment of mycobacterium intracellulare lung disease. *Journal of clinical microbiology*, 55(2):574–584, 2017.

[49] Rebecca Wertman, Melissa Miller, Pamela Groben, Dean S Morrell, and Donna A Culton. Mycobacterium bolletii/mycobacterium massiliense furunculosis associated with pedicure footbaths: a report of 3 cases. *Archives of Dermatology*, 147(4):454–458, 2011.

[50] Byron S Kennedy, Brenden Bedard, Mary Younge, Deborah Tuttle, Eric Ammerman, John Ricci, Andrew S Doniger, Vincent E Escuyer, Kara Mitchell, Judith A Noble-Wang, et al. Outbreak of mycobacterium chelonae infection associated with tattoo ink. *New England Journal of Medicine*, 367(11):1020–1024, 2012.

[51] Michael S Phillips and C Fordham Von Reyn. Nosocomial infections due to nontuberculous mycobacteria. *Clinical infectious diseases*, 33(8):1363–1374, 2001.

[52] Cheryl Squier, Victor L Yu, and Janet E Stout. Waterborne nosocomial infections. *Current Infectious Disease Reports*, 2(6):490–496, 2000.

[53] Sadia Shakoor, Maria Owais, Rumina Hasan, and Seema Irfan. Nosocomial and healthcare-associated ntm infections and their control. In *Nontuberculous Mycobacteria (NTM)*, pages 177–190. Elsevier, 2019.

[54] Imran Ahmed, Simon Tiberi, Joveria Farooqi, Kauser Jabeen, Dorothy Yeboah-Manu, Giovanni Battista Migliori, and Rumina Hasan. Non-tuberculous mycobacterial infections—a neglected and emerging problem. *International Journal of Infectious Diseases*, 92:S46–S50, 2020.

[55] C Kimloi Gomez-Smith, Timothy M LaPara, and Raymond M Hozalski. Sulfate reducing bacteria and mycobacteria dominate the biofilm communities in a chloraminated drinking water distribution system. *Environmental science & technology*, 49(14):8432–8440, 2015.

[56] Michael B Waak, Timothy M LaPara, Cynthia Halle, and Raymond M Hozalski. Nontuberculous mycobacteria in two drinking water distribution systems and the role of residual disinfection. *Environmental Science & Technology*, 53(15):8563–8573, 2019.

[57] Elizabeth D Hilborn, Terry C Covert, Mitchell A Yakrus, Stephanie I Harris, Sandra F Donnelly, Eugene W Rice, Sean Toney, Stephanie A Bailey, and Gerard N Stelma Jr. Persistence of nontuberculous mycobacteria in a drinking water system after addition of filtration treatment. *Applied and environmental microbiology*, 72(9):5864–5869, 2006.

[58] Enrico Tortoli. The new mycobacteria: an update. *FEMS Immunology & Medical Microbiology*, 48(2):159–178, 2006.

[59] Karel Hruska and Marija Kaevska. Mycobacteria in water, soil, plants and air: a review. *Veterinarni Medicina*, 57(11), 2012.

[60] C Fordham Von Reyn, JN Marlow, RD Arbeit, TW Barber, and JO Falkinham. Persistent colonisation of potable water as a source of mycobacterium avium infection in aids. *The Lancet*, 343(8906):1137–1141, 1994.

[61] Charles L Dulberger, Eric J Rubin, and Cara C Boutte. The mycobacterial cell envelope—a moving target. *Nature Reviews Microbiology*, 18(1):47–59, 2020.

[62] Halima Medjahed and Jean-Marc Reyrat. Construction of mycobacterium abscessus defined glycopeptidolipid mutants: comparison of genetic tools. *Applied and environmental microbiology*, 75(5):1331–1338, 2009.

[63] Patrick J Brennan and Hiroshi Nikaido. The envelope of mycobacteria. *Annual review of biochemistry*, 64(1):29–63, 1995.

[64] Antony T Vincent, Sammy Nyongesa, Isabelle Morneau, Michael B Reed, Elitza I Tocheva, and Frederic J Veyrier. The mycobacterial cell envelope: a relict from the past or the result of recent evolution? *Frontiers in microbiology*, 9:2341, 2018.

[65] Vincent Jarlier and Hiroshi Nikaido. Mycobacterial cell wall: structure and role in natural resistance to antibiotics. *FEMS microbiology letters*, 123(1-2):11–18, 1994.

[66] Waldemar Vollmer, Didier Blanot, and Miguel A De Pedro. Peptidoglycan structure and architecture. *FEMS microbiology reviews*, 32(2):149–167, 2008.

[67] Michael McNeil, Stephen J Wallner, Shirley W Hunter, and Patrick J Brennan. Demonstration that the galactosyl and arabinosyl residues in the cell-wall arabinogalactan of mycobacterium leprae and myobacterium tuberculosis are furanoid. *Carbohydrate research*, 166(2):299–308, 1987.

[68] Jun Liu, Clifton E Barry, Gurdyal S Besra, and Hiroshi Nikaido. Mycolic acid structure determines the fluidity of the mycobacterial cell wall. *Journal of Biological Chemistry*, 271(47):29545–29551, 1996.

[69] Katherine A Abrahams and Gurdyal S Besra. Synthesis and recycling of the mycobacterial cell envelope. *Current Opinion in Microbiology*, 60:58–65, 2021.

[70] Werner B Schaefer, Charles L Davis, and Maurice L Cohn. Pathogenicity of transparent, opaque, and rough variants of mycobacterium avium in chickens and mice. *American Review of Respiratory Disease*, 102(4):499–506, 1970.

[71] Halima Medjahed, Jean-Louis Gaillard, and Jean-Marc Reyrat. Mycobacterium abscessus: a new player in the mycobacterial field. *Trends in microbiology*, 18(3):117–123, 2010.

[72] Jeffrey S Schorey and Lindsay Sweet. The mycobacterial glycopeptidolipids: structure, function, and their role in pathogenesis. *Glycobiology*, 18(11):832–841, 2008.

[73] Ana Victoria Gutiérrez, Albertus Viljoen, Eric Ghigo, Jean-Louis Herrmann, and Laurent Kremer. Glycopeptidolipids, a double-edged sword of the mycobacterium abscessus complex. *Frontiers in microbiology*, 9:1145, 2018.

[74] Elizabeth R Rhoades, Angela S Archambault, Rebecca Greendyke, Fong-Fu Hsu, Cassandra Streeter, and Thomas F Byrd. Mycobacterium abscessus glycopeptidolipids mask underlying cell wall phosphatidyl-myo-inositol mannosides blocking induction of human macrophage tnf-α by preventing interaction with tlr2. *The Journal of Immunology*, 183(3):1997–2007, 2009.

[75] Judith Recht, Asunción Martínez, Sandra Torello, and Roberto Kolter. Genetic analysis of sliding motility in mycobacterium smegmatis. *Journal of bacteriology*, 182(15):4348–4351, 2000.

[76] Susan T Howard, Elizabeth Rhoades, Judith Recht, Xiuhua Pang, Anny Alsup, Roberto Kolter, C Rick Lyons, and Thomas F Byrd. Spontaneous reversion of mycobacterium abscessus from a smooth to a rough morphotype is associated with reduced expression of glycopeptidolipid and reacquisition of an invasive phenotype. *Microbiology*, 152(6):1581–1590, 2006.

[77] Keenan Ryan and Thomas F Byrd. Mycobacterium abscessus: shapeshifter of the mycobacterial world. *Frontiers in microbiology*, 9:2642, 2018.

[78] George Carter, Martin Wu, Daryl C Drummond, and Luiz E Bermudez. Characterization of biofilm formation by clinical isolates of mycobacterium avium. *Journal of medical microbiology*, 52(9):747–752, 2003.

[79] Alexandre Pawlik, Guillaume Garnier, Mickael Orgeur, Pin Tong, Amanda Lohan, Fabien Le Chevalier, Guillaume Sapriel, Anne-Laure Roux, Kevin Conlon, Nadine Honore, et al. Identification and characterization of the genetic changes responsible for the characteristic smooth-to-rough morphotype alterations of clinically persistent m ycobacterium abscessus. *Molecular microbiology*, 90(3):612–629, 2013.

[80] Fabienne Ripoll, Caroline Deshayes, Sophie Pasek, Françoise Laval, Jean-Luc Beretti, Franck Biet, Jean-Loup Risler, Mamadou Daffé, Gilles Etienne, Jean-Louis Gaillard, et al. Genomics of glycopeptidolipid biosynthesis in mycobacterium abscessus and m. chelonae. *BMC genomics*, 8(1):1–9, 2007.

[81] Raju Mukherjee and Dipankar Chatterji. Glycopeptidolipids: Immuno-modulators in greasy mycobacterial cell envelope. *IUBMB life*, 64:215–25, 03 2012.

[82] Jesús Rojas Jaimes, Jorge Giraldo-Chavez, Yudit Huyhua-Flores, and Tatiana Caceres-Nakiche. Identificación de micobacterias en medio sólido mediante microscopía de fase invertida y tinción ziehl-neelsen. *Revista Peruana de Medicina Experimental y Salud Pública*, 35:279–284, 2018.

[83] Robert Koch. The etiology of tuberculosis. *Mittheilungen aus dem Kaiserlichen Gesundheitsamte*, 2:1–88, 1884.

[84] Nisha Rao, Laxman S Meena, et al. Biosynthesis and virulent behavior of lipids produced by mycobacterium tuberculosis: Lam and cord factor: an overview. *Biotechnology research international*, 2011, 2011.

[85] DG Macheque. Morphologic assessment of cord factor for rapid and presumptive identification of mycobacterium tuberculosis complex. *International Journal of Infectious Diseases*, 21:368, 2014.

[86] Andrea Gobetti Vieira Coelho, Liliana Aparecida Zamarioli, Clemira Martins Pereira Vidal Reis, and Bruno Francisco de Lima Duca. Detection of cord factor for the presumptive identification of mycobacterium tuberculosis complex. *Jornal Brasileiro de Pneumologia*, 33:707–711, 2007.

[87] Esther Julián, Mónica Roldán, Alejandro Sánchez-Chardi, Oihane Astola, Gemma Agustí, and Marina Luquin. Microscopic cords, a virulence-related characteristic of mycobacterium tuberculosis, are also present in nonpathogenic mycobacteria. *Journal of bacteriology*, 192(7):1751–1760, 2010.

[88] Alejandro Sánchez-Chardi, Francesc Olivares, Thomas F Byrd, Esther Julián, Cecilia Brambilla, and Marina Luquin. Demonstration of cord formation by rough mycobacterium abscessus variants: implications for the clinical microbiology laboratory. *Journal of clinical microbiology*, 49(6):2293–2295, 2011.

[89] Sophie Burbaud, Françoise Laval, Anne Lemassu, Mamadou Daffé, Christophe Guilhot, and Christian Chalut. Trehalose polyphleates are produced by a glycolipid biosynthetic pathway conserved across phylogenetically distant mycobacteria. *Cell chemical biology*, 23(2):278–289, 2016.

[90] Augusto Cesar Hunt-Serracin, Brian J Parks, Joseph Boll, and Cara C Boutte. Mycobacterium abscessus cells have altered antibiotic tolerance and surface glycolipids in artificial cystic fibrosis sputum medium. *Antimicrobial agents and chemotherapy*, 63(7):e02488–18, 2019.

[91] Ayssar A Elamin, Matthias Stehr, and Mahavir Singh. The cord factor: structure, biosynthesis and application in drug research—achilles heel of mycobacterium tuberculosis? *Understanding Tuberculosis—New Approaches to Fighting Against Drug Resistance*, pages 187–206, 2012.

[92] S-J Koh, T Song, YA Kang, JW Choi, KJ Chang, CS Chu, JG Jeong, J-Y Lee, M-K Song, H-Y Sung, et al. An outbreak of skin and soft tissue infection caused by mycobacterium abscessus following acupuncture. *Clinical microbiology and infection*, 16(7):895–901, 2010.

[93] JA Torres-Coy, BA Rodríguez-Castillo, R Pérez-Alfonzo, and JH De Waard. Source investigation of two outbreaks of skin and soft tissue infection by mycobacterium abscessus subsp. abscessus in venezuela. *Epidemiology & Infection*, 144(5):1117–1120, 2016.

[94] DM Grogono, JM Bryant, D Rodriguez-Rincon, I Everall, KP Brown, P Moreno, D Verma, E Hill, J Drijkoningen, CS Haworth, et al. T4 global spread of mycobacterium abscessus clones amongst cystic fibrosis patient, 2016.

[95] Tavs Qvist, Steffen Eickhardt, Kasper N Kragh, Claus B Andersen, Martin Iversen, Niels Høiby, and Thomas Bjarnsholt. Chronic pulmonary disease with mycobacterium abscessus complex is a biofilm infection. *European Respiratory Journal*, 46(6):1823–1826, 2015.

[96] Anne-Laure Roux, Albertus Viljoen, Aïcha Bah, Roxane Simeone, Audrey Bernut, Laura Laencina, Therese Deramaudt, Martin Rottman, Jean-Louis Gaillard, Laleh Majlessi, et al. The distinct fate of smooth and rough mycobacterium abscessus variants inside macrophages. *Open biology*, 6(11):160185, 2016.

[97] Astrid Lewin, Elisabeth Kamal, Torsten Semmler, Katja Winter, Sandra Kaiser, Hubert Schäfer, Lei Mao, Patience Eschenhagen, Claudia Grehn, Jennifer Bender, et al. Genetic diversification of persistent mycobacterium abscessus within cystic fibrosis patients. *Virulence*, 12(1):2415–2429, 2021.

[98] Thomas F Byrd and C Rick Lyons. Preliminary characterization of a mycobacterium abscessus mutant in human and murine models of infection. *Infection and immunity*, 67(9):4700–4707, 1999.

[99] Bodil E Jönsson, Marita Gilljam, Anders Lindblad, Malin Ridell, Agnes E Wold, and Christina Welinder-Olsson. Molecular epidemiology of mycobacterium abscessus, with focus on cystic fibrosis. *Journal of clinical microbiology*, 45(5):1497–1504, 2007.

[100] Crystal J Wiersma, Juan Manuel Belardinelli, Charlotte Avanzi, Shiva Kumar Angala, Isobel Everall, Bhanupriya Angala, Edward Kendall, Vinicius Calado Nogueira de Moura, Deepshikha Verma, Jeanne Benoit, et al. Cell surface remodeling of mycobacterium abscessus under cystic fibrosis airway growth conditions. *ACS Infectious Diseases*, 6(8):2143–2154, 2020.

[101] Gillian Clary, Smitha J Sasindran, Nathan Nesbitt, Laurel Mason, Sara Cole, Abul Azad, Karen McCoy, Larry S Schlesinger, and Luanne Hall-Stoodley. Mycobacterium abscessus smooth and rough morphotypes form antimicrobial-tolerant biofilm phenotypes but are killed by acetic acid. *Antimicrobial agents and chemotherapy*, 62(3):e01782–17, 2018.

[102] Enrico Tortoli, Laura Rindi, Maria J Garcia, Patrizia Chiaradonna, Rosanna Dei, Carlo Garzelli, Reiner M Kroppenstedt, Nicoletta Lari, Romano Mattei, Alessandro Mariottini, et al. Proposal to elevate the genetic variant mac-a, included in the mycobacterium avium complex, to species rank as mycobacterium chimaera sp. nov. *International journal of systematic and evolutionary microbiology*, 54(4):1277–1285, 2004.

[103] Joseph O Falkinham. Mycobacterium avium complex: Adherence as a way of life. *AIMS microbiology*, 4(3):428, 2018.

[104] Jacopo Monticelli, Roberta Maria Antonello, Roberto Luzzati, Marco Gabrielli, Maurizio Ferrarese, Luigi Codecasa, Stefano Di Bella, Daniele Roberto Giacobbe, et al. Mycobacterium chimaera infections: An update. *Journal of Infection and Chemotherapy*, 26(3):199–205, 2020.

[105] Hugo Sax, Guido Bloemberg, Barbara Hasse, Rami Sommerstein, Philipp Kohler, Yvonne Achermann, Matthias Rössle, Volkmar Falk, Stefan P Kuster, Erik C Böttger, et al. Prolonged outbreak of mycobacterium chimaera infection after open-chest heart surgery. *Clinical Infectious Diseases*, 61(1):67–75, 2015.

[106] Philipp Kohler, Stefan P Kuster, Guido Bloemberg, Bettina Schulthess, Michelle Frank, Felix C Tanner, Matthias Rössle, Christian Böni, Volkmar Falk, Markus J Wilhelm, et al. Healthcare-associated prosthetic heart valve, aortic vascular graft, and disseminated mycobacterium chi-

maera infections subsequent to open heart surgery. *European heart journal*, 36(40):2745–2753, 2015.

[107] Rami Sommerstein, Christian Rüegg, Philipp Kohler, Guido Bloemberg, Stefan P Kuster, and Hugo Sax. Transmission of mycobacterium chimaera from heater–cooler units during cardiac surgery despite an ultraclean air ventilation system. *Emerging infectious diseases*, 22(6):1008, 2016.

[108] Meghan M Lyman, Cheri Grigg, Cara Bicking Kinsey, M Shannon Keckler, Heather Moulton-Meissner, Emily Cooper, Minn M Soe, Judith Noble-Wang, Allison Longenberger, Shane R Walker, et al. Invasive nontuberculous mycobacterial infections among cardiothoracic surgical patients exposed to heater–cooler devices. *Emerging infectious diseases*, 23(5):796, 2017.

[109] Jakko van Ingen, Thomas A Kohl, Katharina Kranzer, Barbara Hasse, Peter M Keller, Anna Katarzyna Szafrańska, Doris Hillemann, Meera Chand, Peter Werner Schreiber, Rami Sommerstein, Christoph Berger, Michele Genoni, Christian Rüegg, Nicolas Troillet, Andreas F Widmer, Sören L Becker, Mathias Herrmann, Tim Eckmanns, Sebastian Haller, Christiane Höller, Sylvia B Debast, Maurice J Wolfhagen, Joost Hopman, Jan Kluytmans, Merel Langelaar, Daan W Notermans, Jaap ten Oever, Peter van den Barselaar, Alexander B A Vonk, Margreet C Vos, Nada Ahmed, Timothy Brown, Derrick Crook, Theresa Lamagni, Nick Phin, E Grace Smith, Maria Zambon, Annerose Serr, Tim Götting, Winfried Ebner, Alexander Thürmer, Christian Utpatel, Cathrin Spröer, Boyke Bunk, Ulrich Nübel, Guido V Bloemberg, Erik C Böttger, Stefan Niemann, Dirk Wagner, and Hugo Sax. Global outbreak of severe ¡em¿mycobacterium chimaera¡/em¿ disease after cardiac surgery: a molecular epidemiological study. *The Lancet Infectious Diseases*, 17(10):1033–1041, 2021/09/19 2017.

[110] Peter W Schreiber, Stefan P Kuster, Barbara Hasse, Cornelia Bayard, Christian Rüegg, Philipp Kohler, Peter M Keller, Guido V Bloemberg, Francesco Maisano, Dominique Bettex, et al. Reemergence of mycobacterium chimaera in heater–cooler units despite intensified cleaning and disinfection protocol. *Emerging infectious diseases*, 22(10):1830, 2016.

[111] J William Costerton, Zbigniew Lewandowski, Douglas E Caldwell, Darren R Korber, and Hilary M Lappin-Scott. Microbial biofilms. *Annual review of microbiology*, 49(1):711–745, 1995.

[112] Paula Watnick and Roberto Kolter. Biofilm, city of microbes. *Journal of bacteriology*, 182(10):2675–2679, 2000.

[113] Hans-Curt Flemming, Jost Wingender, Ulrich Szewzyk, Peter Steinberg, Scott A Rice, and Staffan Kjelleberg. Biofilms: an emergent form of bacterial life. *Nature Reviews Microbiology*, 14(9):563–575, 2016.

[114] Karin Sauer, Paul Stoodley, Darla M Goeres, Luanne Hall-Stoodley, Mette Burmølle, Philip S Stewart, and Thomas Bjarnsholt. The biofilm life cycle: expanding the conceptual model of biofilm formation. *Nature Reviews Microbiology*, pages 1–13, 2022.

[115] Jacobs P Richards and Anil K Ojha. Mycobacterial biofilms. *Microbiology spectrum*, 2(5):2–5, 2014.

[116] Albertus Viljoen, Yves F Dufrêne, and Jérôme Nigou. Mycobacterial adhesion: From hydrophobic to receptor-ligand interactions. *Microorganisms*, 10(2):454, 2022.

[117] Sophia A Pacheco, Fong-Fu Hsu, Katelyn M Powers, and Georgiana E Purdy. Mmpl11 protein transports mycolic acid-containing lipids to the mycobacterial cell wall and contributes to biofilm formation in mycobacterium smegmatis. *Journal of Biological Chemistry*, 288(33):24213–24222, 2013.

[118] Catherine C Wright, Fong Fu Hsu, Eusondia Arnett, Jennifer L Dunaj, Patrick M Davidson, Sophia A Pacheco, Melanie J Harriff, David M Lewinsohn, Larry S Schlesinger, and Georgiana E Purdy. The mycobacterium tuberculosis mmpl11 cell wall lipid transporter is important for biofilm formation, intracellular growth, and nonreplicating persistence. *Infection and immunity*, 85(8):e00131–17, 2017.

[119] Anil K Ojha, William R Jacobs, and Graham F Hatfull. Genetic dissection of mycobacterial biofilms. In *Mycobacteria protocols*, pages 215–226. Springer, 2015.

[120] Seenivasan Boopathi, Subbiah Ramasamy, B Haridevamuthu, Raghul Murugan, Maruthanayagam Veerabadhran, Ai-Qun Jia, and Jesu Arockiaraj. Intercellular communication and social behaviors in mycobacteria. *Frontiers in Microbiology*, page 3525, 2022.

[121] J-H Ryu, H Kim, JF Frank, and LR Beuchat. Attachment and biofilm formation on stainless steel by escherichia coli o157: H7 as affected by curli production. *Letters in applied microbiology*, 39(4):359–362, 2004.

[122] Martijn FBG Gebbink, Dennis Claessen, Barend Bouma, Lubbert Dijkhuizen, and Han AB Wösten. Amyloids—a functional coat for microorganisms. *Nature Reviews Microbiology*, 3(4):333–341, 2005.

[123] Mikkel Klausen, Anders Aaes-Jørgensen, Søren Molin, and Tim Tolker-Nielsen. Involvement of bacterial migration in the development of complex multicellular structures in pseudomonas aeruginosa biofilms. *Molecular microbiology*, 50(1):61–68, 2003.

[124] Julian Wimpenny, Werner Manz, and Ulrich Szewzyk. Heterogeneity in biofilms. *FEMS microbiology reviews*, 24(5):661–671, 2000.

[125] Y. El-Naggar and S.E. Finkel. Live wires. *The Scientist*, 27, 05 2013.

[126] Samay Pande, Shraddha Shitut, Lisa Freund, Martin Westermann, Felix Bertels, Claudia Colesie, Ilka B Bischofs, and Christian Kost. Metabolic cross-feeding via intercellular nanotubes among bacteria. *Nature communications*, 6(1):1–13, 2015.

[127] David G Allison. The biofilm matrix. *Biofouling*, 19(2):139–150, 2003.

[128] Hans-Curt Flemming and Jost Wingender. The biofilm matrix. *Nature reviews microbiology*, 8(9):623–633, 2010.

[129] Poushali Chakraborty and Ashwani Kumar. The extracellular matrix of mycobacterial biofilms: could we shorten the treatment of mycobacterial infections? *Microbial cell*, 6(2):105, 2019.

[130] Abhishek Trivedi, Parminder Singh Mavi, Deepak Bhatt, and Ashwani Kumar. Thiol reductive stress induces cellulose-anchored biofilm formation in mycobacterium tuberculosis. *Nature communications*, 7(1):1–15, 2016.

[131] Niël Van Wyk, David Navarro, Mickaël Blaise, Jean-Guy Berrin, Bernard Henrissat, Michel Drancourt, and Laurent Kremer. Characterization of a mycobacterial cellulase and its impact on biofilm-and drug-induced cellulose production. *Glycobiology*, 27(5):392–399, 2017.

[132] David G Davies, Matthew R Parsek, James P Pearson, Barbara H Iglewski, J William Costerton, and Everett P Greenberg. The involvement of cell-to-cell signals in the development of a bacterial biofilm. *Science*, 280(5361):295–298, 1998.

[133] Daniel J Hassett, Ju-Fang Ma, James G Elkins, Timothy R McDermott, Urs A Ochsner, Susan EH West, Ching-Tsan Huang, Jessie Fredericks, Scott Burnett, Philip S Stewart, et al. Quorum sensing in pseudomonas aeruginosa controls expression of catalase and superoxide dismutase genes and mediates biofilm susceptibility to hydrogen peroxide. *Molecular microbiology*, 34(5):1082–1093, 1999.

[134] Martina Hausner and Stefan Wuertz. High rates of conjugation in bacterial biofilms as determined by quantitative in situ analysis. *Applied and environmental microbiology*, 65(8):3710–3713, 1999.

[135] Mathis Steindor, Vanesa Nkwouano, Ertan Mayatepek, Colin R Mackenzie, Dirk Schramm, and Marc Jacobsen. Rapid detection and immune characterization of mycobacterium abscessus infection in cystic fibrosis patients. *PLoS One*, 10(3):e0119737, 2015.

[136] Astrid Lewin, Daniela Baus, Elisabeth Kamal, Fabienne Bon, Ralph Kunisch, Sven Maurischat, Michaela Adonopoulou, and Katharina Eich. The mycobacterial dna-binding protein 1 (mdp1) from mycobacterium bovis bcg influences various growth characteristics. *BMC Microbiology*, 8(1):91, 2008.

[137] T. Seemann. Prokka: rapid prokaryotic genome annotation. *Bioinformatics*, 2014.

[138] Andrew J. Page, Carla A. Cummins, Martin Hunt, Vanessa K. Wong, Sandra Reuter, Matthew T.G. Holden, Maria Fookes, Daniel Falush, Jacqueline A. Keane, and Julian Parkhill. Roary: rapid large-scale prokaryote pan genome analysis. *Bioinformatics*, 31(22):3691–3693, 07 2015.

[139] Joerg Doellinger, Andy Schneider, Marcell Hoeller, and Peter Lasch. Sample preparation by easy extraction and digestion (speed)-a universal, rapid, and detergent-free protocol for proteomics based on acid extraction. *Molecular & Cellular Proteomics*, 19(1):209–222, 2020.

[140] Katharina Konrat, Ingeborg Schwebke, Michael Laue, Christin Dittmann, Katja Levin, Ricarda Andrich, Mardjan Arvand, and Christoph Schaudinn. The bead assay for biofilms: a quick, easy and robust method for testing disinfectants. *PloS one*, 11(6):e0157663, 2016.

[141] Nishant Sharma, Suruchi Aggarwal, Saravanan Kumar, Rahul Sharma, Konika Choudhury, Niti Singh, Praapti Jayaswal, Renu Goel, Saima Wajid, Amit Kumar Yadav, et al. Comparative analysis of homologous aminopeptidase pepn from pathogenic and non-pathogenic mycobacteria reveals divergent traits. *PloS one*, 14(4):e0215123, 2019.

[142] B Murugasu-Oei, A Tay, and T Dick. Upregulation of stress response genes and abc transporters in anaerobic stationary-phase mycobacterium smegmatis. *Molecular and General Genetics MGG*, 262(4):677–682, 1999.

[143] Surendra Singh, Chad Brocker, Vindhya Koppaka, Ying Chen, Brian C Jackson, Akiko Matsumoto, David C Thompson, and Vasilis Vasiliou. Aldehyde dehydrogenases in cellular responses to oxidative/electrophilicstress. *Free radical biology and medicine*, 56:89–101, 2013.

[144] Yongmeng Li, Yan Zhou, Yufang Ma, and Xuebing Li. Design and synthesis of novel cell wall inhibitors of mycobacterium tuberculosis glmm and glmu. *Carbohydrate research*, 346(13):1714–1720, 2011.

[145] Jian Kang, Liming Xu, Shufeng Yang, Wendan Yu, Shuo Liu, Yi Xin, and Yufang Ma. Effect of phosphoglucosamine mutase on biofilm formation and antimicrobial susceptibilities in m. smegmatis glmm gene knockdown strain. *PloS one*, 8(4):e61589, 2013.

[146] Gleiciane Leal Moraes, Guelber Cardoso Gomes, Paulo Robson Monteiro De Sousa, Cláudio Nahum Alves, Thavendran Govender, Hendrik G Kruger, Glenn EM Maguire, Gyanu Lamichhane, and Jerônimo Lameira. Structural and functional features of enzymes of mycobacterium tuberculosis peptidoglycan biosynthesis as targets for drug development. *Tuberculosis*, 95(2):95–111, 2015.

[147] Luis EN Quadri. Biosynthesis of mycobacterial lipids by polyketide synthases and beyond. *Critical reviews in biochemistry and molecular biology*, 49(3):179–211, 2014.

[148] Siyuan Feng, Yan Liu, Wanfei Liang, Mohamed Abd El-Gawad El-Sayed Ahmed, Zihan Zhao, Cong Shen, Adam P Roberts, Lujie Liang, Liya Liao, Zhijuan Zhong, et al. Involvement of transcription elongation factor grea in mycobacterium viability, antibiotic susceptibility, and intracellular fitness. *Frontiers in microbiology*, 11:413, 2020.

[149] Gerd M Seibold and Bernhard J Eikmanns. The glgx gene product of corynebacterium glutamicum is required for glycogen degradation and for fast adaptation to hyperosmotic stress. *Microbiology*, 153(7):2212–2220, 2007.

[150] Chao Wang, Qiaoli Zhang, Yang Wang, Xudong Tang, Yanan An, Shulin Li, Hongyue Xu, Yan Li, Wenjing Luan, Xuefei Wang, et al. Comparative proteomics analysis between biofilm and planktonic cells of mycobacterium tuberculosis. *Electrophoresis*, 40(20):2736–2746, 2019.

[151] Joana Azeredo, Nuno F Azevedo, Romain Briandet, Nuno Cerca, Tom Coenye, Ana Rita Costa, Mickaël Desvaux, Giovanni Di Bonaventura, Michel Hébraud, Zoran Jaglic, et al. Critical review on biofilm methods. *Critical reviews in microbiology*, 43(3):313–351, 2017.

[152] James Harrison, Georgina Lloyd, Maju Joe, Todd L Lowary, Edward Reynolds, Hannah Walters-Morgan, Apoorva Bhatt, Andrew Lovering, Gurdyal S Besra, and Luke J Alderwick. Lcp1 is a phosphotransferase responsible for ligating arabinogalactan to peptidoglycan in mycobacterium tuberculosis. *MBio*, 7(4):e00972–16, 2016.

[153] Hoa T Nguyen, Kerstin A Wolff, Richard H Cartabuke, Sam Ogwang, and Liem Nguyen. A lipoprotein modulates activity of the mtrab two-component system to provide intrinsic multidrug resistance, cytokinetic control and cell wall homeostasis in mycobacterium. *Molecular microbiology*, 76(2):348–364, 2010.

[154] Werner B Schaefer and C Willard Lewis Jr. Effect of oleic acid on growth and cell structure of mycobacteria. *Journal of Bacteriology*, 90(5):1438–1447, 1965.

[155] L Karygianni, Z Ren, H Koo, and T Thurnheer. Biofilm matrixome: extracellular components in structured microbial communities. *Trends in Microbiology*, 28(8):668–681, 2020.

[156] Nicole Billings, Maria Ramirez Millan, Marina Caldara, Roberto Rusconi, Yekaterina Tarasova, Roman Stocker, and Katharina Ribbeck. The extracellular matrix component psl provides fast-acting antibiotic defense in pseudomonas aeruginosa biofilms. *PLoS pathogens*, 9(8):e1003526, 2013.

[157] Siva Wu, Marc M Baum, James Kerwin, Debbie Guerrero, Simon Webster, Christoph Schaudinn, David VanderVelde, and Paul Webster. Biofilm-specific extracellular matrix proteins of nontypeable haemophilus influenzae. *Pathogens and disease*, 72(3):143–160, 2014.

[158] Lone Tang, Andreas Schramm, Thomas R Neu, Niels P Revsbech, and Rikke L Meyer. Extracellular dna in adhesion and biofilm formation of four environmental isolates: a quantitative study. *FEMS microbiology ecology*, 86(3):394–403, 2013.

[159] Cécile Berne, David T Kysela, and Yves V Brun. A bacterial extracellular dna inhibits settling of motile progeny cells within a biofilm. *Molecular microbiology*, 77(4):815–829, 2010.

[160] Rattiyaphorn Pakkulnan, Chitchanok Anutrakunchai, Sakawrat Kanthawong, Suwimol Taweechaisupapong, Pisit Chareonsudjai, and Sorujsiri Chareonsudjai. Extracellular dna facilitates bacterial adhesion during burkholderia pseudomallei biofilm formation. *PloS one*, 14(3):e0213288, 2019.

[161] Mira Okshevsky and Rikke Louise Meyer. The role of extracellular dna in the establishment, maintenance and perpetuation of bacterial biofilms. *Critical reviews in microbiology*, 41(3):341–352, 2015.

[162] Kenneth C Malcolm, Silvia M Caceres, Kerstin Pohl, Katie R Poch, Audrey Bernut, Laurent Kremer, Donna L Bratton, Jean-Louis Herrmann, and Jerry A Nick. Neutrophil killing of mycobacterium abscessus by intra-and extracellular mechanisms. *PLoS One*, 13(4):e0196120, 2018.

[163] Thomas F Byrd and Edward D Chan. Mycobacterium abscessus; the paradox of low pathogenicity and high virulence. *Frontiers in Microbiology*, 13, 2022.

[164] Carme Cucarella, Cristina Solano, Jaione Valle, Beatriz Amorena, Íñigo Lasa, and José R Penadés. Bap, a staphylococcus aureus surface protein involved in biofilm formation. *Journal of bacteriology*, 183(9):2888–2896, 2001.

[165] Junfeng Ma, Xiang Cheng, Zhonghe Xu, Yikan Zhang, Jaione Valle, Shilong Fan, Xiaobing Zuo, Iñigo Lasa, and Xianyang Fang. Structural mechanism for modulation of functional amyloid and biofilm formation by staphylococcal bap protein switch. *The EMBO Journal*, 40(14):e107500, 2021.

[166] Tatsuya Kikuchi, Yoshimitsu Mizunoe, Akemi Takade, Seiji Naito, and Shin-ichi Yoshida. Curli fibers are required for development of biofilm architecture in escherichia coli k-12 and enhance bacterial adherence to human uroepithelial cells. *Microbiology and immunology*, 49(9):875–884, 2005.

[167] Claire Prigent-Combaret, Gérard Prensier, Thanh Thuy Le Thi, Olivier Vidal, Philippe Lejeune, and Corinne Dorel. Developmental pathway for biofilm formation in curli-producing escherichia coli strains: role of flagella, curli and colanic acid. *Environmental microbiology*, 2(4):450–464, 2000.

[168] Marta Martínez-Gil, Fátima Yousef-Coronado, and Manuel Espinosa-Urgel. Lapf, the second largest pseudomonas putida protein, contributes to plant root colonization and determines biofilm architecture. *Molecular microbiology*, 77(3):549–561, 2010.

[169] Morten Rybtke, Jens Berthelsen, Liang Yang, Niels Høiby, Michael Givskov, and Tim Tolker-Nielsen. The lapg protein plays a role in pseudomonas aeruginosa biofilm formation by controlling the presence of the cdra adhesin on the cell surface. *Microbiologyopen*, 4(6):917–930, 2015.

[170] Andrew D McCall, Ruvini U Pathirana, Aditi Prabhakar, Paul J Cullen, and Mira Edgerton. Candida albicans biofilm development is governed by cooperative attachment and adhesion maintenance proteins. *NPJ biofilms and microbiomes*, 5(1):1–12, 2019.

[171] Jiunn NC Fong and Fitnat H Yildiz. Biofilm matrix proteins. *Microbiology spectrum*, 3(2):3–2, 2015.

[172] Zeshan Habib, Weize Xu, Muhammad Jamal, Khaista Rehman, Jinxia Dai, Zhen fang Fu, Xi Chen, and Gang Cao. Adaptive gene profiling of mycobacterium tuberculosis during sublethal kanamycin exposure. *Microbial pathogenesis*, 112:243–253, 2017.

[173] Carla CCR de Carvalho, Raquel Teixeira, and Pedro Fernandes. Mycobacterium vaccae adaptation to disinfectants and hand sanitisers, and evaluation of cross-tolerance with antimicrobials. *Antibiotics*, 9(9):544, 2020.

[174] Christine Vogel and Edward M Marcotte. Insights into the regulation of protein abundance from proteomic and transcriptomic analyses. *Nature reviews genetics*, 13(4):227–232, 2012.

[175] Yuichi Wakamoto, Neeraj Dhar, Remy Chait, Katrin Schneider, François Signorino-Gelo, Stanislas Leibler, and John D McKinney. Dynamic persistence of antibiotic-stressed mycobacteria. *Science*, 339(6115):91–95, 2013.

[176] Kirsi Savijoki, Henna Myllymäki, Hanna Luukinen, Lauri Paulamäki, Leena-Maija Vanha-Aho, Aleksandra Svorjova, Ilkka Miettinen, Adyary Fallarero, Teemu O Ihalainen, Jari Yli-Kauhaluoma, et al. Surface-shaving proteomics of mycobacterium marinum identifies biofilm subtype-specific changes affecting virulence, tolerance, and persistence. *Msystems*, 6(3):e00500–21, 2021.

[177] Wanyan Deng, Chunmei Li, and Jianping Xie. The underling mechanism of bacterial tetr/acrr family transcriptional repressors. *Cellular signalling*, 25(7):1608–1613, 2013.

[178] Min Yang, Chun-Hui Gao, Jialing Hu, Lei Zhao, Qiaoyun Huang, and Zheng-Guo He. Inbr, a tetr family regulator, binds with isoniazid and influences multidrug resistance in mycobacterium bovis bcg. *Scientific reports*, 5(1):1–15, 2015.

[179] Leslie Cuthbertson and Justin R Nodwell. The tetr family of regulators. *Microbiology and Molecular Biology Reviews*, 77(3):440–475, 2013.

[180] Edith NG Houben, Jovanka Bestebroer, Roy Ummels, Louis Wilson, Sander R Piersma, Connie R Jiménez, Tom HM Ottenhoff, Joen Luirink, and Wilbert Bitter. Composition of the type vii secretion system membrane complex. *Molecular microbiology*, 86(2):472–484, 2012.

[181] Catalin M Bunduc, Dirk Fahrenkamp, Jiri Wald, Roy Ummels, Wilbert Bitter, Edith NG Houben, and Thomas C Marlovits. Structure and dynamics of a mycobacterial type vii secretion system. *Nature*, 593(7859):445–448, 2021.

[182] Xiao-Li Zhang, De-Feng Li, Joy Fleming, Li-Wei Wang, Ying Zhou, Da-Cheng Wang, Xian-En Zhang, and Li-Jun Bi. Core component eccb1 of the mycobacterium tuberculosis type vii secretion system is a periplasmic atpase. *The FASEB Journal*, 29(12):4804–4814, 2015.

[183] Daria Bottai and Roland Brosch. Mycobacterial pe, ppe and esx clusters: novel insights into the secretion of these most unusual protein families. *Molecular microbiology*, 73(3):325–328, 2009.

[184] Samantha L Sampson. Mycobacterial pe/ppe proteins at the host-pathogen interface. *Clinical and Developmental Immunology*, 2011, 2011.

[185] Sakshi Kohli, Yadvir Singh, Khushbu Sharma, Aditya Mittal, Nasreen Z Ehtesham, and Seyed E Hasnain. Comparative genomic and proteomic analyses of pe/ppe multigene family of mycobacterium tuberculosis h37rv and h37ra reveal novel and interesting differences with implications in virulence. *Nucleic acids research*, 40(15):7113–7122, 2012.

[186] Li-Yin Lai, Tzu-Lung Lin, Yi-Yin Chen, Pei-Fang Hsieh, and Jin-Town Wang. Role of the mycobacterium marinum esx-1 secretion system in sliding motility and biofilm formation. *Frontiers in microbiology*, 9:1160, 2018.

[187] Marion Lagune, Cecile Petit, Flor Vásquez Sotomayor, Matt D Johansen, Kathrine SH Beckham, Christina Ritter, Fabienne Girard-Misguich, Matthias Wilmanns, Laurent Kremer, Florian P Maurer, et al. Conserved and specialized functions of type vii secretion systems in non-tuberculous mycobacteria. *Microbiology*, 167(7):001054, 2021.

[188] Thottethodi Subrahmanya Keshava Prasad, Renu Verma, Satish Kumar, Raja Sekhar Nirujogi, Gajanan J Sathe, Anil K Madugundu, Jyoti Sharma, Vinuth N Puttamallesh, Anjali Ganjiwale, Vithal P Myneedu, et al. Proteomic analysis of purified protein derivative of mycobacterium tuberculosis. *Clinical proteomics*, 10(1):1–9, 2013.

[189] Joseph O Falkinham III. Factors influencing the chlorine susceptibility of mycobacterium avium, mycobacterium intracellulare, and mycobacterium scrofulaceum. *Applied and environmental microbiology*, 69(9):5685–5689, 2003.

[190] Julie Bonhomme, Murielle Chauvel, Sophie Goyard, Pascal Roux, Tristan Rossignol, and Christophe d'Enfert. Contribution of the glycolytic flux and hypoxia adaptation to efficient biofilm formation by candida albicans. *Molecular microbiology*, 80(4):995–1013, 2011.

[191] Kerry S Williamson, Lee A Richards, Ailyn C Perez-Osorio, Betsey Pitts, Kathleen McInnerney, Philip S Stewart, and Michael J Franklin. Heterogeneity in pseudomonas aeruginosa biofilms includes expression of ribosome hibernation factors in the antibiotic-tolerant subpopulation and hypoxia-induced stress response in the metabolically active population. *Journal of bacteriology*, 194(8):2062–2073, 2012.

[192] Rajoana Rojony, Matthew Martin, Anaamika Campeau, Jacob M Wozniak, David J Gonzalez, Pankaj Jaiswal, L Danelishvili, and Luiz E Bermudez. Quantitative analysis of mycobacterium avium subsp. hominissuis proteome in response to antibiotics and during exposure to different environmental conditions. *Clinical proteomics*, 16(1):1–20, 2019.

[193] Vanja M Bulatovic, Nancy L Wengenack, James R Uhl, Leslie Hall, Glenn D Roberts, Franklin R Cockerill III, and Frank Rusnak. Oxidative stress increases susceptibility of mycobacterium tuberculosis to isoniazid. *Antimicrobial agents and chemotherapy*, 46(9):2765–2771, 2002.

[194] Thomas Trunk, Hawzeen S Khalil, and Jack C Leo. Bacterial autoaggregation. *AIMS microbiology*, 4(1):140, 2018.

[195] Zuzana Bohrerova and Karl G Linden. Ultraviolet and chlorine disinfection of mycobacterium in wastewater: effect of aggregation. *Water environment research*, 78(6):565–571, 2006.

[196] Mette Kolpen, Peter Østrup Jensen, Tavs Qvist, Kasper Nørskov Kragh, Cecillie Ravnholt, Blaine Gabriel Fritz, Ulla Rydahl Johansen, Thomas Bjarnsholt, and Niels Høiby. Biofilms of mycobacterium abscessus complex can be sensitized to antibiotics by disaggregation and oxygenation. *Antimicrobial agents and chemotherapy*, 64(2):e01212–19, 2020.

[197] Catherine R Armbruster, Terri S Forster, Rodney M Donlan, Heather A O'Connell, Alicia M Shams, and Margaret M Williams. A biofilm model developed to investigate survival and disinfection of mycobacterium mucogenicum in potable water. *Biofouling*, 28(10):1129–1139, 2012.

[198] Poushali Chakraborty, Sapna Bajeli, Deepak Kaushal, Bishan Dass Radotra, and Ashwani Kumar. Biofilm formation in the lung contributes to virulence and drug tolerance of mycobacterium tuberculosis. *Nature communications*, 12(1):1–17, 2021.

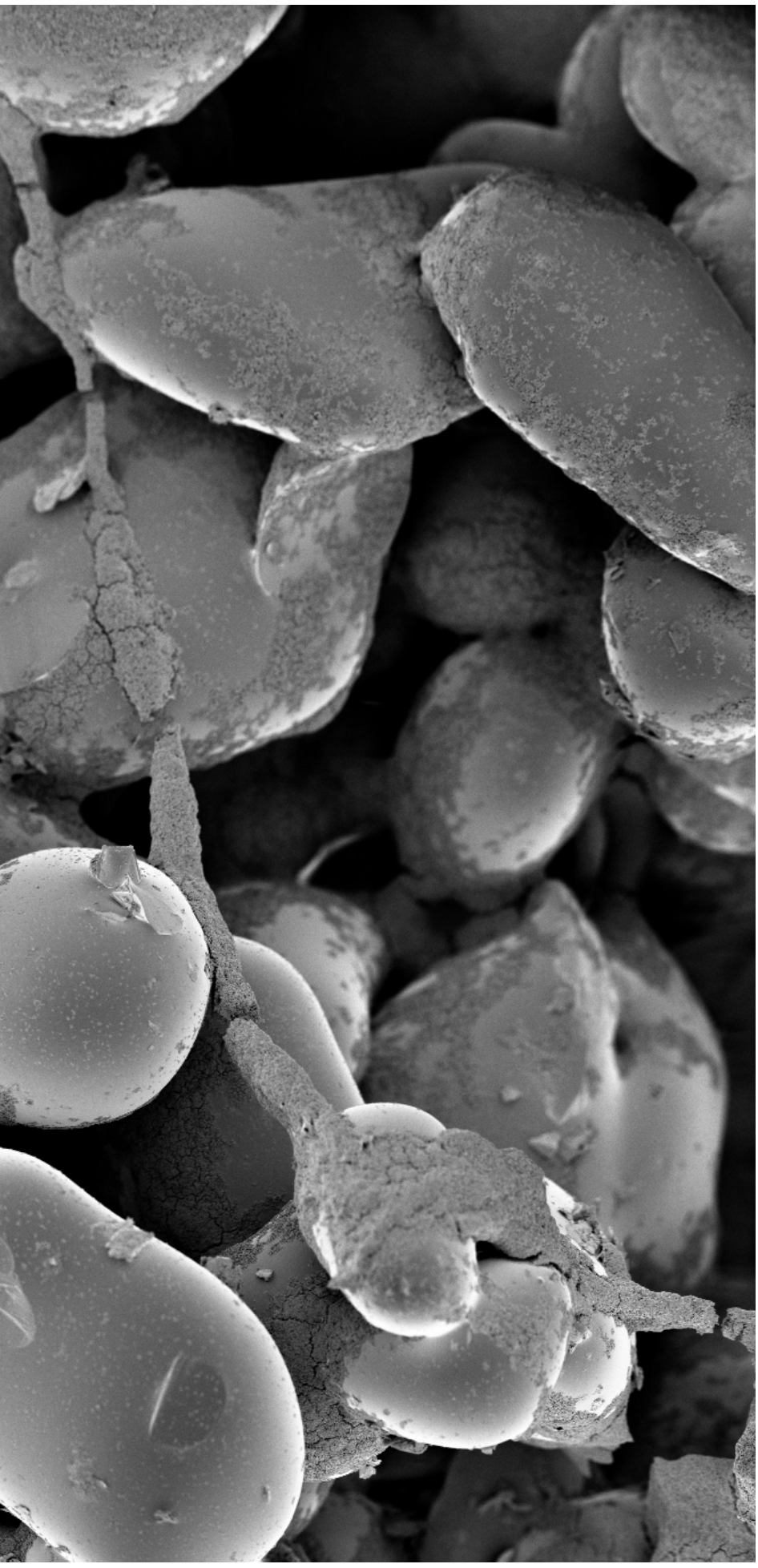

Chapter 5

Appendix

List of Abbreviations

AFB	acid-fast bacteria
AMI	amikacin
ASM	artifical sputum medium
CB	collagen-coated glass beads
CF	cystic fibrosis
CFU	colony forming unit
ECM	extracellular matrix
ECMO	extracorporal membrane oxigenation
eDNA	extracellular DNA
FAC	free active chlorine
GA	glutaraldehyde
GB	glass beads
GPL	glycopeptidolipids
HCU	heater-cooler unit
HCUs	heater-cooler units
MA	mycolic acids
MAB-PD	*M. abscessus* pulmonary disease
MAC	*Mycobacterium avium*-complex
MAC-PD	MAC pulmonary disease
MB-OADC	Middlebrook 7H9 or 7H11 + 10 % OADC
MH	Mueller-Hinton II cation adjusted
MH-OADC	Mueller-Hinton II cation adjusted + 5 % OADC
MOTT	mycobacteria other than tuberculosis
MTB	*Mycobacterium tuberculosis*
MTC	*Mycobacterium tuberculosis*-complex
NTM	nontuberculous mycobacteria
NTM-PD	NTM pulmonary disease
PAA	peracetic acid
PB	plastic beads
PCR	polymerase chain reaction
PGB	porous glass beads
PGL	phenolic glycolipids
RGM	rapid growing mycobacteria
SGM	Slow growing mycobacteria
SNP	single nucleotide polymorphism
ssGPL	serovar-specific GPL
T7SS	type VII secretion system
TDM	trehalose dimycolate
TGC	tigecycline
TMM	trehalose monomycolate

List of Figures

List of Tables

Supplementary

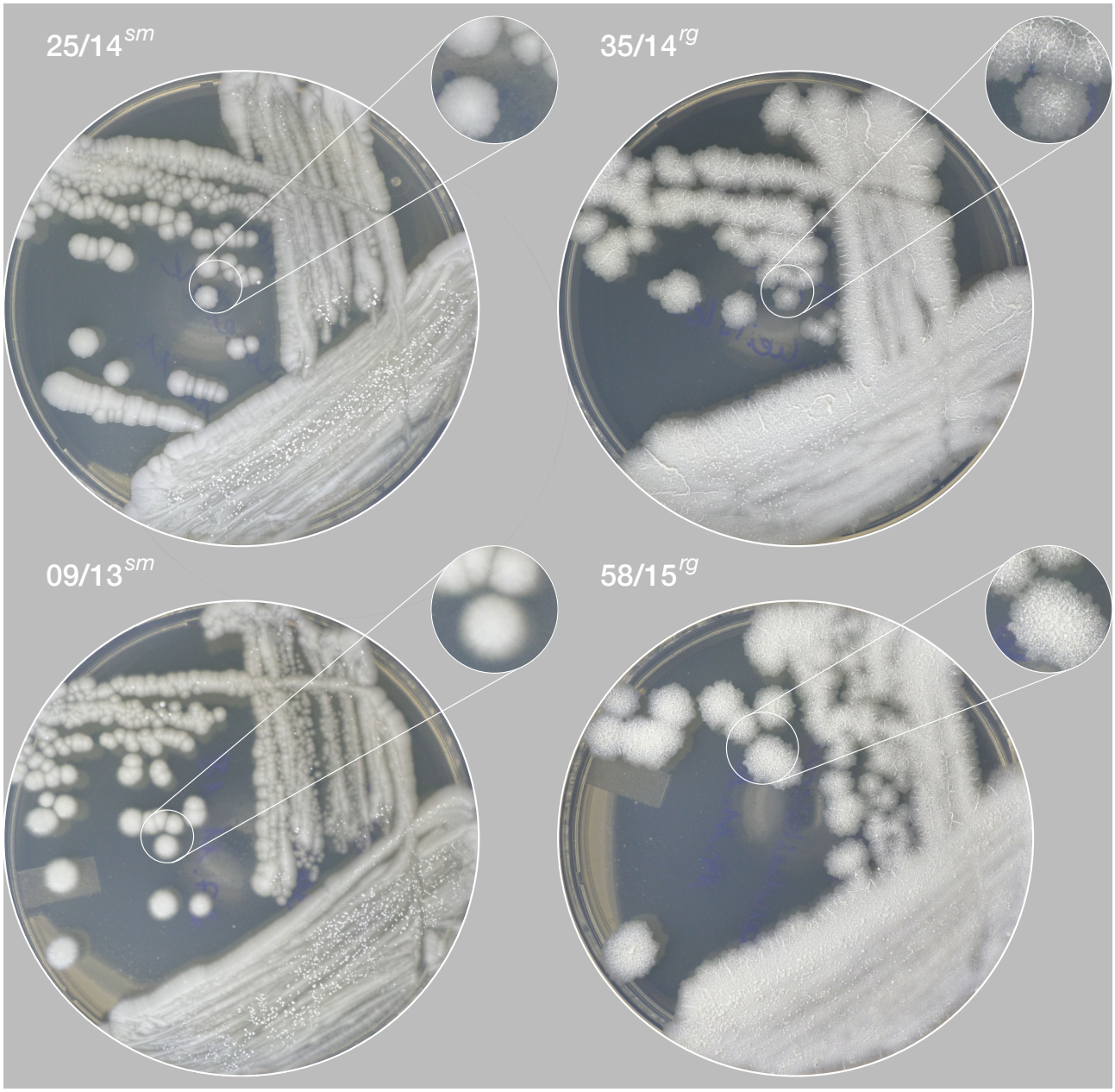

Suppl. Fig. S.1: Photographies of *M. abscessus* isolates
Displayed are photographies of the used *M. abscessus* isolates grown on MB-OADC agar plates for 7 days at 37° C. For better comparison, zooms of single colonies are presented.
The isolates $25/14^{sm}$ and $09/13^{sm}$ grow as smooth morphotype, though the upscaled images of the single colonies show slight differences in the form of the colonies. While $09/13^{sm}$ grows more even in a round shape, single colonies of $25/14^{sm}$ present a slightly frayed shape.
The isolates $35/14^{rg}$ and $58/15^{rg}$ represent the rough morphotype. The colonies of both isolates have a fringed shape and an uneven bumpy surface.

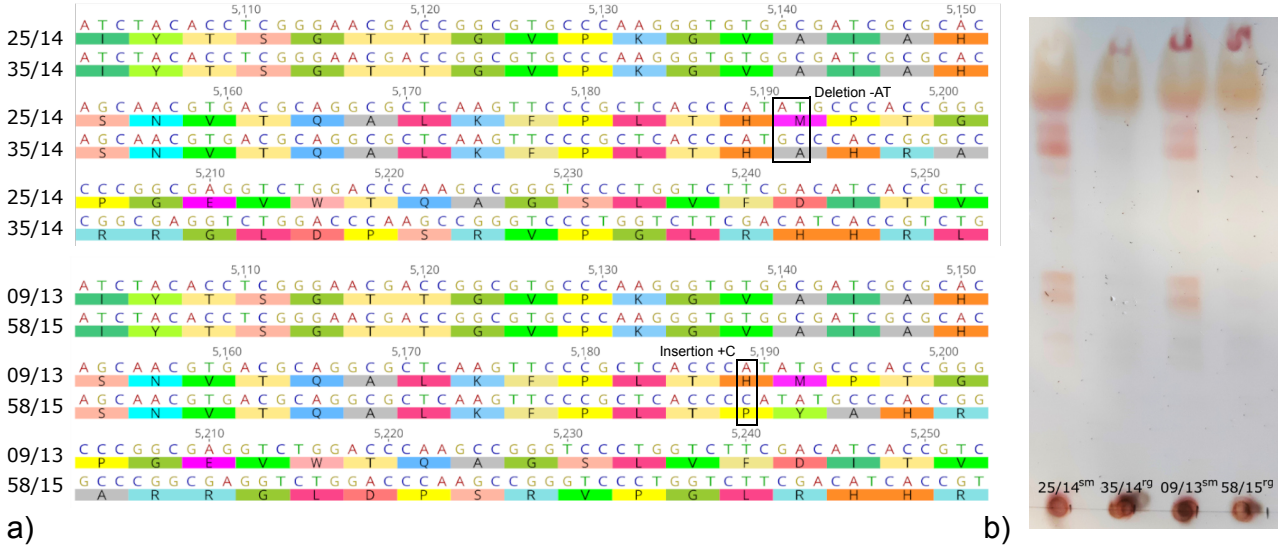

Suppl. Fig. S.2: Schematic representation of the *mps2* gene and a TLC of the isolated GPL of the used *M. abscessus* isolates.

a) Displayed is a section of the *mps2* gene showing the positions of the mutations that occurred in the rough morphotypes and the resulting changes in the amino acid sequence. The gene sequence and the resulting amino acid translation of the *mps2* gene of both smooth isolates is identical.
The isolate 35/14^{rg} has a deletion of two bases (AT) at the position 5191-5192 when compared to its smooth counterpart 25/14^{sm}. The other rough morphotype 58/15^{rg} has instead an insertion of one base (C) at the position 5189 compared to 09/13^{sm}.
These are the only mutations in the GPL gene cluster of both related isoform isolates and result in the phenotypic change from smooth to rough morphotype.
b) In order to analyse the GPL expression in the *M. abscessus* isolates, the bacteria were cultivated as planktonic samples as described above (section 2.2.5) to a optical density (OD_{600}) of 1.8-2.
Thereafter the bacteria were heat-killed and centrifuged (8,000 rpm, 15 min). The supernatant was discarded and the pellet resuspended in 10 mL chloroform/methanol (2:1, vol/vol). Then the bacteria were ultrasonicated (100% power, 1 min; Branson sonifier-450 D, Heinemann, Germany). The resulting liquid phase was then transferred to a fresh tube and hydrolyzed with 3 mL of 0.2 N sodium hydroxide in methanol in order to remove the alkali-labile lipids. The mixture was then neutralized to pH 7 using 6 N HCL und thereafter mixed with 6 mL chloroform and afterwards 5 mL water. This was centrifuged as mentioned above and the bottom phase transferred to a new tube and evaporated completely. The dried pellet was then resuspended in chloroform/methanol (2:1, vol/vol).

For thin-layer chromatography, 5 µL of the dissolved lipids were applied to silica-coated TLC plates (Analtech DC-Uniplates™, Merck, Germany) and dried shortly. Afterwards the TLC plate was put in a chamber containing chloroform/methanol (90:10, vol/vol) as solvent. The lipids were separated for 15 min, then the TLC plate was taken out of the chamber and dried under the fume hood completely. The lipids were made visible by spraying the plates with 10% H_2SO_4 in ethanol and afterwards exposing the plate to hot air until the banding was clearly displayed.

Both smooth isolates show slightly red GPL bands in the upper and the middle part of the plate. These bands are not visible for the rough isolates.

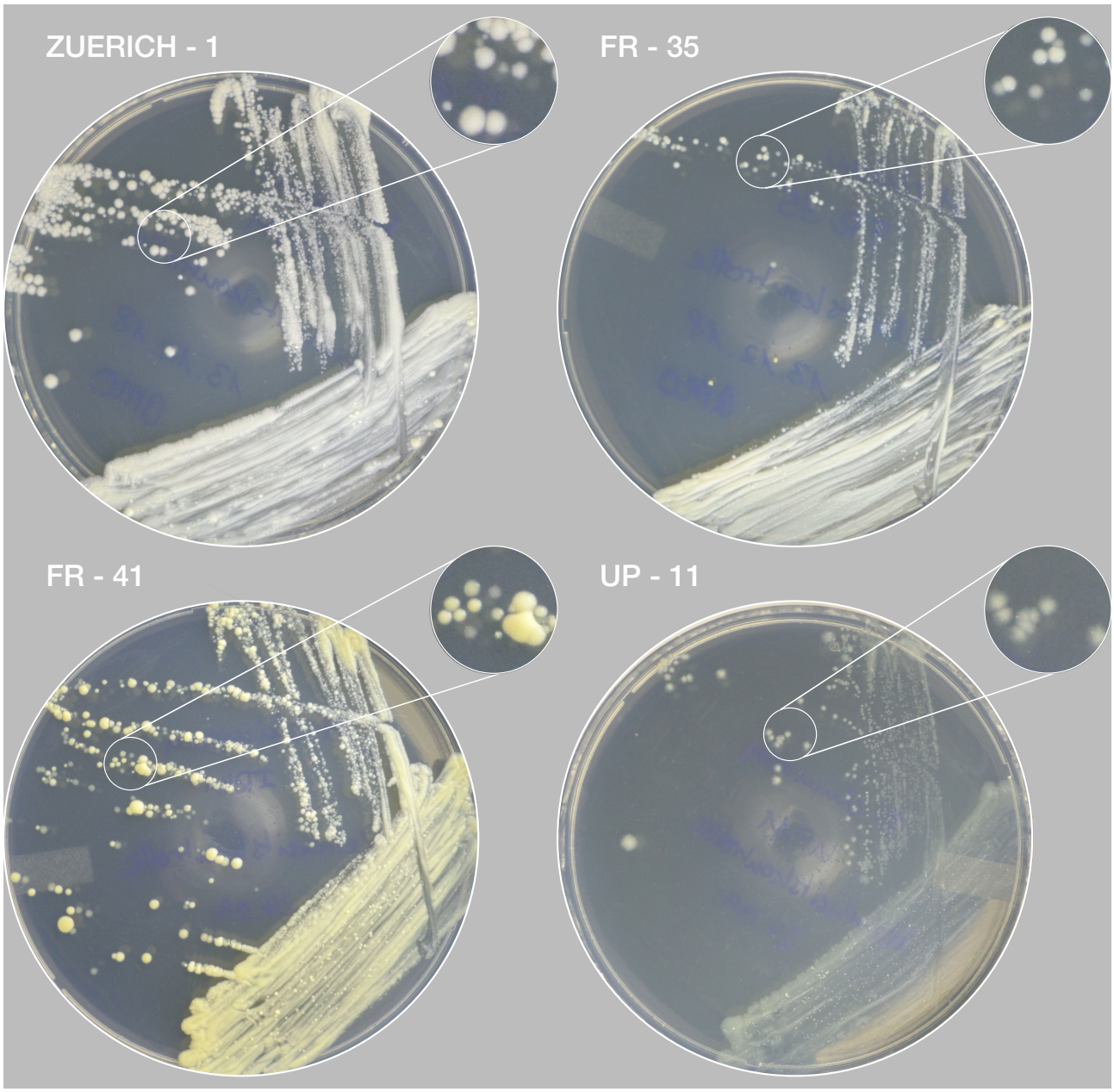

Suppl. Fig. S.3: Photographies of *M. chimaera* isolates
Displayed are photographies of the used *M. chimaera* isolates with zooms to single colonies of each isolate. The bacteria were grown on MB-OADC 10 % agar plates for 21 days at 37 °C. In all cases the colonies are of smooth and circular shape.
Except for UP-11 all isolates show two or more colony types that differ by size and opacity. Especially FR-41 displays a distinct yellowish colouration. The colonies of UP-11 are rather small and of translucent opacity compared to the other isolates.

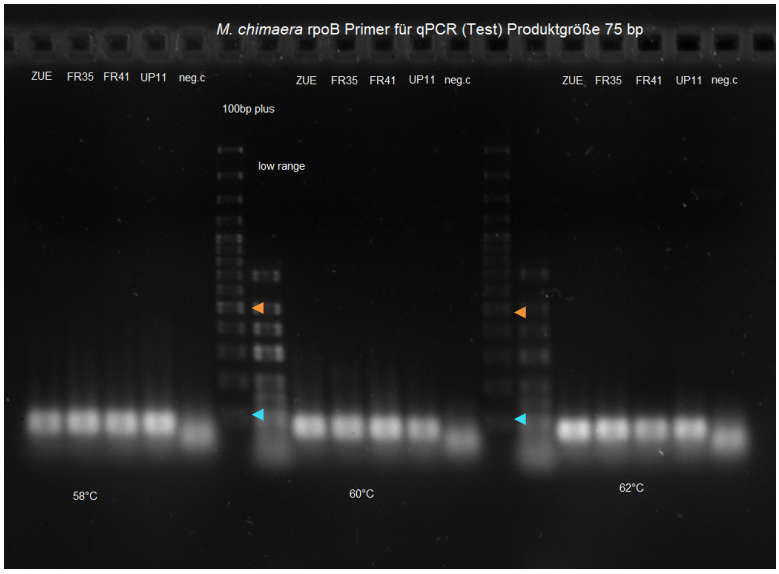

Suppl. Fig. S.4: *M. chimaera rpoB* primers
In order to confirm the optimal conditions for PCR and RT-qPCR, the primers of the *rpoB* gene of *M. chimaera* were tested at different temperatures (58 °C; 60 °C; 62 °C). A product size of 75 basepairs (bp) was expected. The gel electrophoresis was performed with a 2 % agarose gel at 120 V for 1.5 h.
For further analysis the temperature of 60 °C was used. blue arrow = 100 bp; orange arrow = 500 bp

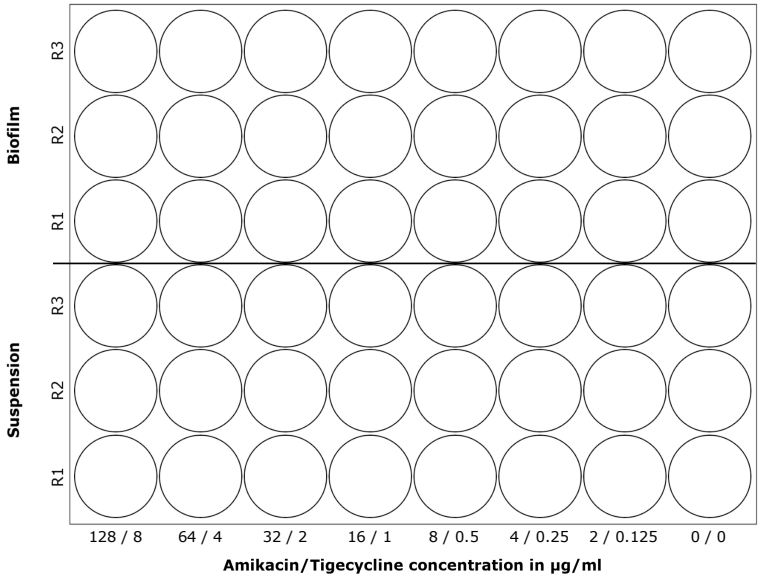

Suppl. Fig. S.5: Antibiotic test plate set-up
Displayed is the common set-up of the antibiotic test plates used. For biofilm and suspension three replicates, respectively, were tested at once, each in eight decreasing concentrations of the chosen antibiotic (AMI or TGC).

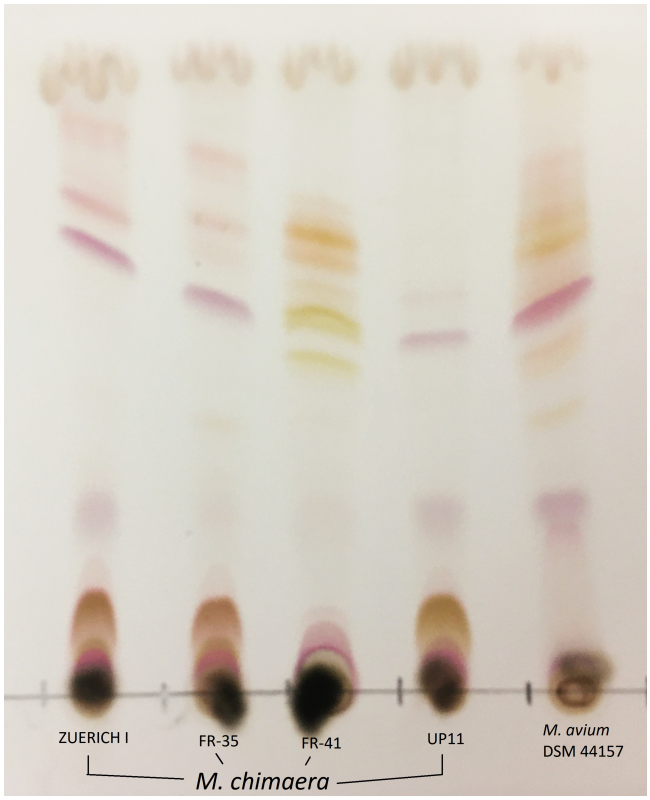

Suppl. Fig. S.6: TLC of slow growing mycobacteria.

In order to analyse the lipid composition of each isolate, the bacteria were cultivated as planktonic samples and prepared as described above (section 2.2.5 & section 2.5.3.3).
After the lipids were completely dried they were resuspended in 1 mL 2:1 chloroform/methanol and stored in a parafilm sealed 2 mL eppendorf tube at -20 °C.

For thin-layer chromatography, 5 µL of the dissolved lipids were applied to silica-coated TLC plates (Analtech DC-Uniplates™, Merck, Germany) and dried shortly. Afterwards the TLC plate was put in a chamber containing chloroform/methanol (90:10, vol/vol) as solvent. The lipids were separated for 15 min then the TLC plate was taken out of the chamber and dried under the fume hood completely.
The lipids were made visible by spraying the plates with 10 % H_2SO_4 in ethanol and afterwards exposing the plate to hot air until the banding was clearly displayed.

Except for FR-41, all *M. chimaera* isolates show similar lipid profiles, while *M. avium* ATCC 15769 displays a more complex pattern, showing similarities to FR-41 and the other *M. chimaera* isolates.

While the isolates ZUERICH-1 FR-35 and UP-11 as well as *M. avium* ATCC 15769 show a violet band in the middle range and less intense violet bands in the upper part of the plate.
FR-41shows multiple bands of yellow and orange color which are not present in any other *M. chimaera* isolate.

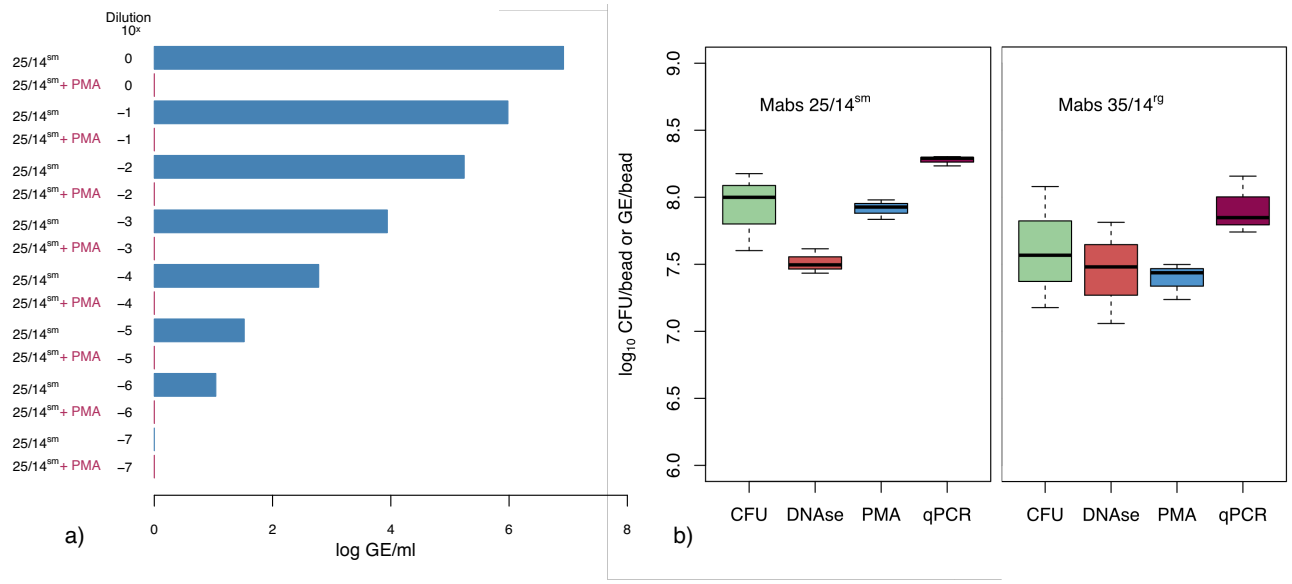

Suppl. Fig. S.7: Functionality testing of PMA
In order to exclude extracellular DNA and dead bacteria as false positive counts from qPCR, the DNA binding dye propidium monoazide (Biotium, CA) was used. The light-activated dye is supposed to bind free available DNA such as eDNA and DNA of dead bacteria (disrupted cell wall).
a) The efficiency of PMA was tested with isolated DNA of $25/14^{sm}$ in different dilutions, down to 10^{-7}. The samples to which PMA was added. were not measured by RT-qPCR, even at the highest amount of DNA. **b)** In a second approach PMA was tested against CFU counting, qPCR and samples to which DNAse was added. and which were afterwards measured by qPCR. The experiment showed that DNAse treatment does not only digests eDNA, but also affects living bacteria. qPCR measurement without PMA recognized more genome equivalents when compared to the expected number of bacteria that has been counted by CFU/mL. The PMA treated samples showed a comparable amount of GE/mL compared to CFU/mL, with a much reduced standard deviation, which is especially for the rough isolate $35/14^{rg}$ an advantage.

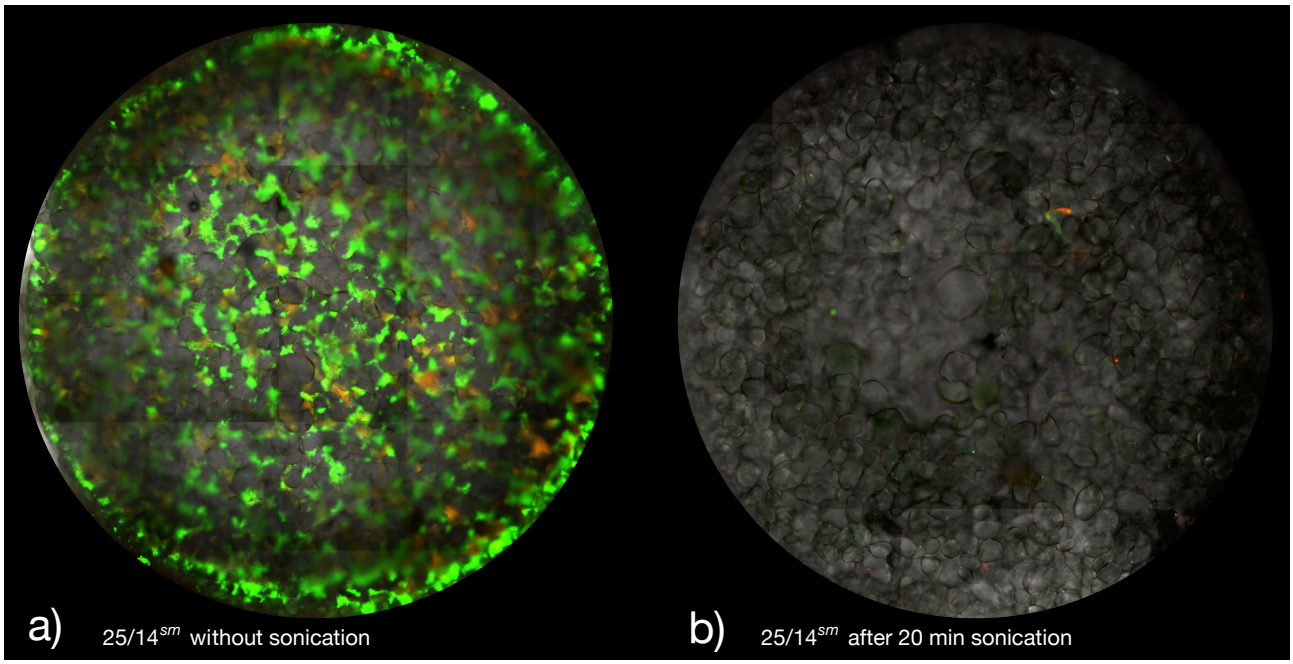

Suppl. Fig. S.8: Efficiency of Sonication
The isolate *M. abscessus* 25/14^{sm} was grown on PGBs for 7 days in optimal medium and stained for 20 min with SYTO9 (green) and propidium iodide (red) (staining solution 1:1000 in 1:1 H_2O/DMSO; see table 2.5.1). The images display the overlay (orange) of both stains.
To test the efficacy of the sonication, one bead (**b**) was sonicated as usually proceeded (see section 2.2.3), the other bead (**a**) was not treated. Afterwards both beads were scanned by fluorescent microscopy using optimal laser settings for each stain.
The comparison shows that after sonication (**b**) the complete biofilm was detached from the bead.

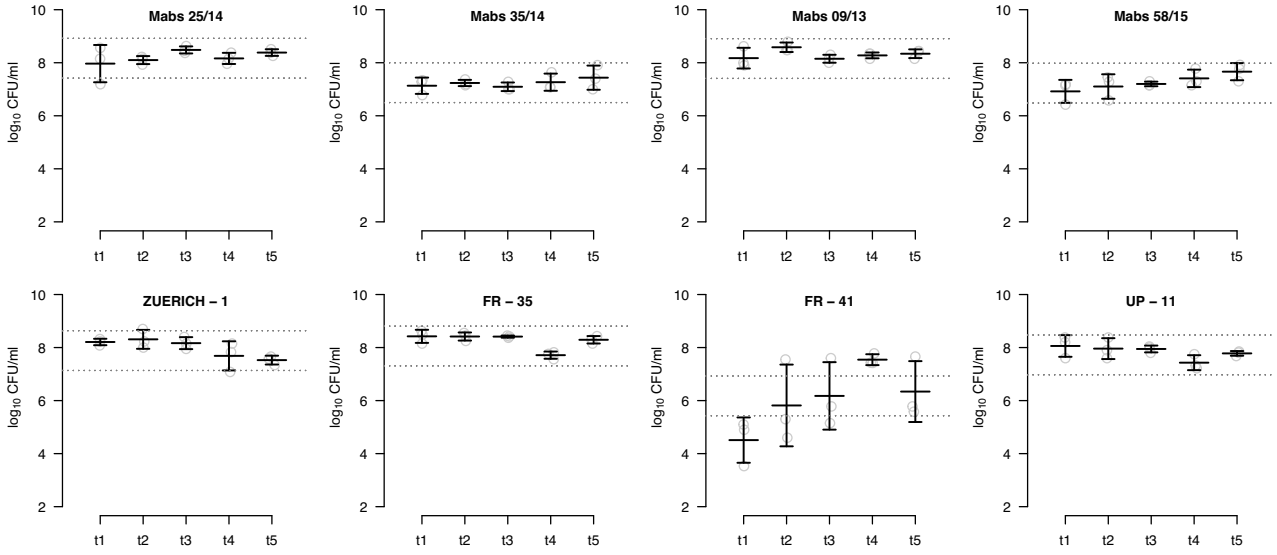

Suppl. Fig. S.9:
Reproducibility of biofilm growth of multiple biological samples of *M. abscessus* and *M. chimaera* on porous glass beads.
Five biological samples of each isolate were cultivated on PGBs and the number of biofilm associated bacteria quantified after 7 days for *M. abscessus* and 21 days for *M. chimaera* isolates. Light grey circles show technical triplicates of each biological sample. Bars represent mean and standard deviation. Dotted lines represent the maximal allowed deviation of 1 log around the overall mean that is necessary to enable reliable disinfectant testing.
While all isolates show a high reproducible biofilm growth on PGBs among multiple biological replicates, the isolate FR-41shows a strong deviation of biofim growth among biological and also technical replicates.

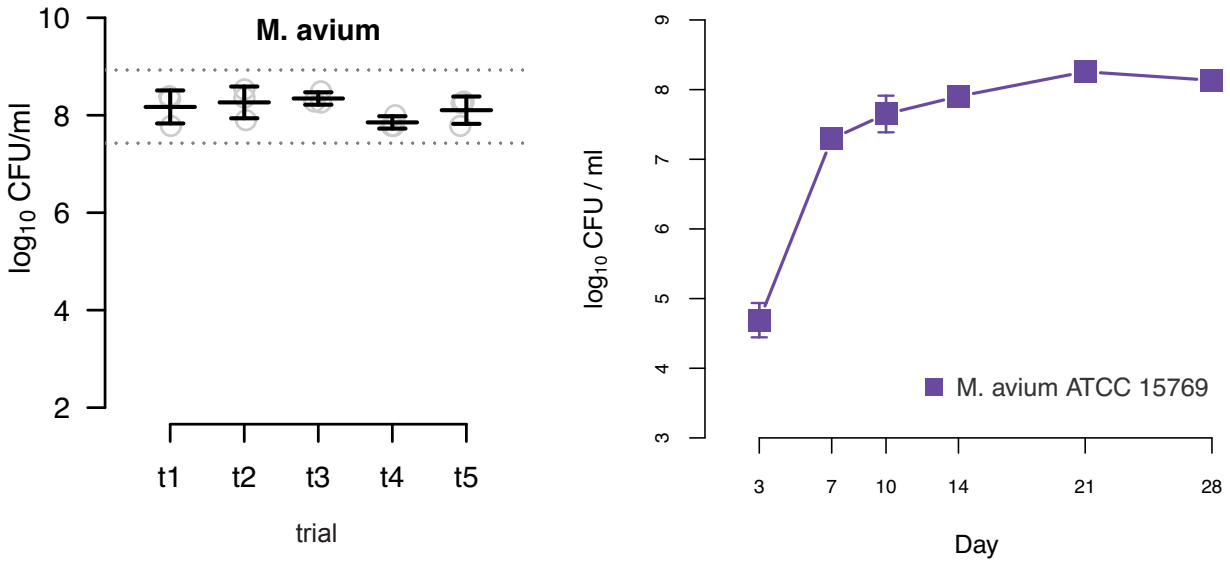

Suppl. Fig. S.10: Growth and Reproducibility of biofilm from *M. avium* ATCC 15769
a) Five biological samples of *M. avium* ATCC 15769 were cultivated on PGBs and the number of biofilm associated bacteria quantified after 21 days. Light grey circles show technical triplicates of each biological sample. The dotted lines represent the maximal allowed deviation of 1 log around the overall mean that is necessary to enable reliable disinfectant testing. In all replications the isolate displayed a constant number of approx. 8 $\log_{10}$ CFU/mL.
b) Displayed is the growth curve of the biofilm growth of *M. avium* ATCC 15769. The isolate shows an exponential growth until day 7 followed by a constant growth until day 21. It grows to a similar level as the *M. chimaera* isolates.
Represented are means and standard deviations of three (growth curve) or five (reproducibility) individual biological replicates, each consisting of three technical replicates.

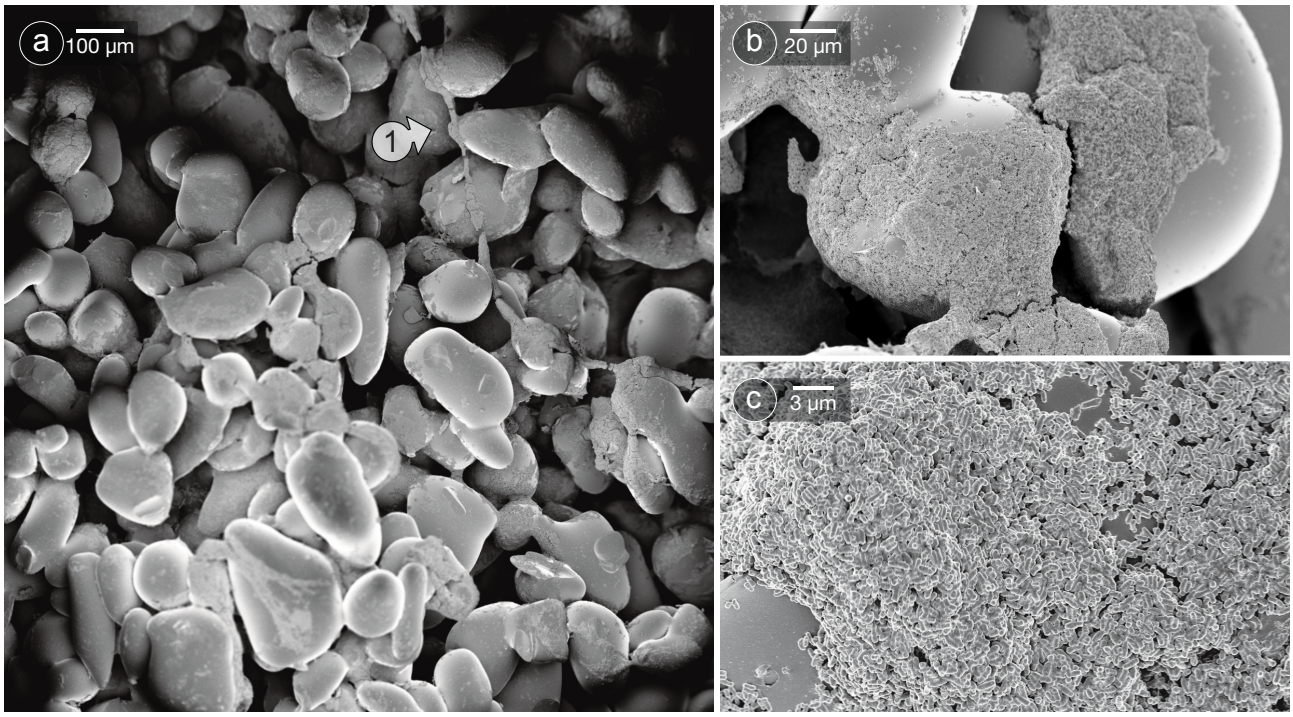

Suppl. Fig. S.11: SEM images of *M. avium* ATCC 15769.
Upscaled SEM images of the disinfectant testing reference isolate *M. avium* ATCC 15769 grown on PGBs.
The isolate was used for standardising the disinfectant testing experiments. It showed similar behaviour as the *M. chimaera* isolates in cases of biofilm growth pattern and ECM composition.
The SEM imaging showed biofilm growth of the *M. avium* ATCC 15769 isolate all over the PGB surface, the outer and inner parts of the glass particles.
The overview image (**a**, arrow 1) shows that the biofilm is partially structured as tubes or lines that link multiple aggregates on the surface of the glass particles (**b**). The aggregates show a dense packing of the bacteria covered with an evenly distributed matrix (**c**).

Suppl. Tab. S.1: Accessory genes of *M. chimaera* ZUERICH-1.
Listed are the first 50 of 513 genes that are only present in the genome of *M. chimaera* ZUERICH-1 when compared to the other isolates. No available UniProtID is indicated by '-'.

ZUERICH-1 genome accession	Unique Gene name	Non-unique Gene name	Description	UniProt ID
FHBAGDFH_03139	hcaF_2		3-phenylpropionate/cinnamic acid dioxygenase subunit beta	A0A1Y0TGD1
FHBAGDFH_04312			AAA domain-containing protein	A0A220YFT7
FHBAGDFH_00348			alpha/beta hydrolase	A0A220YE39
FHBAGDFH_01115			alpha/beta hydrolase	A0A1Y0T6C1
FHBAGDFH_03138			aromatic ring-hydroxylating dioxygenase subunit alpha	A0A220YIM6
FHBAGDFH_00454			arsenate reductase ArsC	A0A1Y0T1E0
FHBAGDFH_00453			arsenical-resistance protein	A0A220Y4T9
FHBAGDFH_00366			ArsR family transcriptional regulator	A0A220YE22
FHBAGDFH_00462			ArsR family transcriptional regulator	A0A1Y0T2E0
FHBAGDFH_00307			ATP-binding protein	A0A220YE75
FHBAGDFH_00363			ATP-binding protein	A0A220YE23
FHBAGDFH_04316			ATP-binding protein	A0A220YFT3
FHBAGDFH_01164			ATP-dependent Clp protease ATP-binding subunit	A0A220YG99
FHBAGDFH_00009	rep		ATP-dependent DNA helicase Rep	A0A220Y6U0
FHBAGDFH_00049			ATPase ParA type	A0A220YEZ9
FHBAGDFH_01160			chromosome partitioning protein ParA	A0A220YG98
FHBAGDFH_03578			cutinase family protein	-
FHBAGDFH_00408			DEAD/DEAH box helicase	A0A1Y0T467
FHBAGDFH_00465	menG		Demethylmenaquinone methyltransferase	A0A220Y5F5
FHBAGDFH_00185			endopeptidase	A0A1Y0T4H1
FHBAGDFH_00198	mazF4		Endoribonuclease MazF4	A0A220YEI1
FHBAGDFH_00364	eccC		ESX secretion system protein EccC	A0A220YE27
FHBAGDFH_00063		eccA3	ESX-3 secretion system protein EccA3	A0A1Y0TAU4
FHBAGDFH_00261			FHA domain-containing protein	A0A220YEB7
FHBAGDFH_01134			four-helix bundle copper-binding protein	A0A220YGC4
FHBAGDFH_00448			glyoxalase/bleomycin resistance/dioxygenase family protein	A0A220Y4U2
FHBAGDFH_00461			heavy metal translocating P-type ATPase	A0A220XMH3
FHBAGDFH_01127			helix-turn-helix domain-containing protein	A0A1Y0TC37
FHBAGDFH_00098			HNH endonuclease	A0A1Y0TAR4
FHBAGDFH_00001			hypothetical protein	A0A220XPQ7
FHBAGDFH_00003			hypothetical protein	A0A1Y0T0V5
FHBAGDFH_00004			hypothetical protein	A0A1Y0T3H0
FHBAGDFH_00005			hypothetical protein	A0A220Y6R9
FHBAGDFH_00006			hypothetical protein	A0A220XPL3
FHBAGDFH_00007			hypothetical protein	A0A220XPJ1
FHBAGDFH_00008			hypothetical protein	A0A1Y0SYB7
FHBAGDFH_00010			hypothetical protein	A0A7U5RTZ9
FHBAGDFH_00011			hypothetical protein	A0A220Y7X9
FHBAGDFH_00012			hypothetical protein	-
FHBAGDFH_00013			hypothetical protein	-
FHBAGDFH_00014			hypothetical protein	-
FHBAGDFH_00015			hypothetical protein	A0A1Y0SY43
FHBAGDFH_00016			hypothetical protein	-
FHBAGDFH_00017			hypothetical protein	A0A1Y0T0U9
FHBAGDFH_00019			hypothetical protein	A0A220XPN0
FHBAGDFH_00020			hypothetical protein	A0A220Y717
FHBAGDFH_00022			hypothetical protein	A0A220XPS8
FHBAGDFH_00023			hypothetical protein	A0A1Y0T8J1
FHBAGDFH_00024			hypothetical protein	A0A220XXB3
FHBAGDFH_00025			hypothetical protein	A0A220XXZ3

The whole table is digital available from Dr. Astrid Lewin, Robert Koch - Insitut, Berlin.

Suppl. Tab. S.2: Significantly regulated proteins of the isolates *M. chimaera* ZUERICH-1 and FR-35.
Listed are the first 50 of 1339 proteins that were significantly regulated in the proteome analysis. The values were rounded to the third decimal place.ZUE - ZUERICH-1; FR35 - FR-35; B - biofilm; S - suspension; P - planktonic

UniprotID	Proteome log_2 fold expression						COG category
	ZUE B	ZUE S	ZUE P	FR35 B	FR35 S	FR35 P	
A0A1Y0SVR0	0,220	0,031	-0,383	-0,396	0,068	-0,010	S
A0A1Y0SVT0	0,410	0,053	-0,106	0,186	0,156	-0,659	M
A0A1Y0SW51	0,213	-0,082	-0,003	-0,234	-0,056	0,342	C
A0A1Y0SW61	0,028	-0,560	0,298	-0,568	0,448	0,280	S
A0A1Y0SWC9	-1,333	-1,640	1,132	-1,275	1,297	1,207	S
A0A1Y0SWP5	0,172	-0,160	0,000	0,573	-0,234	-0,845	S
A0A1Y0SWS9	0,201	0,085	-0,772	-0,632	0,027	0,468	G
A0A1Y0SWV5	-0,072	-0,035	0,497	0,660	-0,025	-0,388	S
A0A1Y0SWY5	0,672	1,328	-0,217	-0,214	-0,512	0,715	S
A0A1Y0SWY6	0,071	1,378	-0,071	0,650	-1,123	-0,469	S
A0A1Y0SX05	-0,035	1,756	0,117	-0,395	-0,717	0,538	S
A0A1Y0SXC1	0,217	-0,160	0,010	0,205	-0,010	-0,394	I
A0A1Y0SXG5	-0,572	0,126	0,553	1,357	-0,311	-0,209	Q
A0A1Y0SXS7	-1,827	-0,963	1,175	0,101	0,000	-0,093	T
A0A1Y0SXU2	-3,009	-1,781	2,085	-0,898	0,685	0,000	-
A0A1Y0SXU2	-3,009	-1,781	2,085	-0,898	0,685	0,000	S
A0A1Y0SXX3	-0,028	0,160	0,147	0,485	-0,263	-0,333	K
A0A1Y0SY51	-1,201	-0,331	0,904	0,299	-0,844	-0,904	P
A0A1Y0SY71	0,249	0,228	-0,689	-0,270	-0,007	0,007	I
A0A1Y0SYA7	0,276	0,006	-0,581	-1,162	0,036	0,061	-
A0A1Y0SYB6	-0,295	0,094	0,483	0,796	-0,171	-1,368	-
A0A1Y0SYB7	-0,994	-0,918	-0,272	-1,135	0,000	0,402	L
A0A1Y0SYB7	-0,994	-0,918	-0,272	-1,135	0,000	0,402	L
A0A1Y0SYG5	0,022	-0,073	0,610	0,472	-0,243	-0,610	C
A0A1Y0SYG9	-0,188	-0,084	0,371	0,270	-0,298	0,018	O
A0A1Y0SYH8	0,450	0,303	-0,297	0,016	-0,113	-0,028	I
A0A1Y0SYJ8	-0,221	-0,011	0,301	0,312	-0,060	-0,499	-
A0A1Y0SYK0	-0,301	-0,153	0,433	0,435	0,621	-1,206	I
A0A1Y0SYN5	-0,602	0,110	0,685	1,394	-0,629	-0,534	Q
A0A1Y0SYR7	-2,437	-1,866	1,309	-1,008	0,627	0,487	S
A0A1Y0SYU0	-0,412	-0,225	0,616	-0,480	0,801	1,047	S
A0A1Y0SYV5	0,062	0,361	-0,472	-0,174	-0,194	0,480	-
A0A1Y0SYZ3	0,079	1,752	-0,661	-0,705	-0,848	0,851	-
A0A1Y0SZ12	-1,035	-0,880	-0,128	-1,047	0,278	-0,312	-
A0A1Y0SZ76	0,183	-0,007	-0,245	-0,235	-0,044	0,469	P
A0A1Y0SZB1	0,575	0,470	-0,103	-0,375	-1,025	0,372	T
A0A1Y0SZB3	0,314	-0,008	-0,553	-0,625	0,175	0,363	K
A0A1Y0SZC2	0,199	0,101	-0,478	-0,240	0,161	-0,003	IQ
A0A1Y0SZE5	0,069	0,068	-0,444	-0,471	0,391	0,296	KT
A0A1Y0SZG6	-0,020	-0,044	0,719	0,664	-0,068	-0,033	-
A0A1Y0SZK9	-0,134	-0,008	1,002	1,123	0,008	-0,418	H
A0A1Y0SZL3	-0,223	-0,565	0,726	1,801	-0,094	-2,273	S
A0A1Y0SZU1	0,501	0,122	-0,227	-0,237	0,234	-0,006	M
A0A1Y0SZU2	0,204	0,151	-0,319	0,141	-0,000	-1,222	C
A0A1Y0SZX2	-0,068	-0,162	0,138	0,154	0,174	-0,946	NU
A0A1Y0T019	0,186	0,009	-0,066	0,331	-0,164	-0,401	S
A0A1Y0T024	-0,033	0,189	-0,091	-0,549	0,008	0,291	G
A0A1Y0T036	-0,198	-0,020	0,231	0,602	0,204	-0,732	IQ
A0A1Y0T041	0,003	0,157	-0,402	-0,765	-0,128	1,034	S
A0A1Y0T046	-0,104	-0,009	0,374	0,563	0,280	-0,567	Q
A0A1Y0T047	-0,042	0,190	-1,330	-1,190	0,002	0,534	-

The whole table is digital available from Dr. Astrid Lewin, Robert Koch - Insitut, Berlin.

Suppl. Tab. S.3: Significantly regulated genes of the isolates *M. chimaera* ZUERICH-1 and FR-35.
Listed are the first 50 of 4733 genes that were significantly regulated in the transcriptome analysis. The values were rounded to the third decimal place. ZUE - ZUERICH-1; FR35 - FR-35; B - biofilm; S - suspension; P - planktonic

UniprotID	Transcriptome $\log_2$ fold expression						COG category
	ZUE B	ZUE S	ZUE P	FR35 B	FR35 S	FR35 P	
A0A0P7HPK6	-0,126	-5,061	0,411	0,343	-3,773	0,901	S
A0A1Y0SVR9	-0,414	-0,203	0,409	0,354	-1,044	1,171	K
A0A1Y0SVT0	-0,410	1,015	-0,157	-0,124	-0,064	0,230	M
A0A1Y0SVU0	-0,186	-0,184	-0,205	0,409	-0,006	0,171	S
A0A1Y0SVW2	0,305	-1,543	0,544	0,683	-1,404	0,088	C
A0A1Y0SVX3	-0,219	1,073	-0,322	-0,255	0,427	0,007	S
A0A1Y0SVX4	-0,106	-1,685	0	0,013	-0,702	2,611	S
A0A1Y0SVY2	0,219	0,092	0,072	-0,621	-0,124	0,973	K
A0A1Y0SVZ3	-0,276	0,951	-0,139	-0,476	-0,164	0,498	KLT
A0A1Y0SVZ4	0,755	-0,717	0,278	1,491	-0,553	-0,812	O
A0A1Y0SW07	-1,276	-3,216	-0,852	3,972	-0,166	1,117	Q
A0A1Y0SW12	-0,231	-0,858	0,138	0,444	-0,817	0,423	-
A0A1Y0SW61	-0,340	-0,180	0,135	0,947	-0,308	0,830	S
A0A1Y0SW76	0,463	-0,848	0,870	0,512	-0,280	-0,145	D
A0A1Y0SW81	-1,983	-1,631	-0,663	0,457	0,276	1,154	S
A0A1Y0SW89	-0,275	-0,740	0,322	0,258	-0,090	0,125	K
A0A1Y0SWC4	-0,451	1,223	-0,537	-0,271	-0,112	0,315	M
A0A1Y0SWC9	-0,259	-0,817	0,439	0,790	-0,708	1,105	S
A0A1Y0SWD3	-0,256	0,765	-0,369	-0,747	-0,648	0,507	M
A0A1Y0SWD4	0,707	3,805	3,182	-1,473	-1,161	-1,094	-
A0A1Y0SXH7	0,107	0,063	0,093	-0,146	-1,198	0,024	IQ
A0A1Y0SXI4	0,752	-0,589	-0,506	1,278	-2,439	0,200	C
A0A1Y0SXJ2	0,919	-1,792	0,359	0,692	-2,375	-0,179	V
A0A1Y0SXK8	-0,793	0,660	-0,445	0,188	0,078	-0,141	S
A0A1Y0SXM0	-0,516	0,118	0,808	0,000	-0,796	-0,052	S
A0A1Y0SXQ0	0,593	0,122	0,586	0,210	-1,616	0,084	-
A0A1Y0SXR5	-0,155	-0,121	0,083	1,436	-1,272	0,276	-
A0A1Y0SXR9	0,285	-0,777	0,017	0,566	-0,229	0,433	-
A0A1Y0SXS6	0,000	-0,578	0,264	0,239	-0,853	0,695	-
A0A1Y0SXS7	-0,298	1,825	0,000	-0,457	-0,916	0,062	T
A0A1Y0SXT1	0,028	-0,233	0,053	0,223	0,165	0,233	-
A0A1Y0SWQ1	-0,123	-1,835	-0,241	0,423	-1,923	0,770	IQ
A0A1Y0SWQ3	-0,048	-1,620	-0,013	0,328	-1,866	1,213	S
A0A1Y0SWS9	-0,214	-1,016	0,027	0,328	-1,137	0,689	G
A0A1Y0SWT7	0,054	-0,625	0,220	0,405	-1,422	0,286	L
A0A1Y0SWT9	-0,800	0,957	0,255	-0,454	-0,832	-0,123	S
A0A1Y0SWV1	-0,513	1,326	-0,177	-0,517	-0,281	0,025	V
A0A1Y0SWV5	0,233	-0,720	0,318	-0,151	-0,581	1,670	S
A0A1Y0SWX1	0,035	-1,436	0,100	0,364	-1,548	0,635	I
A0A1Y0SWY5	-1,826	0,628	-1,171	-1,463	0,380	0,559	S
A0A1Y0SWY6	-1,536	1,854	-0,715	-1,845	-0,310	0,748	S
A0A1Y0SWZ6	-2,638	2,203	-1,229	-2,851	-1,053	1,593	S
A0A1Y0SX04	-0,359	-0,118	0,160	-0,006	-0,191	0,608	J
A0A1Y0SX36	-0,960	0,148	-0,071	-0,376	-0,402	0,624	S
A0A1Y0SX37	-0,699	0,866	-0,185	-0,036	0,253	0,100	S
A0A1Y0SX48	0,213	0,186	1,350	0,794	-0,015	-1,334	N
A0A1Y0SX57	0,133	-0,263	-0,104	0,410	-0,546	0,779	-
A0A1Y0SXB2	-1,056	0,236	-0,343	2,957	-1,790	0,928	P
A0A1Y0SXB3	-1,454	-0,436	0	0	-1,821	-3,720	I
A0A1Y0SXB4	-0,716	0,822	-0,198	3,460	-1,088	-0,415	K
A0A1Y0SXC1	-0,252	-0,233	0,208	0,837	-0,946	0,316	I

The whole table is digital available from Dr. Astrid Lewin, Robert Koch - Insitut, Berlin.

Suppl. Tab. S.4: Presence of the genes identified in the upper quartile of the isolates *M. chimaera* ZUERICH-1 and FR-35in the specific cultivation forms.
Listed are the first 50 of 236 genes that were identified in the upper quartiles (Q4) of all cultivation forms in both isolates. The presence of a gene is indicated with '+', the absence is displayed by '-'. Six of the genes are present in both biofilms, but not in the other forms. These were further analysed in table table 3.4.3.

UniprotID	ZUE B	ZUE S	ZUE P	FR35 B	FR35 S	FR35 P
A0A7U5RY31	+	-	-	-	+	-
A0A222S6U2	+	+	+	+	+	+
A0A220YKI6	+	+	+	+	+	+
A0A220YKG7	-	-	-	-	+	-
A0A220YKF1	+	+	+	+	+	+
A0A220YKB3	+	+	+	+	-	+
A0A220YK69	-	-	+	+	+	+
A0A220YJU4	+	+	+	+	+	+
A0A220YJS1	-	-	-	-	+	-
A0A220YJR5	+	+	+	+	+	-
A0A220YJG9	-	-	-	-	+	-
A0A220YJE0	+	+	+	+	+	+
A0A220YJ52	-	-	-	-	+	-
A0A220YJ46	+	-	-	-	-	-
A0A220YIX3	+	+	+	+	+	+
A0A220YIQ1	+	+	+	+	+	+
A0A220YII3	-	-	-	-	+	-
A0A220YI16	-	+	-	-	+	+
A0A220YHL9	-	-	-	+	-	-
A0A220YHH7	+	+	-	+	-	-
A0A220YHG8	-	+	-	-	-	-
A0A220YHG5	+	-	-	+	-	-
A0A220YGT9	+	-	+	+	+	-
A0A220YGT9	+	+	-	+	-	-
A0A220YGQ5	+	+	+	+	-	-
A0A220YGP6	-	-	-	+	+	-
A0A220YGM5	+	+	+	+	+	+
A0A220YGF3	-	-	-	-	+	-
A0A220YG36	+	-	-	-	-	-
A0A220YG19	+	-	-	-	-	-
A0A220YFV9	-	-	-	-	-	+
A0A220YFR8	-	-	-	-	+	-
A0A220YFN7	-	-	+	-	-	-
A0A220YFN1	+	+	+	+	+	+
A0A220YFL9	+	+	+	-	+	+
A0A220YF74	-	+	-	-	-	-
A0A220YEU2	+	-	+	+	-	+
A0A220YEP6	+	-	+	+	-	+
A0A220YEP3	-	+	-	-	-	-
A0A220YEN1	+	+	+	-	-	-
A0A220YEL5	-	-	-	-	+	+
A0A220YEH4	-	+	-	-	-	-
A0A220YEH1	+	-	-	-	-	-
A0A220YED6	-	-	-	-	+	+
A0A220YE92	+	-	+	+	+	+
A0A220YE82	+	-	-	-	-	-
A0A220YE78	+	-	+	+	-	+
A0A220YE63	-	-	+	+	-	-
A0A220YE59	+	-	-	+	+	+
A0A220YE21	+	-	+	-	-	-
A0A220YDZ1	-	-	-	-	+	-

The whole table is digital available from Dr. Astrid Lewin, Robert Koch - Insitut, Berlin.